I.R.Iran

ISSN:2423-5547
e-ISSN:2423-7469

Journal of Renewable Energy and Environment

Volume 9, Number 2, Spring 2022

Materials and Energy Research Center

Iranian Association of Chemical Engineers

ISSN: 2423-5547; e-ISSN: 2423-7469

Journal of Renewable Energy and Environment (JREE): Vol. 9, No. 2, (Spring 2022), 1-106

CONTENTS

AIMS AND SCOPE

Journal of Renewable Energy and Environment (JREE) publishes original papers, review articles, short communications and technical notes in the field of science and technology of renewable energies and environmental-related issues including:

- Generation
- Storage
- Conversion
- Distribution
- Management (economics, policies and planning)
- Environmental Sustainability

INSTRUCTIONS FOR AUTHORS

Submission of manuscript represents that it had neither been published nor submitted for publication elsewhere and is result of research carried out by author(s). Only the extended and upgraded articles presented in a conference and/or appeared in a symposium proceedings could be evaluated for publication.
Authors are required to include a list describing all the symbols and abbreviations in the paper. Use of the international system of measurement units is mandatory.

- On-line submission of manuscripts results in faster publication process and is recommended. Instructions are given in the JREE web sites: www.jree.ir
- References should be numbered in brackets and appear in sequence through the text. List of references should be given at the end of the paper. All journal articles listed in the References section must follow with article doi.
- Figure captions are to be indicated under the illustrations. They should sufficiently explain the figures.
- Illustrations should appear in their appropriate places in the text.
- Tables and diagrams should be submitted in a form suitable for reproduction.
- Photographs should be of high quality saved as jpg files.
- Tables' illustrations, figures and diagrams will be normally printed in single column width (8 cm). Exceptionally large ones may be printed across two columns (17 cm).

Journal of Renewable Energy and Environment

Journal Homepage: www.jree.ir

Materials and Energy Research Center

MERC

Research Article

Control of Pitch Angle in Wind Turbine Based on Doubly Fed Induction Generator Using Fuzzy Logic Method

Ehsan Hosseini [a,b], Neda Behzadfar [a,b*], Mahnaz Hashemi [a,b], Majid Moazzami [a,b], Majid Dehghani [a,b]

[a] *Department of Electrical Engineering, Najafabad Branch, Islamic Azad University, Najafabad, Isfahan, Iran.*
[b] *Smart Microgrid Research Center, Najafabad Branch, Islamic Azad University, Najafabad, Isfahan, Iran.*

PAPER INFO

Paper history:
Received: 07 July 2021
Revised in revised form: 17 November 2021
Scientific Accepted: 11 January 2022
Published: 11 January 2022

Keywords:
Doubly Fed Induction Generator (DFIG),
Fuzzy Logic Controller,
PI Controller,
Pitch Angle,
Wind Turbine

ABSTRACT

Wind turbines can be controlled by controlling the generator speed and adjusting the blade angle and the total rotation of a turbine. Wind energy is one of the main types of renewable energy and is geographically extensive, scattered and decentralized and is almost always available. Pitch angle control in wind turbines with Doubly Fed Induction Generator (DFIG) has a direct impact on the dynamic performance and oscillations of the power system. Due to continuous changes in wind speed, wind turbines have a multivariate nonlinear system. The purpose of this study is to design a pitch angle controller based on fuzzy logic. According to the proposed method, nonlinear system parameters are automatically adjusted and power and speed fluctuations are reduced. The wind density is observed by the fuzzy controller and the blade angle is adjusted to obtain appropriate power for the system. Therefore, the pressure on the shaft and the dynamics of the turbine are reduced and the output is improved, especially in windy areas. Finally, the studied system is simulated using Simulink in MATLAB and the output improvement with the fuzzy controller is shown in the simulation results compared to the PI controller. Fuzzy control with the lowest cost is used to control the blade angle in a wind turbine. Also, in this method, the angle is adjusted automatically and it adapts to the system in such a way that the input power to the turbine is limited. Compared to the PI controller, by calculating different parameters, the power quality for fuzzy controller is enhanced from 2.941 % to 4.762 % for wind with an average speed of 12 meters per second.

https://doi.org/10.30501/jree.2021.293546.1226

1. INTRODUCTION

Dynamics governs most industrial processes and the real system is nonlinear. The analysis and design of the control system in the nonlinear mode is very difficult [1]. The power system is a very complex system whose equations are nonlinear and its parameters may vary due to various factors such as noise and local loads [2, 3]. Considering the environmental and economical concerns, energy should be produced at places away from consumption centers [4, 5].

In today's world, due to the decline of non-renewable energy reserves, renewable energy has gained importance due to its significant role and much research has been done to exploit these resources [6, 7]. So far, many studies have stressed the importance and application of new energies [8, 9].

Wind energy is used as a sustainable energy [10, 11]. One of the main types of renewable energy is wind energy, which is geographically extensive, scattered, decentralized, and widely accessible [12, 13]. To get maximum energy from the wind and according to the aerodynamic requirements of the generators, it is important to provide an accurate controller resistant to disturbances [14, 15].

When the wind speed and the speed of the turbine exceed their nominal values, the angle controller operates and decreases the power received from the wind by increasing the angle [16, 17]. To this end, various control methods such as proportional controller-integrator-derivative (PID) [18], linear matrix of inequality [19], fuzzy logic [20], quadratic linear equations [21], conventional predictive control [22], and a sliding mode control scheme [23] are proposed. In [24] and [25], the advantages and disadvantages of some examples of controllers were listed.

Effects of various environmental and mechanical factors on increased energy extraction by wind farm systems in [26] were investigated using artificial network modeling, which is the best model of artificial neural network based on annual wind speed changes and diameter, in order to predict the energy increase rate from wind farm. Turbine rotor and turbine power were used.

A step angle control strategy using fuzzy logic control for the DFIG wind turbine system was presented in [27], which did not require system information and wind speed. Also, an adaptive PI control loop was added to the fuzzy logic control

*Corresponding Author's Email: n.behzadfar@pel.iaun.ac.ir (N. Behzadfar)
URL: https://www.jree.ir/article_143158.html

Please cite this article as: Hosseini, E., Behzadfar, N., Hashemi, M., Moazzami, M. and Dehghani, M., "Control of pitch angle in wind turbine based on doubly fed induction generator using fuzzy logic method", ***Journal of Renewable Energy and Environment (JREE)***, Vol. 9, No. 2, (2022), 1-7. (https://doi.org/10.30501/jree.2021.293546.1226).

and used as a step angle controller in a variable-speed wind turbine system.

The most common controller in variable-speed wind turbines to obtain the desired output power is the blade angle controller. Blade angle control in wind turbines has a direct impact on a machine's dynamic performance and power system oscillations. Wind turbines have a nonlinear and multivariate system; hence, it is very important to design controllers that adapt to the system at any time [28].

In this paper, fuzzy control is used to control the blade angle. In this method, the blade angle is automatically adjusted and adapts to the system in a way that increases the input power to the system by taking into account the aerodynamic conditions.

Compared to previous designs, the designed fuzzy controller features no wind speed at the fuzzy input, which eliminates the need for an anemometer. Using a regular pattern wind speed is another feature of the proposed method which is suitable for gaining a better understanding of the performance of controllers. Several previous studies have pointed out that the use of irregularly patterned wind speeds causes no differences in the output of controllers in case of sudden wind changes. Based on a comparison between the simulation results, the superiority of the fuzzy controller is proven. The use of the proposed controller in wind farms will increase the efficiency and service life of mechanical parts and ensures cheaper maintenance.

2. WIND TURBINE SYSTEM MODEL

Wind turbines consist of two main parts: mechanical power generation and conversion of mechanical power to electrical, done by the turbine and the generator, respectively [29]. In this section, their relations and equations are briefly mentioned.

2.1. Turbine

The two-mass model is used in the study of transient stability to model the mechanical and electrical connection between the generator and the wind turbine [30]. If T_M, T_S, and T_E are considered as mechanical, axial, and electrical torques in the turbine, respectively, the equations are:

$$\frac{d\omega_r}{dt} = \frac{1}{2H_R}(T_E + T_S) \quad (1)$$

$$\frac{d\omega_t}{dt} = \frac{1}{2H_T}(T_M + T_S) \quad (2)$$

$$\frac{d\beta}{dt} = \omega_b(\omega_t + \omega_r) \quad (3)$$

where H_T is the moment of inertia of the turbine, H_R the moment of inertia of the turbine rotor, ω_r the frequency angle of the rotor and turbine, and β the angle of the pitch tip. Wind kinetic energy is proportional to the second power of wind speed while wind power is proportional to the cubic speed of wind. Therefore, upon increasing wind speed, wind power will increase. Technical use of wind energy is possible when the average wind speed is in the range of 5 meters per second to 25 meters per second (90 Km/h). The mechanical equation of the turbine is given below [31, 32]:

$$P_W = \frac{1}{2}\pi\rho C_P(\lambda,\beta)R^2V_w^3 \quad (4)$$

where ρ (kg/m^3), R (m), V_w (m/s), and S_b (VA) are air density, pitch diameter, wind speed, and apparent power, respectively. Wind turbine power factor (C_p) is equal to [33]:

$$C_P(\lambda,\beta) = c_1\left(\frac{c_2}{\lambda_i} - c_3\beta - c_4\right)e^{\frac{-c_5}{\lambda_i}} + c_6\lambda \quad (5)$$

where β is the pitch tip angle and the coefficient λ_i is equal to:

$$\lambda_i = \left[\frac{1}{\lambda + c_7\beta} - \frac{c_8}{\beta^3 + 1}\right]^{-1} \quad (6)$$

Blade tip speed to wind speed ratio (λ) is [34]:

$$\lambda = \frac{\omega_t R}{V_\omega} \quad (7)$$

Therefore, at a given wind speed, there is only one specific angular velocity for maximum power.

Wind speed is a determining factor in power reference, torque, or turbine speed. Depending on the wind speed, the operation of the turbine can be divided into four general modes. The mechanical output power of a wind turbine is divided into four regions in terms of wind speed, as shown in Figure 1 [23].

The angular velocity of the turbine is set to be less than the nominal wind speed in $C_{p,max}$. When the wind speed is higher than the nominal wind speed, the blade angle control is activated and by adjusting the blade and limiting the energy received from the wind, the blade angle can be adjusted to determine the proper power of the generator and gearbox. The blade control mechanism can be modeled using the following fixed time system (T_β) [35, 36]:

$$\frac{d\beta_P}{dt} = \frac{1}{T_\beta}(\beta_{P\,ref} - \beta_P) \quad (8)$$

When the wind speed is less than the nominal wind speed, β_{pref} is maintained at zero; however, when it exceeds the nominal value, the actual power is modeled by the PI controller via the following relations [37]:

$$\beta_{p\,ref} = K_{P\beta}(P_t - P_{t\,ref}) + x_\beta \quad (9)$$

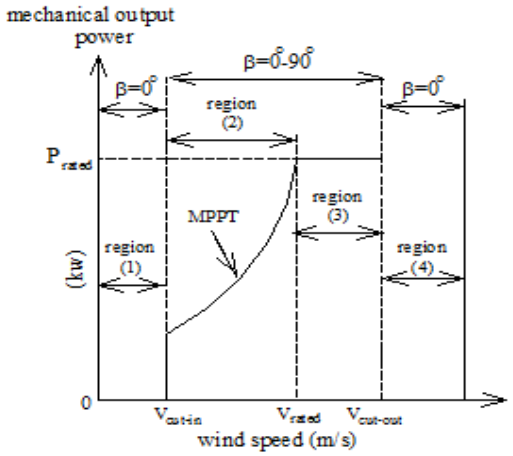

Figure 1. Wind turbine operating areas in terms of wind speed

$$\frac{dx_\beta}{dt} = K_{I\beta}(P_t - P_{t\,ref}) \quad (10)$$

where $K_{I\beta}$ and $K_{P\beta}$ are the integral interest rates, which are proportional. The blade angle control block diagram in Figure 2 shows that the PI controller is used for adjustment. The speed or mechanical power of the generator is expressed by X. A summary of the parameters used to model the turbine is given in Table 1.

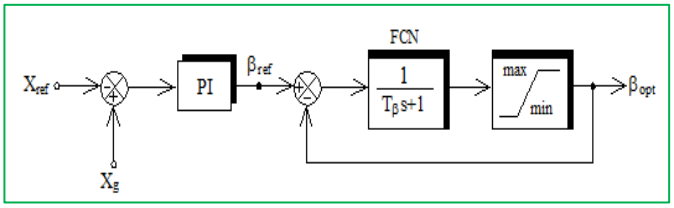

Figure 2. Application of PI controller to controlling blade angle

Table 1. Turbine modeling parameters

Parameter	Symbol	Unit
Frequency angles of the rotor	ω_r	Rad/s
Mechanical torque	T_M	N.m
Axial torque	T_S	N.m
Electrical torque	T_E	N.m
Wind turbine power factor	C_P	-
Angles of the pitch tip	β	degree
Moment of inertia of the turbine	H_T	s
Moment of inertia of the turbine rotor	H_R	s
Apparent power	S_b	VA
Air density	ρ	kg/m^3
Pitch diameter	R	M
Wind speed	V_w	m/s

2.2. DFIG wind turbine system

Figure 3 shows the block diagram of the system under study, including the wind turbine and the controller. The turbines used are Horizontal-Axis Wind Turbines (HAWTs). HAWTs are typically either two- or three-bladed and operate at high blade tip speeds [38, 39]. The system model is derived from the mechanical model of the blades, hub, and shaft; a magnetic model of a three-phase transformer; and a back-to-back converter of transmission line and network [40, 41]. The back-to-back converter is formed of separate parts on the side of the device and the network that are connected to each other via a DC connector capacitor [42, 43].

2.3. Control with fuzzy logic

Fuzzy generator, inference motor, fuzzy rules, and non-fuzzy generator are the four main parts of a fuzzy controller. A fuzzy inference system has fuzzy inputs and outputs; however, the inputs and outputs of the target system are numerical [44, 45]. Based on the experience, language variables are used to set fuzzy rules. All calculations and rules are done and considered at the heart of the fuzzy system, the inference engine [46, 47]. In the studied system, the multiplication inference engine, singleton fuzzy maker, and center interpolation maker are used. The block diagram using fuzzy logic is shown in Figure 4. The error in the generator output power (ΔP), the variation of the output power error (δΔp), and rotor speed (ω_r) are considered as inputs for the proposed fuzzy controller [48].

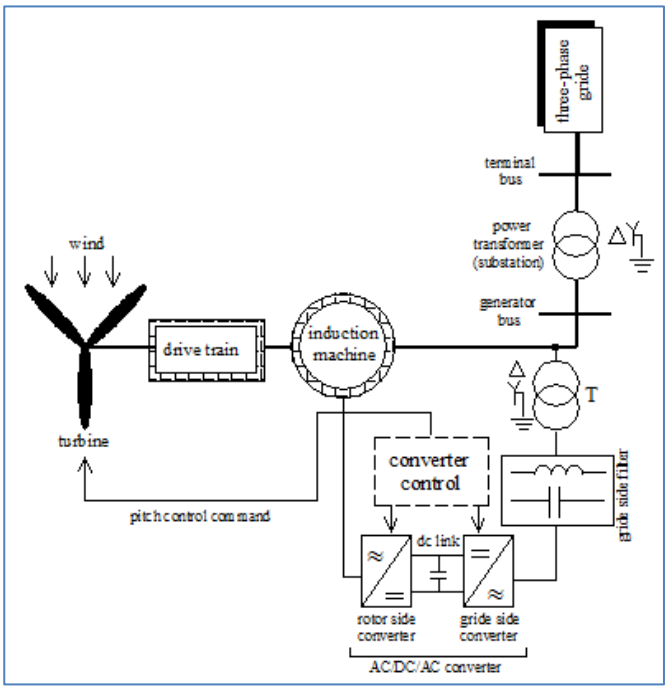

Figure 3. Target system block diagram

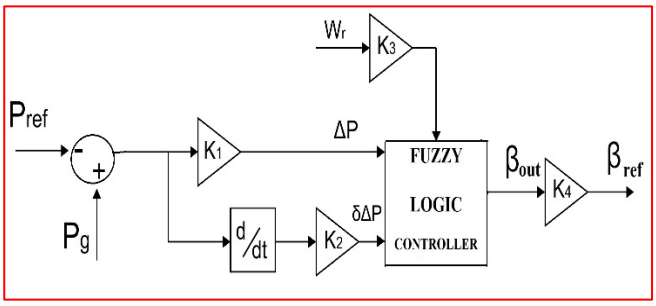

Figure 4. Block blade angle control diagram using fuzzy logic

3. SIMULATION RESULTS

In this section, to demostrate different performances of the controllers, two wind speeds with averages of 12 m/s and 16 m/s were used. The system parameters including turbine, generator, and network are given in Tables 2 and 3. The power coefficient of wind turbines depends on the wind speed and is not constant. In the simulation, the maximum value for Cp is 0.48. Fuzzy controller input and output adjustment constants are K_1=0.44×10-6, K_2=0.0035, K_3=0.006, and K_4=100.

The membership functions of the first fuzzy input (output power) in the range of [-1 – +1] are considered. Generator output power is in the MW limit and by multiplying it by K_1, it becomes the desired input for the fuzzy. The wind speed pattern, which has an average value of 12 meters per second as shown in Figure 5, is given below, including mechanical torque in Figure 6, output power in Figure 7, dc link voltage in Figure 8, reactive power in Figure 9, rotor speed in Figure 10, and angle blades in Figure 11. Rotor speed and reactive power are given in terms of pu. In case of sudden changes in the wind speed, its effects are seen on each of the system parameters. Two fuzzy and PI controllers were used to compare the results. Increase in active power input, rotor speed, and torque is well known in the fuzzy controller. Also,

reducing the DC link voltage fluctuations and the reactive transmission power are other advantages of this controller. All of these advantages result from the lower blade angle engagement.

Table 2. System and generator parameters

Component	Value
Nominal value of power	9×10^3 W
Network voltage	575 V
Network frequency	60 Hz
Voltage in infinite bus	120 KV
Magnetic inductance	3 pu
Resistance in stator	7×10^{-3} pu
Inductance in stator	17×10^{-2} pu
Number of poles	3
Moment of inertia	5.04
Maximum converter power	0.5 pu
Network side coupled indicator	0.15-0.0015 pu
Nominal voltage of dc bus	1.2×10^3 V
Capacitor in dc link	6×10^{-2} F
Network side control pins (Kp Ki)	1.25-300
Rotor side control pins [Kp Ki]	1-100
Line length	20×10^3 m

Table 3. Nominal parameters of the turbine

Component	Value
Power rate	9 MW
Wind speed rate	12 m/s
Maximum blade angle	45º
Maximum blade angle changes	2º/s
Wind cut-off speed	24 m/s

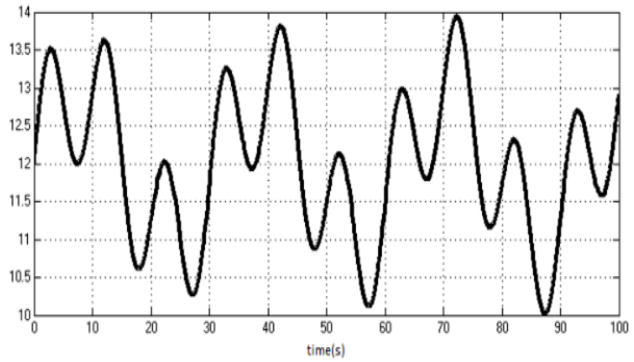

Figure 5. Display wind speed with an average value of 12 m/s

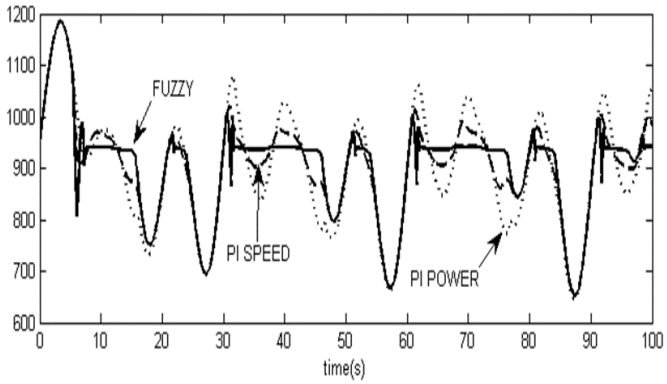

Figure 6. Mechanical torque (Nm) with an average value of 12 m/s

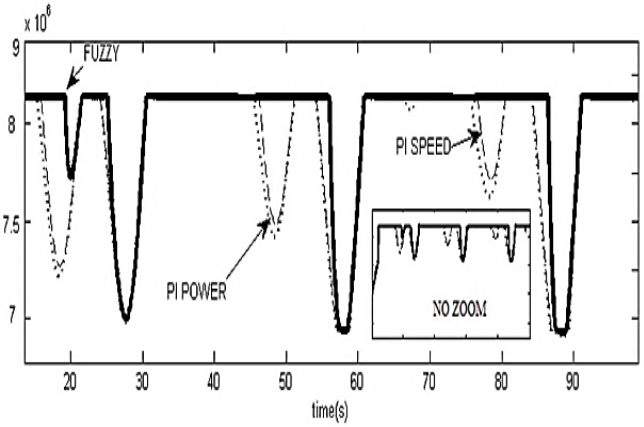

Figure 7. Output power (w) with an average value of 12 m/s

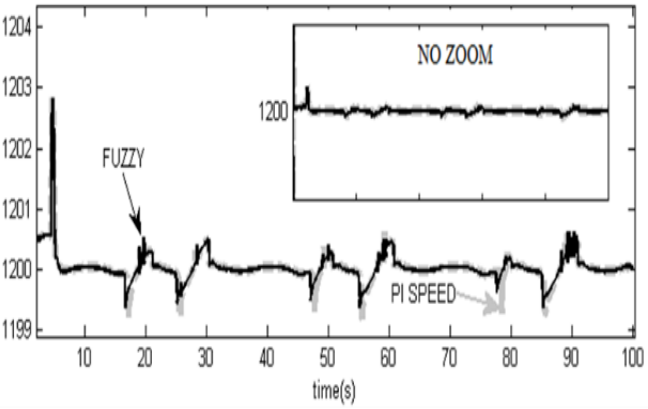

Figure 8. DC link voltage with an average value of 12 m/s

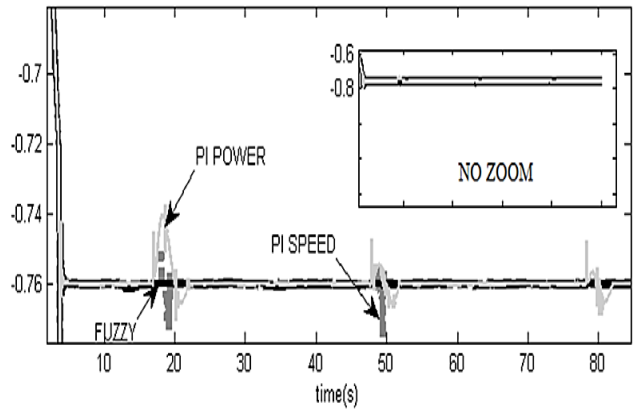

Figure 9. Reactive power with an average value of 12 m/s

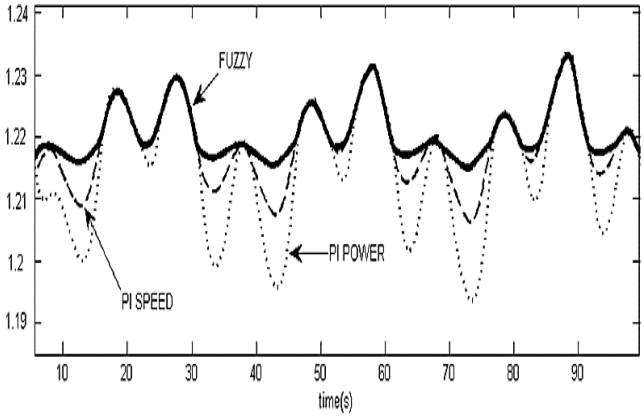

Figure 10. Rotor speed (pu) with an average value of 12 m/s

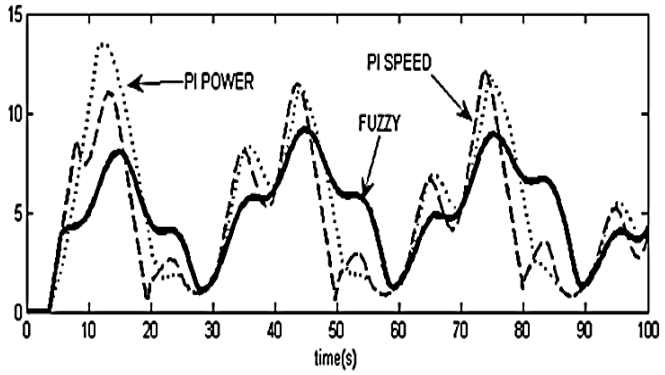

Figure 11. Pitch angle at an average value of 12 m/s with fuzzy and PI controllers

Next, the wind speed pattern with an average of 16 meters per second is given in Figure 12; in addition, simulation results for mechanical torque, transmission power, rotor speed, and pitch angle are shown in Figures 13, 14, 15, 13, respectively. The speed of the rotor is given in terms of prionite. In this wind speed pattern, PI power and speed controllers as well as fuzzy ones are used to compare the results better. The blade angle control is adjusted to increase wind power. This increase rate augments the mechanical torque and speed of the rotor. The fuzzy controller does not experience unnecessary fluctuations in the PI control of the blade angle. For this reason, it has increased the efficiency of the system. By changing the angle control gain, the superiority of the fuzzy controller over the PI is shown in Figures 14 and 15.

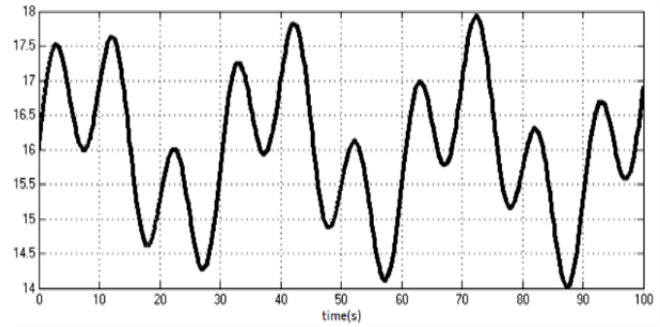

Figure 12. Display wind speed with an average value of 16 m/s

The application of an anemometer to have wind speed information increases costs and reduces system reliability. The use of fuzzy logic control to control the pitch angle is reliable and robust in terms of nonlinear pitch angle properties with wind speed. The advantages of fuzzy logic controllers over conventional controllers include the following: cheap development, coverage of a wide range of operating conditions, and easy customizability in terms of natural language.

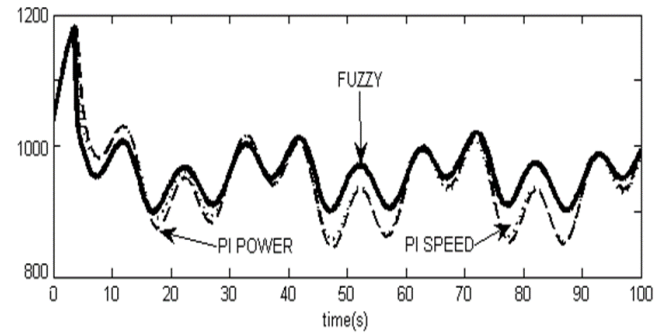

Figure 13. Mechanical torque (Nm) at an average value of 16 m/s

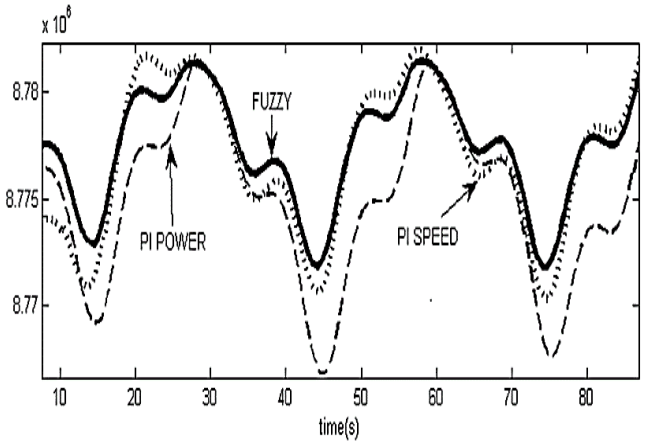

Figure 14. Zoom output power at an average value of 16 m/s

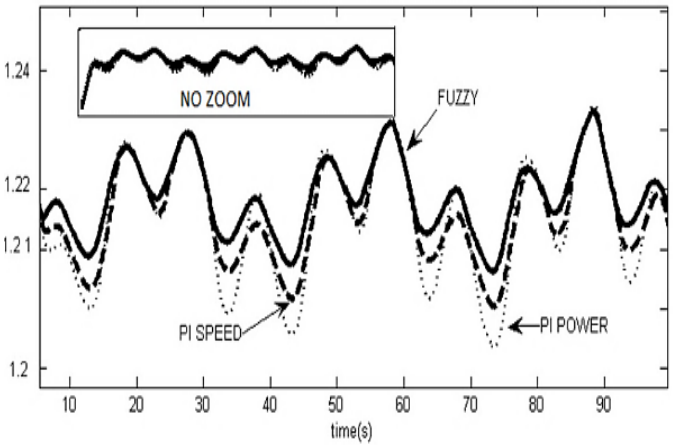

Figure 15. Rotor speed (pu) at an average value of 16 m/s

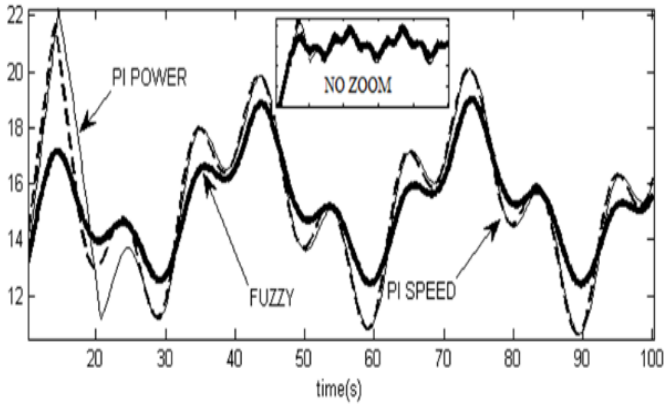

Figure 16. Pitch angle in wind speed with an average value of 16 m/s

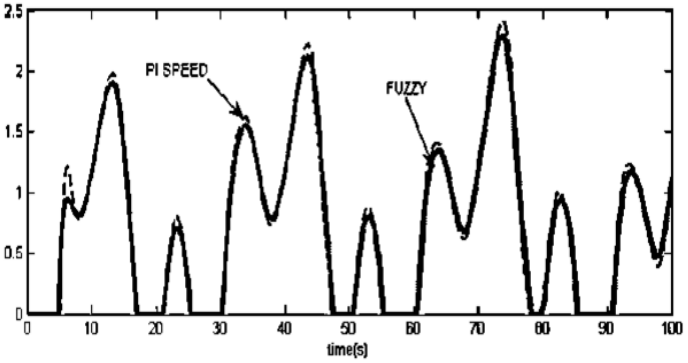

Figure 17. Pitch angle at an average value of 16 m/s withh fuzzy and PI controller

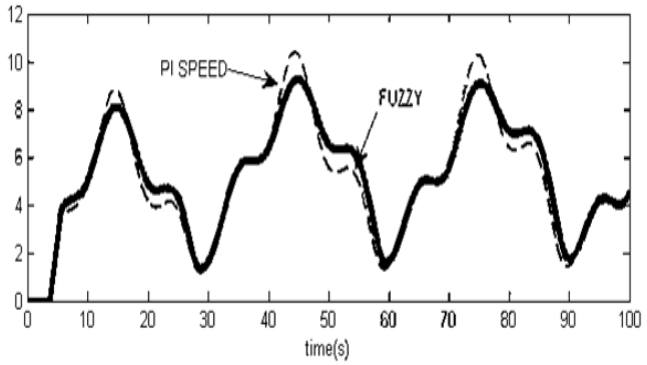

Figure 18. Pitch angle at an average value of 16 m/s with fuzzy and PI controllers

4. CONCLUSIONS

The aim of this paper is to model and simulate a DFIG-based wind turbine. An automatic controller based on fuzzy algorithm was designed for wind turbine and it was compared with traditional PI controllers. This controller enjoys independence from wind speed at the fuzzy input. The simulation results were obtained and demonstrated using MATLAB software Simulink. The superiority of the fuzzy controller in the simulation results was quite clear in case of sudden wind changes. Turbine power stability and reliable dynamic response resulted from the application of the proposed controller. By comparing various parameters, including the minimum values, and the ratio of harmonic distortions to the principal component, power quality was improved from 2.941 % to 4.762 % for the fuzzy controller, compared to the PI controller, at an average wind speed of 12 m/s. At a wind speed of 16 m/s, the quality improvement of 2 % to 45.5 % was observed for the fuzzy controller, compared to the PI controller.

5. ACKNOWLEDGEMENT

The authors would like to thank the editor, the journal's editors, the executive agents of the journal, and the judges for their suggestions that helped improve the quality of this article. This research was conducted at the Smart Microgrid Research Center, Najafabad Branch, Islamic Azad University, Najafabad, Isfahan, Iran. We thank the esteemed colleagues of the Research Center.

REFERENCES

1. Hashemi, M. and Shahgholian, G., "Distributed robust adaptive control of high order nonlinear multi agent systems", ***ISA Transactions***, Vol. 74, (2018), 14-27. (https://doi.org/10.1016/j.isatra.2018.01.023).
2. Jafari, E., Marjanian, A., Silaymani, S. and Shahgholian, G., "Designing an emotional intelligent controller for IPFC to improve the transient stability based on energy function", ***Journal of Electrical Engineering and Technology***, Vol. 8, No. 3, (2013), 478-489. (https://doi.org/10.5370/JEE¬T.2013.8.3.478).
3. Shahgholian, G., Arezoomand, M. and Mahmoodian, H., "Analysis and simulation of the single-machine infinite-bus with power system stabilizer and parameters variation effects", ***Proceedings of the IEEE/ICIAS***, Kuala Lumpur, Malaysia, Vol. 1, (2007), 167-171. (https://doi.org/10.1109/ICIAS.2007.4658368).
4. Khosravi, A., Malekan, M., Pabon, J.J.G., Zhao, X. and Assad, M.E.H., "Design parameter modelling of solar power tower system using adaptive neuro-fuzzy inference system optimized with a combination of genetic algorithm and teaching learning-based optimization algorithm", ***Journal of Cleaner Production***, Vol. 244, (2020), Article Number: 118904. (https://doi.org/10.1016/j.jclepro.2019.118904).
5. Aghadavoodi, E. and Shahgholian, G., "A new practical feed-forward cascade analyze for close loop identification of combustion control loop system through RANFIS and NARX", ***Applied Thermal Engineering***, Vol. 133, (2018), 381-395. (https://doi.org/10.1016/j.applthermaleng.2018.01.075).
6. Kiani, A., Fani, B. and Shahgholian, G., "A multi-agent solution to multi-thread protection of DG-dominated distribution networks", ***International Journal of Electrical Power and Energy Systems***, Vol. 130, (2021), Article Number: 106921. (https://doi.org/10.1016/j.ijepes.2021.106921).
7. Fani, B., Dadkhah, M. and Karami, A., "Adaptive protection coordination scheme against the staircase fault current waveforms in PV-dominated distribution systems", ***IET Generation, Transmission and Distribution***, Vol. 12, No. 9, (2018), 2065-2071. (https://doi.org/10.1049/iet-gtd.2017.0586).
8. Rahmani, M., Faghihi, F., Moradi-Cheshmeh-Beigi, M. and Hosseini, S., "Frequency control of islanded microgrids based on fuzzy cooperative and influence of STATCOM on frequency of microgrids", ***Journal of Renewable Energy and Environment (JREE)***, Vol. 5, No. 4, (2018), 27-33. (https://doi.org/10.30501/jree.2018.94119).
9. Ahmadi, S., Sadeghkhani, I., Shahgholian, G., Fani, B. and Guerrero, J.M., "Protection of LVDC microgrids in grid-connected and islanded modes using bifurcation theory", ***IEEE Journal of Emerging and Selected Topics in Power Electronics***, Vol. 9, (2019), 2597-2604. (https://doi.org/10.1109/JESTPE.2019.2961903).
10. Mahdavian, M. and Behzadfar, N., "A review of wind energy conversion system and application of various induction generators", ***Journal of Novel Researches on Electrical Power***, Vol. 8, No. 4, (2020), 55-66. (http://jeps.iaud.ac.ir/article-1-255-en.html).
11. AlShabi, M. and Assad, M.E.H., "Chapter 16- Artificial intelligence applications in renewable energy systems", ***Design and Performance Optimization of Renewable Energy Systems***, Vol. 1, (2021), 251-295. (https://doi.org/10.1016/B978-0-12-821602-6.00018-3).
12. Shahgholian, G., Khani, K. and Moazzami, M., "Frequency control in autanamous microgrid in the presence of DFIG based wind turbine", ***Journal of Intelligent Procedures in Electrical Technology***, Vol. 6, No. 21, (2015), 3-12. (https://dorl.net/dor/20.1001.1.23223871.1394.6.23.1.9).
13. Zou, J., Peng, C., Xu, H. and Yan, Y., "A fuzzy clustering algorithm-based dynamic equivalent modeling method for wind farm with DFIG", ***IEEE Transactions on Energy Conversion***, Vol. 30, No. 4, (2015), 1329-1337. (https://doi.org/10.1109/TEC.2015.2431258).
14. Sedaghat, A., Assad, M.E.H. and Gaith, M., "Aerodynamics performance of continuously variable speed horizontal axis wind turbine with optimal blades", ***Energy***, Vol. 77, (2014), 752-759. (https://doi.org/10.1016/j.energy.2014.09.048).
15. Sedaghat, A., Samani, I., Ahmadi-Baloutaki, M., Assad, M.E.H. and Gaith, M., "Computational study on novel circulating aerofoils for use in Magnus wind turbine blades", ***Energy***, Vol. 91, (2015), 393-403. (https://doi.org/10.1016/j.energy.2015.08.058).
16. Prasad, R. and Padhy, N.P., "Synergistic frequency regulation control mechanism for DFIG wind turbines with optimal pitch dynamics", ***IEEE Transactions on Power Systems***, Vol. 35, No. 4, (2020), 3181-3191. (https://doi.org/10.1109/TPWRS.2020.2967468).
17. Xiahou, K.S., Liu, Y., Li, M.S. and Wu, Q.H., "Sensor fault-tolerant control of DFIG based wind energy conversion systems", ***International Journal of Electrical Power and Energy Systems***, Vol. 117, (2020), Article 105563. (https://doi.org/10.1016/j.ijepes.2019.105563).
18. Fan, L., Kavasseri, R., Miao, Z.L. and Zhu, C., "Modeling of DFIG-based wind farms for SSR analysis", ***IEEE Transactions on Power Delivery***, Vol. 25, No. 4, (2010), 2073-2082. (https://doi.org/10.1109/TPWRD.2010.2050912).
19. Duong, M.Q., Grimaccia, F., Leva, S., Mussetta, M. and Ogliari, E., "Pitch angle control using hybrid controller for all operating regions of SCIG wind turbine system", ***Renewable Energy***, Vol. 70, (2014), 197-203. (https://doi.org/10.1016/j.renene.2014.03.072).
20. Naik, K.A., Gupta, C.P. and Fernandez, E., "Design and implementation of interval type-2 fuzzy logic-PI based adaptive controller for DFIG based wind energy system", ***International Journal of Electrical Power and Energy Systems***, Vol. 115, (2020), Article 105468. (https://doi.org/10.1016/j.ijepes.2019.105468).
21. Hossain, M.J., Pota, H.R. nad Ramos, R.A., "Improved low-voltage-ride-through capability of fixedspeed wind turbines using decentralised control of STATCOM with energy storage system", ***IET Generation,***

Transmission and Distribution, Vol. 6, No. 8, (2012), 719-730. (https://doi.org/10.1049/iet-gtd.2011.0537).

22. Merabet, A., Beguenane, R., Thongam, J.S. and Hussein, I., "Adaptive sliding mode speed control for wind turbine systems", ***Proceedings of the IEEE/IECON***, (2011), 2461-2466. (https://doi.org/10.1109/I-ECON.2011.6119696).
23. Hyun, S.H. and Wang, J., "Pitch angle control and wind speed prediction method using inverse input-output relation of a wind generation system", ***Journal of Electrical Engineering and Technology***, Vol. 8, No. 5, (2013), 1040-1048. (https://doi.org/10.5370/JEET.2013.8.5.1040).
24. Van, T.L., Nguyen, T.H. and Lee, D.C., "Advanced pitch angle control based on fuzzy logic for variable-speed wind turbine systems", ***IEEE Transactions on Energy Conversion***, Vol. 30, No. 2, (2015), 578-587. (https://doi.org/10.1109/TEC.2014.2379293).
25. Hosseini, E. and Shahgholian, G., "Different types of pitch angle control strategies used in wind turbine system applications", ***Journal of Renewable Energy and Environment (JREE)***, Vol. 4, No. 1, (2017), 20-35. (http://dx.doi.org/10.30501/jree.2017.70103).
26. Abidoye, L.K, Bani-Hani, E., Assad, M.E.H., AlShabi, M., Soudan, B. and Oriaje, A.T., "Effects of environmental and turbine parameters on energy gains from wind farm system: Artificial neural network simulations", ***Wind Engineering***, Vol. 44, No. 2, (2020), 181-195. (https://doi.org/10.1177/0309524X19849834).
27. Van, T.L., Dang, N.K., Doan, X.N., Truong, T.H. and Minh, H.N., "Adaptive fuzzy logic control to enhance pitch angle controller for variable-speed wind turbines", ***Proceedings of the 10th International Conference on Knowledge and Systems Engineering (KSE)***, Ho Chi Minh City, Vietnam, (2018), 225-229. (https://doi.org/10.1109/KSE.2018.8573332).
28. Hosseini, E. and Shahgholian, G., "Partial- or full-power production in WECS: A survey of control and structural strategies", ***European Power Electronics and Drives***, Vol. 27, No. 3, (2017), 125-142. (https://doi.org/10.1080/09398368.2017.1413161).
29. Wu, F., Zhang, X.P., Godfrey, K. and Ju, P., "Small signal stability analysis and optimal control of a wind turbine with doubly fed induction generator", ***IET Generation, Transmission and Distribution***, Vol. 1, No. 5, (2007), 751-760. (https://doi.org/10.1049/iet-gtd:20060395).
30. Yang, L., Xu, Z., Ostergaard, J. and Dong, Z.Y., "Advanced control strategy of DFIG wind turbines for power system fault ride through", ***IEEE Transactions on Power Systems***, Vol. 27, No. 2, (2012), 713-722. (https://doi.org/10.1109/TPWRS.2011.2174387).
31. Yang, L., Xu, Z., Ostergaard, I. and Dong, Z.Y., "Oscillatory stability and eigenvalue sensitivity analysis of a DFIG wind turbine system", ***IEEE Transactions on Energy Conversion***, Vol. 26, No. 1, (2011), 328-339. (https://doi.org/10.1109/TEC.2010.2091130).
32. Shaker, M.S. and Patton, R.J., "Active sensor fault tolerant output feedback tracking control for wind turbine systems via T–S model", ***Engineering Applications of Artificial Intelligence***, Vol. 34, (2014), 1-12. (https://doi.org/10.1016/j.engappai.2014.04.005).
33. Lin, W.M. and Hong, C.M., "Intelligent approach to maximum power point tracking control strategy for variable-speed wind turbine generation", ***Energy***, Vol. 35, No. 6, (2010), 2440-2447. (https://doi.org/10.1016/j.energy.2010.02.033).
34. Lin, W.M., Hong, C.M., Ou, T.C. and Chiu, T.M., "Hybrid intelligent control of PMSG wind generation system using pitch angle control with RBFN", ***Energy Conversion and Management***, Vol. 52, No. 2, (2011), 1244-1251. (https://doi.org/10.1016/j.enconman.2010.09.020).
35. Linus, R.M. and Damodharan, P., "Maximum power point tracking method using a modified perturb and observe algorithm for grid connected wind energy conversion systems", ***IET Renewable Power Generation***, Vol. 9, No. 6, (2015), 682-689. (https://doi.org/10.1049/iet-rpg.2014.0070).
36. Bhukya, J. and Mahajan, V., "Optimization of damping controller for PSS and SSSC to improve stability of interconnected system with DFIG based wind farm", ***International Journal of Electrical Power and Energy Systems***, Vol. 108, (2019), 314-335. (https://doi.org/10.1016/j.ijepes.2019.01.017).
37. Duong, M.Q., Grimaccia, F., Leva, S., Mussetta, M. and Ogliari, E., "Pitch angle control using hybrid controller for all operating regions of SCIG wind turbine system", ***Renewable Energy***, Vol. 70, (2014), 197-203. (https://doi.org/10.1016/j.renene.2014.03.072).
38. Hyams, M.A., 20- Wind energy in the built environment, Metropolitan sustainability: Understanding and improving the urban environment, Woodhead Publishing Series in Energy, (2012), 457-499. (https://doi.org/10.1533/9780857096463.3.457).
39. Lampinen, M.J., Kotiaho, V.W. and Assad, M.E.H., "Application of axial fan theory to horizontal-axis wind turbine", ***International Journal of Energy Research***, Vol. 30, No. 13, (2006), 1093-1107. (https://doi.org/10.1002/er.1208).
40. Shahgholian, G., "Analysis and simulation of dynamic performance for DFIG-based wind farm connected to a distrubition system", ***Energy Equipment and Systems***, Vol. 6, No. 2, (2018), 117-130. (https://doi.org/10.22059/ees.2018.31531).
41. Jafari, A. and Shahgholian, G., "Analysis and simulation of a sliding mode controller for mechanical part of a doubly-fed induction generator based wind turbine", ***IET Generation, Transmission and Distribution***, Vol. 11, No. 10, (2017), 2677-2688. (https://doi.org/10.1049/iet-gtd.2016.1969).
42. Mahvash, H., Taher, S.A. and Rahimi, M., "A new approach for power quality improvement of DFIG based wind farms connected to weak utility grid", ***Ain Shams Engineering Journal***, Vol. 8, No. 3, (2017), 415-430. (https://doi.org/10.1016/j.asej.2015.09.001).
43. Samanes, J., Gubia, E., Lopez, J. and Burgos, R., "Sub-synchronous resonance damping control strategy for DFIG wind turbines", ***IEEE Access***, Vol. 8, (2020), 223359-223372. (https://doi.org/10.1109/ACCESS.2020.3043818).
44. Shahgholian, G., Maghsoodi, M. and Movahedi, A., "Fuzzy proportional integral controller design for thyristor controlled series capcitor and power system stabilizer to improve power system stability", ***Revue Roumaine Des Sciences Techniques***, Vol. 61, No. 4, (2016), 418-423. (http://revue.elth.pub.ro/index.php?action=details&id=627).
45. Shahgholian, G., Maghsoodi, M., Mahdavian, M., Janghorbani, M,. Azadeh, M., and Farazpey, S., "Analysis of speed control in DC motor drive by using fuzzy control based on model reference adaptive control", ***Proceedings of the 13th International Conference on Electrical Engineering/Electronics, Computer, Telecommunications and Information Technology (ECTI-CON)***, Chiang Mai, Thailand, (2016). (https://doi.org/10.1109/ECTICon.2016.7561239).
46. Ouyang, J., Tang, T., Yao, J. and Li, M., "Active voltage control for DFIG-based wind farm integrated power system by coordinating active and reactive powers under wind speed variations", ***IEEE Transactions on Energy Conversion***, Vol. 34, No. 3, (2019), 1504-1511. (https://doi.org/10.1109/TEC.2019.2905673).
47. Fooladgar, M., Rok-Rok, E., Fani, B. and Shahgholian, G., "Evaluation of the trajectory sensitivity analysis of the DFIG control parameters in response to changes in wind speed and the line impedance connection to the grid DFIG", ***Journal of Intelligent Procedures in Electrical Technology***, Vol. 5, No. 20, (2015), 37-54. (In Farsi). (http://jipet.iaun.ac.ir/index.php/images/article_555948.html?lang=en).
48. Hosseini, E. and Shahgholian, G., "Output power levelling for DFIG wind turbine system using intelligent pitch angle control", ***Automatika***, Vol. 58, No. 4, (2017), 363-374. (https://doi.org/10.1080/00051144.2018.1455017).
49. Sharmila, V., Rakkiyappan, R. and Joo, Y.H., "Fuzzy sampled-data control for dfig-based wind turbine with stochastic actuator failures", ***IEEE Transactions on Systems, Man, and Cybernetics: Systems***, Vol. 51, No. 4, (2021), 2199-2211. (https://doi.org/10.1109/TSMC.2019.2946873).

Journal of Renewable Energy and Environment

Journal Homepage: www.jree.ir

Materials and Energy Research Center

MERC

Research Article

Environmental and Economic Sustainability Assessment of Rainfed Agro-Systems in Northern Iran

Alireza Taheri-Rad, Abbas Rohani *, Mehdi Khojastehpour

Department of Biosystems Engineering, Ferdowsi University of Mashhad, P. O. Box: 91779-48974, Mashhad, Khorasan Razavi, Iran.

PAPER INFO

Paper history:
Received: 26 May 2021
Revised in revised form: 25 November 2021
Scientific Accepted: 11 October 2021
Published: 29 January 2022

Keywords:
Barley,
Canola,
Eco-Efficiency,
Triticale,
Wheat

ABSTRACT

Environmental and economic aspects are two remarkable pillars toward a sustainable agro-system. Accordingly, this study aimed to assess the sustainability of autumn rainfed agro-systems in northern Iran by the Eco-Efficiency (EF) indicator. The data of the production processes of wheat, barley, canola, and triticale were collected in the three crop years of 2016-2019. Results indicated that the canola production system with 720 $kgCO_{2eq}$ ha^{-1} had the highest greenhouse gas (GHG) emissions; however, wheat with 604 $kgCO_{2eq}$ ha^{-1} was attributed to the lowest GHG emissions. The results of the economic analysis also highlighted that the barley production system had the lowest while the canola production system had the highest production costs. The canola production system had the highest profitability, while the barley production system had the lowest in terms of net income and average benefit to cost ratio indicators. The EF indicator for wheat, barley, canola, and triticale was determined to be 1.4, 0.6, 1.8, and 1.1, respectively, indicating the highest EF value for the canola production system.

https://doi.org/10.30501/jree.2021.287947.1212

1. INTRODUCTION

The agricultural sector is the largest economic sector in the world and its growth and development are of great importance not only from an economic viewpoint but also in various social and environmental dimensions. In this regard, the analysis of agricultural systems can have a significant role in reducing the destructive impacts on the environment and, thus, achieving sustainable agriculture [1]. Today, the growing trend of GHG emissions arising from burning fossil fuels has led to greater attention to reduction of energy consumption in various fields [2]. Therefore, considering environmental issues has become one of the main components in global planning and the most critical factor in and prerequisite for many activities in the world [3, 4]. In addition to environmental issues, increasing economic productivity is also essential to achieving greater profits. In this regard, paying attention to the profitability of production in line with environmental issues leads the EF indicator to be defined. The EF with the definition of "The ratio of product value to environmental issues" is considered a useful tool for improving economic and environmental sustainability simultaneously [5]. The EF includes strategies that both increase the efficiency of energy consumption and reduce the production costs [6]. In this regard, using the indicator can be a proper criterion to investigate the sustainability of agricultural production [7, 8].

*Corresponding Author's Email: arohani@um.ac.ir (A. Rohani)
URL: https://www.jree.ir/article_143969.html

Due to the climatic conditions of Iran, about 75 % of agricultural lands (11 million hectares) are rainfed. Mazandaran province in northern Iran, having 83,000 hectares of rainfed farms, is known as one of the major production regions of rainfed crops. The most important rainfed crops in the province include wheat, barley, canola, triticale, soybeans, and vegetables and the four autumn crops, i.e., wheat, barley, canola, and triticale with a total area of 71,000 hectares, have the highest area among rainfed crops in the province [9]. Given the importance of producing rainfed crops to increase income and meet food needs, improving these production systems can be essential. In other words, the growing trend of consuming energy and chemical inputs per unit area in recent years has increased the amount of pollutants emitted to the environment in the agro-systems. Since optimal input consumption is a primary aim in the development of sustainable agriculture, it is vital to consider the consumption of input energies in agricultural production processes [10]. Therefore, various studies have been conducted recently to examine agricultural inputs and production costs of various crops in Iran and the world. An economic and environmental study of a wheat production system in western Iran claimed that net income and benefit to cost ratio were 488 \$ ha^{-1} and 2.33, respectively. Moreover, the highest GHG emissions belonged to electricity and nitrogen fertilizer [11]. The economic analysis of wheat production in Turkey claimed that the benefit to cost ratio was 1.2 and agricultural machinery and chemical fertilizers attended to the highest contribution to variable costs [12]. The study of canola production in

Please cite this article as: Taheri-Rad, A.R., Rohani, A. and Khojastehpour, M., "Environmental and economic sustainability assessment of rainfed agro-systems in northern Iran", ***Journal of Renewable Energy and Environment (JREE)***, Vol. 9, No. 2, (2022), 8-17. (https://doi.org/10.30501/jree.2021.287947.1212).

Golestan province approved that the chemical fertilizers and diesel fuel had the highest contributions to GHG emissions with 51.23 % and 30.16 %, respectively [13]. Another study on wheat, barley, canola, soybean, paddy, and corn silage crops in northern Iran pointed out that three crops of canola, barley, and wheat had the lowest GHG emissions with 1,064, 1,106, and 1,171 $kgCO_{2eq}$ ha^{-1}, respectively, and paddy with 6,094 $kgCO_{2eq}$ ha^{-1} had the highest GHG emissions [14].

Various studies have also focused on evaluating the EF value in agricultural production. For instance, the results of a study on the EF value of paddy production in Thailand indicated that under equal income conditions, GHG emissions in the rainfed system were lower than that in the irrigated system [15]. In another research in Italy, the results of a study on the EF value of rapeseed and sunflower production highlighted that the EF value of rapeseed production was lower than sunflower. The results also revealed that sunflower production was more environmentally friendly than rapeseed [16]. It was also stated that in wheat production in Japan, nitrogen fertilizer was the main contributor to increasing the EF value and, thus, to sustainable development of wheat production [17]. In another study, an assessment of the EF value of tangerine production in northern Iran showed that the net income was 2.18 \$ $kgCO_{2eq}^{-1}$. It was also stated that chemical fertilizers had the highest contribution to both environmental and economic sustainability of tangerine production [18].

This study aimed to investigate the sustainability of autumn rainfed agro-systems in northern Iran using the Eco-Efficiency (EF) indicator. This indicator has recently become a key tool for assessing different agricultural systems in Iran and across the world, due to its potential ability to quantify and integrate two major pillars of sustainable development, i.e., economic and environmental aspects. This point can lead to providing a powerful tool for investigating and comparing various crops in terms of how it is possible to make a balance between economic outputs and environmental effects of an agricultural system. However, according to the literature review, no research has been done so far on the sustainability of autumn rainfed agro-systems from environmental and economic points of view. Therefore, although different evaluation indices can be considered to estimate the EF of a crop production system, this study followed the procedure proposed by previous studies as in [18] due to the availability and simplicity of data collection. Besides, unlike other studies, three-year classified data have been used in this research, allowing for the investigation of the inputs flows over the time. Therefore, the main objectives of this research were to do (i) economic analysis and determine the economic indicators in the production of autumn rainfed crops including wheat, barley, canola, and triticale, (ii) conduct environmental analysis of autumn rainfed crops production, and finally (iii) compare the EF values of these crops to investigate the overall sustainability of the production systems.

2. METHOD

2.1. Data collection and study area

The study area was Mazandaran province located in northern Iran. Dasht-E Naz Sari Agricultural Company is of the main agricultural companies in northern Iran, which is located in Mazandaran with an area under cultivation of about 3,900 hectares. Irrigated and rainfed systems are being used for crop production in this company. Given the large area under cultivation of autumn rainfed crops in this company and also access to accurate data about using inputs, this company was selected to be the study area. Since the main rainfed systems of this company are located in Galugah County in this province, this region was selected as the study area. The mean values of some climatic parameters of Galugah County during 2006-2020 are shown in Table 1. Four major rainfed crops in this region, i.e., wheat, barley, canola, and triticale, were investigated during three crops years from 2017 to 2019. The total areas occupied by the four crops were 800, 770, and 685 ha in these three years, respectively, in the study area. In this company, the crops are cultivated in several smaller fields with different sizes. Accordingly, the required data were collected from all fields in each year and the average consumption of inputs was expressed per hectare (Table 2).

Table 1. Climatic conditions of Galugah, on average

Daily temperature (°C)	Annual precipitation (mm)	Total rainy days (day)	Total sunny hours (h)	Air relative humidity (%)	Annual evaporation (mm)
17.7	617	91	1962	75	1148

Table 2. Consumed inputs in wheat, barley, canola, and triticale production systems per unit area

Variables	Wheat (Unit ha^{-1})				Barley (Unit ha^{-1})		
	1st year (2016-2017)	2nd year (2017-2018)	3rd year (2018-2019)		1st year (2016-2017)	2nd year (2017-2018)	3rd year (2018-2019)
Machinery (h)	7.32	6.51	6.15		7.89	8.99	7.78
Diesel fuel (l)	94.08	92.40	98.54		88.42	107.10	98.00
Biocides (kg)	3.72	2.88	3.92		2.5	5.78	6.18
Chemical fertilizers (kg)	291.80	382.83	275.70		319.30	343.75	203.06
Manure (kg)	5040.00	5016.00	5038.50		4970.00	5000.00	5277.00
Seed (kg)	259.44	261.73	252.12		200.7	196.74	240.22
Human labor (h)	7.20	6.44	7.88		7.16	9.39	7.22
Output (kg)	2786.88	4057.73	3586.35		1587.34	3707.55	2164.11
Total area (ha)	250	300	260		342	200	180
	Canola (Unit ha^{-1})				Triticale (Unit ha^{-1})		
Machinery (h)	9.89	9.52	8.76		6.78	5.58	6.17
Diesel fuel (l)	121.33	120.40	118.05		106.78	104.30	100.80

Biocides (kg)	4.35	3.26	7.81		3.00	5.06	6.14
Chemical fertilizers (kg)	610.56	623.33	478.51		356.36	275.42	426.67
Manure (kg)	5000.00	4933.00	4865.00		5085.00	5000.00	5000.00
Seed (kg)	7.44	7.57	5.54		205.00	250.25	231.50
Human labor (h)	12.22	13.82	12.43		6.78	7.30	6.67
Output (kg)	2299.89	2754.67	2525.89		3065.59	3382.83	4168.00
Total area (ha)	90	150	185		118	120	60

2.2. GHG emissions analysis

The GHG emissions of the investigated systems were estimated by multiplying the value of inputs consumed in each system by its emission coefficient (Table 3). The investigated inputs were diesel fuel, manure, agricultural machinery, chemical fertilizers, and biocides.

Table 3. GHG emission coefficient of consumed inputs

Inputs	Unit	GHG emissions coefficient ($kgCO_{2eq}$)	Reference
Agricultural machinery	MJ	0.071	[19]
Diesel fuel	L	2.76	[20]
Biocides			
(a) Herbicides	kg	6.3	[21]
(b) Pesticides	kg	5.1	[21]
(c) Fungicides	kg	3.9	[21]
Chemical fertilizers			
(a) Nitrogen	kg	0.09	[22]
(b) Phosphate	kg	0.15	[22]
(c) Potassium	kg	0.51	[22]
Manure	kg	0.0462	[23]

The GHG emission (G_M) of agricultural machines was estimated in terms of the energy value of this input (Eq. 1). Accordingly, G_M can be obtained from the machine working hours (H_M) and the energy equivalent coefficient of machines (0.62 MJ h^{-1}) [24] and GHG emission coefficient (C_M) are presented in Table 2. The GHG emissions of other inputs were determined using Eq. 2. In this equation, G_I and C_I donate the values and coefficients of GHG emissions, respectively, and W refers to the inputs used in the production process. W_I included electricity (kWh), diesel fuel (L), and chemical fertilizers (kg), biocides (kg), and manure (kg) [25]. Various biocides and chemical fertilizers used in the production process can be attended at different energy levels. Therefore, to obtain GHG emissions from the inputs, biocides were divided into three sub-groups, i.e., herbicides, fungicides, and insecticides. Similarly, chemical fertilizers were divided into three sub-groups of nitrogen, phosphorus, and potash [21].

$$G_M = 0.62 \times H_M \times C_M \quad (1)$$

$$G_I = W_I \times C_I \quad (2)$$

2.3. Economic analysis

The economic analysis of autumn rainfed agro-systems in Mazandaran province was conducted based on the amount of consumed inputs for each crop (wheat, barley, canola, and triticale). The total production costs and the total production value for each crop were computed per unit area. The economic indicators, i.e., gross income, net income, benefit to cost ratio, and economic productivity associated with each crop were estimated (Eqs. (3) to (6)) and compared [26-28].

$$\text{Gross income} = \text{Total production value} \left(\$\ ha^{-1}\right) - \text{Variable costs} \left(\$\ ha^{-1}\right) \quad (3)$$

$$\text{Net income} = \text{Total production value} \left(\$\ ha^{-1}\right) - \text{Total production cost} \left(\$\ ha^{-1}\right) \quad (4)$$

$$\text{Benefit to cost ratio} = \frac{\text{Total production value} \left(\$\ ha^{-1}\right)}{\text{Total production cost} \left(\$\ ha^{-1}\right)} \quad (5)$$

$$\text{Economic productivity} = \frac{\text{Yield} \left(kg\ ha^{-1}\right)}{\text{Total production cost} \left(\$\ ha^{-1}\right)} \quad (6)$$

2.4. EF indicator

The EF is the main indicator for improving both economic and environmental sustainability in agricultural production. In this study, the EF value was determined for investigated agro-systems. The indicator is calculated by dividing the economic output indicator (I_{eco}) to the environmental impact indicator (I_{env}) [29] (Eq. 7). In this regard, economic output and environmental impact indicators were considered to be the net income and GHG emissions in the production process of each crop per unit area, respectively.

$$EF = \frac{I_{eco}}{I_{env}} \quad (7)$$

3. RESULTS AND DISCUSSION

3.1. GHG emission analysis

Table 4 presents the average inputs consumption and the average GHG emissions from investigated agro-systems in Mazandaran province. The average yield of wheat, barley, canola, and triticale was 3,476.99, 2,486.33, 2,526.82, and 3,538.81, respectively, which was remarkably higher than the average yield of these crops in Iran [9]. The total GHG emissions derived from producing wheat, barley, canola, and triticale were found to be 604.34, 619.94, 720.38, and 628.62 $kgCO_{2eq}$ ha^{-1}, respectively, among which canola had the highest GHG emissions, while wheat had the lowest GHG emissions. It can be due to the difference in the amounts of inputs consumption in the investigated agro-systems. Accordingly, results exhibit that chemical fertilizers, particularly nitrogen fertilizers, were the main reason of the higher value of GHG emissions in the canola agro-system. Similar findings were reported in previous studies [13, 30, 31], where the highest GHG emissions of canola production belonged to the chemical fertilizers. The higher consumption of chemical fertilizers in canola production can be associated with higher nutritional needs of the crop. A study on how nitrogen fertilizer can affect seed yield of wheat and canola approved that at a given level of N-fertilizer, the yield of wheat was significantly higher than canola [32]. Another

study also claimed that for producing 90 % of the maximum yield, N and k-fertilizer requirements of canola were 26 % and 32 % higher than those of wheat, respectively [33]. However, the excessive use of chemical fertilizers can be managed by replacing bio-sources of nutrition such as crop residues, or manure, as well as applying the optimal level of fertilizers based on the local conditions [34-38]. Gao et al. reported that at similar N levels, manure application sometimes led to greater production of oil content in canola than fertilizers [39]. The contribution of the consumed inputs to GHG emissions is presented in Figure 1. The diesel fuel input was attended to the highest GHG emission rate in four investigated agro-systems, and the highest and lowest GHG emission rates from this input belonged to the canola production process with 331.00 $kgCO_{2eq}$ ha^{-1} and 46 % and wheat production with 262.22 $kgCO_{2eq}$ ha^{-1} and 22.4 %, respectively. The manure input was the second greatest contributor to GHG emissions in all investigated agro-systems. The input had the highest GHG emissions with 234.83 $kgCO_{2eq}$ ha^{-1} in the barley production, while the canola production with 227.89 $kgCO_{2eq}$ ha^{-1} had the lowest emission. According to Figure 1, the two inputs of diesel fuel and manure contributed to 77.6 % to 82.6 % of total GHG emissions, in producing autumn rainfed crops in Mazandaran province. The manure input had a high consumption in autumn rainfed agro-systems in this region, such that, according to Table 2, the average consumption of this input in all investigated agro-systems was about 5,000 kg ha^{-1}. Chemical fertilizers ranked third in GHG emissions in all studied agro-systems. The GHG emission from this input in canola production with 89.77 $kgCO_{2eq}$ ha^{-1} and 12.4 % was the highest and in barley production, with 52.80 $kgCO_{2eq}$ ha^{-1} and 8.5 % was the lowest. In this province, farmers use a combination of manure and chemical fertilizers to feed farms. Therefore, the consumption of chemical fertilizers in the production of rainfed crops in this region was much lower than that in similar studies [11, 40]. Other studies have reported that the simultaneous use of manure and chemical fertilizers can result in a significant reduction in chemical fertilizers consumption [41, 42]. The GHG emissions of the two inputs of agricultural machinery and biocides also were the lowest in the studied agro-systems. According to Table 4, the GHG emissions from consuming these inputs in the canola production were the highest and in the production of triticale and wheat were the lowest. Overall, the results indicated that canola had the highest GHG emissions, while wheat had the lowest GHG emissions among studied crops. Therefore, the GHG emissions from all inputs consumption except manure for canola were higher than those for other investigated agro-systems.

Table 4. Consumed inputs and GHG emissions of autumn rainfed agro-systems

Variables	Consumed inputs (Unit ha^{-1})					GHG emissions ($kgCO_{2eq}$ ha^{-1})			
	Wheat	Barley	Canola	Triticale		Wheat	Barley	Canola	Triticale
Inputs									
Machinery (MJ)	6.66	8.22	9.39	6.18		29.66	36.60	41.80	27.50
Diesel fuel (kg)	95.01	97.84	119.93	103.96		262.22	270.04	331.00	286.93
Biocides (kg)	3.51	4.82	5.14	4.73		19.16	25.68	29.92	25.08
(a) Herbicides	1.94	2.48	3.88	2.37		12.12	15.63	24.42	14.92
(b) Insecticides	0.69	0.78	0.48	0.78		3.51	3.96	2.44	3.99
(c) Fungicides	0.88	1.56	0.78	1.58		3.43	6.09	3.06	6.18
Chemical fertilizers (kg)	316.78	288.70	570.80	352.81		60.84	52.80	89.77	56.81
(a) Nitrogen	169.54	165.77	402.63	215.30		15.26	14.92	36.24	19.38
(b) Phosphorous	81.98	68.94	89.55	90.84		12.30	10.34	13.43	13.63
(c) Potassium	65.26	54.00	78.62	46.67		33.28	27.54	40.10	23.80
Manure (kg)	5031.71	5082.85	4932.73	5028.25		232.46	234.83	227.89	232.31
Seed (kg)	257.76	212.35	6.85	228.92		-	-	-	-
Human labor (h)	7.17	7.92	12.82	6.92		-	-	-	-
Total GHG emissions	-	-	-	-		604.34	619.94	720.38	628.62
Output									
Yield (kg)	3476.99	2486.33	2526.82	3538.81		-	-	-	-

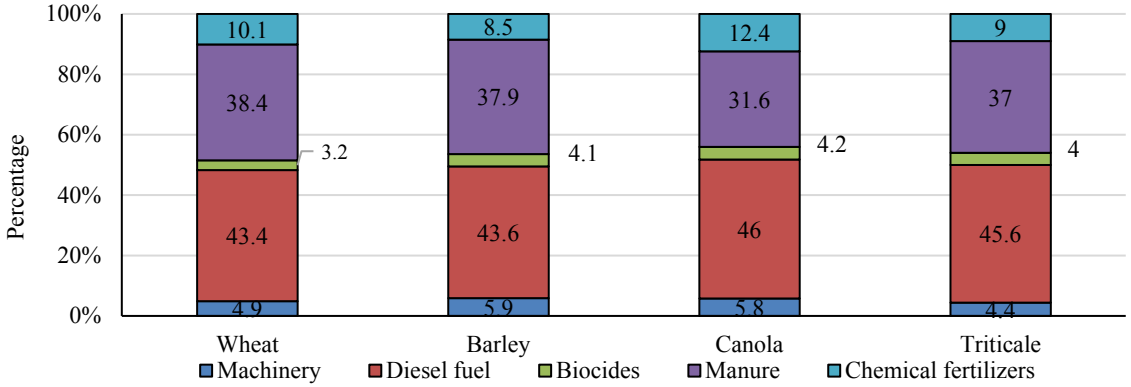

Figure 1. Share of GHG emissions of consumed inputs in wheat, barley, canola, and triticale productions

The GHG emissions from autumn rainfed agro-systems were also investigated in terms of crop years (Figure 2). The results for wheat production revealed that although the total GHG emissions varied over three years, the differences were not significant. According to Figure 2(a), the emissions from all inputs were equal every three years, and only the input of chemical fertilizers in the second year had a higher GHG emission rate than in other years. The results of the study of barley production claimed that the total GHG emissions of the second year (666.2 $kgCO_{2eq}$ ha^{-1}) were estimated significantly higher than in the other two years. According to Figure 2(b) in the second year, GHG emissions of diesel fuel, chemical fertilizers, and agricultural machinery inputs were higher than in the other years. Figure 2(c) depicts the results of studying the canola production, where although the GHG emissions of diesel fuel, manure, and agricultural machinery in the first year were greater than the other years and the total GHG emission in the third year (740.6 $kgCO_{2eq}$ ha^{-1}) was obtained to be more than that in other years. The difference can be associated with the higher GHG emissions of biocides and chemical fertilizers in the third crop year. However, overall, the difference in GHG emissions was not significant in different years. The results of studying the triticale production (Figure 2(d)) also highlighted that although the total GHG emissions were higher in the third year, this difference was not significant. The difference can be associated with the higher GHG emissions of biocides and chemical fertilizers in the third crop year.

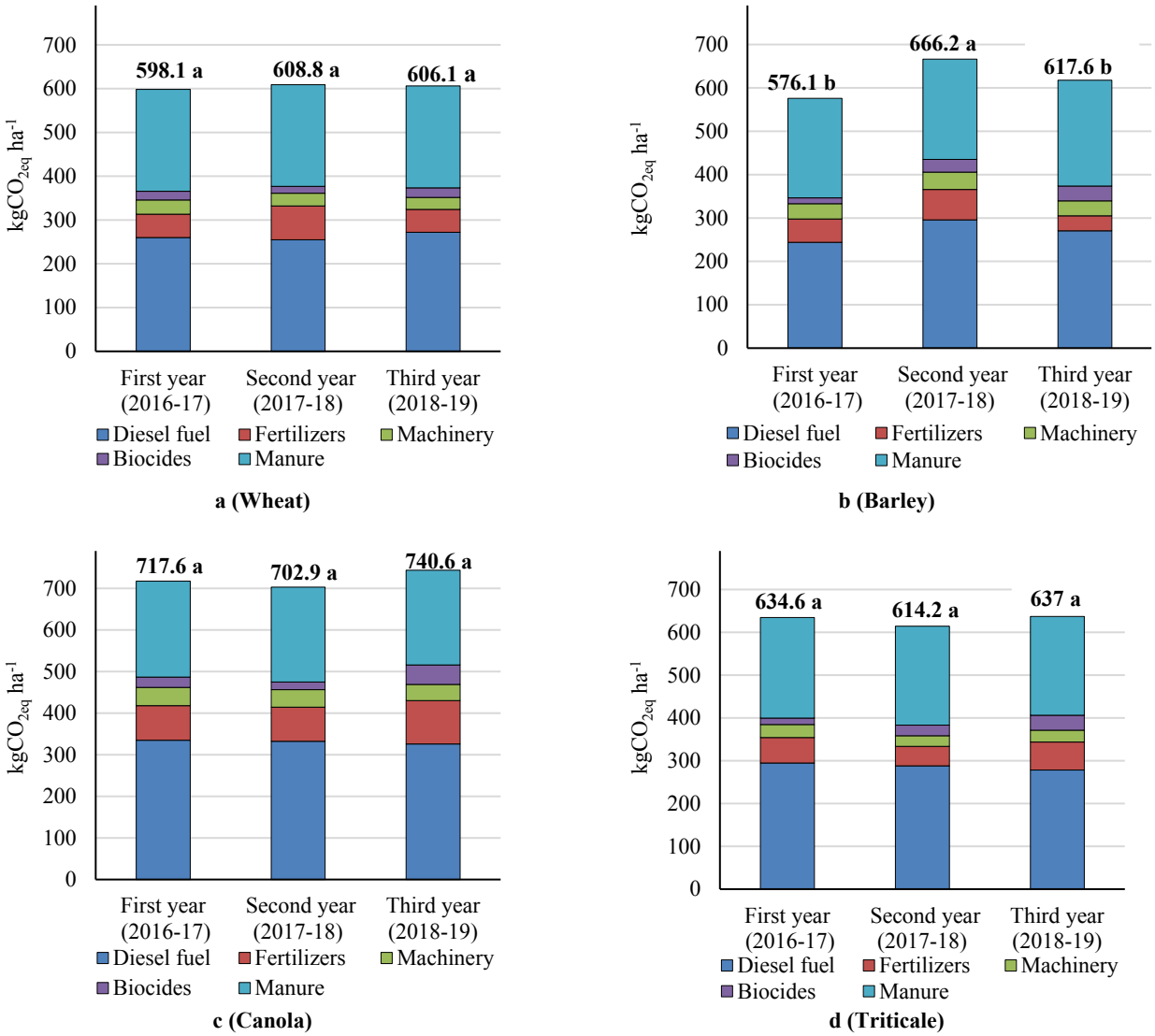

Figure 2. The GHG emissions of consumed inputs in (a) wheat, (b) barley, (c) canola, and (d) triticale production during three crop years (2016-2019) in Mazandaran province

3.2. Economic analysis

Table 5 presents the economic indicators and production costs of autumn rainfed crops in Mazandaran province. The total production costs for wheat, barley, canola, and triticale were 623.20, 596.81, 671.41, and 597.64 \$ ha^{-1}, respectively. Barley had the lowest and canola had the highest production costs. The gross income of producing these crops was found to be 1490.14, 947.17, 1949.26, and 1263.86 \$ ha^{-1}, respectively, in which canola had the highest gross income and the lowest value of the indicator belonged to the barley production system. In general, among the rainfed autumn crops in this region, canola had the highest production costs as well as the highest gross income. The economic analysis of crops in Moghan Plain indicated that canola had the highest production costs and income, while the values for barley were lower than canola and wheat [43].

Figure 3 depicts the contribution of consumed inputs to the production costs for investigated agro-systems. Examining the

variable costs revealed that seed, chemical fertilizers, manure, and agricultural machinery were among the costliest inputs in all the investigated agro-systems. In wheat production, seed and manure had the highest costs, with 150.36 and 119.80 \$ ha^{-1}, respectively, and with a total share of 51.1 %. In wheat production, the average seed consumption was approximately 258 kg ha^{-1}, which was higher than that of the wheat production systems in other parts of Iran [26, 40]. In barley production, manure input with 121.02 \$ ha^{-1} and 23.9 % had the highest production costs. Agricultural machinery and seed inputs with 23.2 % and 18 %, respectively, were among the most expensive inputs in the production. In another study on barley production, it was reported that seed input was one of the most consumed inputs [44]. In canola production, chemical fertilizers with 151.66 \$ ha^{-1} and 26.6 % had the highest production costs due to the high consumption of nitrogen fertilizer. Accordingly, the highest costs associated with the chemical fertilizers belonged to the nitrogen fertilizer with 95.86 \$ ha^{-1} for the consumption value of 402.63 kg ha^{-1}. The consumption of chemical fertilizers in this study was found to be higher than that in other regions of Iran [13, 45]. In general, the high nutritional needs of canola to nitrogen fertilizer [46] and the semi-mechanized distribution systems of spreading nitrogen fertilizer (using fertilizer broadcaster) in farms increased the consumption of this input. In this regard, by using a proper combination of manure and chemical fertilizers, the consumption of this input can be reduced [42, 47]. In the triticale production system, similar to wheat, the two inputs of manure and seeds with 119.72 and 109.01 \$ ha^{-1}, respectively, and with a total share of 45.1 % had the highest production costs.

Biocides, human labor, and diesel fuel were also in the next ranks of production costs for all the investigated crops. Although biocides were responsible for the lowest GHG emissions, their contribution to the production costs was significant due to the high consumption rates of herbicides in all studied agro-systems. In other words, according to Table 5, the cost of herbicides was at least two times higher than that of fungicides and insecticides. The lowest costs also belonged to the diesel fuel. This input was the highest contributor to GHG emissions in all the investigated crops. However, the contribution of diesel fuel to production costs varied from 1.3 to 1.5 % and it results from low price of diesel fuel and consequently, high and overuse of this input in Iran. Similar findings are also reported in previous studies on various crop production systems in the same region [28, 48] (Esmailpour-Troujeni et al., 2018; Mirkarimi et al., 2021).

Assessing the economic indicators revealed that the net income of wheat, barley, canola, and triticale was 866.94, 350.37, 1,277.85, and 666.22 \$ ha^{-1}, respectively. The average benefit to cost ratio of these crops was also 2.39, 1.59, 2.90, and 2.11, respectively. The results of these two indicators indicated the high profitability of canola production and the low profitability of barley production. The economic productivity of these crops was also estimated at 5.85, 4.17, 3.76, and 5.92 kg ha^{-1}, respectively, indicating that for every dollar spent on production, more wheat and triticale were produced. Overall, the results of studying economic indicators highlighted that canola and barley had the highest and lowest profitability among autumn rainfed crops, respectively. Unakitan et al. [49] in assessing the canola production in Turkey, reported that the crop production in Turkey was highly profitable. They found the benefit to cost ratio and net income in canola production to be 2.09 and 916.63 \$ ha^{-1}, respectively, which was less than that of the current study. Mousavi-Avval et al. [45] in the economic assessment of canola production in three different farm sizes in northern Iran stated that the maximum values of benefit to cost ratio and net incomes were 1.59 and 532.81 \$ ha^{-1}, indicating high profitability of canola production.

Table 5. Production costs and economic indicators of wheat, barley, canola, and triticale

Items	Unit	Wheat	Barley	Rapeseed	Triticale
A. Inputs					
1.Machinery	\$ ha^{-1}	95.18	117.44	134.12	88.24
2.Human labor	\$ ha^{-1}	15.37	16.98	27.48	14.82
3.Ch fertilizers	\$ ha^{-1}	89.05	80.09	151.66	96.05
(a) Nitrogen	\$ ha^{-1}	40.37	39.47	95.86	51.26
(b)Phosphorous	\$ ha^{-1}	25.37	21.34	27.72	28.12
(c) Potassium	\$ ha^{-1}	23.31	19.29	28.08	16.67
4.Seed	\$ ha^{-1}	150.36	91.01	57.07	109.01
5.Biocides	\$ ha^{-1}	51.58	72.25	72.64	71.22
(a) Herbicides	\$ ha^{-1}	25.85	33.07	51.68	31.57
(b) Insecticides	\$ ha^{-1}	10.00	11.28	6.95	11.35
(c) Fungicides	\$ ha^{-1}	15.73	27.89	14.02	28.29
6. manure	\$ ha^{-1}	119.80	121.02	117.45	119.72
7.Diesel fuel	\$ ha^{-1}	6.79	6.99	8.57	7.43
B. indices					
Variable cost	\$ ha^{-1}	528.13	505.77	569.0	506.47
Fixed cost	\$ ha^{-1}	95.06	91.04	102.42	91.17
Total cost	\$ ha^{-1}	623.20	596.81	671.41	597.64
Sale price	\$ kg^{-1}	0.43	0.38	0.77	0.36
production value	\$ ha^{-1}	1490.14	947.17	1949.26	1263.86
Benefit to cost ratio	-	2.39	1.59	2.90	2.11
Eco-productivity	kg $\$^{-1}$	5.58	4.17	3.76	5.92
Gross income	\$ ha^{-1}	962.01	441.41	1380.26	757.39
Net income	\$ ha^{-1}	866.94	350.37	1277.85	666.22

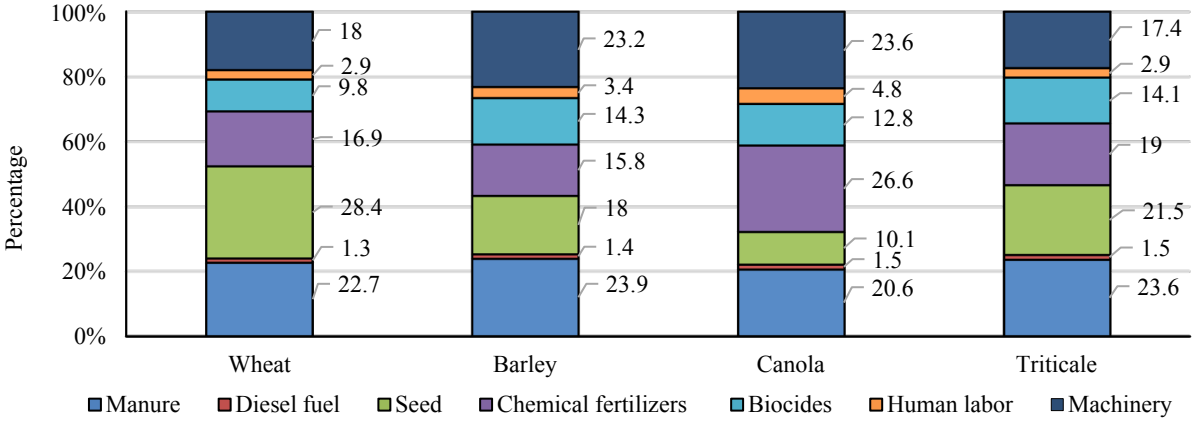

Figure 3. The share of consumed inputs in the average production costs of wheat, barley, canola, and triticale

Figure 4 depicts the share of each input in the production cost of autumn rainfed crops in terms of different crop years. In wheat production (Figure 4(a)), however, production costs in the first and second years were higher than in the third year and the differences were not significant. The reason for this difference was the higher cost of two inputs of agricultural machinery and chemical fertilizers, respectively, in the first and second crop years. In barley production (Figure 4(b)), it can be stated that the total production costs for the second year with 644.1 \$ ha^{-1} were significantly higher than the first year with 547.9 \$ ha^{-1}. Therefore, the costs of all inputs, except seed and manure, were higher in the second year than in the first year. According to Figure 4(c), the results of the study on canola revealed that there was no significant difference between production costs in three years and the consumption of inputs in different years was almost equal. The study on triticale also indicated an upward trend in production costs over three years (Figure 4(d)). Thus, total production costs for the third year (639.4 \$ ha^{-1}) were significantly higher than the first year (568.7 \$ ha^{-1}). Overall, the results of the study on production costs in different years pointed out that the two crops of wheat and canola had the least changes in production costs and the two crops of barley, while triticale, had significant changes in production costs.

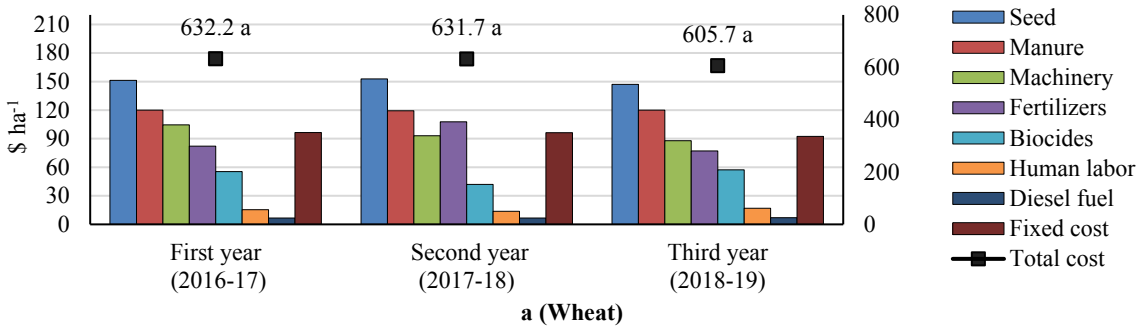

a (Wheat)

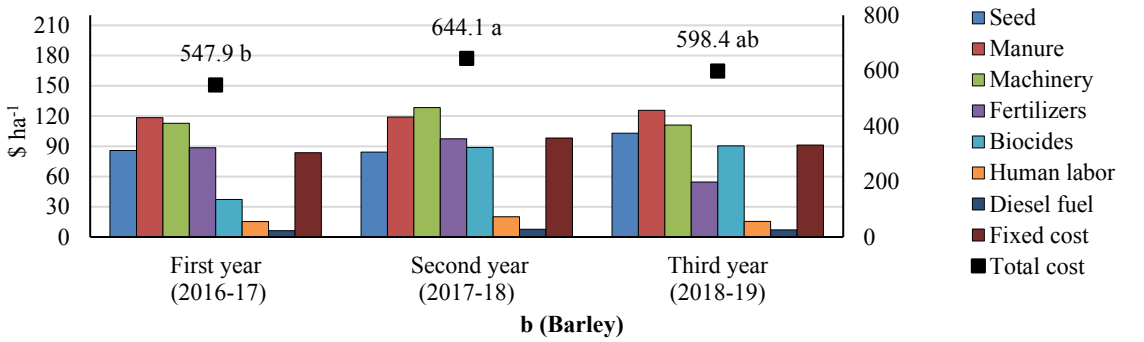

b (Barley)

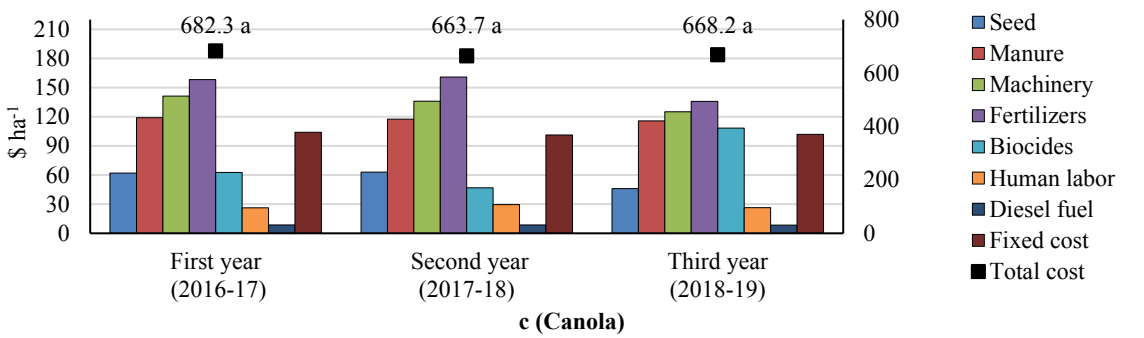

c (Canola)

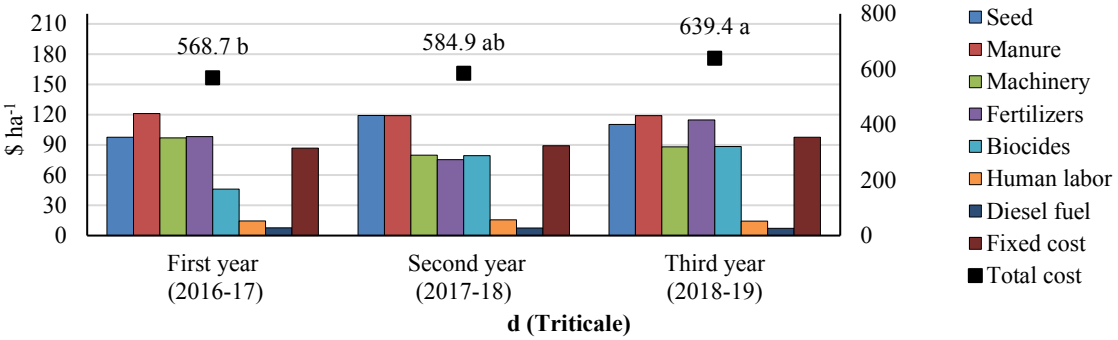

d (Triticale)

Figure 4. Share of consumed inputs in the production costs of (a) wheat, (b) barley, (c) canola, and (d) triticale

3.3. EF Indicator analysis

Figure 5 presents the EF value of investigated autumn rainfed agro-systems in Mazandaran province. The EF values for producing wheat, barley, canola, and triticale were calculated as 1.43, 0.57, 1.77, and 1.06 \$ $kgCO_{2eq}^{-1}$, respectively, resulting in the highest EF value of canola production. However, GHG emissions from canola production were higher than other crops (according to Table 3), the EF value of canola production was the highest. It can be associated with the higher net income of canola production. According to Table 4, the net income of canola production was about four times higher than that of barley production and about two-fold higher than that of triticale production. In general, by reducing GHG emissions and increasing net income, the EF value could be increased in the production of these crops. In the study of rapeseed and sunflower production in Italy, the maximum values of EF were reported to be 0.82 and 0.30 \$ $kgCO_{2eq}^{-1}$, respectively [50], which was much lower than that of autumn rainfed crops in Mazandaran province. The EF value of sugarcane production in Thailand was determined to be 2.8 \$ $kgCO_{2eq}^{-1}$ [51] and higher than that of the investigated agro-systems in the current research.

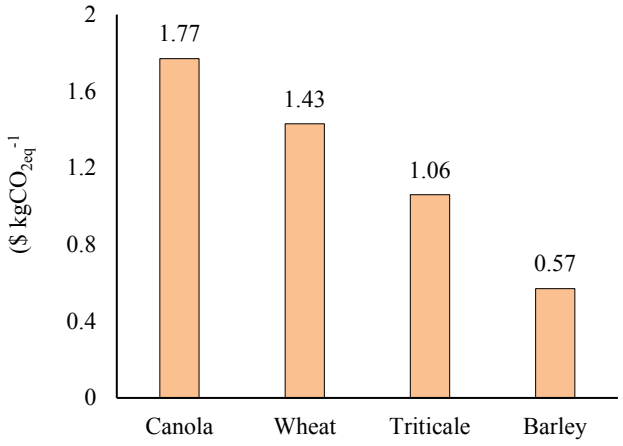

Figure 5. The EF value of wheat, barley, canola, and triticale production systems, on average

The EF value of the investigated agro-systems in terms of different crop years is presented in Table 6. Accordingly, the difference between the EF values in three years was significant for wheat and barley, while it was not significant for canola and triticale in different years. The EF values of wheat production in the second and third years were higher than in the first year, and for barley in the second year was much higher than in the first and third years, which was significant at a 5 % level. In general, the EF values in all investigated agro-systems were higher in the second year than in the first year, which can be due to the weather conditions and the amount of annual rainfall in the region.

Table 6. The EF value of wheat, barley, canola, and triticale production per hectare (\$ $kgCO_{2eq}^{-1}$)

Crop	EF (Based on net income)		
	1st year (2016-2017)	2nd year (2017-2018)	3rd year (2018-2019)
Wheat	0.94[b]	1.82[a]	1.53[a]
Barley	0.10[b]	1.15[a]	0.37[b]
Canola	1.52[a]	2.08[a]	1.73[a]
Triticale	0.83[a]	1.01[a]	1.33[a]

4. CONCLUSIONS

The study investigated the sustainability of autumn rainfed agro-systems (wheat, barley, canola, and triticale) in northern Iran using the EF indicator. The investigated inputs included seed, human labor, manure, diesel fuel, agricultural machinery, chemical fertilizers, and biocides in three crop years of 2016-2019. GHG emissions from inputs were obtained through GHG emission coefficients, and the EF was estimated based on the ratio of the net income indicator to the environmental impact indicator. The total GHG emissions from wheat, barley, canola, and triticale production were determined to be 604.34, 619.94, 720.38, and 628.62 $kgCO_{2eq}$ ha^{-1}, respectively, in which the diesel fuel had the highest GHG emissions in all the investigated agro-systems. In general, canola had the highest GHG emissions, while the lowest GHG emissions belonged to the wheat production system. The GHG emissions from all inputs consumption except manure for canola production were higher than those for other investigated crops production systems. In the wheat and triticale production systems, the semi-mechanized sowing system caused increase in the consumption and cost of seeds, and in the canola production, use of the semi-mechanized system for distributing the nitrogen fertilizer (using fertilizer broadcaster) in farms was the most effective factor in increasing the chemical fertilizers consumption. In determining the economic indicators, the net income of wheat, barley, canola, and triticale production was found to be 866.94, 350.37, 1277.85, and 666.22 \$ ha^{-1}, respectively, and the average benefit to cost ratios of these products were 2.39, 1.59, 2.90, and 2.11, respectively. The results of these two indicators presented high profitability of canola production and low profitability of barley production. The EF values for wheat, barley, canola, and triticale production systems were determined to be 1.43, 0.57, 1.77, and 1.06 \$ $kgCO_{2eq}^{-1}$, respectively, in which canola had the highest EF value. In conclusion, canola can be recommended as the most sustainable crop in terms of economic and environmental

points of view. Further research is required to investigate the third pillar of sustainability of the investigated production systems as the social aspect.

5. ACKNOWLEDGEMENT

The authors would like to acknowledge the support provided by the Ferdowsi University of Mashhad for funding this work.

REFERENCES

1. Rathke, G.W. and Diepenbrock, W., "Energy balance of winter oilseed rape (*Brassica napus* L.) cropping as related to nitrogen supply and preceding crop", ***European Journal of Agronomy***, Vol. 24, No. 1, (2006), 35-44. (https://doi.org/10.1016/j.eja.2005.04.003).
2. Nikkhah, A., Khojastehpour, M., Emadi, B., Taheri-Rad, A. and Khorramdel, S., "Environmental impacts of peanut production system using life cycle assessment methodology", ***Journal of Cleaner Production***, Vol. 92, (2015), 84-90. (https://doi.org/10.1016/j.jclepro.2014.12.048).
3. Taheri-Rad, A., Khojastehpour, M., Rohani, A., Khoramdel, S. and Nikkhah, A., "Energy flow modeling and predicting the yield of Iranian paddy cultivars using artificial neural networks", ***Energy***, Vol. 135, (2017), 405-412. (https://doi.org/10.1016/j.energy.2017.06.089).
4. Khoshnevisan, B., Bolandnazar, E., Barak, S., Shamshirband, S., Maghsoudlou, H., Altameem, T.A. and Gani, A., "A clustering model based on an evolutionary algorithm for better energy use in crop production", ***Stochastic Environmental Research and Risk Assessment***, Vol. 29, No. 8, (2015), 1921-1935. (https://doi.org/10.1007/s00477-014-0972-6).
5. United Nations, Eco-efficiency indicators: Measuring resource-use efficiency and the impact of economic activities on the environment, Greening of economic growth series, United Nations Publication, (2009). (https://sustainabledevelopment.un.org/content/documents/785eco.pdf).
6. UNEP, "Eco-efficiency for the dairy processing industry", The UNEP Working Group for Cleaner Production in the Food Industry. Environmental Management Centre, The University of Queensland, St Lucia. Australia, (2004). (https://www.worldcat.org/title/unep-working-group-for-cleaner-production-in-the-food-industry/oclc/224393021).
7. Ho, T.Q., Hoang, V.N., Wilson, C. and Nguyen, T.T., "Eco-efficiency analysis of sustainability-certified coffee production in Vietnam", ***Journal of Cleaner Production***, Vol. 183, (2018), 251-260. (https://doi.org/10.1016/j.jclepro.2018.02.147).
8. Bonfiglio, A., Arzeni, A. & Bodini, A., "Assessing eco-efficiency of arable farms in rural areas", ***Agricultural Systems***, Vol. 151, (2017), 114-125. (https://doi.org/10.1016/j.agsy.2016.11.008).
9. Ministry of Agriculture of Iran, Iran Agriculture Statistics, (2019). (http://www.maj.ir/Dorsapax/userfiles/Sub65/Amarnamehj195-96-site.pdf).
10. Nabavi-Pelesaraei, A., Abdi, R. and Rafiee, S., "Neural network modeling of energy use and greenhouse gas emissions of watermelon production systems", ***Journal of the Saudi Society of Agricultural Sciences***, Vol. 15, No. 1, (2016), 38-47. (https://doi.org/10.1016/j.jssas.2014.05.001).
11. Ghasemi-Mobtaker, H., Kaab, A. and Rafiee, S., "Application of life cycle analysis to assess environmental sustainability of wheat cultivation in the west of Iran", ***Energy***, Vol. 193, (2020), 116768. (https://doi.org/10.1016/j.energy.2019.116768).
12. Unakıtan, G. and Aydın, B., "A comparison of energy use efficiency and economic analysis of wheat and sunflower production in Turkey: A case study in Thrace region", ***Energy***, Vol. 149, (2018), 279-285. (https://doi.org/10.1016/j.energy.2018.02.033).
13. Kazemi, H., Bourkheili, S.H., Kamkar, B., Soltani, A., Gharanjic, K. and Nazari, N.M., "Estimation of greenhouse gas (GHG) emission and energy use efficiency (EUE) analysis in rainfed canola production (Case study: Golestan province, Iran)", ***Energy***, Vol. 116, Part 1, (2016), 694-700. (https://doi.org/10.1016/j.energy.2016.10.010).
14. Mohammadi, A., Rafiee, S., Jafari, A., Keyhani, A., Mousavi-Avval, S.H. and Nonhebel, S., "Energy use efficiency and greenhouse gas emissions of farming systems in north Iran", ***Renewable and Sustainable Energy Reviews***, Vol. 30, (2014), 724-733. (https://doi.org/10.1016/j.rser.2013.11.012).
15. Thanawong, K., Perret, S.R. and Basset-Mens, C., "Eco-efficiency of paddy rice production in Northeastern Thailand: A comparison of rain-fed and irrigated cropping systems", ***Journal of Cleaner Production***, Vol. 73, (2014), 204-217. (https://doi.org/10.1016/j.jclepro.2013.12.067).
16. Forleo, M.B., Palmieri, N. and Salimei, E., "The eco-efficiency of the dairy cheese chain: An Italian case study", ***Italian Journal of Food Science***, Vol. 30, No. 2, (2018). (https://doi.org/10.14674/IJFS-1077).
17. Masuda, K., "Measuring eco-efficiency of wheat production in Japan: A combined application of life cycle assessment and data envelopment analysis", ***Journal of Cleaner Production***, Vol. 126, (2016), 373-381. (https://doi.org/10.1016/j.jclepro.2016.03.090).
18. Besharatdeh, M., Norouzi, Gh. and Feizabadi, Y., "Eco-efficiency assessment of tangerine production in Mazandaran province, with rural economic development approach", ***Quarterly Journal of Space Economy & Rural Development***, Vol. 30, No. 8, (2020), 195-218. (In Farsi). (https://iranjournals.nlai.ir/handle/123456789/501403).
19. Dyer, J.A. and Desjardins, R.L., "Carbon dioxide emissions associated with the manufacturing of tractors and farm machinery in Canada", ***Biosystems Engineering***, Vol. 93, No. 1, (2006), 107-118. (https://doi.org/10.1016/j.biosystemseng.2005.09.011).
20. Dyer, J.A. and Desjardins, R.L., "Simulated farm fieldwork, energy consumption and related greenhouse gas emissions in Canada", ***Biosystems Engineering***, Vol. 85, (2003), 503-513. (https://doi.org/10.1016/S1537-5110(03)00072-2).
21. Lal, R. "Carbon emission from farm operations", ***Environment International***, Vol. 30, No. 7, (2004), 981-990. (https://doi.org/10.1016/j.envint.2004.03.005).
22. Yildizhan, H., "Energy, exergy utilization and CO_2 emission of strawberry production in greenhouse and open field", ***Energy***, Vol. 143, (2018), 417-423. (https://doi.org/10.1016/j.energy.2017.10.139).
23. Ozilgen, M. and Oner, E.S., Biothermodynamics: Principles and applications, CRC Press, (2016). (https://www.routledge.com/Biothermodynamics-Principles-and-Applications/Ozilgen-Oner/p/book/9780367868123).
24. Singh, S. and Mittal, J.P., Energy in production agriculture, Mittal Publications, New Delhi, India, (1992). (https://www.econbiz.de/Record/energy-in-production-agriculture-singh-surendra/10000874369).
25. Mondani, F., Aleagha, S., Khoramivafa, M. and Ghobadi, R., "Evaluation of greenhouse gases emission based on energy consumption in wheat Agroecosystems", ***Energy Reports***, Vol. 3, (2017), 37-45. (https://doi.org/10.1016/j.egyr.2017.01.002).
26. Sahabi, H., Feizi, H. and Karbasi, A., "Is saffron more energy and economic efficient than wheat in crop rotation systems in northeast Iran?", ***Sustainable Production and Consumption***, Vol. 5, (2016), 29-35. (https://doi.org/10.1016/j.spc.2015.11.001).
27. Amoozad-Khalili, M., Rostamian, R., Esmaeilpour-Troujeni, M. and Kosari-Moghaddam, A., "Economic modeling of mechanized and semi-mechanized rainfed wheat production systems using multiple linear regression model", ***Information Processing in Agriculture***, Vol. 7, No. 1, (2020), 30-40. (https://doi.org/10.1016/j.inpa.2019.06.002).
28. Esmailpour-Troujeni, M., Khojastehpour, M., Vahedi, A. and Emadi, B., "Sensitivity analysis of energy inputs and economic evaluation of pomegranate production in Iran", ***Information Processing in Agriculture***, Vol. 5, No. 1, (2018), 114-123. (https://doi.org/10.1016/j.inpa.2017.10.002).
29. Van-Middelaar, C.E., Berentsen, P.B.M., Dolman, M.A. and De Boer, I.J.M., "Eco-efficiency in the production chain of Dutch semi-hard cheese", ***Livestock Science***, Vol. 139, No. 1-2, (2011), 91-99. (https://doi.org/10.1016/j.livsci.2011.03.013).
30. Shrestha, B.M., Desjardins, R.L., McConkey, B.G., Worth, D.E., Dyer, J.A. and Cerkowniak, D.D., "Change in carbon footprint of canola production in the Canadian Prairies from 1986 to 2006", ***Renewable Energy***, Vol. 63, (2014), 634-641. (https://doi.org/10.1016/j.renene.2013.10.022).
31. Eady, S., "Greenhouse gas emissions from the cultivation of canola oilseed in Australia." (2017). (http://australianoilseeds.com/__data/assets/pdf_file/0010/11440/Australian_Country_Report_for_Canola_Nov2017-_Updated_with_CO2_MJ_FAME.pdf).
32. Mason, M.G. and Brennan, R.F., "Comparison of growth response and nitrogen uptake by canola and wheat following application of nitrogen

fertilizer", ***Journal of Plant Nutrition***, Vol. 21, No. 7, (1998), 1483-1499. (https://doi.org/10.1080/01904169809365497).

33. Brennan, R.F. and Bolland, M.D.A., "Comparing the nitrogen and potassium requirements of canola and wheat for yield and grain quality", ***Journal of Plant Nutrition***, Vol. 32, No. 12, (2009), 2008-2026. (https://doi.org/10.1080/01904160903308127).
34. Paramesh, V., Arunachalam, V., Nikkhah, A., Das, B. and Ghnimi, S., "Optimization of energy consumption and environmental impacts of arecanut production through coupled data envelopment analysis and life cycle assessment", ***Journal of Cleaner Production***, Vol. 203, (2018), 674-684. (https://doi.org/10.1016/j.jclepro.2018.08.263).
35. Nikkhah, A., Firouzi, S. Assad, M.E.H. and Ghnimi, S., "Application of analytic hierarchy process to develop a weighting scheme for life cycle assessment of agricultural production", ***Science of the Total Environment***, Vol. 665, (2019), 538-545. (https://doi.org/10.1016/j.scitotenv.2019.02.170).
36. Firouzi, S., Nikkhah, A. and Rosentrater, K.A., "An integrated analysis of non-renewable energy use, GHG emissions, carbon efficiency of groundnut sole cropping and groundnut-bean intercropping agro-ecosystems", ***Environmental Progress & Sustainable Energy***, Vol. 36, No. 6, (2017), 1832-1839. (https://doi.org/10.1002/ep.12621).
37. Nikkhah, A., Kosari-Moghaddam, A., Troujeni, M.E., Bacenetti, J. and Van Haute, S., "Exergy flow of rice production system in Italy: Comparison among nine different varieties", ***Science of The Total Environment***, Vol. 781, (2021), 146718. (https://doi.org/10.1016/j.scitotenv.2021.146718).
38. Firouzi, S., Nikkhah, A. and Aminpanah, H., "Resource use efficiency of rice production upon single cropping and ratooning agro-systems in terms of bioethanol feedstock production", ***Energy***, Vol. 150, (2018), 694-701. (https://doi.org/10.1016/j.energy.2018.02.155).
39. Gao, J., Thelen, K.D., Min, D.-H., Smith, S., Hao, X. and Gehl, R., "Effects of manure and fertilizer applications on canola oil content and fatty acid composition", ***Agronomy Journal***, Vol. 102, No. 2, (2010), 790-797. (https://doi.org/10.2134/agronj2009.0368).
40. Nabavi-Pelesaraei, A., Hosseinzadeh-Bandbafha, H., Qasemi-Kordkheili, P., Kouchaki-Penchah, H. and Riahi-Dorcheh, F., "Applying optimization techniques to improve of energy efficiency and GHG (greenhouse gas) emissions of wheat production", ***Energy***, Vol. 103, (2016), 672-678. (https://doi.org/10.1016/j.energy.2016.03.003).
41. Kapoor, R., Giri, B. and Mukerji, K.G., "Improved growth and essential oil yield and quality in Foeniculum vulgare mill on mycorrhizal inoculation supplemented with P-fertilizer", ***Bioresource Technology***, Vol. 93, No. 3, (2004), 307-311. (https://doi.org/10.1016/j.biortech.2003.10.028).
42. Megawer, E.A. and Mahfouz, S.A., "Response of canola (*Brassica napus* L.) to biofertilizers under Egyptian conditions in newly reclaimed soil", ***International Journal of Agriculture Sciences***, Vol. 2, No. 1, (2010), 12. (http://www.fayoum.edu.eg/stfsys/stfPdf/242/476/201212313817.pdf).
43. Farahza, M.N., Nazari, B., Akbari, M.R., Naeini, M.S. and Liaghat, A., "Assessing the physical and economic water productivity of annual crops in Moghan plain and analyzing the relationship between physical and economic water productivity", ***Irrigation and Water Engineering***, Vol. 11, No. 2, (2020), 166-179. (https://doi.org/10.22125/IWE.2020.120729).
44. Ghasemi-Mobtaker, H., Keyhani, A., Mohammadi, A., Rafiee, S. and Akram, A., "Sensitivity analysis of energy inputs for barley production in Hamedan province of Iran", ***Agriculture, Ecosystems & Environment***, Vol. 137, No. 3-4, (2010), 367-372. (https://doi.org/10.1016/j.agee.2010.03.011)..
45. Mousavi-Avval, S.H., Rafiee, S., Jafari, A. and Mohammadi, A., "Energy efficiency and cost analysis of canola production in different farm sizes", ***International Journal of Energy and Environment***, Vol. 2, No. 5, (2011), 845-852. (https://www.researchgate.net/profile/S_Hashem_Mousavi_Avval/publication/229053446_Energy_efficiency_and_cost_analysis_of_canola_production_in_different_farm_sizes/links/0deec538738e46d8ec000000/Energy-efficiency-and-cost-analysis-of-canola-production-in-different-farm-sizes.pdf).
46. Ozer, H., "Sowing date and nitrogen rate effects on growth, yield and yield components of two summer rapeseed cultivars", ***European Journal of Agronomy***, Vol. 19, No. 3-4, (2003), 453-463. (https://doi.org/10.1016/S1161-0301(02)00136-3).
47. Roy, D.K. and Singh, B.P., "Effect of level and time of nitrogen application with and without vermicompost on yield, yield attributes and quality of malt barley (Hordeum vulgare)", ***Indian Journal of Agronomy***, Vol. 51, No. 1, (2006), 40-42. (https://www.indianjournals.com/ijor.aspx?target=ijor:ija&volume=51&issue=1&article=013).
48. Mirkarimi, S.R., Ardakani, Z. and Rostamian, R., "Economic and environmental assessment of tobacco production in Northern Iran", ***Industrial Crops and Products***, Vol. 161, (2021), 113171. (https://doi.org/10.1016/j.indcrop.2020.113171).
49. Unakitan, G., Hurma, H. and Yilmaz, F., "An analysis of energy use efficiency of canola production in Turkey", ***Energy***, Vol. 35, No. 9, (2010), 3623-3627. (https://doi.org/10.1016/j.energy.2010.05.005).
50. Forleo, M.B., Palmieri, N., Suardi, A., Coaloa, D. and Pari, L., "The eco-efficiency of rapeseed and sunflower cultivation in Italy, Joining environmental and economic assessment", ***Journal of Cleaner Production***, Vol. 172, (2018), 3138-3153. (https://doi.org/10.1016/j.jclepro.2017.11.094).
51. Silalertruksa, T., Gheewala, S.H., and Pongpat, P., "Sustainability assessment of sugarcane biorefinery and molasses ethanol production in Thailand using eco-efficiency indicator", ***Applied energy***, Vol. 160, (2015), 603-609. (https://doi.org/10.1016/j.apenergy.2015.08.087).

JREE: Vol. 9, No. 2, (Spring 2022) 18-26

Journal of Renewable Energy and Environment

Journal Homepage: www.jree.ir

Materials and Energy Research Center

MERC

Research Article

Performance of Microtabs and Trailing Edge Flaps in Wind Turbine Power Regulation: A Numerical Analysis Using WTSim

Alireza Maheri [a*], I. Kade Wiratama [b], Terence Macquart [c]

[a] School of Engineering, Centre for Energy Transition, University of Aberdeen, Aberdeen, Scotland, United Kingdom.
[b] Faculty of Engineering, University of Mataram, Mataram, West Nusa Tenggara, Indonesia.
[c] Department of Aerospace Engineering, University of Bristol, Bristol, England, United Kingdom.

PAPER INFO

Paper history:
Received: 27 June 2021
Revised in revised form: 15 November 2021
Scientific Accepted: 10 September 2021
Published: 20 February 2022

Keywords:
Microtab,
Trailing Edge Flap,
Smart Blade,
Power Control,
Load Alleviation,
WTSim

ABSTRACT

The effectiveness of trailing-edge flaps and microtabs in damping 1P-3P loads has been proven through a series of research work during the past decade. This paper presents the results of an investigation into the effectiveness of these devices in power enhancement and power control for responding to the issue of where these devices can be used with dual function of load and power control on a medium size turbine. The 300 kW-AWT27 wind turbine is used as the base wind turbine and the effects of adding trailing-edge flaps and string of microtabs of different lengths positioned at different span locations on the aerodynamic performance of the rotor are studied. In each case, the wind turbine simulator WTSim is used to obtain the aerodynamic performance measures. In the next step, the original blade twist is redesigned to ensure that the blade is optimized upon the addition of these active flow controllers. It is found that blades equipped with flaps can increase the annual average power and reduce the blade loading at the same time for constant speed and variable speed generators. Power enhancement is more visible on constant speed rotors, while load reduction is more significant on variable speed rotors. To achieve constant speed rotors, an average power enhancement of around 12 % is achieved for a flap of size 25 % of the blade span located at about 72 % of the blade span. Microtabs are less effective in power control and can improve the produced power only by a few percentage points.

https://doi.org/10.30501/jree.2021.291397.1220

1. INTRODUCTION

Power and aerodynamic load control systems in wind turbines have multiple functions. All wind turbines need a power control system, which improves the extracted wind power at wind speeds below the rated wind speed and regulates the power at its rated value above the rated wind speed. In large-scale wind turbines, the blades experience significant loads. Hence, load alleviation becomes also a function of control systemin order to reduce the quasi-steady loads on blades due to gradual change in wind speed or in azimuth angle and/or to damp unsteady fluctuating loads, which are mainly produced by wind turbulence. Reducing fatigue loads produced by cyclic or stochastic forces due to tower shadow, yaw misalignment, wind shear, wind turbulence, and the wake effects of other turbines can result in a significant reduction in cost [1]. This remains a motivation for many research works during the past two decades, with growing interests in the past few years. These research works have focused on a variety of concepts for load reduction, some rooted in the already existing and well-established fixed-wing and rotary wing aircraft systems, and some specifically developed for wind turbines. A review of the state-of-the-art research in this field can be found in [1-3].

Conventional and some of the nonconventional power and load control mechanisms are shown in Figure 1. The control systems shown in this figure use different controlling parameters to control the power and/or load. Since the power extracted by a blade is in close relation to the aerodynamic load on the blade, some of these control systems inherently affect both power and load. The control parameters are blade span, aerofoil topology, and blade twist. Some of these control systems respond only to wind variations on large time scales, while some others have a shorter response time and can, therefore, be used for controlling the effect of wind variations with smaller timescales.

Controllers affecting the blade twist influence the performance of wind turbines by varying angles of attack α and the flow kinematics. As shown in Figure 1, the angle of attack depends on the inflow angle φ, elastic twist of the blade β_e, blade pretwist β_0, and pitch angle pitch. Collective and individual pitch control systems employ pitch as the controlling parameter. Bend-twist or stretch-twist adaptive

*Corresponding Author's Email: alireza.maheri@abdn.ac.uk (A. Maheri)
URL: https://www.jree.ir/article_145119.html

Please cite this article as: Maheri, A., Wiratama, I.K. and Macquart, T., "Performance of microtabs and trailing edge flaps in wind turbine power regulation: A numerical analysis using WTSim", ***Journal of Renewable Energy and Environment (JREE)***, Vol. 9, No. 2, (2022), 18-26. (https://doi.org/10.30501/jree.2021.291397.1220).

blades control the performance by the blade elastic torsional displacement β_e which is produced as a result of elastic coupling in the blade material. Those controllers affecting the cross-sectional topology of the blade (e.g., via morphing or deploying an active flow controller) affect the form of the function $\vec{f}$ relating the aerodynamic coefficients C_L, C_D, and C_M to the flow kinematics.

Most of modern wind turbines use individual pitch control systems for alleviating loads of 1P (rotor rotational frequency) [4] up to 3P [5]. However, these systems do not have any significant impact on stochastic loads with higher frequencies. Furthermore, IPC exacerbates pitch actuations leading to an increase in wear and risk of failure of the blade-root connection. On the other hand, smaller active flow controllers, such as microtabs and trailing edge flaps, modify the flow kinematics locally instead of changing the flow kinematics around the entire of the blade [6, 7]. This led the researchers to investigating the potential benefits of implementation of these active flow controllers as auxiliary control surfaces for providing more effective load alleviation, particularly in damping fluctuating and stochastic loads with higher frequencies [8-13].

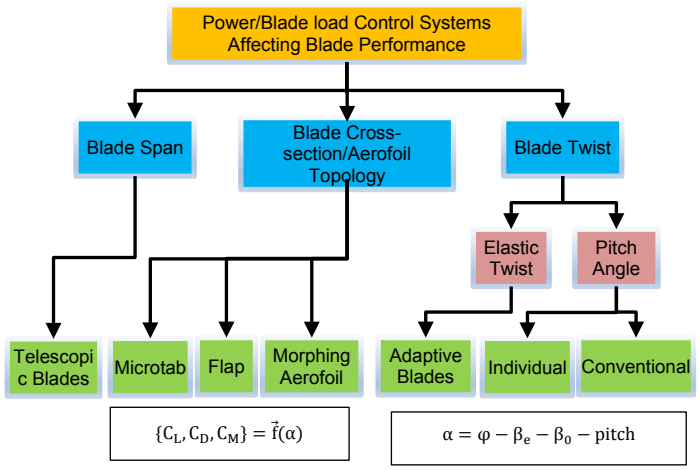

Figure 1. Different control systems affecting blade performance

Although the results of the above-mentioned studies have proven the potentials of these active flow controllers in load alleviation, utilization of these devices may take some time to be realized due to two main drawbacks of these systems. First, the integration of active flow controllers in wind turbine blades makes the blade manufacturing process more complicated due to required alteration in the process, particularly necessary modifications in moulding process and adding precise machining. Second, the integration of active flow controllers in wind turbine blades means the addition of moving mechanical parts to the structure of the blade. The maintenance and reliability of these systems become another concern for blade manufacturers.

Given that the previous research has focused on load alleviation and assumed that active flow controllers are accompanied by the main controller such as pitch system (for instance, see [14]) with the function of improving power at low winds and regulating the power at high winds, the capability of these devices in power control has not been investigated thoroughly. If these systems are capable of controlling the power as well as load alleviation, there will not be a need for the main control system and significant cost saving over the lifespan of the wind turbine can be achieved. This issue together with their proven potential in load alleviation and extension of the lifespan of the blades could circumvent the above-mentioned drawbacks. Ebrahimi and Movahhedi [15] conducted a numerical simulation of the performance of microtabs in improving the power of a 20-kW stall-regulated wind turbine below rated wind speed. Their results show some improvement in the average power for this small wind turbine. However, the issue of the suitability of microtabs for larger wind turbines remains unanswered.

In view of the above discussion, this paper aims to investigate the potential benefits of these control systems in power enhancement and regulation and to explore the possibility of using these devices as the only controlling systems with both functions of load alleviation and power regulation.

2. BLADES UTILIZING NONCONVENTIONAL CONTROL SURFACES

A wind turbine blade is defined by its span, chord, pretwist, aerofoil, and maximum thickness distributions: $\{R, c(r), \beta_0(r), AF(r), t_{max}(r)\}$. Three more parameters, namely inboard radial location $R_{F,s}$, outboard radial location $R_{F,e}$, and width of the flap as a fraction of the chord length at the centre of the flap $d_F^* = d_F/c_F$, are also required to define the location and size of the flap. These parameters are shown in Figure 2.

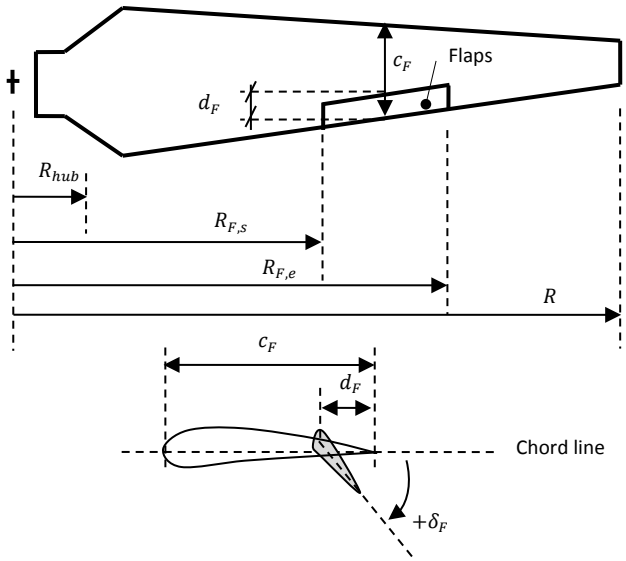

Figure 2. Blade with trailing edge flap

Once a flap is deployed by an angle of δ_F, it changes the flow kinematics around the blade at that location. This leads to a change in local lift and drag coefficients $\Delta C_L|_{\delta_F}$ and $\Delta C_D|_{\delta_F}$:

$$\Delta C_L|_{\delta_F} = C_L|_{\delta_F} - C_L|_{\delta_F=0} \quad (1.a)$$

$$\Delta C_D|_{\delta_F} = C_D|_{\delta_F} - C_D|_{\delta_F=0} \quad (1.b)$$

where, $C_L|_{\delta_F}$ and $C_D|_{\delta_F}$ are the aerodynamic coefficients at that deployment angle δ_F, and $C_L|_{\delta_F=0}$ and $C_D|_{\delta_F=0}$ are the original aerodynamic coefficients ($\delta_F = 0$). Besides the deployment angle, ΔC_L and ΔC_D depend on the aerofoil shape, flap width, and the angle of attack of the aerofoil α.

In case of blades equipped with microtabs, five parameters are required to define a string of microtabs on a blade. These parameters are the inboard and outboard radial locations of the string of microtabs $R_{MT,s}$ and $R_{MT,e}$; normalized distance from the leading edge $d^*_{MT} = d_{MT}/c_{MT}$; microtab length s_{MT} and actuation height $h^*_{MT} = h_{MT}/c_{MT}$. The distance from the leading edge and the actuation height are normalized by c_{MT}, which is the chord length at the centre of microtab. These parameters are shown in Figure 3.

Each microtab, in a string of microtabs, depending on its location can get two positions. Microtabs on the suction side of the aerofoil can be deployed upward only (coded by -1), while those on the pressure side of the aerofoil can be deployed downward (coded by +1). A deployed microtab changes lift and drag coefficients. These changes can be presented as follows:

$$\Delta C_L|_{MT} = C_L|_{MT} - C_L|_{MT=0};\ \ MT \in \{-1, +1\} \quad (2.a)$$

$$\Delta C_D|_{MT} = C_D|_{MT} - C_D|_{MT=0};\ \ MT \in \{-1, +1\} \quad (2.b)$$

where, $\Delta C_L|_{MT}$ and $\Delta C_D|_{MT}$ are the variations in aerodynamic coefficients as a result of the deployment of a microtab on the suction side ($MT = -1$) or pressure side ($MT = +1$); $C_L|_{MT}$ and $C_D|_{MT}$ are the aerodynamic coefficients; and $C_L|_{MT=0}$ and $C_D|_{MT=0}$ are the original aerodynamic coefficients without the presence or the deployment of microtabs. The amount of changes in lift and drag coefficients, ΔC_L and ΔC_D, depends on the local angle of attack, α, microtab location d^*_{MT}, and actuation height h^*_{MT}. An undeployed microtab in its neutral position has no effect on the flow kinematics.

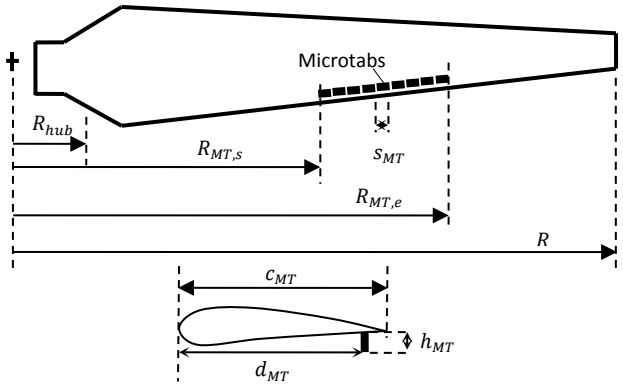

Figure 3. Blade with a string of microtabs

The analysis tool used for this study, WTSim (Wind Turbine Simulator), has a BEMT-based (blade element momentum theory) aerodynamic module and a controller simulator. This tool is capable of simulation of wind turbines with conventional and nonconventional blades (adaptive blades, telescopic blades, and blades equipped with active flow controllers). WTSim calculates the wind turbine aerodynamic performance, including the blade and rotor aerodynamic loads, blade internal forces, the rotor mechanical power in a given operating condition, and the annual average power. More information on the application of WTSim and the background theory of simulating smart blades can be found in [16] and [17], respectively. The BEMT module in WTSim is a modified version of that reported in [18] and [9]. The original version uses axial induction factor convergence algorithms [19, 20] and is evaluated against WTPerf in [18] and against FAST and DU_SWAMP in [9] for conventional blades. This module has been modified for blades equipped with microtabs and trailing edge flaps.

For this study, the lookup tables for ΔC_L and ΔC_D due to the presence of mictotabs and flaps are obtained using XFOIL [21].

3. PRETWIST MODIFICATION

Since the addition of microtab or flap to the blade changes the flow kinematics around the blade, the original topology will not be optimum anymore. That is, we need to redesign the blade to ensure it is optimized for the new purpose. However, if we redesign the entire of the blade topology (chord, pretwist, and aerofoil distributions) and the rotor radius, we lose our ground for evaluating how much of the improvement results from the added active controller. Therefore, this study redesigns the pretwist distribution only. The pretwist has the highest effect on the flow kinematics around the blade; on the other hand, changing the pretwist does not directly lead to a change in the blade mass (as opposed to changing the chord and aerofoil distribution or rotor radius).

In all cases, the blade is modified to ensure that the full potential of active flow controllers is achieved without increasing the cost or the mass of the blade (except for the added cost or mass of the active flow controller itself). The optimization problem is, therefore, formulated as follows:

$$\max P_{av} = \int_{V_i}^{V_o} P(V)R(V)dV \quad (3.a)$$

subject to:

$$P \le P_{rated} \quad (3.b)$$

$$m_{blade,opt} \le m_{blade,original} \quad (3.c)$$

where P_{av} is the annual average power produced by the wind turbine if installed on a site with an average wind speed of V_{av}, $P(V)$ is the rotor power at wind speed V, $R(V)$ is the wind speed probability density function, V_i and V_o are the cut-in and cut-out velocities, respectively, P_{rated} is the rated power, and m_{blade} is the mass of the blade. Generally speaking, to ensure that Constraint (3.c) above is satisfied, we need to analyze the blade both aerodynamically and structurally. However, since the rotor radius and the chord and aerofoil distributions remain the same as the original blades, there is no need to increase the thickness of the blade shell and, hence, increase the mass of the blade if the loading on the optimized blade is equal to or less than the loading on the original blade. In other words, Constraint (3.c) is automatically satisfied if the following constraint on the flap bending moment, as the dominant load, is satisfied:

$$M_{flap,opt} \le M_{flap,original} \quad (3.d)$$

By replacing Constraint (3.c) with Constraint (3.d) and keeping the rotor radius, chord and aerofoil distributions constant, there is no need to include any structural analysis in the optimization process. This study calculates the average power based on a Rayleigh probability density function and site average wind speed of $V_{av} = 5.7\ m/s$ and cut-in and cut-out velocities of $V_i = 5\ m/s$ and $V_o = 25\ m/s$, respectively.

The optimization tool employed for solving this optimization problem is a Genetic Algorithm (GA) that

requires the BEMT module and the controller simulator for evaluating the design candidates (for calculating P(V), $M_{flap}(V)$, and (P_{av}). The GA has special features such as geometric crossover for better exploitation of the solutions, dynamic mutation, and semi-heuristic initial population generation [22, 23]. A chromosome containing the aerodynamic design variables of a blade is a string of real numbers, integer numbers/coded parameters representing the chord, pretwist, and aerofoil distributions at some design points (n_{dp}) along the span of the blade. For blades equipped with mictotabs and flaps, assuming that the size and chordwise locations of these flow controllers are fixed, their span locations ($R_{F,s}, R_{F,e}, R_{MT,s}, R_{MT,e}$) are also added to the set of design variables.

4. POTENTIALS OF TRAILING EDGE FLAPS IN POWER ENHANCEMENT AND REGULATION

AWT27 wind turbine is adopted as the baseline turbine for this study. It is a two-bladed stall-regulated constant-speed wind turbine with a rotor diameter of 27.4 m. The blade profile is made of S800 series aerofoils. The rotor produces a rated power of about 300 kW at a rotor speed of 53.3 rpm. This turbine is a well-known research wind turbine with its technical data available in the public domain (e.g., see [24]). The advantage of AWT27 over newer research wind turbines such as variable-speed pitch-controlled NREL 5MW turbine is due to its type. A stall-regulated constant-speed turbine makes an ideal test case for studying the power control capabilities of control systems under investigation as it does not have any form of active control in place.

We deal with three design variables when conducting a design optimization of blades equipped with trailing edge flaps. These parameters are blade pretwist distribution, flap location, and flap length. As shown in Figure 2, parameter ($R_{F,e} - R_{F,s}$) is the flap length and $0.5(R_{F,e} + R_{F,s})$, the radial location of the centre of the flap, represents the flap location. Here, the length of the flap is limited to 5 % of the rotor radius to restrict the added mass and cost. Since the inner parts of the blade are aerodynamically less effective and since the flap cannot be installed at the tip of the blade, the position of the flap is limited between 60 % and 95 % of the rotor radius. The optimization problem of (3) is reformulated as follows:

$$\max P_{av} = f(X) \quad (4.a)$$

where

$$X = \{\beta_0(r), R_{F,s}, R_{F,e}\} \quad (4.b)$$

subject to:

$$P \le P_{rated} \quad (4.c)$$

$$M_{flap,opt} \le M_{flap,original} \quad (4.d)$$

$$R_{F,s} \ge 0.6R \quad (4.e)$$

$$R_{F,e} \le 0.95R \quad (4.f)$$

$$R_{F,e} - R_{F,s} \le 0.05R \quad (4.g)$$

The pretwist distribution $\beta_0(r)$ is defined using $n_{dp} = 5$ design points. The width of the flap d_F is considered as 10 % of the local chord c_F, where c_F is the chord @ $0.5(R_{F,e} + R_{F,s})$. The flap deployment angle is assumed to be limited to the lower and upper limits of 20 degrees: $\delta_{F,l} = -20°$ and $\delta_{F,u} = +20°$.

The optimum solution is found to have a pretwist distribution, as shown in Figure 4.a, with a flap extended between 70-75 % of the rotor radius. Figures 4.b through 4.d show the performances of original AWT-27 without installing flap, AWT-27 blades equipped with flap but with original pretwist, and AWT-27 blades equipped with flap with an optimized pretwist. It is evident that the addition of flap to the original blades without modifying them has some positive effect on the power capture capability (improving the average power from 43.9 kW to 44.8 kW and showing the increase of 2.1 %). However, this slight improvement comes at a cost of 4.6 % increase in the flap bending moment at the root (176.5 kNm versus 168.7 kNm). On the other hand, comparing the performances of the optimized blades equipped with flaps and the original blades, we observe a significant 8.84 % improvement in the average power (47.7 kW versus 43.9 kW) as well as a 2.9 % reduction in the root bending moment (163.8 kNm versus 168.7 kNm).

The behavior of the power curve of Figure 4.b for blades equipped with flap and optimized pretwist suggests that flap can be used instead of traditional pitch control system to regulate the rotor power at wind speeds above the rated speed. This is consistent with the behavior of blade root bending moment curve shown in Figure 4.d, in which the bending moment increases to its maximum value at a rated wind speed (similar to pitch-controlled rotors) and, then, decreases at higher wind speeds. A slight reduction in power curve at wind speeds above 23 m/s and increase in blade bending moment for wind speeds above 20 m/s result from flap saturation. A perfect power regulation and a continuous bending moment reduction at higher wind speeds (similar to pitch-controlled rotors) can be achieved by using a bigger flap or allowing higher deployment angles beyond $\pm 20°$.

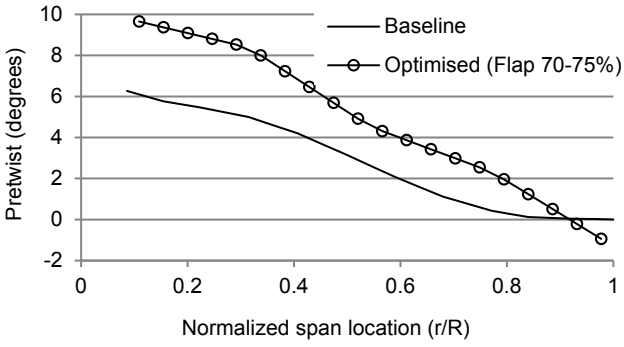

(a)

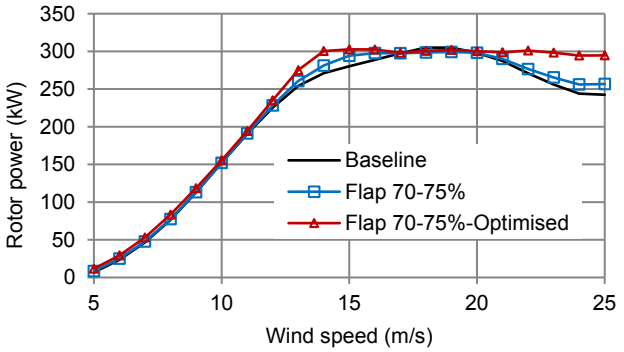

(b)

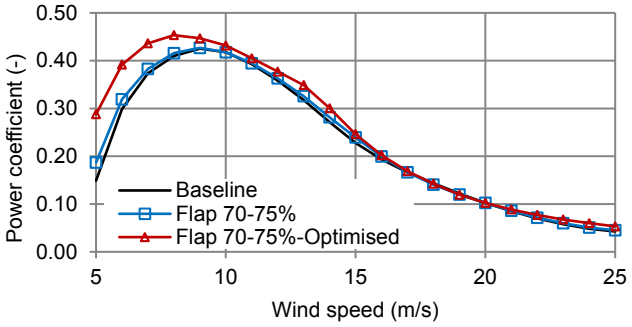

(c)

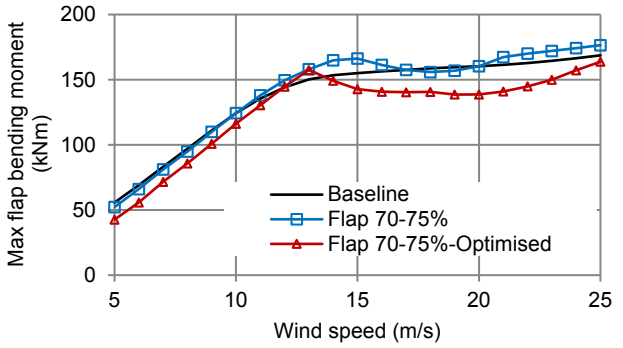

(d)

Figure 4. Blade with trailing edge flap @ 70-75 % of the span - Constant speed rotor

The optimization problem (4) can be also solved in the case of variable speed rotors, where all parameters are the same as those used in the case of constant speed rotor except the rotor speed which is treated here as a controlling parameter. For simulating the rotor speed, the following parameters are used: $\Omega_l = 30$ rpm, $\Omega_u = 65$ rpm, and $\varepsilon_\Omega = 0.1$ rpm. For the variable speed rotor, the optimum solution is found to have a pretwist distribution, as shown in Figure 5.a, with the optimum flap location between 70-75 % of the rotor radius. Figures 5.b to 5.d show the performance of the unit with original blades, original blades with flap, and optimized blade with flap.

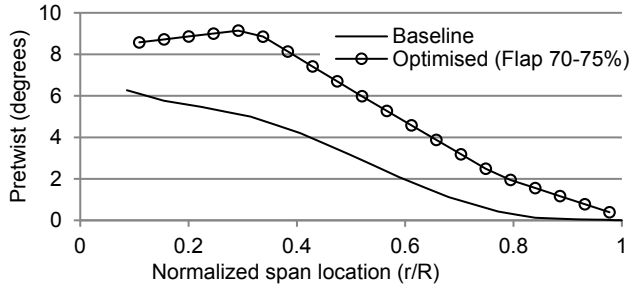

(a)

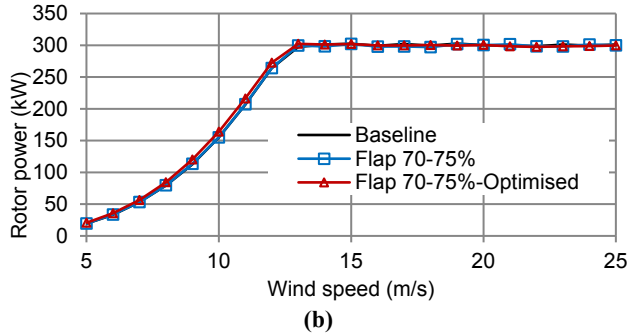

(b)

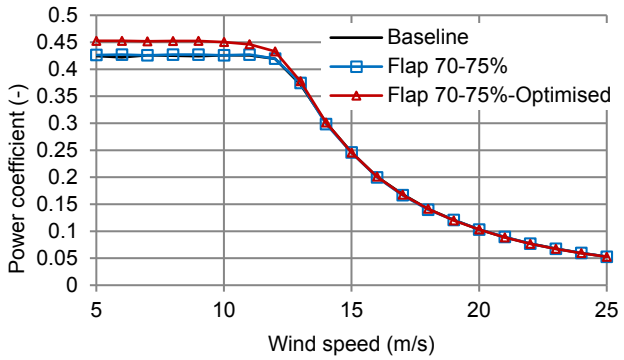

(c)

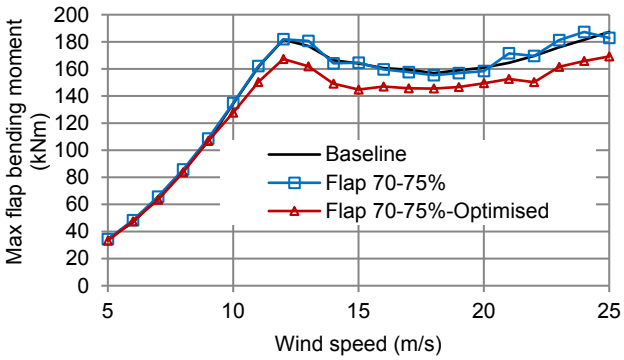

(d)

Figure 5. Blade with trailing edge flap @ 70-75% of the span – Variable-speed rotor

As expected, in the case of turbines with variable speeds, since the dominant controlling parameter is the rotor speed, the contribution of other active flow controllers, such as trailing edge flaps, in improving the energy capture capability is very small. This contribution, however, increases notably as a result of optimization (here, a 4.8 % increase in the average power from 49.7 kW to 52.1 kW). Moreover, with reference to Figure 5.d, one can see that the blade optimization leads to the reduction of blade loading as well (here, 9.6 % from 187.3 kNm to 169.2 kNm). Moreover, the same argument regarding flap saturation and its effect on the behavior of blade root bending moment curve can be made for rotors with variable speeds.

4.1. Parametric study

Reference [25] reports the results of a parametric study on exploring the potential benefit and effect of using trailing edge flaps on constant speed rotors. Here, by adopting the same approach, the effect of the size and location of flap on the power capture capability of variable speed rotors is investigated for 11 cases of different flap sizes and locations, as shown in Table 1. For each case, the optimum pretwist is found upon solving an optimization problem similar to that of (5.a), in which $X = \{\beta_0(r)\}$ with Constraint (5.c) as the only constraint applied. The results of performance simulation are shown in Figures 6 and 7.

In Figure 7.a, all flaps start at 60 % of the rotor radius (Cases 1 and 8 through 11 in Table 1). In Figure 7.b, all flaps have a span of 5 % of rotor radius (Cases 1 through 7 in Table 1). By using the data shown in Figure 7, the share of blade pretwist optimization in the power enhancement is shown in Figure 8.

Table 1. Studied flap lengths and flap locations (in % of R)

Case	$R_{F,s}$	$R_{F,e}$	Flap location $0.5(R_{F,e}+R_{F,s})$	Flap length $R_{F,e}-R_{F,s}$
1	60	65	62.5	5
2	65	70	67.5	5
3	70	75	72.5	5
4	75	80	77.5	5
5	80	85	82.5	5
6	85	90	87.5	5
7	90	95	92.5	5
8	60	70	65.0	10
9	60	75	67.5	15
10	60	80	70.0	20
11	60	85	72.5	25

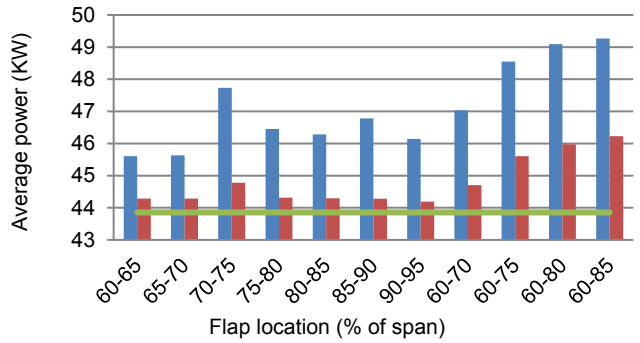

(a)

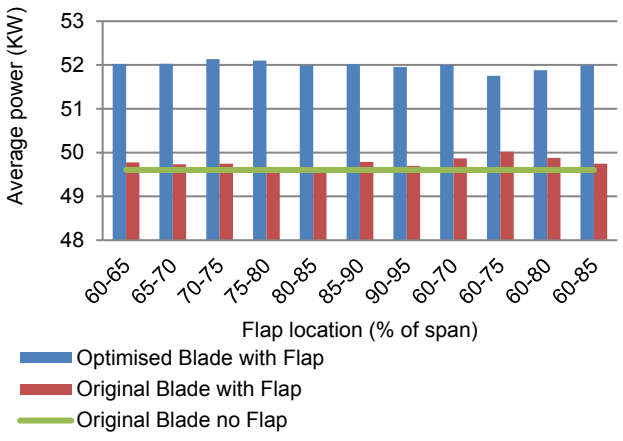

(b)

Figure 6. Average power for different flap sizes and locations: (a) constant speed [25] and (b) variable-speed rotors

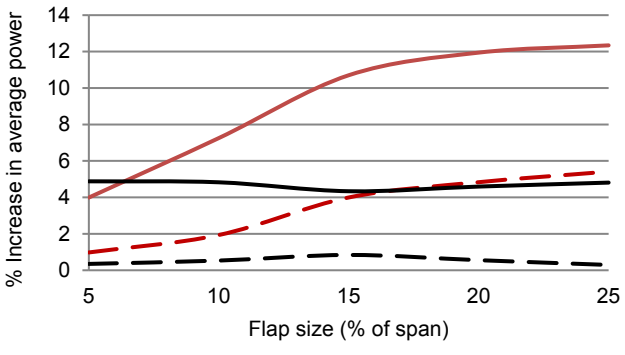

(a)

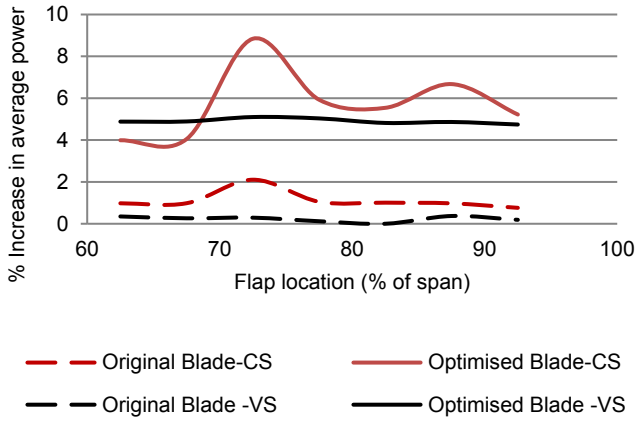

(b)

Figure 7. Effects of the (a) flap size and (b) flap location on the improvement in the average power

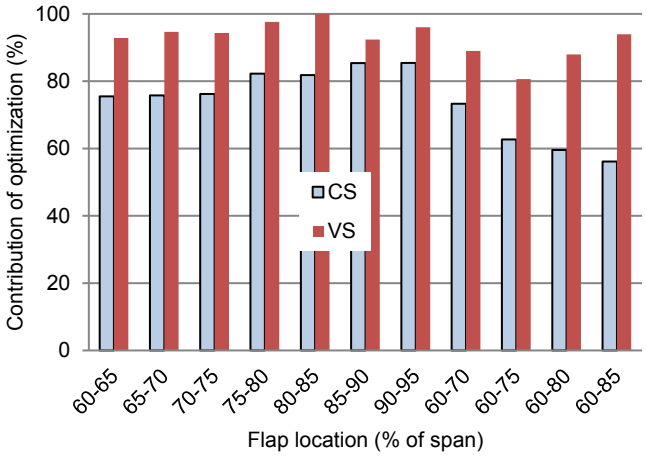

Figure 8. Contribution of optimization to the power enhancement

In view of these results, the following conclusions can be drawn:

- For CS rotors, the size of the flap has a significant effect on the amount of enhancement in the average power. This effect, however, reduces dramatically as the size increases (also reported in [25]).
- For CS rotors, the location of flap is a key parameter influencing the amount of improvement in the power extraction. The best location for placing a flap is at about 70 % of the blade span from the root of the blade (also reported in [25]).
- In contrast to CS rotors, neither the location of the flap nor its size affect the performance significantly. This is mainly due to having a rotor speed as the dominant controlling system in place.
- Effect of flap on CS is greater than that of flap on VS.
- Contribution of the pretwist optimization to enhancing the power capture capability in both CS and VS rotors is significant. Contribution of the blade optimization in VS rotors is greater than that in CS rotors.

Optimization has the highest effect on shorter flaps located towards the tip of the blade. This is due to the facts that the outer parts of the blade are aerodynamically more sensitive and that flow kinematics can be more optimized locally around shorter flaps.

5. POTENTIALS OF MICROTABS IN POWER ENHANCEMENT AND REGULATION

Since we are using a string of microtabs over a portion of the blade rather than a single microtab, the length of the string does not make a meaningful design variable. The reason is that some part of the string (the inner parts) might be always in a neutral position with no effect on the power. Therefore, we assume that the string of microtabs has a fixed length of 20 % of the span, extended from $R_{MT,s} = 0.7R$ to $R_{MT,e} = 0.9R$. The optimization problem of (4) is then reformulated as follows:

$$\max P_{av} = f(X) \quad (5.a)$$

where

$$X = \{\beta_0(r)\} \quad (5.b)$$

subject to:

$$P \leq P_{rated} \quad (5.c)$$

$$M_{flap,opt} \leq M_{flap,original} \quad (5.d)$$

Using $d^*_{MT} = 80$ % and $d^*_{MT} = 95$ % of the chord from the leading edge on the upper and lower surfaces, respectively, with an actuation height of $h^*_{MT} = 3.3$ % of the chord length, the blade is optimized for pretwist, as shown in Figure 9.a.

In Figures 9.b and 9.c, the curves representing the baseline blade and the baseline blade with microtabs are almost identical. With reference to Figure 9, it is evident that the baseline blades extract more or less the same amount of power, with or without microtab, unless the pretwist is optimized. The pretwist optimization leads to some improvement of 4.2 % in the average power (45.7 kW versus 43.9 kW).

By repeating the optimization problem above for the case of variable speed rotor, no improvement was observed due to the dominance of the rotor speed as the controlling parameter.

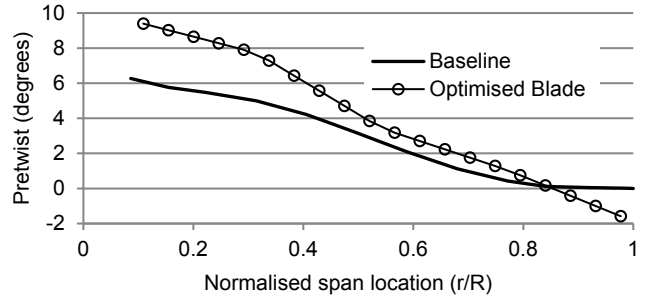

(a)

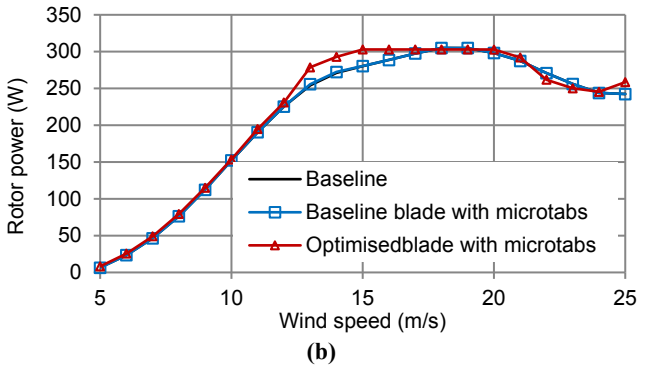

(b)

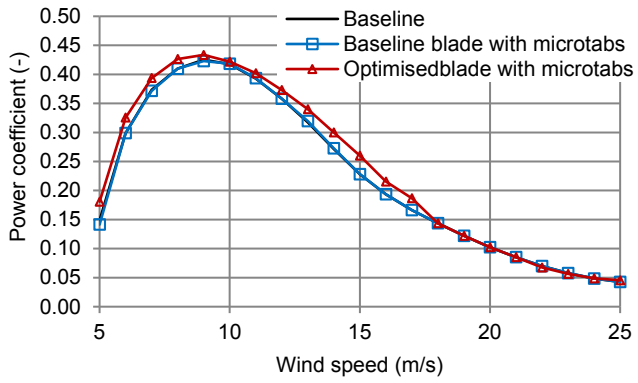

(c)

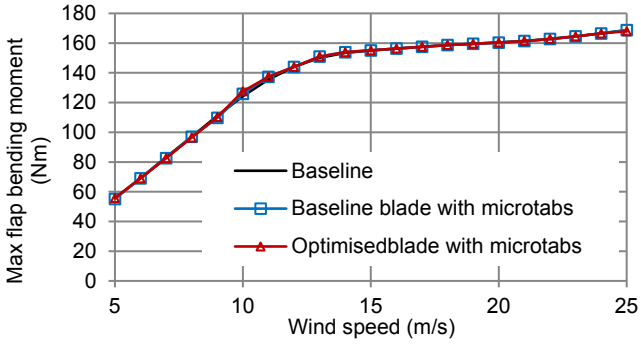

(d)

Figure 9. Microtab on optimised blades

6. SUMMARY AND CONCLUSION

Active flow controllers such as trailing edge flaps and microtabs were proposed and developed for damping 1P-3P cyclic and stochastic loads on wind turbine blades. Their effectiveness in load alleviation and their potential in increasing the lifespan of blades were proven through a series of researches during the past decade. This paper explored the effectiveness of these devices in power enhancement at low winds and power regulation at high winds towards answering the issue of whether these devices can be used with the dual function of load and power control.

The constant-speed stall-regulated 300 kW AWT 27 wind turbine was adopted as the case for studying the effect of trailing edge flaps and microtabs on power enhancement at low winds and power regulation at high winds. In all cases, the pretwist of the blades was optimized to ensure that the full potential of active flow controllers is realized without increasing the cost and mass of the blade (except for the added cost or mass of the active flow controller itself). The optimization objective was taken as the annual average power (to be maximised) with constraints on power (for power regulation) and flap bending moment of the blades at root (to ensure that the mass of the optimized blade is not larger than the mass of the original blade). The following conclusions can be drawn from the results of these case studies:

- In both constant speed and variable speed rotors, adding flaps to the original blades without pretwist optimization has some positive effect on the power capture capability. However, this slight improvement comes at the cost of an increase in blade loading. Optimized blades equipped with flaps can increase the annual average power and reduce blade loading at the same time for both constant speed and variable speed rotors. The effect of power

enhancement is more visible on constant speed rotors, while load reduction is more significant for variable-speed rotors. In variable-speed rotors, since the dominant controlling parameter is the rotor speed, the effect of adding trailing edge flap on improving the energy capture capability is lower.

- For variable-speed generators, neither the position nor the size of flap affects the extracted power significantly. On the other hand, in the case of constant-speed generators, the position of flap along the blade span plays a key role in influencing the amount of improvement in the rotor power. At the examined positions, it was found that the best location for positioning a flap was at about 70 % of the blade span. The flap size is also found to have a significant effect on the average power enhancement. However, this effect is not linear and reduces significantly as the size of flap increases.
- Contribution of the pretwist optimization to enhancing the power capture capability in both constant-speed and variable-speed rotors is significant. Contribution of the blade optimization to variable-speed rotors is greater than that to constant speed rotors. Optimization has the highest effect on shorter flaps located towards the tip of the blade. This is due to the facts that the outer parts of the blade are aerodynamically more sensitive and that flow kinematics can be more optimized locally around shorter flaps.
- Flap is much more efficient than microtabs in power control. The baseline blades extract almost the same amount of power, with or without microtab. However, with an optimized pretwist, microtabs can improve the power produced by up to 4 %.

Most likely, more improvements could be made by removing some of the optimization constraints. For example, removing Constraint (5.g) $R_{F,e} - R_{F,s} \leq 0.05R$ allows the optimizer to explore the longer flaps. The addition of chord as a design variable in the optimization process needs conducting a cost analysis, but makes the design space more flexible and, therefore, provides a greater chance for finding superior solutions in terms of power enhancement and load reduction compared to the reported ones.

7. ACKNOWLEDGEMENT

This research has received no external funding.

NOMENCLATURE

AF	Aerofoil index
c	Chord length (m)
c_F	Chord length at flap location (m)
c_M	Chord length at microtab location (m)
C_D	Drag coefficient
C_L	Lift coefficient
C_M	Pitching moment coefficient
d_F	Flap width (m)
d_{MT}	Microtab distance from the leading edge (m)
h_{MT}	Microtab actuation height (m)
M_{flap}	Blade flapwise bending moment at root (Nm)
m_{blade}	Blade mass (kg)
pitch	Pitch angle (°)
P	Rotor power (W)
P_{av}	Site average power (W)
P_{rated}	Rated power (W)
R	Rotor radius (m); probability density function
$R_{F,e}$	Flap outboard radial location (m)
$R_{F,s}$	Flap inboard radial location (m)
$R_{MT,e}$	Microtab outboard radial location (m)
$R_{MT,s}$	Microtab inboard radial location (m)
r	Span location (m)
s_{MT}	Single microtab length (m)
t_{max}	Aerofoil maximum thickness (% of chord)
V	Wind speed at hub height (m/s)
V_i	Cut in wind speed (m/s)
V_o	Cut out wind speed (m/s)
V_{rated}	Rated wind speed (m/s)
Greek letters	
α	Angle of attack
β_0	Blade pretwist (°)
β_e	Blade elastic twist (°)
δ_F	Flap deployment angle (°)
φ	Inflow angle (°)
Ω	Rotor speed (rpm)
Subscripts	
F	Flap
l	Lower limit
MT	Microtab
opt	Optimum
origin	Original
u	Upper limit
Superscript	
*	Normalised

REFERENCES

1. Barlas, T.K. and van Kuik, G.A.M., "Review of state of the art in smart rotor control research for wind turbines", ***Progress in Aerospace Sciences***, Vol. 46, No. 1, (2010), 1-27. (https://doi.org/10.1016/j.paerosci.2009.08.002).
2. Yuan, Y. and Tang, J., "On advanced control methods toward power capture and load mitigation in wind turbines", ***Engineering***, Vol. 3, No. 4, (2017), 494-503. (https://doi.org/10.1016/J.ENG.2017.04.023).
3. Menezes, E.J.N., Araújo, A.M. and da Silva, N.S.B., "A review on wind turbine control and its associated methods", ***Journal of Cleaner Production***, Vol. 174, (2018), 945-953. (https://doi.org/10.1016/j.jclepro.2017.10.297).
4. Larsen, T.J., Madsen, H.A. and Thomsen, K., "Active load reduction using individual pitch, based on local blade flow measurements", ***Wind Energy***, Vol. 8, No. 1, (2005), 67-80. (https://doi.org/10.1002/we.141).
5. van Engelen, T.G., "Design model and load reduction assessment for multirotational mode individual pitch control (higher harmonics control)", ***Proceedings of European Wind Energy Conference***, Athens, (2006). (https://publicaties.ecn.nl/PdfFetch.aspx?nr=ECN-RX--06-068).
6. Johnson S.J., Baker J.P., van Dam, C.P. and Berg, D., "An overview of active load control techniques for wind turbines with an emphasis on microtabs", ***Wind Energy***, Vol. 13, No. (2-3), (2010), 239-253. (https://doi.org/10.1002/we.356).
7. Bæk, P., Gaunaa, M., Sørensen, N.N. and Fuglsang, P., "Comparative study of distributed active load control concepts for wind turbine blades", ***Proceedings of Science of Making Torque from Wind Conference***, Heraklion, Greece, (2010), 611-617. (https://doi.org/10.2514/6.2011-348).
8. Macquart, T., Maheri, A. and Busawon, K., "Microtab dynamic modelling for wind turbine blade load rejection", ***Renewable Energy***, Vol. 64, (2014), 144-152. (https://doi.org/10.1016/j.renene.2013.11.011).
9. Macquart, T. and Maheri, A., "Integrated aeroelastic and control analysis of wind turbine blades equipped with microtabs", ***Renewable Energy***, Vol. 75, (2015), 102-114. (https://doi.org/10.1016/j.renene.2014.09.032).
10. Macquart, T., Maheri, A. and Busawon, K., "A decoupling control strategy for wind turbine blades equipped with active flow controllers", ***Wind Energy***, Vol. 20, (2017), 569-584. (https://doi.org/10.1002/we.2024).
11. Chen, H. and Qin, N., "Trailing-edge flow control for wind turbine performance and load control", ***Renewable Energy***, Vol. 105, (2017), 419-435. (https://doi.org/10.1016/j.renene.2016.12.073).

12. Oltmann, N.C., Sobotta, D. and Hoffmann, A., "Load reduction of wind turbines using trailing edge flaps", ***Energy Procedia***, Vol. 136, (2017), 176-181. (https://doi.org/10.1016/j.egypro.2017.10.316).
13. Zhuang, C., Yang, G., Zhu, Y. and Hu, D., "Effect of morphed trailing-edge flap on aerodynamic load control for a wind turbine blade section", ***Renewable Energy***, Vol. 148, (2020), 964-974. (https://doi.org/10.1016/j.renene.2019.10.082).
14. Chen, Z.J., Stol, K.A. and Mace, B.R., "Wind turbine blade optimisation with individual pitch and trailing edge flap control", ***Renewable Energy***, Vol. 103, (2017), 750-765. (https://doi.org/10.1016/j.renene.2016.11.009).
15. Ebrahimi, A. and Movahhedi, M., "Wind turbine power improvement utilizing passive flow control with microtab", ***Energy***, Vol. 150, (2018), 575-582. (https://doi.org/10.1016/j.energy.2018.02.144).
16. Maheri, A., "Simulation of wind turbines utilising smart blades", ***Journal of Thermal Engineering***, Vol. 2, No. 1, (2016), 557-565. (https://doi.org/10.18186/jte.01522).
17. Maheri, A., "Multiobjective optimisation and integrated design of wind turbine blades using WTBM-ANSYS for high fidelity structural analysis", ***Renewable Energy***, Vol. 145, (2020), 814-834. (https://doi.org/10.1016/j.renene.2019.06.013).
18. Maheri, A., Noroozi, S., Toomer C. and Vinney, J., "WTAB, a computer program for predicting the performance of horizontal axis wind turbines with adaptive blades", ***Renewable Energy***, Vol. 31, No. 11, (2006), 1673-1685. (https://doi.org/10.1016/j.renene.2005.09.023).
19. Maheri, A., Noroozi, S., Toomer C. and Vinney, J., "Damping the fluctuating behaviour and improving the convergence rate of the axial induction factor in the BEMT-based rotor aerodynamic codes", ***Proceedings of European Wind Energy Conference and Exhibition 2006, EWEC (2006)***, Athens, Greece, Vol. 2, (2006), 1176-1179. (https://www.researchgate.net/publication/277016534_Damping_the_fluctuating_behaviour_and_improving_the_convergence_rate_of_the_axial_induction_factor_in_the_BEMT_based_rotor_aerodynamic_codes).
20. Macquart, T., Maheri, A. and Busawon, K., "Improvement of the accuracy of the blade element momentum theory method in wind turbine aerodynamics analysis", ***Proceedings of 2nd International Symposium on Environment Friendly Energies and Applications***, Newcastle, UK, (2012). (https://doi.org/10.1109/EFEA.2012.6294047).
21. Drela, M., "XFOIL: An analysis and design system for low Reynolds number airfoils", Low Reynolds number aerodynamics, Lecture notes in engineering, Mueller, T.J. (eds.), Springer, Berlin, Heidelberg, (1989). (https://web.mit.edu/drela/Public/papers/xfoil_sv.pdf).
22. Maheri, A., Macquart, T., Safari, D. and Maheri, M., "Phenotype building blocks and geometric crossover in structural optimisation", ***Proceedings of ECT2012: Eighth International Conference on Engineering Computational Technology***, Dubrovnik, Croatia, (2012). (https://doi.org/10.4203/ccp.100.51).
23. Kahwash, F. and Maheri, A., "A genetic algorithm for optimal distribution of aerofoils on wind turbine blades", ***Proceedings of 1st International Conference on Engineering of Tarumanagara (ICET 2013)***, Jakarta, (2013). (https://www.researchgate.net/publication/261285892).
24. Poore, R., "NWTC AWT-26 research and retrofit project -Summary of AWT-26/27 turbine research and development", NREL report NREL/SR-500-26926, (2000). (https://www.nrel.gov/docs/fy00osti/26926.pdf).
25. Wiratama, I.K. and Maheri, A., "Optimal design of wind turbine blades equipped with flaps", ***ARPN Journal of Engineering and Applied Sciences***, Vol. 9, No. 9, (2014), 1511-1515. (http://www.scopus.com/inward/record.url?eid=2-s2.0-84907258786&partnerID=MN8TOARS).

JREE: Vol. 9, No. 2, (Spring 2022) 27-36

Journal of Renewable Energy and Environment

Journal Homepage: www.jree.ir

Materials and Energy Research Center

MERC

Research Article

Dynamic Simulation of Solar-Powered Heating and Cooling System for an Office Building Using TRNSYS: A Case Study in Kerman

Hadi Farzan *

Department of Mechanical Engineering, Faculty of Engineering, Higher Education Complex of Bam, P. O. Box: 76615-314, Bam, Kerman, Iran.

PAPER INFO

Paper history:
Received: 18 October 2021
Revised in revised form: 18 December 2021
Scientific Accepted: 07 December 2021
Published: 05 March 2022

Keywords:
Solar-Powered Heating System,
Solar-Powered Cooling System,
Evacuated-Tube Collectors,
Energy Saving,
TRNSYS,
Transient Dynamics Simulation

ABSTRACT

Recently, novel techniques have been developed in building industries to use solar heating and cooling systems. The current study develops a Solar-powered Heating and Cooling (SHC) system for an office building in Kerman and assesses the transient dynamics of this system and office indoor temperature. To this end, TRNSYS simulation software is utilized to simulate system dynamics. The developed system comprises Evacuated-Tube solar Collectors (ETCs), heat storage tank, heat exchanger, circulating pumps, axillary furnace, cooling tower, single-effect absorption chiller, and air handling unit. The office indoor temperature is assessed in two scenarios, including commonly-insulated and well-insulated envelopes, while window awnings are used to prevent the sun from shining directly through the windows. The results illustrate that the SHC system can meet the thermal loads and provide thermal comfort in line with ASHRAE standards. The indoor temperature reaches 21 °C and 24 °C on cold winter and hot summer days by using the SHC system; however, without the SHC system, the indoor temperature experiences 15 °C and 34 °C on cold and hot days, respectively. The SHC system provides 45 °C and 15 °C supply air on cold and hot days to keep the indoor temperature in the desired range. A thermostat monitors the indoor temperature and saves energy by turning off the system when no heating or cooling is required. Furthermore, the ETCs can run the SHC system for a long time during daytime hours, but the axillary heater is still essential to work at the beginning of the morning.

https://doi.org/10.30501/jree.2021.310980.1272

1. INTRODUCTION

Buildings consume nearly 40 % of global energy, and this demand has grown dramatically in recent years. Since fossil fuels have been mainly used to meet this huge energy demand, policymakers have been encouraged to utilize green energy sources to improve sustainability and reduce greenhouse gas (GHG) emissions. Buildings consume approximately 35 % of total energy for Heating, Ventilation, and Air Conditioning (HVAC) systems; hence, renewable energy-driven HVAC systems can significantly affect and reduce required energy demands and improve building energy performance.

In 2008, the building sector in Iran accounted for 41.9 % of total energy demands, and this energy demand was mainly provided by utilizing fossil fuels, including natural gas 66 %, petroleum 20 %, electricity 2.5 %, and other sources 1.5 % [1]. Unfortunately, renewable energy sources do not effectively participate in meeting energy demands in this sector. However, Iran has great potential in renewable resources, especially solar energy, as the most affordable renewable energy source.

*Corresponding Author's Email: hadi.farzan@bam.ac.ir (H. Farzan)
URL: https://www.jree.ir/article_145858.html

Using renewable resources to run heating, cooling, and air condition systems is a sustainable approach that easily improves building efficiency [2]. However, building efficiency is enhanced by considering a complex system designed to provide a comfortable, safe, and attractive living and work environment and increase its performance. This crucial issue requires superior engineering designs such as using sustainable and easily accessible energy resources. The major area of energy consumption in buildings is HVAC systems, i.e., nearly 35 % of total building energy demand [3]. In this case, there are opportunities for improving energy performance by using solar-powered HVAC systems. Numerous literature studies have evaluated solar-powered HVAC systems in different technical, environmental, and economic terms [4]. Hobbi and Siddiqui [5] designed and evaluated a solar water heating system for a residential building in Montreal, Canada using TRNSYS. They optimized and sized the designed system components including collector array area, fluid type, and heat storage tank, while employing this approach helped them achieve a 54 % solar contribution to meeting demands. Monne et al. [6] evaluated the efficiency of a solar-powered cooling system consisting of a 37.5 m^2 flat plate collector and a 4.5 kW absorption chiller to obtain the impacts of cooling water temperature and generator driving temperature on the COP of used solar-powered chiller.

Please cite this article as: Farzan, H., "Dynamic simulation of solar-powered heating and cooling system for an office building using TRNSYS: A case study in Kerman", ***Journal of Renewable Energy and Environment (JREE)***, Vol. 9, No. 2, (2022), 27-36. (https://doi.org/10.30501/jree.2021.310980.1272).

Tashtoush et al. [7] performed a dynamics simulation of a solar ejector cooling system in Jordan by using TRNSYS. This study also optimized the cooling system components such as collector type and area; they concluded that 60-70 m^2 ETCs could meet the energy required for the 7.0 kW ejector cooling system. A review study [8, 9] represented a comprehensive review of various solar-powered systems with focus on Building-Integrated Solar Thermal systems (BISTs) and compared these systems with Building-Added (BA) installations. Safa et al. [10] simulated the performance of a Ground Source Heat Pump (GSHP) to obtain GSHPs performance curve versus building loads and evaluate the heat pump's efficiency at different source temperatures. Asim et al. [11] utilized TRNSYS software to simulate a solar-powered cooling system consisting of ETCs, a hot water storage tank, and an absorption chiller in Pakistan to maintain a typical room temperature at 26 °C. A research study conducted by Guillen-Lambea et al. [12] reviewed various strategies to meet cooling & heating demands in residential buildings in European countries and compared them with strategies used in the USA. This study used a model developed in TRNSYS for a dwelling and performed a simulation with different ventilation strategies and envelope transmittance in numerous countries in Europe and the USA.

Alibabaei et al. [13] developed a MATLAB-TRNSYS co-simulator to investigate the effectiveness of predictive strategy planning in energy cost saving in an HVAC system. These controlling strategies include load shifting and dual fuel switching systems. The simulation indicated that these strategies effectively optimized energy cost saving; however, they depended on the outdoor temperature. Ghaith [14] used a parabolic trough solar collector and an absorption chiller to meet the cooling load of a residential building in the UAE, and a bio-mass heater was used as an auxiliary heater. The obtained results showed that this hybrid system made a 30 % solar contribution in to its optimal configuration. Angrisani et al. [15] carried out a thermo-economic analysis of an SHC system for an office building in Italy. They developed a TRNSYS model to assess different solar panel technologies and collector areas. The obtained results demonstrated that the solar-powered system could reduce CO_2 emissions by up to 23 %. Antoniadis and Martinopoulos [16] used TRNSYS simulation software to calculate space heating load and annual domestic hot water need in a residential building in Greece. Furthermore, they optimized the designed heating system, and the optimal system obtained a seasonal solar fraction of 39 %. Jani et al. [17] investigated a drawback of traditional HVAC systems in humid climate conditions with high latent cooling loads. They proposed and analyzed a solid desiccant-assisted space cooling system using TRNSYS modeling to handle this problem and reduce energy consumption. The obtained results proved that the proposed system could provide a desirable thermal comfort. Wu and Skye [18] and Irfan et al. [19] investigated numerous scenarios used in the USA and subzero temperature areas for photovoltaic and HVAC systems and evaluated these strategies in different technical and economic aspects.

Several studies have analyzed solar-powered heating & cooling systems from an economic point of view in different climate conditions [20, 21]. Pirmohamadi et al. [22] developed an optimization algorithm to transform an existing office building into a zero-energy building using an efficient solar thermal system to reduce CO_2 emissions. They used TRNSYS and DesignBuilder simulation software to evaluate the feasibility of this conversion. Ahmed et al. [23] and Rosato et al. [24] carried out transient building energy simulations for a residential building in Canada and Italy. In these studies, they designed, optimized, and assessed these solar-powered systems from different technical viewpoints.

The current investigation utilizes TRNSYS simulation software to develop a numerical model and study the dynamics of an SHC system to meet heating & cooling loads for an office building in Kerman, Iran. Furthermore, this model investigates and analyzes the indoor office temperature in the presence or absence of the SHC system.

2. EXPERIMENTAL

The user in the current study is an office building whose schematic and floor plan are shown in Figure 1. The building modeling process was carried out in Sketch up software. This office is a four-story building with a 960 m^2 surface area and 48 working people. Window awnings are attached to the exterior walls of the building to prevent the sun from shining directly through the windows while still allowing natural light to pour through the windows. An air handling unit is utilized to meet heating & cooling loads in the building. Each floor is considered as a thermal zone to monitor indoor air temperature more precisely. The working hour is 8:00 to 16:00, and the office is closed on the weekends. The building envelope is thermally well insulated by polystyrene boards. The building envelope characteristics are shown in Table 1.

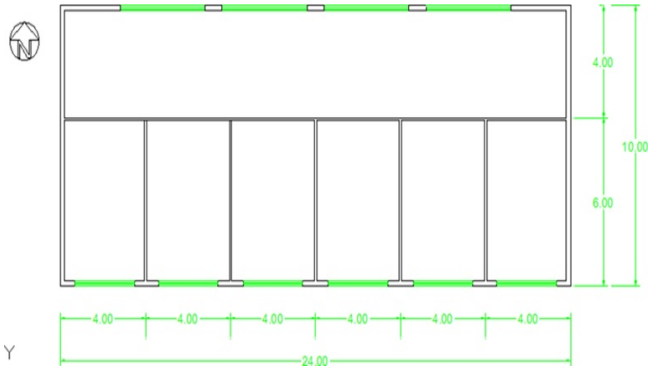

(a)

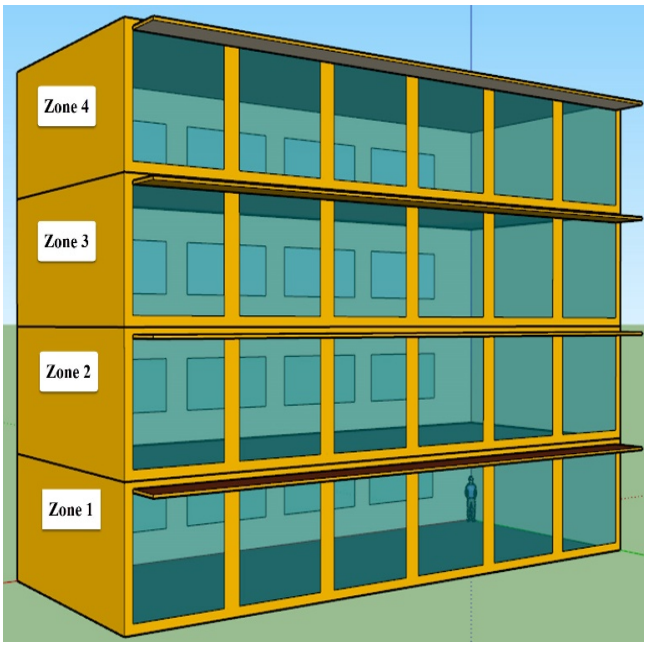

(b)

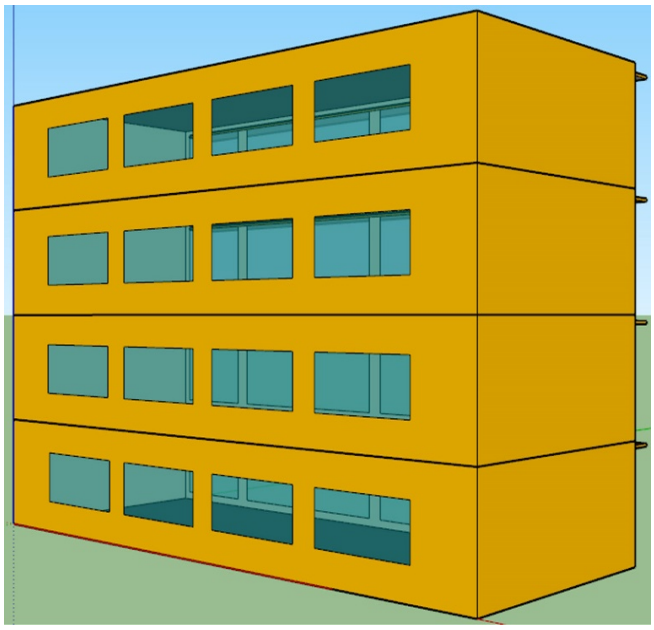

(c)

Figure 1. Building (a) floor plan and (b) south view (c) north view

Table 1. Main characteristics of building envelope

Insulation type	Envelope	U-value (W/m^{2}K)
Thermally well-Insulated envelope	External walls	0.501
	Internal walls	1.386
	Roof	0.497
	Floor	0.452
	Window	2.58

The people inside the office need fresh air. This air can be provided by infiltration or a designed HVAC system. The required air change rate for the people inside the building is assumed to be equal to 15 CFM per person, according to [27]. For this application, the required air change to satisfy ASHRAE standards is obtained nearly 720 CFM. The air infiltration depends on the wind velocity and is given as [25]:

$$\mathrm{ACH} = 0.07 v_w + 0.4 \quad (1)$$

where v_w is the wind velocity, and ACH defines the air change due to the infiltration.

The people working inside the office are seated and have a light activity. By assuming this scenario, the heat gain for a seated person is 400 Btu/hr and a total of 19200 Btu/hr [25]. Furthermore, each person has a personal PC, and the heat released to the space for each PC is equal to 100 W. ASHRAE handbook suggests a lighting power density of 1.11 W/ft^2 for office spaces [25].

The modeled office building is located in Kerman, Iran (30.2839° N, 57.0834° E). Kerman has hot arid climate conditions with an average elevation of 1755 m from the sea level. On average, July is the sunniest month with 329 hours of sunshine, and February has the lowest sunshine duration with 192 hours. The warmest month is July, with an average maximum temperature of 35 °C and the coldest month is January, with an average maximum temperature of 11 °C. Kerman has great potential in solar energy with the monthly average global solar radiation of 4.0 to 4.2 kW/m^2.day in winter and 7.0 to 7.3 kW/m^2.day in summer [26].

The heating and cooling loads were calculated using TRNSYS software considering internal gains (PCs, people, lightings), infiltration heat load, and solar radiation. The peak of heating and cooling loads is 455607 Btu/hr and 468702 Btu/hr, respectively.

3. SHC SYSTEM CONFIGURATION

Figures 2 and 3 show the schematic of the designed SHC system in the current study to satisfy heating & cooling demands and provide thermal comfort in the office building. It is worth noting that the TESS library was used in TRNSYS modeling. The developed SHC system is described as:

3.1. Solar heating system: The solar cooling system consists of the key components given as:

Evacuated tube solar collectors (Type 71): Type 71 simulates the transient thermal dynamics and efficiency of various ETCs. This type can consider ETCs in different parallel or series arrangements to obtain their performance and heat dynamics.

Storage tank (Type 4): This component models a stratified fluid-filled storage tank while the cold liquid enters the tank from the bottom side. The tank is divided into N sections with an equal volume to carry out the simulation. The N value determines the stratification degree. The current study assumes that the storage tank is well insulated to reduce heat loss to ambient environments.

Auxiliary heater (Type 700): The type simulates a fluid boiler and uses a user-defined set point temperature limited by the boiler capacity. The capacity defines heat amount delivered to fluid.

Shell & tube heat exchanger (Type 5): This component defines a shell & tube device. The performance of this type is achieved by determining inlet hot and cold fluid streams temperatures, their flow rates, and heat exchanger overall heat transfer coefficient.

Air handling unit (Type 752): Type 752 simulates a cooling or heating coil which cools or heats passing air stream. This component considers a bypass fraction required to obtain the outlet air temperature.

Mixing and diverting valves (Type 648): This component simulates an air plenum to determine the properties of leaving airflows mixed in the plenum.

Occupancy (Type 14): This type is a forcing function that defines a user-defined pattern that occurs several times throughout one cycle.

Building (Type 56): Type 56 models the thermal behavior of a building with several thermal zones.

3.2. Solar cooling system: The modeled cooling system has some auxiliary components compared to the heating system. These components are given as:

Single-effect absorption chiller (Type 909): Type 909 models a single-effect absorption chiller; based on data files containing the chiller performance in different operating scenarios.

Cooling tower (Type 126): This component estimates the dynamics of a cooling tower and uses weather data, inlet conditions, and overall heat transfer coefficient to calculate performance.

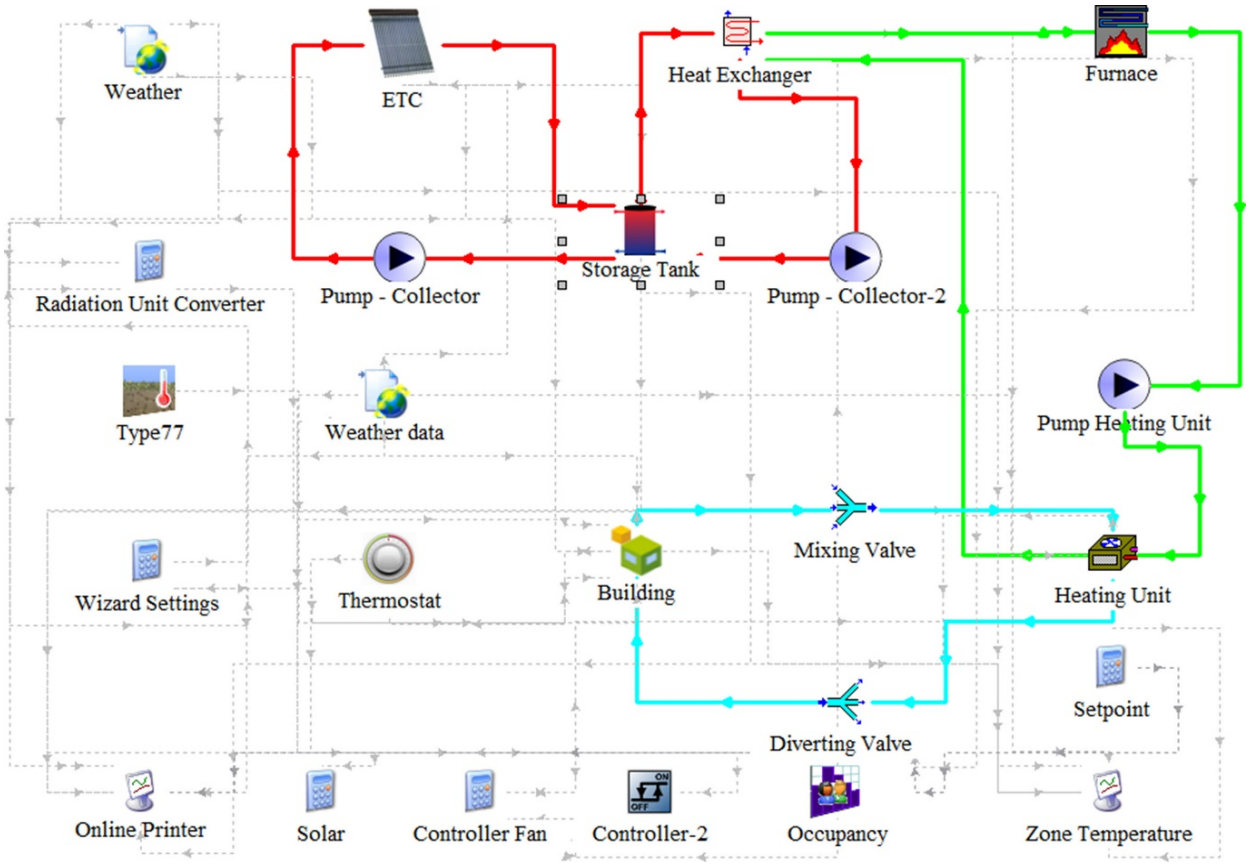

Figure 2. Schematic of the heating system in TRNSYS

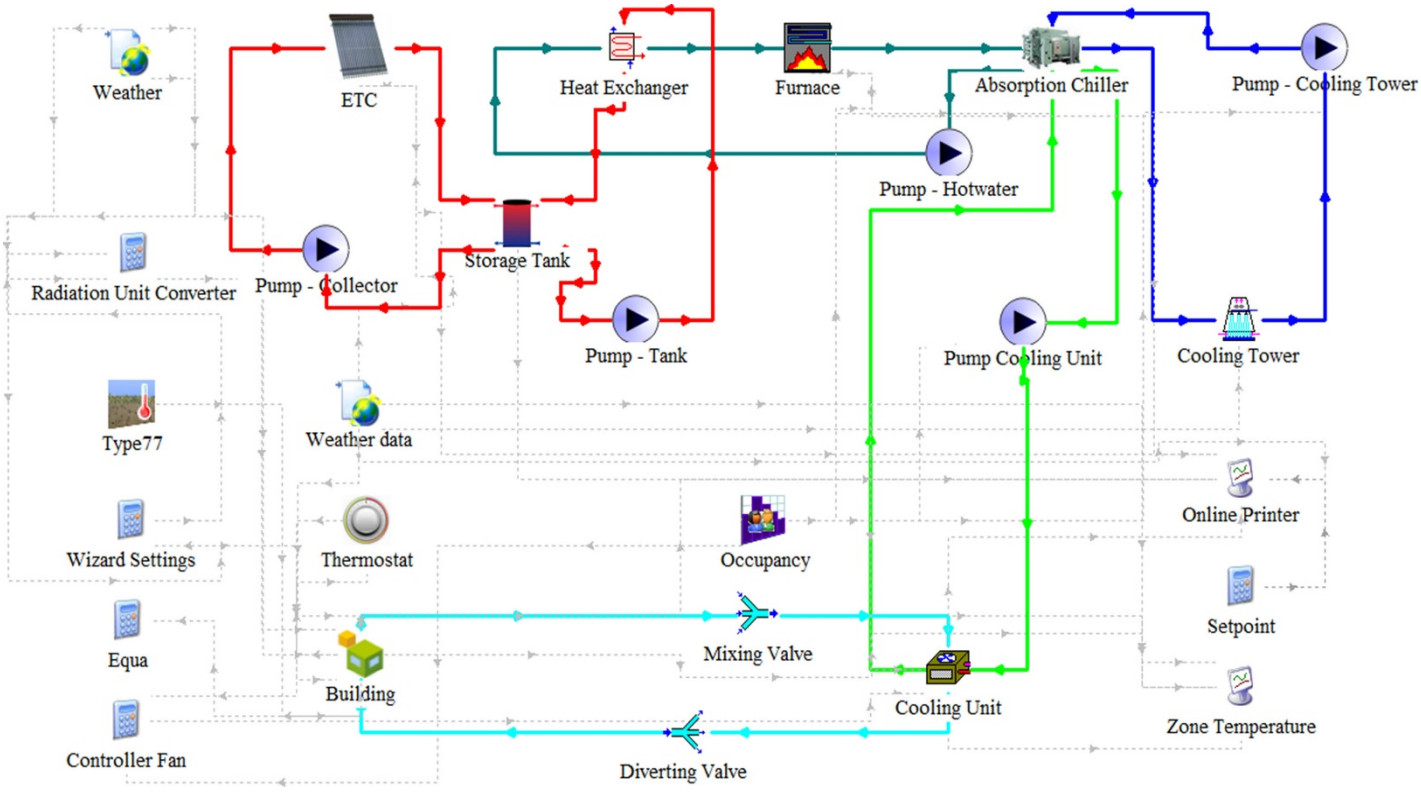

Figure 3. Schematic of the cooling system in TRNSYS

Table 2 shows the technical specifications of the used components in the SHC system. The installed thermostat monitors the indoor office temperature and controls the fan of the air handling unit during working hours. Using this strategy helps keep the indoor temperature in the thermal comfort temperature range and improve the system's energy efficiency. According to ASHRAE standards, the installed thermostat is set to 21 °C in winter and 24 °C in summer [25] with a 3 °C dead band.

Table 2. Main components of SHC system

System	Component	Technical specification	Value
Heating	Evacuated solar collector	Collector area array	200 m^2
	Storage tank	Volume	5 m^3
	Auxiliary furnace	Rated capacity	100 kW
		Setpoint temperature	90 °C
	Shell & tube heat exchanger	Overall heat transfer coefficient	500 W/K
Cooling	Evacuated solar collector	Collector area array	200 m^2
	Storage tank	Volume	5 m^3
	Auxiliary furnace	Rated capacity	100 kW
		Setpoint temperature	90 °C
	Shell & tube heat exchanger	Overall heat transfer coefficient	500 W/K
	Single effect absorption chiller	Rated capacity	50 TR
		COP	0.83
	Cooling tower	Rated capacity	90 tons

4. SHC SYSTEM DEESCRIPTION

In the heating system, the ETCs heat the circulating water-glycol mixture in the solar loop. The heat exchanger helps the heated water-glycol mixture transfers its heat content to the circulating water used in the air heating system. The used water-glycol mixture has a specific heat of 3.709 kJ/kg K and returns to the solar heating loop after heat exchange with the recirculating water in the air heating loop. The installed fan in the air handling unit has a design capacity of 45000 CFM. Furthermore, the outside air damper position is 10 % open to supply outside fresh air to the office. This heated air is carried and distributed equally in each thermal zone.

Same as the heating system, the ETCs produce a hot water flow stream used in the generator of the single effect absorption chiller to provide refrigeration. The chilled water is recirculating in the coils installed in the air handling unit and cools the supply air. As for the heating system, the outside damper position is 10 % open, and the cooled supply air is carried to the office space.

The thermostat monitors the indoor office temperature, and a forcing function named occupancy defines the working hours or people's presence inside the building. These two factors, including thermal comfort temperature range and people presence, serve as inputs to a control system that turns on/off the fan of the air handling unit. This strategy helps improve energy-saving costs by turning off the SHC system when the indoor temperature is in the desired range and no heating or cooling is required.

Since the building is exposed to cold ambient temperature on winter days, the indoor temperature may be so cold and intolerable for people starting to work in the morning. A strategy used on cold winter days is that the system is turned on one hour sooner. This strategy helps the indoor temperature reach thermal comfort temperature as soon as possible.

5. SIMULATION RESULTS AND DISCUSSION

The current study simulates the transient dynamics of the developed SHC system and indoor temperature for an office building located in arid hot climate conditions in Kerman, Iran. The weather conditions play a key role in the dynamics of an SHC system; hence, Figure 4 shows outdoor temperature and solar radiation intensity variations in February 1st and July 1st. The data shown in Figure 4 were obtained using a synoptic weather station in Kerman; however, the simulations were carried out utilizing Meteonorm software. The measured weather data have good agreement with the simulated one. Furthermore, February 1st and July 1st are assumed as the sample cold and hot days to perform simulation and investigate the transient dynamics of the SHC system and indoor office temperature.

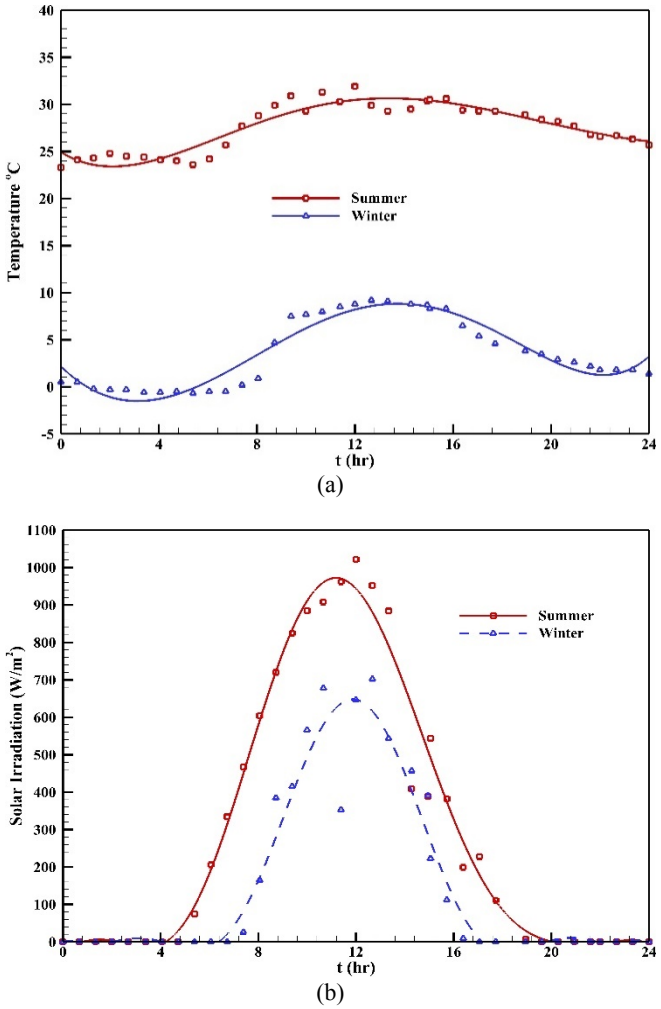

Figure 4. (a) outdoor air temperature and (b) solar intensity in February 1st and July 1st in Kerman

Figure 5 shows the transient dynamics of the indoor office temperature on the considered cold winter day when no heating system is used. As seen in Figure 5, the indoor temperature decreases during the cold night, while the building interacts with a cold ambient and the heating system is off. These two factors are the reaons why the indoor temperature reaches nearly 7 °C at 7 A.M. During daytime hours, the building is exposed to incoming solar radiation and internal gains. Hence, the indoor temperature starts to grow to nearly 15 °C at 4 P.M. The indoor temperature is still so far from the desired thermal comfort temperature without using the heating system.

It is interesting to note that the fourth floor (fourth thermal zone) has the worst condition, and its indoor temperature is the lowest on cold winter days. However, the building is well-insulated, but the fourth floor is adjacent to the roof that is exposed to the cold outside air. This issue results in increase in heat losses from the fourth floor to the outside, and its indoor temperature drastically decreases compared to the other thermal zones.

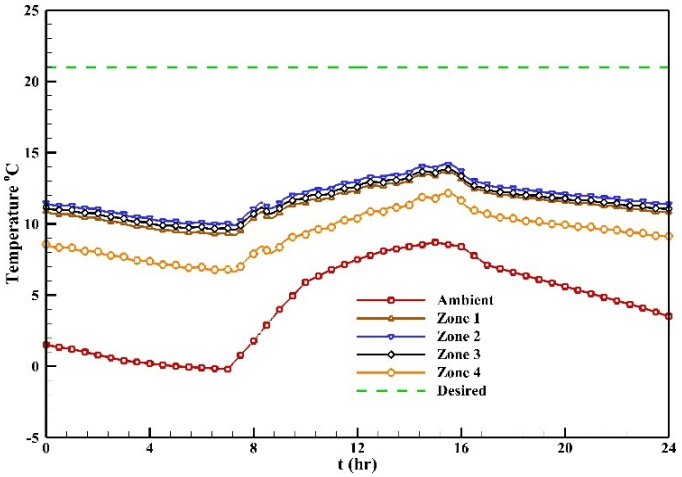

Figure 5. Transient dynamics of the indoor office temperature without using heating system

Figure 6 shows the transient dynamics of the indoor office temperature using the heating system. Figure 6 illustrates that the heating system can meet the required heating demands on cold winter days and maintain the indoor temperature in the desired range during long working hours. It is clear that the thermostat turns on and off the fan during the daytime hours. This factor causes the heating system to turn off when heating is not required and to save energy. On the other hand, the considered occupancy forcing function turns the heating system off when the people are not present in the office after 4 P.M.

The indoor office temperature is a function of the energy saved in the envelope mass and ambient temperature when the heating system is off. After 4 P.M., the indoor temperature is reduced due to interaction with cold environments. However, the indoor temperature is still higher than the outside air. Indeed, the energy is saved in the envelope mass during the period that the heating system is on. This saved energy releases and heats the indoor temperature when the heating system is off.

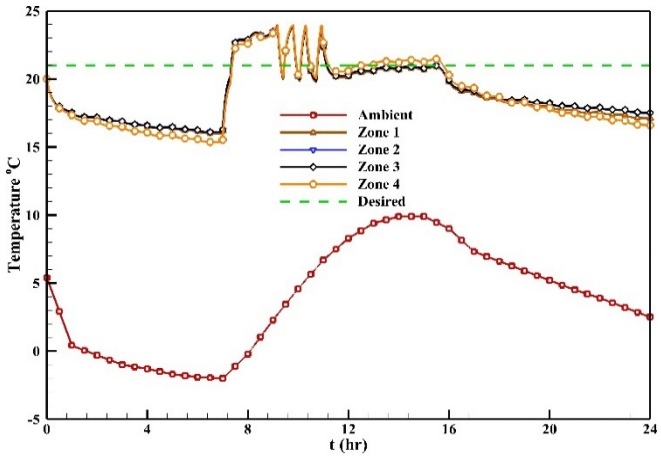

Figure 6. Transient dynamics of the indoor office temperature using heating system

Figure 7 represents the transient dynamics of the heating system. As seen in Figure 7, the collector outlet temperature increases in the beginning of the morning and reaches nearly 70 °C at noon. The collector outlet temperature remains maximum until 15:30 and, then, reduces when the solar intensity approaches zero. Furthermore, since the collector outlet is at its maximum temperature for approximately 8 hours, it provides this opportunity to use maximum solar energy during daytime hours.

In addition, Figure 7 shows the tank outlet temperature profile toward the heat source (ETCs). It shows that hot water-glycol inside the tank exchanges its heat content in the heat exchange with the recirculating water in the air heating system and its temperature reduces. Hence, it returns toward ETCs with a lower temperature. Since the solar intensity is too insufficient to heat water-glycol in the beginning of the morning at 7:00 A.M., the tank loses its heat content faster and its outlet temperature reduces in a steeper gradient. However, this trend is changed by increasing the solar intensity and the tank outlet temperature starts to increase after nearly 9:00 A.M.

The supply air temperature leaving the air handling unit is also shown in Figure 7. It is implied that the fan runs continuously to supply hot air to the office until noon due to the cold outside weather conditions. The thermostat turns off the fan sometimes in the afternoon since the indoor air temperature is in the desired thermal comfort range. The supply air temperature leaving the air handling unit reaches nearly 50 °C during the periods that the fan is working. During the times that the office is closed, the supply air temperature is near outside air temperature.

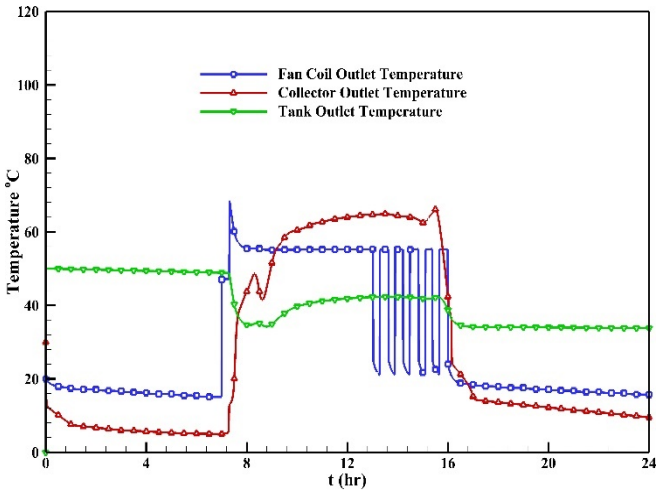

Figure 7. Transient dynamics of the heating system

Figure 8 shows the transient dynamics of the indoor temperature on the considered hot summer day without using the cooling system. During the daytime hours, the building is exposed to high solar intensity, and the internal heat gains release heat to the space. Therefore, the indoor office temperature increases during daytime hours. However, the indoor temperature reduces in the evening when the solar intensity is negligible or absent, and the people are not present in the office. Like on the considered cold winter day, the fourth floor has the hottest indoor temperature due to the interaction with the hot outside temperature through the roof exposure.

Since the building envelope is exposed to the solar intensity, the thermal energy is saved in the envelope. This energy

releases in the evening and keeps the indoor temperature higher than the outside air temperature.

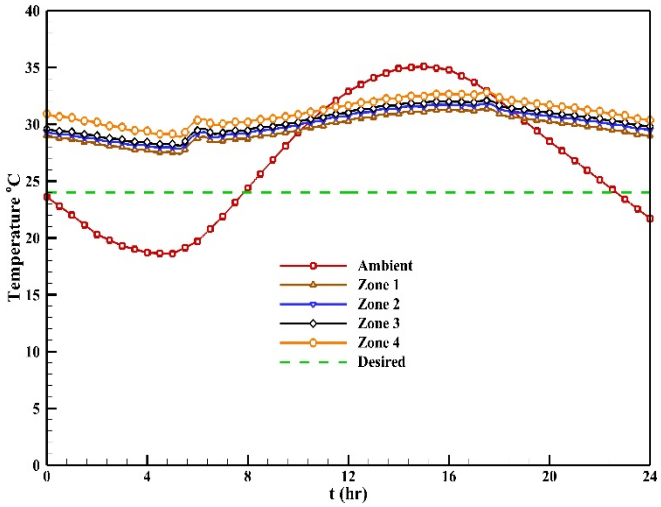

Figure 8. Transient dynamics of the indoor office temperature without using cooling system

Figure 9 represents the indoor temperature variation on the considered hot summer day using the cooling system. Using the cooling system results in keeping the indoor temperature in the desired thermal comfort range. As discussed in the heating system analysis, the thermostat monitors the indoor temperature and sends a control signal to turn the cooling unit fan on or off. The cooling air is supplied to the space by turning on the fan, reducing the indoor temperature, and satisfying the cooling load. As the people exit the office in the evening, the forced occupancy function turns off the fan and the indoor temperature grows in the absence of the cooling system.

Interestingly, since the cooling system meets the thermal loads during daytime hours, the office experiences lower indoor temperatures in the evening than the scenario where no cooling system is used.

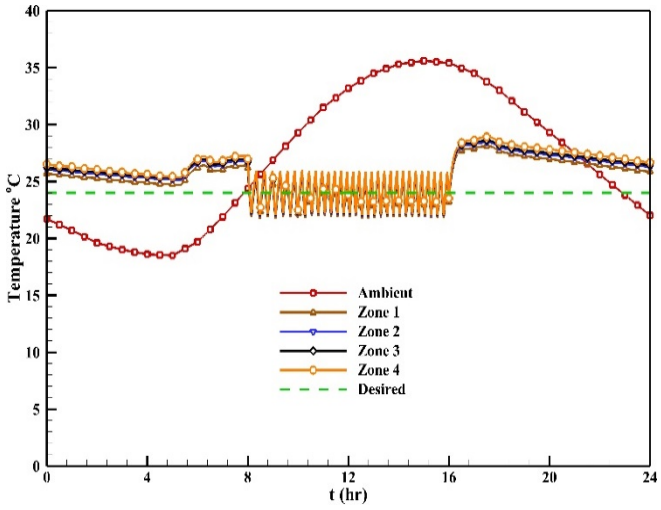

Figure 9. Transient dynamics of the office indoor temperature using cooling system

Figure 10 depicts the transient dynamics of the cooling system. This figure shows the ETCs outlet temperature, storage tank outlet temperature toward the ETCs, and supply air leaving the air handling unit. The ETCs outlet temperature grows in the beginning of the morning and increases the solar intensity. This temperature reaches up to nearly 100 °C at noon and reduces in the evening by reducing the solar intensity. This hot water-glycol mixture is used to heat the recirculating hot water that runs the single-effect absorption chiller. Fortunately, the high solar intensity in Kerman results in a high-temperature water-glycol mixture and, consequently, recirculates the hot water used in the refrigeration cycle. The hotter the recirculating water, the higher the COP. The tank outlet temperature has the same trend as the ETCs outlet temperature. However, the difference between the tank and the ETCs outlet temperatures implies the amount of thermal energy delivered to the recirculating water in the heat exchanger. When the solar intensity is low in the beginning of the morning, the auxiliary furnace must heat the recirculating hot water in the refrigeration cycle.

The supply air temperature profile shows that the fan works in specific periods when the thermostat sends an ON signal. This important issue shows the significant impact of the installed thermostat on saving energy and controlling the indoor temperature in the desired temperature range. When the fan is working, the supply air temperature is nearly 12 °C, which is a suitable temperature for cooling a space.

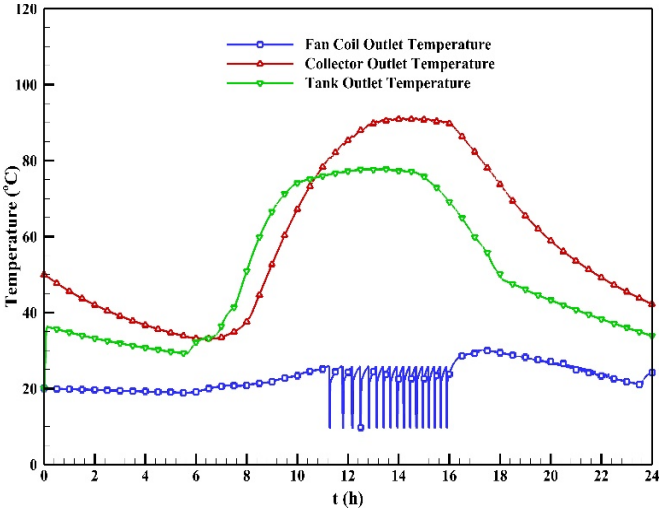

Figure 10. Transient dynamics of cooling system

Building insulation is an affordable approach to optimizing energy consumption in a building and minimizing its heat exchange with its hot or cold ambient. Since insulation materials have low thermal conductivity, the conduction heat exchange with the outside environment through building envelopes reduces drastically. Hence, the energy consumed to provide thermal comfort will be saved. Table 3 shows the main characteristics of the building envelope in the commonly-insulated scenario.

Table 3. Main characteristics of commonly-insulated envelope

Insulation type	Envelope	U-value (W/m^{2}K)
Thermally commonly-insulated envelope	External walls	1.567
	Internal walls	1.732
	Roof	1.654
	Floor	1.234
	Window	2.58

This section analyzes the effects of building envelope characteristics on the transient dynamics of indoor office temperature. To this end, a commonly insulated building is

considered, while the size and configuration of the SHC system are the same as those in the scenario discussed in the previous sections. Figure 11 shows the transient indoor temperature on a cold day when a commonly insulated envelope is used. According to Figure 11, the indoor temperature is far from the desired setpoint in the beginning of working hours, and this situation lasts till noon. Interestingly, the internal gains and solar radiation on the building surface help the indoor temperature increase during daytime hours in this scenario, but the thermostat does not turn off the heating system. This issue proves that the cold outside temperature can easily affect the indoor temperature due to unsuitable insulation. Great heat losses through the building envelope cause the indoor temperature to slowly reach the desired set point compared to the scenario with the well-insulated envelope (Figure 6). Furthermore, the indoor temperature decreases drastically by turning off the SHC system and approaching outside temperature due to heat conduction through the building envelope.

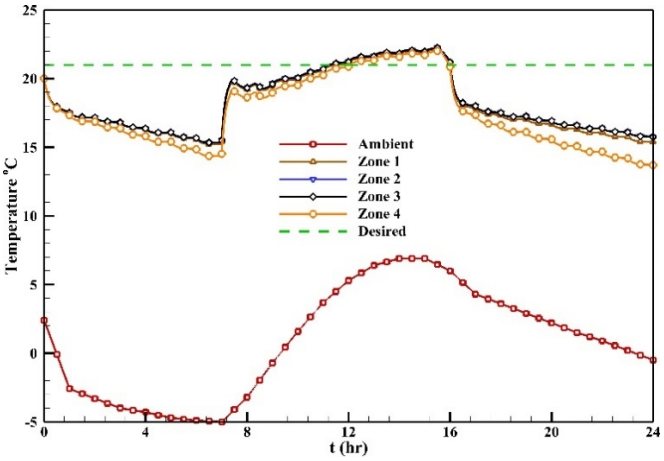

Figure 11. Transient dynamics of the indoor office temperature using heating system with commonly-insulated envelope

Figure 12 shows the indoor temperature on a hot summer day when a commonly insulated envelope is used. The indoor temperature in the commonly insulated building is higher than that in the well-insulated building in the beginning of the morning. Hence, the SHC system needs to meet higher cooling loads at 8:00 A.M. when the system turns ON. Since the simulation was carried out on hot arid climate conditions, the outdoor temperature would decrease drastically at night. Therefore, the energy saved in the envelope mass during daytime hours causes the indoor temperature not to change remarkably at night. Then, the system can start on summer mornings more easily than on winter mornings with severe cold conditions at night.

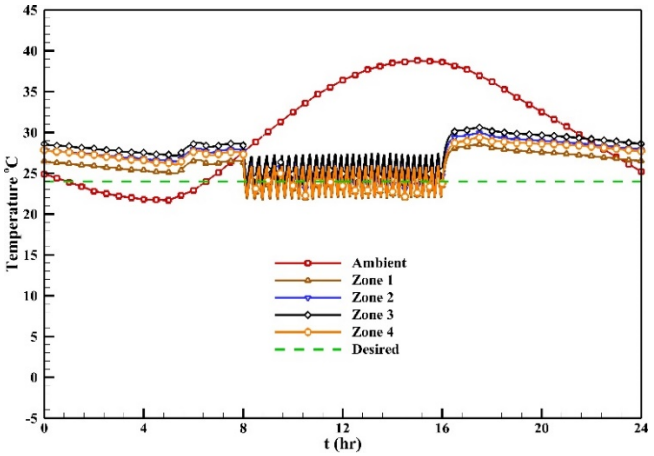

Figure 12. Transient dynamics of the indoor office temperature using cooling system with commonly-insulated envelope

Table 4 represents a brief comparison between the current and previous studies. These studies assessed the indoor temperature dynamics when an SHC system was used to provide thermal comfort in a building. Each study investigated a crucial factor that affected the indoor temperature dynamics of a building. Like the current study, these investigations illustrate that SHC systems can promisingly meet the required thermal load and maintain the zones temperatures in the desired temperature range.

Table 4. Brief comparison between available studies

Reference	Method	SHC system type	Target
Alibabaei et al. [13]	Numerical approach using MATLAB-TRNSYS co-simulator	Solar-powered heating system	Investigation on effectiveness of different predictive strategy planning models in Canada
Rosato et al. [24]	Numerical approach using TRNSYS software	A centralized solar hybrid heating and cooling system	Study on performance of proposed system from energy, environmental and economic points of view in Italy
Altun and Kilic [21]	Numerical approach using TRNSYS software	Solar-powered absorption cooling system	Investigation on performance of cooling system in different climate conditions in Turkey
Figaj and Zoladek [20]	Experimental and Numerical approach	Solar-powered heating & cooling system	Study on solar contribution in heating and cooling in Poland

6. CONCLUSIONS

Nowadays, fossil fuels are consumed mainly to meet energy demands in buildings. However, this approach is beginning to change toward using renewable resources due to the global warming crisis. Recently, novel techniques have been developed to use renewable energy for meeting heating & cooling requirements, which are the major energy consumers in buildings. Iran has great potential in solar energy that

provides an opportunity to convert incoming solar energy to heating & cooling energy. This study investigated the possibility of using solar energy to meet heating & cooling loads in an office building in Kerman with hot arid climate conditions. The transient simulation software, TRNSYS, was used to carry out the simulation and evaluate the transient dynamics of the indoor building temperature and SHC system. The obtained results demonstrated that:

- The indoor air temperature without a heating & cooling system was far from the desired thermal comfort range.
- The indoor office temperature was a function of outside air temperature and envelope mass without using heating & cooling systems. The energy saved in the building envelope was released during the afternoon and affected indoor temperature.
- The solar-powered heating system could meet the heating load in the office building and provide thermal comfort conditions.
- The maximum ETCs and storage tank outlet temperature on cold winter days reached nearly 70 °C and 50 °C, respectively. On the other hand, due to higher solar intensity on hot summer days, the maximum outlet temperature of the ETCs and storage tank reached nearly 100 °C and 80 °C, respectively.
- Indoor temperature specified whether the occupant thermal comfort would be satisfied or not. When no heating or cooling system is used, the indoor temperature is far from the desired temperature on cold winter or hot summer days. In this case, during working hours, the indoor temperature reaches nearly 15 °C on cold winter days and 34 °C on hot summer days.
- Using the SHC system caused the indoor temperature to be in the desired range during working hours. In this case, the indoor temperature oscillated between 20 °C to 24 °C and 23 °C to 27 °C on cold winter and hot summer days.
- The supply air temperature leaving the air handling unit is a suitable range using the developed SHC system. The supply air temperature was nearly 50 °C and 12 °C on cold winter and hot summer days, respectively.
- An axillary furnace was required in the solar-powered heating system when the solar intensity was low in the beginning of the morning.
- The solar-powered cooling system met the cooling load in the office building. However, in the beginning of the morning, the axillary furnace must heat hot water in the refrigeration cycle.
- The thermostat is an affordable approach to monitoring the indoor temperature and control the SHC system. The thermostat saves energy by turning the air handling unit off when the indoor temperature is in the desired temperature range.
- The thermostat assists the indoor temperature to be in the desired range according to the ASHRAE standard (21 °C in winter and 24 °C in summer) and provide thermal comfort in the office.
- A suitable dead band for the thermostat helps the indoor temperature oscillate within the thermal comfort temperature range and increase the lifecycle of the SHC system.
- Suitable envelope insulation helps the indoor temperature reach the desired temperature sooner and remain in this range for a longer period.
- In arid climate conditions, the outside temperature decreases drastically at night, especially in cold winters. In the commonly insulated building, the indoor temperature is significantly affected by the outdoor conditions at night.
- In the commonly insulated building, the indoor temperature is far from the desired setpoint in the beginning of the morning. In this case, the indoor temperature reaches 21 °C (setpoint temperature) at noon. This issue illustrates the remarkable effects of the building's heat exchange with surroundings through its envelope.

7. ACKNOWLEDGEMENT

The authors appreciatively acknowledge the Research Council of the Higher Education Complex of Bam.

REFERENCES

1. Riazi, M. and Hosseyni, S., "Overview of current energy policy and standards in the building sector in Iran", ***Sustainable Development and Planning V***, Vol. 150, (2011), 189-200. (http://doi.org/10.2495/SDP110171).
2. Farzan, H., "The study of thermostat impact on energy consumption in a residential building by using TRNSYS", ***Journal of Renewable Energy and Environment (JREE)***, Vol. 6, No. 1, (2019), 15-20. (http://doi.org/10.30501/jree.2019.95531).
3. "An assessment of energy technologies and research opportunities", ***Quadrennial Technology Review***, United States Department of Energy, (2015). (https://energy.gov/sites/prod/files/2015/09/f26/Quadrennial-Technology-Review-2015_0.pdf).
4. Bellos, E., Tzivanidis, C., Kouvari, A. and Antonopoulos, K.A., Comparison of heating and cooling loads of a typical building with TRNSYS and Equest", Energy, Transportation and Global Warming, Green Energy and Technology, Springer, (2016), 327-338. (http://doi.org/10.1007/978-3-319-30127-3_25).
5. Hobbi, A. and Siddiqui, K., "Optimal design of a forced circulation solar water heating system for a residential unit in cold climate using TRNSYS", ***Solar Energy***, Vol. 83, No. 5, (2009), 700-714. (http://doi.org/10.1016/j.solener.2008.10.018).
6. Monné, C., Alonso, S., Palacín, F. and Serra, L., "Monitoring and simulation of an existing solar powered absorption cooling system in Zaragoza (Spain)", ***Applied Thermal Engineering***, Vol. 31, No. 1, (2011), 28-35. (http://doi.org/10.1016/j.applthermaleng.2010.08.002).
7. Tashtoush, B., Alshare, A. and Al-Rifai, S., "Hourly dynamic simulation of solar ejector cooling system using TRNSYS for Jordanian climate", ***Energy Conversion and Management***, Vol. 100, (2015), 288-299. (http://doi.org/10.1016/j.enconman.2015.05.010).
8. Lamnatou, C., Mondol, J.D., Chemisana, D. and Maurer, C., "Modelling and simulation of building-integrated solar thermal systems: Behaviour of the coupled building/system configuration", ***Renewable and Sustainable Energy Reviews***, Vol. 48, (2015), 178-191. (http://doi.org/10.1016/j.rser.2015.03.075).
9. Lamnatou, C., Mondol, J.D., Chemisana, D. and Maurer, C., "Modelling and simulation of building-integrated solar thermal systems: Behaviour of the system", ***Renewable and Sustainable Energy Reviews***, Vol. 45, (2015), 36-51. (http://doi.org/10.1016/j.rser.2015.01.024).
10. Safa, A.A., Fung, A.S. and Kumar, R., "Heating and cooling performance characterisation of ground source heat pump system by testing and TRNSYS simulation", ***Renewable Energy***, Vol. 83, (2015), 565-575. (http://doi.org/10.1016/j.renene.2015.05.008).
11. Asim, M., Dewsbury, J. and Kanan, S., "TRNSYS simulation of a solar cooling system for the hot climate of pakistan", ***Energy Procedia***, Vol. 91, (2016), 702-706. (http://doi.org/10.1016/j.egypro.2016.06.233).

12. Guillén-Lambea, S., Rodríguez-Soria, B. and Marín, J.M., "Review of european ventilation strategies to meet the cooling and heating demands of nearly zero energy buildings (NZEB)/passivhaus, Comparison with the USA", ***Renewable and Sustainable Energy Reviews***, Vol. 62, (2016), 561-574. (http://doi.org/10.1016/j.rser.2016.05.021).
13. Alibabaei, N., Fung, A.S. and Raahemifar, K., "Development of Matlab-TRNSYS co-simulator for applying predictive strategy planning models on residential house HVAC system", ***Energy and Buildings***, Vol. 128, (2016), 81-98. (http://doi.org/10.1016/j.enbuild.2016.05.084).
14. Ghaith, F.A., "Performance of solar powered cooling system using parabolic trough collector in UAE", ***Sustainable Energy Technologies and Assessments***, Vol. 23, (2017), 21-32. (http://doi.org/10.1016/j.seta.2017.08.005).
15. Angrisani, G., Entchev, E., Roselli, C., Sasso, M., Tariello, F. and Yaïci, W., "Dynamic simulation of a solar heating and cooling system for an office building located in Southern Italy", ***Applied Thermal Engineering***, Vol. 103, (2016), 377-390. (http://doi.org/10.1016/j.applthermaleng.2016.04.094).
16. Antoniadis, C.N. and Martinopoulos, G., "Optimization of a building integrated solar thermal system with seasonal storage using TRNSYS", ***Renewable Energy***, Vol. 137, (2019), 56-66. (http://doi.org/10.1016/j.renene.2018.03.074).
17. Jani, D., Mishra, M. and Sahoo, P., "Performance analysis of a solid desiccant assisted hybrid space cooling system using TRNSYS", ***Journal of Building Engineering***, Vol. 19, (2018), 26-35. (http://doi.org/10.1016/j.jobe.2018.04.016).
18. Wu, W. and Skye, H.M., "Net-zero nation: HVAC and PV systems for residential net-zero energy buildings across the united states", ***Energy Conversion and Management***, Vol. 177, (2018), 605-628. (http://doi.org/10.1016/j.enconman.2018.09.084).
19. Irfan, M., Abas, N. and Saleem, M.S., "Thermal performance analysis of net zero energy home for sub zero temperature areas", ***Case Studies in Thermal Engineering***, Vol. 12, (2018), 789-796. (http://doi.org/10.1016/j.csite.2018.10.008).
20. Figaj, R. and Żołądek, M., "Experimental and numerical analysis of hybrid solar heating and cooling system for a residential user", ***Renewable Energy***, Vol. 172, (2021), 955-967. (http://doi.org/10.1016/j.renene.2021.03.091).
21. Altun, A. and Kilic, M., "Economic feasibility analysis with the parametric dynamic simulation of a single effect solar absorption cooling system for various climatic regions in Turkey", ***Renewable Energy***, Vol. 152, (2020), 75-93. (http://doi.org/10.1016/j.renene.2020.01.055).
22. Pirmohamadi, A., Dastjerdi, S.M., Ziapour, B.M., Ahmadi, P. and Rosen, M.A., "Integrated solar thermal systems in smart optimized zero energy buildings: Energy, environment and economic assessments", ***Sustainable Energy Technologies and Assessments***, Vol. 48, (2021), 101580. (http://doi.org/10.1016/j.seta.2021.101580).
23. Ahamed, M.S., Guo, H. and Tanino, K., "Modeling heating demands in a Chinese-style solar greenhouse using the transient building energy simulation model TRNSYS", ***Journal of Building Engineering***, Vol. 29, (2020), 101114. (http://doi.org/10.1016/j.jobe.2019.101114).
24. Rosato, A., Ciervo, A., Guarino, F., Ciampi, G., Scorpio, M. and Sibilio, S., "Dynamic simulation of a solar heating and cooling system including a seasonal storage serving a small Italian residential district", ***Thermal Science***, Vol. 24, (2020). (http://doi.org/10.2298/TSCI200323276R).
25. Handbook-Fundamentals, ASHRAE Inc., (2011). (https://www.ashrae.org/technical-resources/ashrae-handbook).
26. Edalati, S., Ameri, M. and Iranmanesh, M., "Estimating and modeling monthly mean daily global solar radiation on horizontal surfaces using artificial neural networks in South East of Iran", ***Journal of Renewable Energy and Environment (JREE)***, Vol. 2, No. 1, (2015). 41-47. (http://dx.doi.org/10.30501/jree.2015.70063).

JREE: Vol. 9, No. 2, (Spring 2022) 37-48

Journal of Renewable Energy and Environment

Journal Homepage: www.jree.ir

Materials and Energy Research Center

MERC

Research Article

Analytical Approach to Exploring the Missing Data Behavior in Smart Home Energy Consumption Dataset

Kasaraneni Purna Prakash [a], Yellapragada Venkata Pavan Kumar [b*]

[a] School of Computer Science and Engineering, VIT-AP University, Amaravati-522237, Andhra Pradesh, India.
[b] School of Electronics Engineering, VIT-AP University, Amaravati-522237, Andhra Pradesh, India.

PAPER INFO

Paper history:
Received: 04 November 2021
Revised in revised form: 04 December 2021
Scientific Accepted: 12 December 2021
Published: 07 March 2022

Keywords:
Behavior Analysis,
Data Analysis,
Energy Consumption Data,
Missing Data Anomalies,
Smart Homes,
Smart Meter Data

ABSTRACT

Smart homes are considered to be the subset of smart grids that have gained widespread popularity and significance in the present energy sector. These homes are usually equipped with different kinds of sensors that communicate between appliances and the metering infrastructure to monitor and trace the energy consumption details. The smart meters trace the energy consumption data continuously or in a period of intervals as required. Sometimes, these traces will be missed due to errors in communication channels, an unexpected breakdown of networks, malfunctioning of smart meters, etc. This missingness greatly impacts smart home operations such as load estimation and management, energy pricing, optimizing assets, planning, decision making, etc. Moreover, to implement a suitable precautionary measure to eliminate missing of data traces, it is required to understand the past behavior of the data anomalies. Hence, it is essential to comprehend the behavior of missing data in the smart home energy consumption dataset. In this regard, this paper proposes an analytical approach to detect and quantify the missing data instants in all days for all appliances. Using this quantification, the behavior of missing data anomalies is analyzed during the day. For the analysis, a practical smart home energy consumption dataset 'Tracebase' is considered. Initially, the existence and the count of missing instants are computed. From this, the appliance 'MicrowaveOven' is considered for further analysis as it comprises the highest count of missing instants (84740) in a day when compared to all other appliances. Finally, the proposed analysis reveals that the large number of missing instants is occurring during the daylight period of a day.

https://doi.org/10.30501/jree.2021.313536.1277

1. INTRODUCTION

In recent years, smart homes have become very popular and grabbed the attention of people around the world. Smart homes provide access to a modern style of living with greater comfort and security. Besides, smart homes enable control over the appliance functionality, energy usage, billing, etc. Hence, the consumers are ready to avail the benefits of smart homes and make their homes automated. This automation includes different kinds of sensors, communication channels, computer-controlled equipment, etc., which are formed as a controlled network. This installed equipment captures the energy consumption data 24 × 7 from all the appliances connected in a smart home. The analysis of this data is essential to understanding the functionality of appliances. For this purpose, the availability of high-quality data is always desired. But, the data capturing process is often associated with certain anomalies due to several problems and failures in the power and communication networks. Among such anomalies, missing data records is a major issue, which deludes the analysis and decision-making about energy consumption.

There are several literature works available on the analysis of smart home datasets and detection of various anomalies present in it, as described in Table 1. All these state-of-the-art literature works can be segregated as works related to general concepts, complexities, challenges, and advancements in smart homes; IoT role in the smart home application; smart home environment, technology, and energy management; data analytics in smart grids/homes; data anomalies and their detection. As per the description provided in Table 1 on these works, it is clearly understood that all these works represent the preliminary requirements or supports for the smart home deployments. Further, in the context of data anomalies and missing data, conventional works have focused on identification, preprocessing, and visualization. These approaches help to rectify the data anomalies, thereby improving the data quality.

Along with the preprocessing methods available in the literature, it is also important to have some precautionary measures to avoid data quality issues. To identify the cause of data quality issues or implement a suitable precautionary measure, it is important to know the behavior of the data

*Corresponding Author's Email: pavankumar.yv@vitap.ac.in (Y.V. Pavan Kumar)
URL: https://www.jree.ir/article_146038.html

Please cite this article as: Purna Prakash, K. and Pavan Kumar, Y.V., "Analytical approach to exploring the missing data behavior in smart home energy consumption dataset", ***Journal of Renewable Energy and Environment (JREE)***, Vol. 9, No. 2, (2022), 37-48. (https://doi.org/10.30501/jree.2021.313536.1277).

anomaly. However, there is no work in the literature that discussed the behavioral analysis of missing data anomalies present in the smart home energy consumption data, to the best of the authors' knowledge. This is a major gap in the literature. To address this gap, this paper proposes an analytical approach to exploring the missing data behavior in the smart home energy consumption dataset. This proposed approach quantifies the missing data records in all days for different appliances and analyzes the behavior of these missing data anomalies. The proper identification and behavior analysis of missing data anomalies enables the engineers to implement preventive measures to stop the occurrence of missing data anomalies. This is the motivation, main idea, and novelty of the proposed work of this paper.

The remaining part of the paper is organized as follows. Section 2 presents the methodology of the proposed approach. Section 3 presents the simulation results with their analysis, Finally, Section 4 concludes the findings and achievements of this paper along with the future scope.

Table 1. Review of literature works

Key topic	Reference	Year	Author(s)	Description of the literature work carried
General concepts, complexities, challenges, and advancements in smart homes	[1]	2021	Zielonka et al.	Performed a study and extensive analysis on the recent trends and advancements in smart homes to learn that how they support the users.
	[2]	2021	DeFranco et al.	Emphasized that smart homes were advanced and complex systems. To cope up with this complexity and for further improvement of smart homes' functionality, a comprehensive review and analysis are carried out.
	[3]	2021	Pira	Presented the social issues associated with living in smart homes and made suggestions to reduce the effect of those issues.
	[4]	2020	Kim et al.	Focused on developing design solutions based on user-centered scenarios that include the health issues and daily activities of users.
	[5]	2020	Benjamin et al.	Discussed the pros and cons of smart home technologies by examining the real data drawn in the United Kingdom.
	[6]	2020	Diahovchenko et al.	Reviewed the development and challenges involved in distributed generation, energy storage technologies, deployment of smart meters, microgrids, etc.
IoT role in smart home application	[7]	2021	Wonyoung et al.	Performed a thorough bibliometric study to understand the key trends and the role of the internet of things (IoT) in smart homes.
	[8]	2020	Lin et al.	Discussed the utilization of IoT platforms in the development of smart home applications such as PlantTalk, FishTalk, BreathTalk, TheaterTalk, FrameTalk, and GardenTalk. All these applications were developed under the project 'HomeTalk' which facilitates the flexibility of using appliances.
	[9]	2019	Almusaylim et al.	Conducted a review on the current status and challenges incurred with the implementation of IoT in smart homes.
	[10]	2017	Chen et al.	Introduced a new version of the smart home i.e., Smart Home 2.0. This was designed and implemented using botanical IoT and emotional detection.
Smart home environment, technology, and energy management	[11]	2021	Rasha	Reviewed smart home energy management schemes and also discussed the challenges implicated in smart home power quality.
	[12]	2021	Zhibin et al.	Presented a Spatio-temporal graphical analysis method to understand the behavior of users' energy requirements based on the analytics of smart meter data.
	[13]	2020	Yamauchi et al.	Realized approaches to recognize users' behavior based on their activities and detect anomalies using sensor data in smart homes.
	[14]	2018	Darby	Emphasized the importance of understanding the viability of smart home technologies and users' roles in the smart home environment.
	[15]	2018	Barsocchi et al.	Presented an affordable, easily installable, and accessible smart home environment in turn to reduce the user efforts in managing and improving smart homes.
	[16]	2018	Albuquerque et al.	Suggested a model to maximize energy efficiency and optimize the level of comfort in smart homes.
	[17]	2017	Fan et al.	Discussed cutting-edge visualization techniques and analyzed their merits and demerits to enhance the efficiency of smart home electricity by perceiving the user habits.
	[18]	2017	Martinez-Pabon et al.	Suggested a methodology to forecast the customers who will be eligible for demand response programs using real-time smart meter data.
	[19]	2016	Hare et al.	Conducted a comprehensive review on different modes of faults occurring in microgrids. This review was carried out on both renewable and traditional energy generation systems.
Data analytics in smart grids/homes	[20]	2020	Kezunovic et al.	Discussed the importance of big data analytics to achieve goals in future power grids.
	[21]	2020	vom Scheidt et al.	Performed an extensive quantitative and qualitative literature review on data analytics in the areas of electric power generation, market, transmission, distribution, and utilization.

	[22]	2019	Wang et al.	Conducted an application-oriented review of data analytics in smart meter data in terms of descriptive, predictive, and prescriptive analytics. This review also discussed various challenges and applications concerned with smart meter data analytics.
	[23]	2016	Chou et al.	Developed a framework based on smart grid data analytics for conserving energy in residential buildings. The electricity cost reduction and optimal scheduling of operations depend on the decision made by the decision support system of this framework.
Data anomalies and their detection	[24]	2021	Prakash et al.	Implemented a simple approach to detecting and quantifying the missing data anomalies in smart home energy consumption data.
	[25]	2021	Gilani Fahad et al.	Implemented an approach to detect the anomalies in daily activities of smart home users.
	[26]	2019	Ariyaluran Habeeb et al.	Reviewed the state-of-the-art technologies for detecting anomalies and discussed the challenges of big data processing in real-time.
	[27]	2018	Moghaddass et al.	Designed a framework to detect anomalies in large volumes of smart meter data.
	[28]	2018	Hela et al.	Implemented an association-rule based approach to anticipate the risk of anomalies in the smart home with regard to the activities of users.
	[29]	2017	Wen et al.	Studied the data quality issues such as incomplete data, noisy data, and outliers in energy consumption data of smart grids.

2. METHODOLOGY

The implementation steps of the proposed analytical approach are shown in Figure 1. The process starts with data preparation. The original Tracebase dataset is available with a single column and in string format [30]. The analysis of such a kind of format is difficult. Hence, the dataset is split into the desired columns such as REC_DATE, REC_HOUR, REC_MINUTE, REC_SECOND, and READING. An appropriate type of conversion is applied. The required variables vec, hourly_missing, and day_missing are initialized. The Tracebase dataset consists of Comma-Separated Value (CSV) files in each subdirectory. Each CSV file represents a full day. To access these CSV files, read the directory and subdirectories. Read each CSV file and proceed with the calculation of the number of instants missing at each hour. To accomplish this, filter the data based on the REC_DATE, REC_HOUR, and REC_MINUTE at each hour 'h' and each minute 'm' [for (h in 0:23) and for (m in 0:59)]. These filtered data are saved into an object called 'instants_traces'. To verify whether any instants are missing in the dataset, compare the values of the variable 'vec' with the seconds of the variable REC_SECOND of instants_traces. This comparison gives the information of instants missing at each hour and saved into the variable hourly_missing. The number of instants on each day is calculated by using hourly_missing information and saved into the variable day_missing. Finally, calculate the maximum instants missing at each hour.

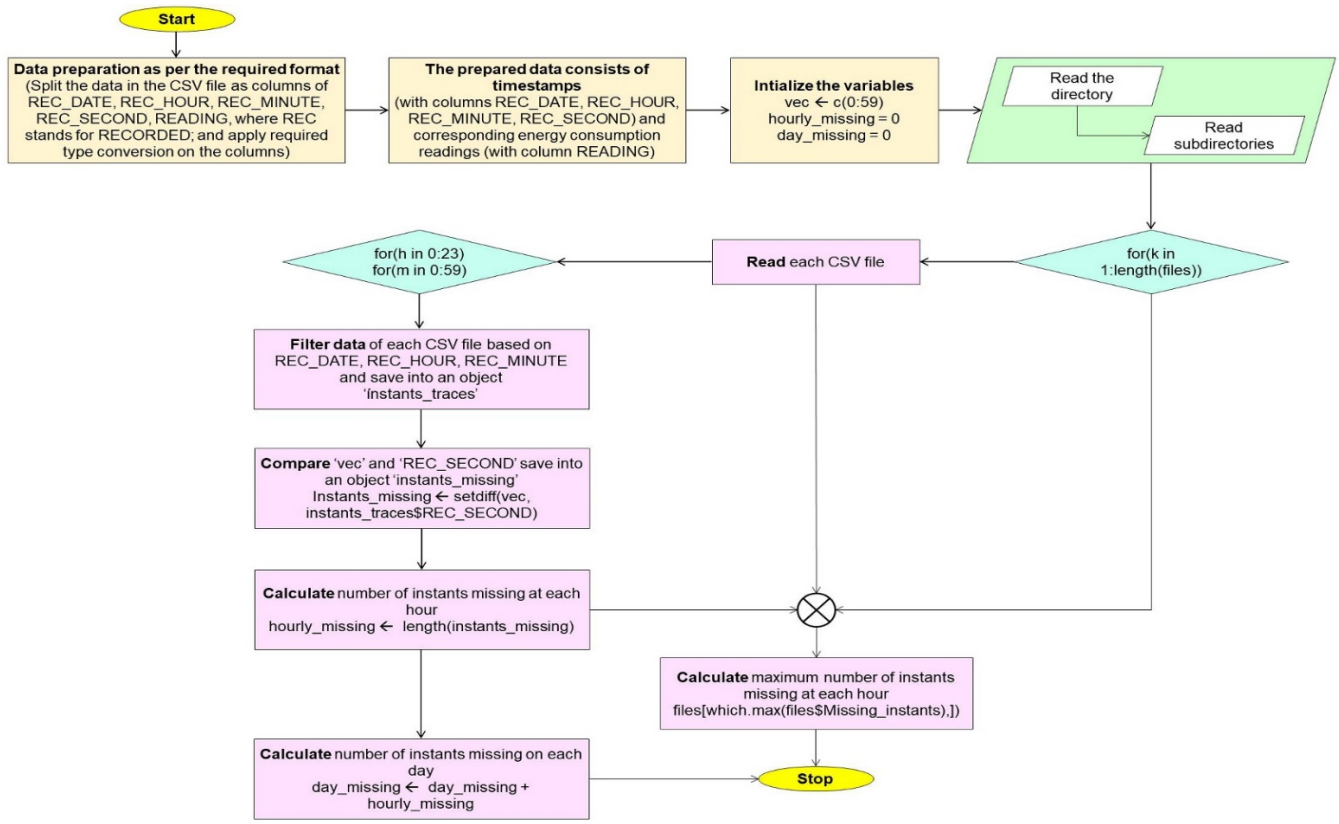

Figure 1. Implementation flow of the proposed analytical approach

3. RESULTS AND ANALYSIS

The subplots represented in Figure 2. showcase the variation in the count of missing instants in different appliances of the smart home energy consumption dataset. These subplots are drawn based on the date (the day where the appliance is connected) on the x-axis and the count of missing instants on the y-axis. The observations made from Figure 2. are given below.

Alarmclock is connected for 5 days and the highest count of missing instants (49826) was observed on 01/09/11, while the lowest count of missing instants (46608) was observed on 03/09/11. Charger-Smartphone is connected for 5 days and the highest count of missing instants (76364) was observed on 22/01/12, while the lowest count of missing instants (70389) was observed on 20/01/12.

Charger-PSP is connected for 2 days and the highest count of missing instants (64442) was observed on 19/11/11, while the lowest count of missing instants (54905) was observed on 18/11/11. CdPlayer is connected for 2 days and the highest count of missing instants (78289) was observed on 21/01/12, while the lowest count of missing instants (70781) was observed on 20/01/12. SolarThermalSystem is connected for 8 days and the highest count of missing instants (64553) was observed on 24/01/12, while the lowest count of missing instants (7560) was observed on 26/01/12. XmasLights is connected for 6 days and the highest count of missing instants (79128) was observed on 06/01/12, while the lowest count of missing instants (73968) was observed on 08/01/12. DvdPlayer is connected for 5 days and the highest count of missing instants (59412) was observed on 20/01/12, while the lowest count of missing instants (55728) was observed on 31/12/11. WaterBoiler is connected for 2 days and the highest count of missing instants (64490) was observed on 24/01/12, while the lowest count of missing instants (61618) was observed on 25/01/12. VacuumCleaner is connected for 1 day and the count of missing instants (57830) was observed on 21/01/12. Iron is connected for 3 days and the highest count of missing instants (34570) was observed on 25/12/11, while the lowest count of missing instants (34488) was observed on 24/12/11.

BeanToCupCoffeemaker is connected for 44 days and the highest count of missing instants (2899) was observed on 19/08/11, while the lowest count of missing instants (827) was observed on 30/08/11. Breadcutter is connected for 13 days and the highest count of missing instants (76612) was observed on 27/01/12, while the lowest count of missing instants (66214) was observed on 25/01/12. Cookingstove is connected for 16 days and the highest count of missing instants (63638) was observed on 01/01/12, while the lowest count of missing instants (52199) was observed on 20/12/11. DigitalTvReceiver is connected for 24 days and the highest count of missing instants (63638) was observed on 01/01/12, while the lowest count of missing instants (52070) was observed on 09/01/12. EthernetSwitch is connected for 33 days and the highest count of missing instants (71657) was observed on 29/11/11, while the lowest count of missing instants (26802) was observed on 20/01/12. Freezer is connected for 9 days and the highest count of missing instants (64565) was observed on 24/01/12, while the lowest count of missing instants (4130) was observed on 26/01/12.

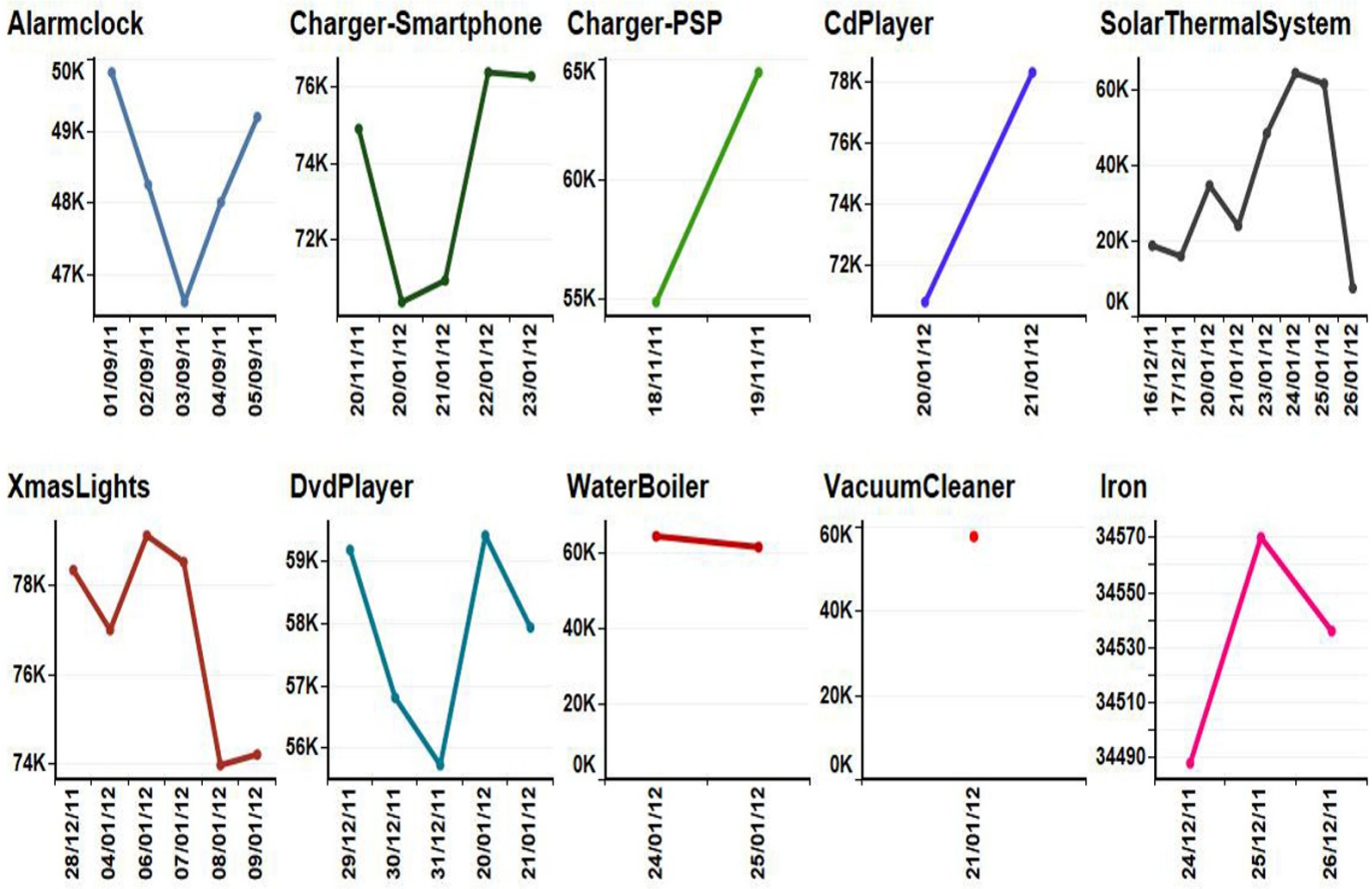

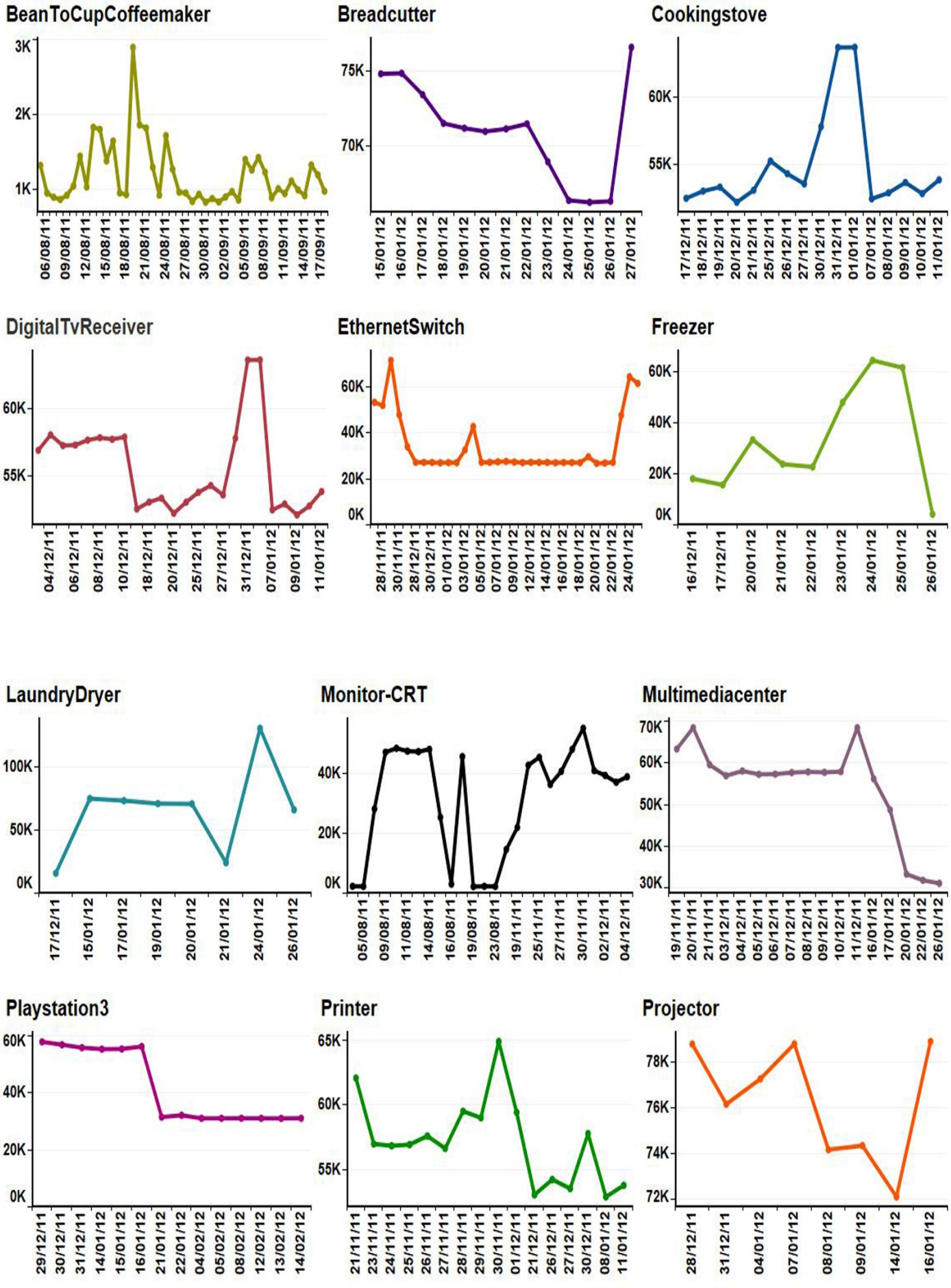
BeanToCupCoffeemaker
Breadcutter
Cookingstove
DigitalTvReceiver
EthernetSwitch
Freezer
LaundryDryer
Monitor-CRT
Multimediacenter
Playstation3
Printer
Projector

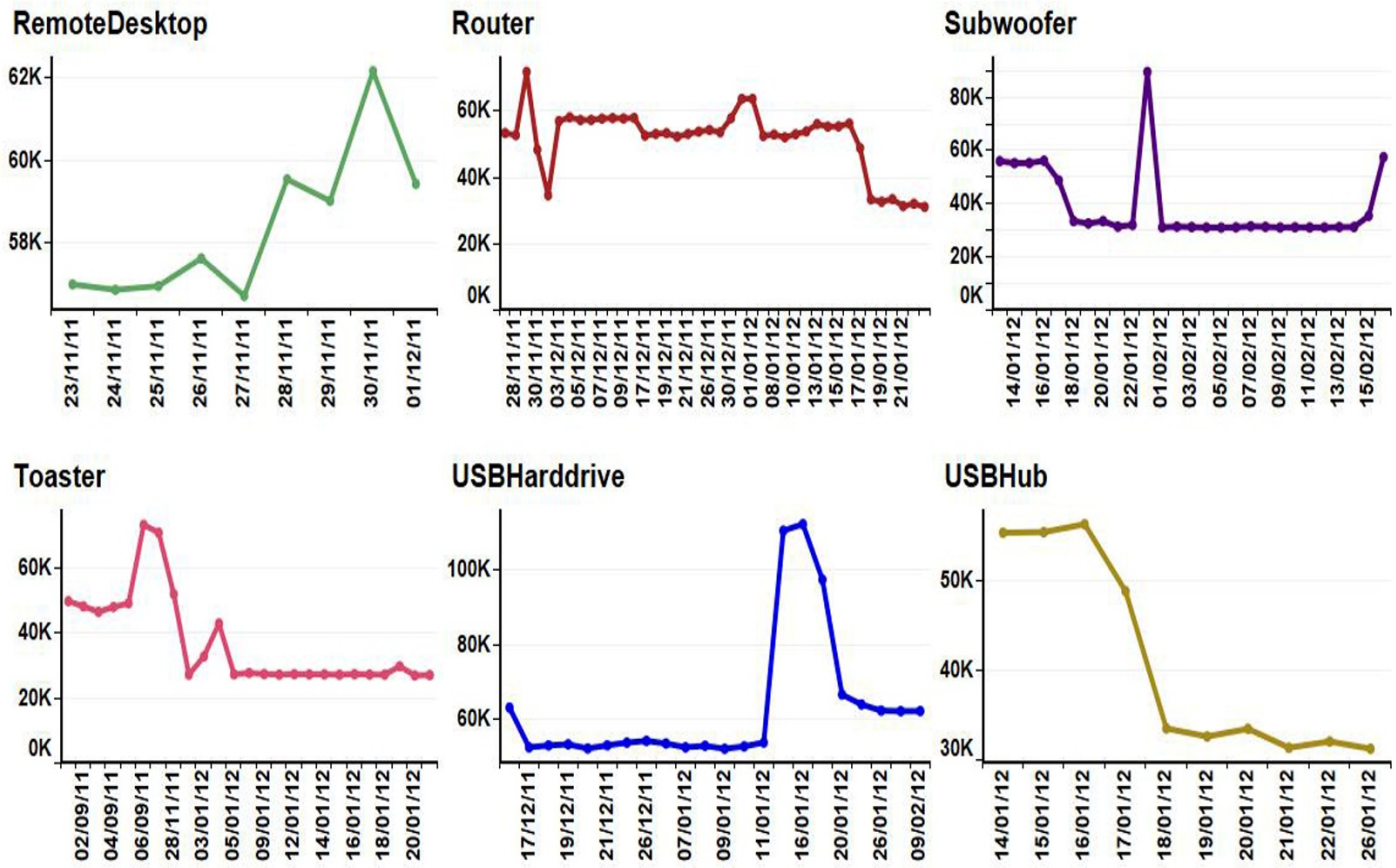
RemoteDesktop
62K
60K
58K
23/11/11
24/11/11
25/11/11
26/11/11
27/11/11
28/11/11
29/11/11
30/11/11
01/12/11
Router
60K
40K
20K
0K
28/11/11
30/11/11
03/12/11
05/12/11
07/12/11
09/12/11
17/12/11
19/12/11
21/12/11
26/12/11
30/12/11
01/01/12
08/01/12
10/01/12
13/01/12
15/01/12
17/01/12
19/01/12
21/01/12
Subwoofer
80K
60K
40K
20K
0K
14/01/12
16/01/12
18/01/12
20/01/12
22/01/12
01/02/12
03/02/12
05/02/12
07/02/12
09/02/12
11/02/12
13/02/12
15/02/12
Toaster
60K
40K
20K
0K
02/09/11
04/09/11
06/09/11
28/11/11
03/01/12
05/01/12
09/01/12
12/01/12
14/01/12
16/01/12
18/01/12
20/01/12
USBHarddrive
100K
80K
60K
17/12/11
19/12/11
21/12/11
26/12/11
07/01/12
09/01/12
11/01/12
16/01/12
20/01/12
26/01/12
09/02/12
USBHub
50K
40K
30K
14/01/12
15/01/12
16/01/12
17/01/12
18/01/12
19/01/12
20/01/12
21/01/12
22/01/12
26/01/12

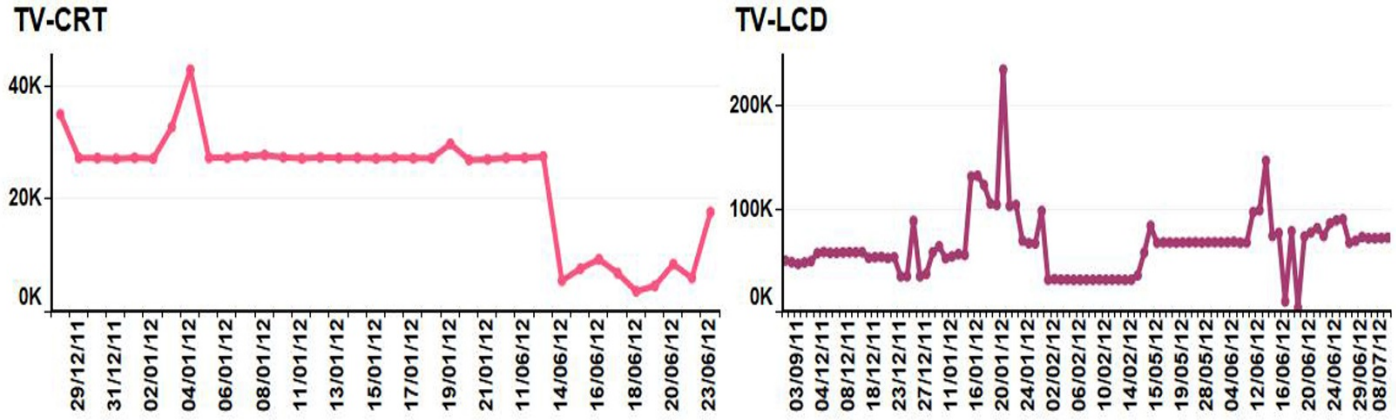
TV-CRT
40K
20K
0K
29/12/11
31/12/11
02/01/12
04/01/12
06/01/12
08/01/12
11/01/12
13/01/12
15/01/12
17/01/12
19/01/12
21/01/12
11/06/12
14/06/12
16/06/12
18/06/12
20/06/12
23/06/12
TV-LCD
200K
100K
0K
03/09/11
04/12/11
08/12/11
18/12/11
23/12/11
27/12/11
11/01/12
16/01/12
20/01/12
24/01/12
02/02/12
06/02/12
10/02/12
14/02/12
15/05/12
19/05/12
28/05/12
04/06/12
12/06/12
16/06/12
20/06/12
24/06/12
29/06/12
08/07/12

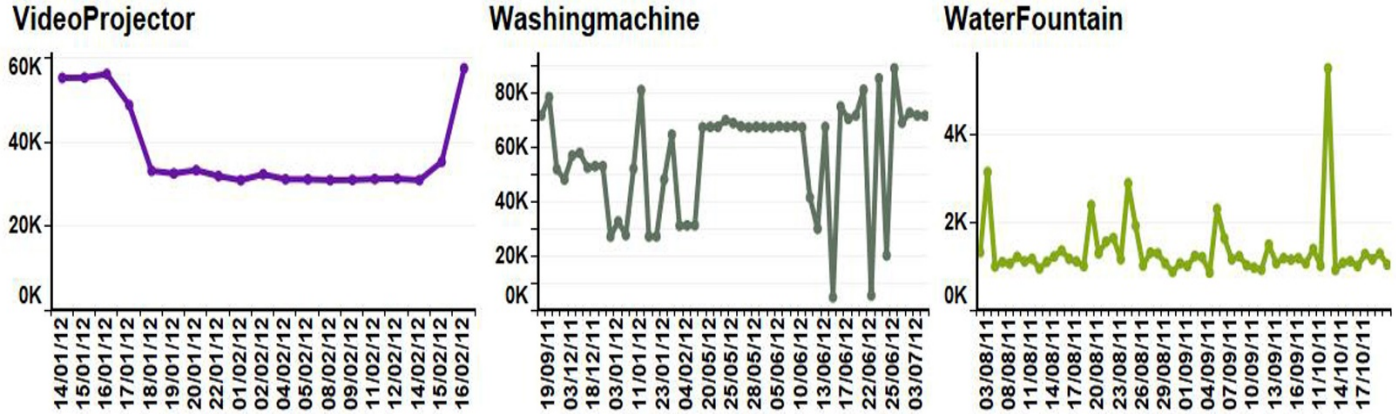
VideoProjector
60K
40K
20K
0K
14/01/12
15/01/12
16/01/12
17/01/12
18/01/12
19/01/12
20/01/12
22/01/12
01/02/12
02/02/12
04/02/12
05/02/12
08/02/12
09/02/12
11/02/12
12/02/12
14/02/12
15/02/12
16/02/12
Washingmachine
80K
60K
40K
20K
0K
19/09/11
03/12/11
18/12/11
03/01/12
11/01/12
23/01/12
04/02/12
20/05/12
25/05/12
28/05/12
05/06/12
10/06/12
13/06/12
17/06/12
22/06/12
25/06/12
03/07/12
WaterFountain
4K
2K
0K
03/08/11
08/08/11
11/08/11
14/08/11
17/08/11
20/08/11
23/08/11
26/08/11
29/08/11
01/09/11
04/09/11
07/09/11
10/09/11
13/09/11
16/09/11
11/10/11
14/10/11
17/10/11

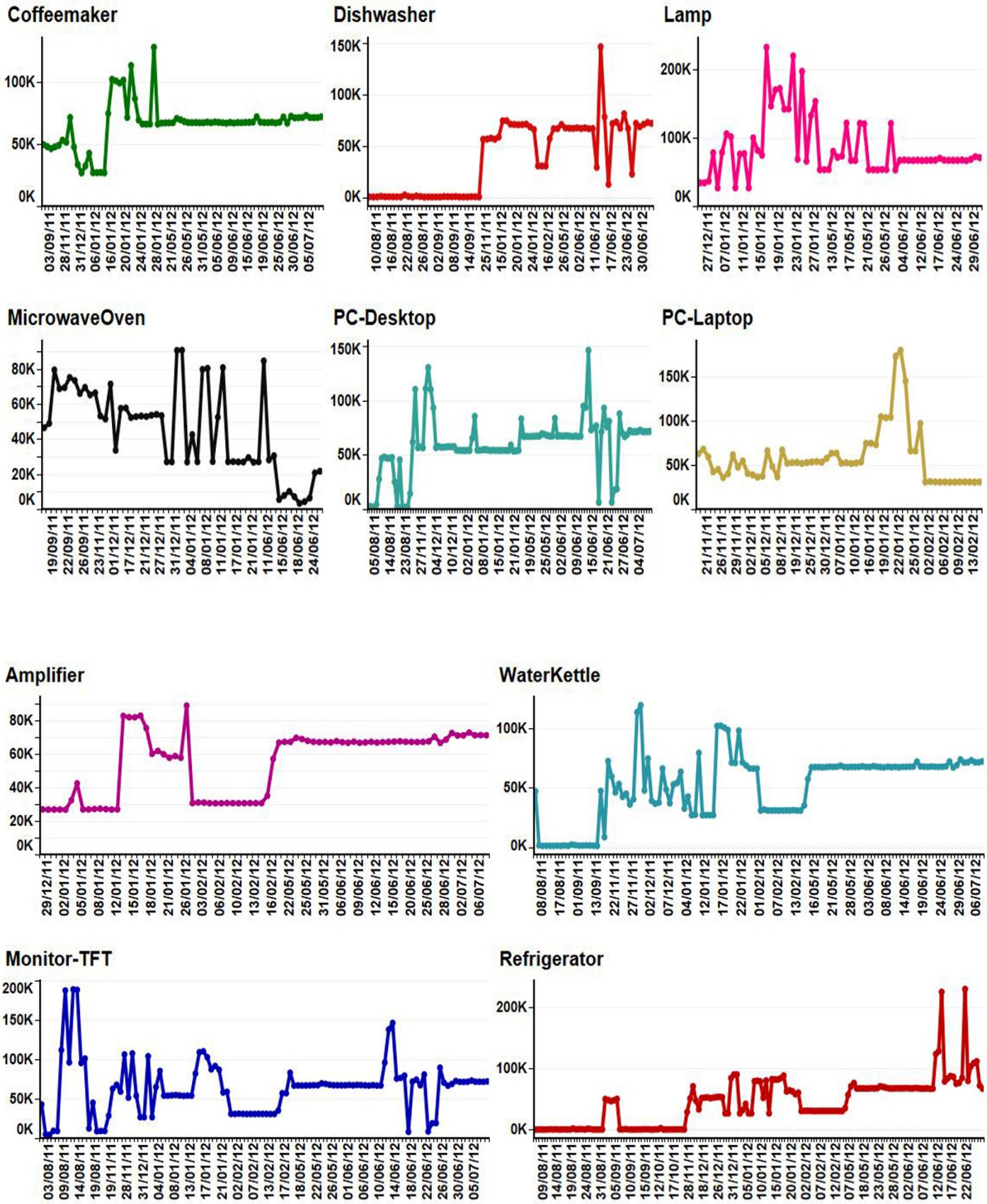

Figure 2. Quantification of missing data anomalies in different appliances (x-axis represents the date and y-axis represents the count of missing instants corresponding to the date)

LaundryDryer is connected for 9 days and the highest count of missing instants (130995) was observed on 24/01/12, while the lowest count of missing instants (15863) was observed on 17/12/11. Monitor-CRT is connected for 26 days and the highest count of missing instants (54858) was observed on 30/11/11, while the lowest count of missing instants (2195)

was observed on 19/08/11. Multimediacenter is connected for 17 days and the highest count of missing instants (68409) was observed on 20/11/11, while the lowest count of missing instants (31085) was observed on 26/01/12. Playstation3 is connected for 14 days and the highest count of missing instants (57798) was observed on 29/12/11, while the lowest count of missing instants (30981) was observed on 13/02/12. Printer is connected for 16 days and the highest count of missing instants (64877) was observed on 30/11/11, while the lowest count of missing instants (52919) was observed on 08/01/12. Projector is connected for 8 days and the highest count of missing instants (78873) was observed on 16/01/12, while the lowest count of missing instants (72117) was observed on 14/01/12.

RemoteDesktop is connected for 9 days and the highest count of missing instants (62149) was observed on 30/11/11, while the lowest count of missing instants (56722) was observed on 27/11/11. Router is connected for 40 days and the highest count of missing instants (71741) was observed on 29/11/11, while the lowest count of missing instants (31101) was observed on 26/01/12. Subwoofer is connected for 28 days and the highest count of missing instants (89521) was observed on 26/01/12, while the lowest count of missing instants (31042) was observed on 05/02/12. Toaster is connected for 25 days and the highest count of missing instants (73077) was observed on 06/09/11, while the lowest count of missing instants (26886) was observed on 20/01/12. USBHarddrive is connected for 30 days and the highest count of missing instants (112335) was observed on 16/01/12, while the lowest count of missing instants (52133) was observed on 09/01/12. USBHub is connected for 10 days and the highest count of missing instants (56175) was observed on 16/01/12, while the lowest count of missing instants (31293) was observed on 26/01/12. TV-CRT is connected for 36 days and the highest count of missing instants (42852) was observed on 04/01/12, while the lowest count of missing instants (3654) was observed on 18/06/12. TV-LCD is connected for 119 days and the highest count of missing instants (234864) was observed on 20/01/12, while the lowest count of missing instants (4090) was observed on 18/06/12. VideoProjector is connected for 19 days and the highest count of missing instants (57509) was observed on 16/02/12, while the lowest count of missing instants (30950) was observed on 01/02/12.

Washingmachine is connected for 56 days and the highest count of missing instants (88890) was observed on 25/06/12, while the lowest count of missing instants (4913) was observed on 14/06/12. WaterFountain is connected for 56 days and the highest count of missing instants (5502) was observed on 12/10/11, while the lowest count of missing instants (864) was observed on 04/09/11. Coffeemaker is connected for 82 days and the highest count of missing instants (127944) was observed on 27/01/12, while the lowest count of missing instants (27090) was observed on 31/12/11. Dishwasher is connected for 76 days and the highest count of missing instants (146443) was observed on 13/06/12, while the lowest count of missing instants (944) was observed on 26/08/11. Lamp is connected for 86 days and the highest count of missing instants (232192) was observed on 16/01/12, while the lowest count of missing instants (27237) was observed on 05/01/12. MicrowaveOven is connected for 60 days and the highest count of missing instants (90825) was observed on 01/01/12, while the lowest count of missing instants (3557) was observed on 18/06/12. PC-Desktop is connected for 151 days and the highest count of missing instants (146357) was observed on 13/06/12, while the lowest count of missing instants (2251) is observed on 04/08/11. PC-Laptop is connected for 67 days and the highest count of missing instants (179830) was observed on 22/01/12, while the lowest count of missing instants (30981) was observed on 07/02/12. Amplifier is connected for 89 days and the highest count of missing instants (89375) was observed on 26/01/12, while the lowest count of missing instants (27094) was observed on 02/01/12. WaterKettle is connected for 134 days and the highest count of missing instants (119492) was observed on 29/11/11, while the lowest count of missing instants (1378) was observed on 13/09/11. Monitor-TFT is connected for 190 days and the highest count of missing instants (189047) was observed on 11/08/11, while the lowest count of missing instants (4836) was observed on 03/08/11. Refrigerator is connected for 206 days and the highest count of missing instants (230645) was observed on 21/06/12, lowest count of missing instants (700) is observed on 17/09/11. The observations made on the count of missing instants in different appliances are summarized in Table 2.

The highest count of missing instants for each appliance is plotted as shown in Figure 3. Using this plot, the highest count of missing instants at a particular device in each appliance revealed that the appliance 'MicowaveOven' had the highest count of missing instants. In total, 84740 instants were missing at the device with identifier 'dev_768D06' on 20/05/12. Hence, all the days of MicrowaveOven appliance are considered for further analysis to know how many hours are there with the highest counts of instants missing. For this purpose, the frequency of hours with the highest missing instants in MicrowaveOven appliance is plotted as shown in Figure 4. During the analysis, it is observed that all the hours except hours 1, 4, and 5 are containing the highest counts of instants missing in the considered 60 days. Out of these hours, hour '0' has the highest frequency with the value 8 and represents the occurrence of the highest count of data instants missing.

Table 2. Summary of observations on the count of missing instants

S.No.	Appliance	No. of days connected	Observation on highest missing instants counts		Observation on lowest missing instants counts	
			Date(s) with highest missing instants	Corresponding missing instants count	Date(s) with lowest missing instants	Corresponding missing instants count
1	Alarmclock	5	01/09/11	49826	03/09/11	46608
2	Charger-Smartphone	5	22/01/12	76364	20/01/12	70389
3	Charger-PSP	2	19/11/11	64442	18/11/11	54905
4	CdPlayer	2	21/01/12	78289	20/01/12	70781
5	SolarThermalSystem	8	24/01/12	64553	26/01/12	7560

6	XmasLights	6	06/01/12	79128	08/01/12	73968
7	DvdPlayer	5	20/01/12	59412	31/12/11	55728
8	WaterBoiler	2	24/01/12	64490	25/01/12	61618
9	VacuumCleaner	1	21/01/12	57830	-	-
10	Iron	3	25/12/11	34570	24/12/11	34488
11	BeanToCupCoffeemaker	44	19/08/11	2899	30/08/11	827
12	Breadcutter	13	27/01/12	76612	25/01/12	66214
13	Cookingstove	16	01/01/12	63638	20/12/11	52199
14	DigitalTvReceiver	24	01/01/12	63638	09/01/12	52070
15	EthernetSwitch	33	29/11/11	71657	20/01/12	26802
16	Freezer	9	24/01/12	64565	26/01/12	4130
17	LaundryDryer	9	24/01/12	130995	17/12/11	15863
18	Monitor-CRT	26	30/11/11	54858	19/08/11	2195
19	Multimediacenter	17	20/11/11	68409	26/01/12	31085
20	Playstation3	14	29/12/11	57798	13/02/12	30981
21	Printer	16	30/11/11	64877	08/01/12	52919
22	Projector	8	16/01/12	78873	14/01/12	72117
23	RemoteDesktop	9	30/11/11	62149	27/11/11	56722
24	Router	40	29/11/11	71741	26/01/12	31101
25	Subwoofer	28	26/01/12	89521	05/02/12	31042
26	Toaster	25	06/09/11	73077	20/01/12	26886
27	USBHarddrive	30	16/01/12	112335	09/01/12	52133
28	USBHub	10	16/01/12	56175	26/01/12	31293
29	TV-CRT	36	04/01/12	42852	18/06/12	3654
30	TV-LCD	119	20/01/12	234864	18/06/12	4090
31	VideoProjector	19	16/02/12	57509	01/02/12	30950
32	Washingmachine	56	25/06/12	88890	14/06/12	4913
33	WaterFountain	56	12/10/11	5502	04/09/11	864
34	Coffeemaker	82	27/01/12	127944	31/12/11	27090
35	Dishwasher	76	13/06/12	146443	26/08/11	944
36	Lamp	86	16/01/12	232192	05/01/12	27237
37	MicrowaveOven	60	01/01/12	90825	18/06/12	3557
38	PC-Desktop	151	13/06/12	146357	04/08/11	2251
39	PC-Laptop	67	22/01/12	179830	07/02/12	30981
40	Amplifier	89	26/01/12	89375	02/01/12	27094
41	WaterKettle	134	29/11/11	119492	13/09/11	1378
42	Monitor-TFT	190	11/08/11	189047	03/08/11	4836
43	Refrigerator	206	21/06/12	230645	17/09/11	700

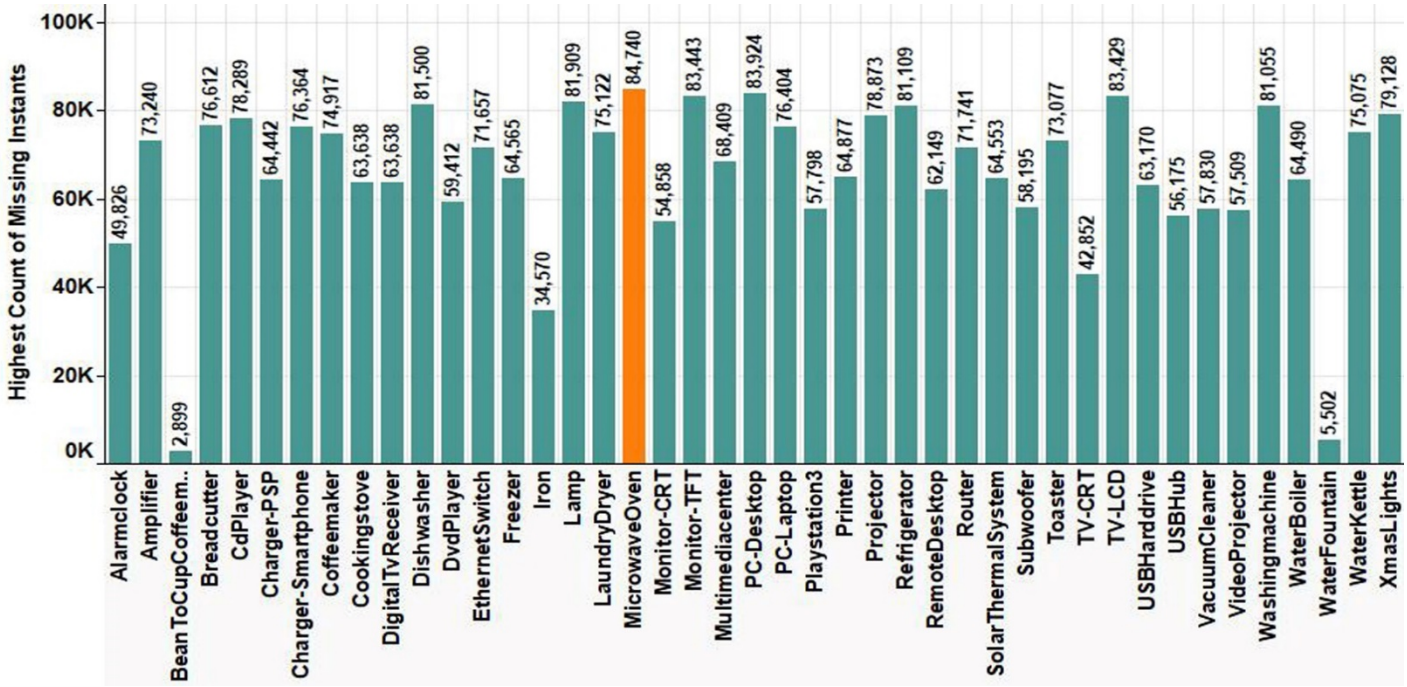

Figure 3. Highest count of missing instants in the readings of different appliances

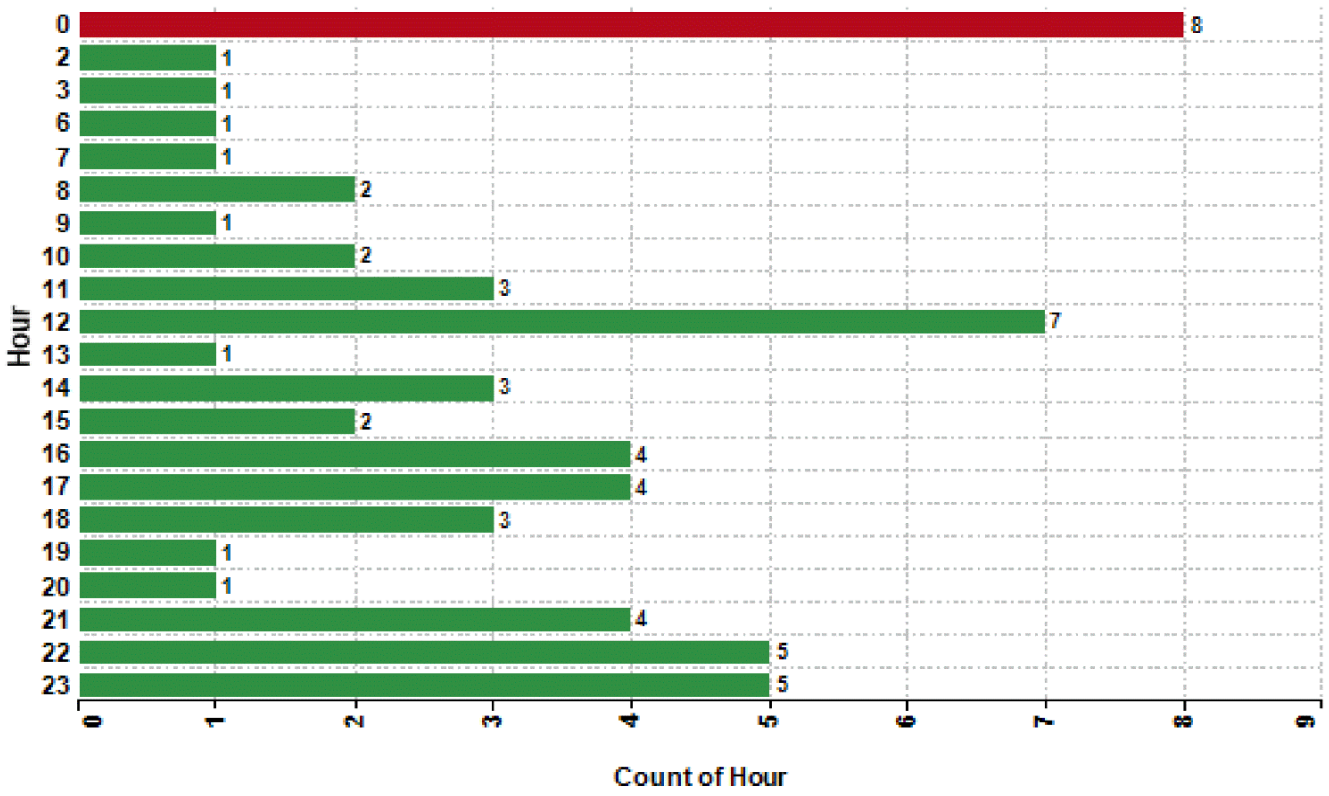

Figure 4. Frequency of hours with highest missing instants in MicrowaveOven

The parts of the day in Darmstadt, Germany are considered Night, Twilight, and Daylight [31]. The hours 00:00 to 06:00 represent Night time. The Astro, Twilight, Nautical Twilight, and Civil Twilight are together considered as Twilight. The hours 07:00, and 20:00 to 23:00 represent Twilight time. The hours 08:00 to 19:00 represent Daylight. All files (60 days) of the appliance "MicrowaveOven" are considered for further analysis as it has the highest count of missing instants. From this analysis, the behavior of missing data in MicrowaveOven appliance during various parts of a day is plotted as shown in Figure 5. From this, it is observed that the highest missing is on Daylight time (33 hours), the next highest is on Twilight time (16 hours), and the lowest is on Nighttime (11 hours).

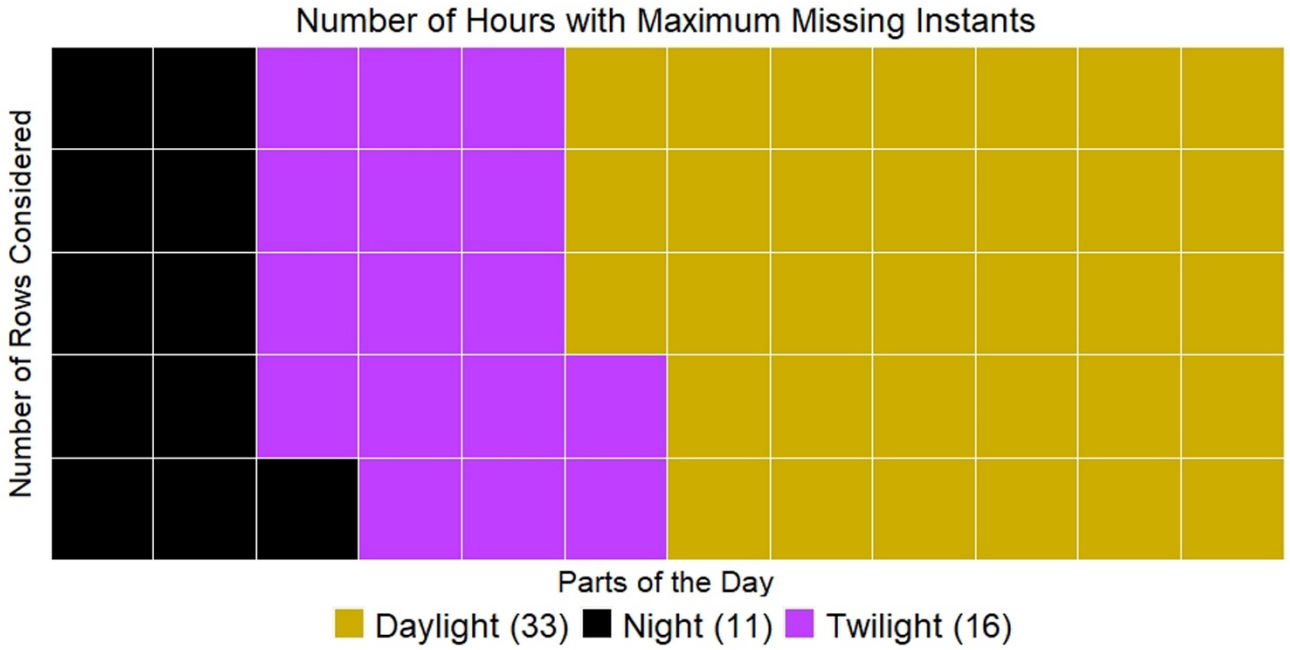

Figure 5. Behavior of missing data in MicrowaveOven appliance during various parts of a day

4. CONCLUSIONS AND FUTURE SCOPE

This paper proposed an analytical approach to exploring the missing data behavior in the smart home energy consumption dataset. The proposed approach successfully explored and quantified the missing data anomalies on all days for all the given appliances in the considered dataset. This analysis revealed that the appliance 'MicrowaveOven' had the highest

count (84740) of missing instants. Further, this proposed approach finds the behavior of missing data anomalies by considering the appliance 'MicrowaveOven' as a test case. The conclusions drawn from the implementation of the proposed approach are given as follows:

- In some appliances, the devices have the same count of missing instants on the same day. For e.g., the device 'dev_D33097' of 'CookingStove' appliance and the device 'dev_D330A3' of 'DigitalTvReceiver' appliance consists of the same count (63638) of missing instants on the same day (01/01/2012). This analysis may help the engineers to suspect and identify some common factors that cause the same count of missing data records across various devices/appliances at the same instants of the time.
- Unexpectedly, in some appliances, more than one lakh missing instants are observed. The reason for this is explained below.
  - In general, the expected number of records in a day is 86400 (24 h × 60 m × 60 s) as there is one trace per second is desired. But, due to the redundancy in the energy consumption data records, the total number of records exceeds the ideal expected count (86400). This further increases the count of missing data instants than the actual count. Hence, these redundant records increase the complexity of the missing data analysis and further delude the identification of missing records correctly. So, it is expected that the dataset be free from such redundant records to have an accurate behavioral analysis of missing data.
  - This opens up a new investigation requirement on the redundant data anomalies to further enhance the data quality and purification process.
- The highest count of missing instants is observed during the Daylight period of a day.

Therefore, it is concluded that the proposed comprehensive exploration of missing data anomalies helps the engineers and researchers to understand the presence and the behavior of missing data anomalies that help for accurate analytics.

5. ACKNOWLEDGEMENT

This work was supported in part by Project Grant No: SRG/2019/000648, sponsored by the Start-up Research Grant (SRG) scheme of the Science and Engineering Research Board (SERB), a statutory body under the Department of Science and Technology (DST), Government of India.

REFERENCES

1. Zielonka, A., Woźniak, M., Garg, S., Kaddoum, G., Piran, Md. J. and Muhammad, G., "Smart homes: How much will they support us? A research on recent trends and advances", ***IEEE Access***, Vol. 9, (2021), 26388-26419. (https://doi.org/10.1109/ACCESS.2021.3054575).
2. DeFranco, J.F. and Kassab, M., "Smart home research themes: An analysis and taxonomy", ***Procedia Computer Science***, Vol. 185, (2021), 91-100. (https://doi.org/10.1016/j.procs.2021.05.010).
3. Pira, S., "The social issues of smart home: A review of four European cities' experiences", ***European Journal of Futures Research***, Vol. 9, No. 3, (2021), 1-15. (https://doi.org/10.1186/s40309-021-00173-4).
4. Kim, M.J., Cho, M.E. and Jun, H.J., "Developing design solutions for smart homes through user-centered scenarios", ***Frontiers in Psychology***, Vol. 11, (2020), 1-12. (https://doi.org/10.3389/fpsyg.2020.00335).
5. Benjamin, K.S. and Dylan, D.F.D.R., "Smart home technologies in Europe: A critical review of concepts, benefits, risks and policies", ***Renewable and Sustainable Energy Reviews***, Vol. 120, (2020), 109663. (https://doi.org/10.1016/j.rser.2019.109663).
6. Diahovchenko, I., Kolcun, M., Čonka, Z., Savkiv, V. and Roman, M., "Progress and challenges in smart grids: Distributed generation, smart metering, energy storage and smart loads", ***Iranian Journal of Science and Technology, Transactions of Electrical Engineering***, Vol. 44, (2020), 1319-1333. (https://doi.org/10.1007/s40998-020-00322-8).
7. Wonyoung, C., Kim, J., SangEun, L. and Park E., "Smart home and internet of things: A bibliometric study", ***Journal of Cleaner Production***, Vol. 301, (2021), 126908. (https://doi.org/10.1016/j.jclepro.2021.126908).
8. Lin, Y.W., Tseng, S.K., Liao, J.K. and Hsu, T.H., "Developing smart home applications", ***Mobile Networks and Applications***, Vol. 27, (2022), 181-195. (https://doi.org/10.1007/s11036-020-01639-8).
9. Almusaylim, Z.A. and Zaman, N., "A review on smart home present state and challenges: Linked to context-awareness internet of things (IoT)", ***Wireless Networks***, Vol. 25, (2019), 3193-3204. (https://doi.org/10.1007/s11276-018-1712-5).
10. Chen, M., Yang, J., Zhu, X., Wang, X., Mengchen, L. and Jeungeun, S., "Smart home 2.0: Innovative smart home system powered by botanical IoT and emotion detection", ***Mobile Networks and Applications***, Vol. 22, (2017), 1159-1169. (https://doi.org/10.1007/s11036-017-0866-1).
11. Rasha, E.A., "Smart homes: Potentials and challenges", ***Clean Energy***, Vol. 5, No. 2, (2021), 302-315. (https://doi.org/10.1093/ce/zkab010).
12. Zhibin, N., Junqi, W., Liu, X., Huang, L. and Nielsen, P.S., "Understanding energy demand behaviors through spatio-temporal smart meter data analysis", ***Energy***, Vol. 226, (2021), 120493. (https://doi.org/10.1016/j.energy.2021.120493).
13. Yamauchi, M., Ohsita, Y., Murata, M., Ueda, K. and Kato, Y., "Anomaly detection in smart home operation from user behaviors and home conditions", ***IEEE Transactions on Consumer Electronics***, Vol. 66, No. 2, (2020), 183-192. (https://doi.org/10.1109/TCE.2020.2981636).
14. Darby, S.J., "Smart technology in the home: Time for more clarity", ***Building Research & Information***, Vol. 46, No. 1, (2018), 140-147. (https://doi.org/10.1080/09613218.2017.1301707).
15. Barsocchi, P., Calabrò, A., Ferro, E., Gennaro, C., Marchetti, E. and Vairo, C., "Boosting a low-cost smart home environment with usage and access control rules", ***Sensors***, Vol. 18, No. 6, (2018), 1-22. (https://doi.org/10.3390/s18061886).
16. Albuquerque, P.U.B., Ohi, D.K.d.A., Pereira, N.S., Prata, B.d.A. and Barroso, C.G., "Proposed architecture for energy efficiency and comfort optimization in smart homes", ***Journal of Control, Automation and Electrical Systems***, Vol. 29, (2018), 718-730. (https://doi.org/10.1007/s40313-018-0410-y).
17. Fan, X., Qiu, B., Liu, Y., Zhu, H. and Han, B., "Energy visualization for smart home", ***Energy Procedia***, Vol. 105, (2017), 2545-2548. (https://doi.org/10.1016/j.egypro.2017.03.732).
18. Martinez-Pabon, M., Eveleigh, T. and Tanju, B., "Smart meter data analytics for optimal customer selection in demand response programs", ***Energy Procedia***, Vol. 107, (2017), 49-59. (https://doi.org/10.1016/j.egypro.2016.12.128).
19. Hare, J., Shi, X., Gupta, S. and Bazzi, A., "Fault diagnostics in smart micro-grids: A survey", ***Renewable and Sustainable Energy Reviews***, Vol. 60, (2016), 1114-1124. (http://dx.doi.org/10.1016/j.rser.2016.01.122).
20. Kezunovic, M., Pinson, P., Obradovic, Z., Grijalva, S., Hong, T. and Bessa, R., "Big data analytics for future electricity grids", ***Electric Power Systems Research***, Vol. 189, (2020), 106788. (https://doi.org/10.1016/j.epsr.2020.106788).
21. vom Scheidt, F., Medinová, H., Ludwig, N., Richter, B., Staudt, P. and Weinhardt, C., "Data analytics in the electricity sector –A quantitative and qualitative literature review", ***Energy and AI***, Vol. 1, (2020), 100009. (https://doi.org/10.1016/j.egyai.2020.100009).
22. Wang, Y., Chen, Q., Hong, T. and Kang, C., "Review of smart meter data analytics: Applications, methodologies, and challenges", ***IEEE Transactions on Smart Grid***, Vol. 10, No. 3, (2019), 3125-3148. (https://doi.org/10.1109/TSG.2018.2818167).
23. Chou, J.S. and Ngo, N.T., "Smart grid data analytics framework for increasing energy savings in residential buildings", ***Automation in Construction***, Vol. 72, No. 3, (2016), 247-257. (http://dx.doi.org/10.1016/j.autcon.2016.01.002).

24. Purna Prakash, K. and Pavan Kumar, Y.V., "Simple and effective descriptive analysis of missing data anomalies in smart home energy consumption readings", ***Journal of Energy Systems***, Vol. 5, No. 3, (2021), 199-220. (https://doi.org/10.30521/jes.878318).

25. Gilani Fahad, L. and Tahir, S.F., "Activity recognition and anomaly detection in smart homes", ***Neurocomputing***, Vol. 423, (2021), 362-372. (https://doi.org/10.1016/j.neucom.2020.10.102).

26. Ariyaluran Habeeb, RA., Nasaruddin, F., Gani, A., Abaker Targio Hashem, I., Ahmed, E. and Imran, M., "Real-time big data processing for anomaly detection: A Survey", ***International Journal of Information Management***, Vol. 45, (2019), 289-307. (https://doi.org/10.1016/j.ijinfomgt.2018.08.006).

27. Moghaddass, R. and Wang, J., "A hierarchical framework for smart grid anomaly detection using large-scale smart meter data", ***IEEE Transactions on Smart Grid***, Vol. 9, No. 6, (2018), 5820-5830. (https://doi.org/10.1109/TSG.2017.2697440).

28. Hela, S., Amel, B. and Badran, R., "Early anomaly detection in smart home: A causal association rule-based approach", ***Artificial Intelligence in Medicine***, Vol. 91, (2018), 57-71. (https://doi.org/10.1016/j.artmed.2018.06.001).

29. Wen, C., Zhou, K., Yang, S. and Cheng, W., "Data quality of electricity consumption data in a smart grid environment", ***Renewable and Sustainable Energy Reviews***, Vol. 75, (2017), 98-105. (http://dx.doi.org/10.1016/j.rser.2016.10.054).

30. Andreas, R., "The tracebase appliance-level power consumption dataset", (2020). (https://github.com/areinhardt/tracebase/tree/master/complete), (Accessed: 28 February 2022).

31. Time and Date AS | Darmstadt, HE, Germany — Sunrise, Sunset, and Moon Times for Today, Parts of a Day in Darmstadt, Germany, (2022). (https://www.timeanddate.com/astronomy/germany/darmstadt), (Accessed: 28 February 2022).

JREE: Vol. 9, No. 2, (Spring 2022) 49-58

Journal of Renewable Energy and Environment

Journal Homepage: www.jree.ir

Materials and Energy Research Center

MERC

Research Article

Multi-Response Optimization of Tubular Microbial Fuel Cells Using Response Surface Methodology (RSM)

Maryam Keshavarz [a], Davod Mohebbi-Kalhori [a,b*], Vajihe Yousefi [a]

[a] *Department of Chemical Engineering, Faculty of Engineering, University of Sistan and Baluchestan, Zahedan, Sistan and Baluchestan, Iran.*
[b] *University of Sistan and Baluchestan Central Laboratory, Zahedan, Sistan and Baluchestan, Iran.*

PAPER INFO

Paper history:
Received: 14 June 2021
Revised in revised form: 03 January 2022
Scientific Accepted: 11 October 2021
Published: 19 March 2022

Keywords:
Microbial Fuel Cell,
Response Surface Methodology (RSM),
Separator-Electrode Assembly,
J-Cloth,
Nylon-Cloth,
Domestic Wastewater Treatment

ABSTRACT

Response surface methodology is employed to statistically identify the significance of three parameters of separator assembly arrangement, wastewater flow rate, and relative flow patterns of anode and cathode influencing the generation of power and coulombic efficiency of Microbial Fuel Cells (MFCs). Three different assemblies of Nylon-Cloth (NC), artificial rayon cloth as Absorbent Layer (AL), and J-Cloth (JC) were investigated as proton exchange mediums instead of common expensive polymeric membranes. Statistical analyses (ANOVA) revealed that although the addition of the AL after the JC layer had no significant impact on the enhancement of maximum power density, it could improve the coulombic efficiency of the MFCs by 15 %, owing to the crucial impact of oxygen permeability control between the MFC chambers. In the counter-current flow pattern, higher trans-membrane pressure and more oxygen concentration differences diminished the MFC performance and marked the importance of efficient separator layer arrangement, compared to co-current influents. The maximum power density of 285.89 mW/m^2, the coulombic efficiency of 4.97 %, and the internal resistance of 323.9 Ω were achieved for the NC-JC-Al arrangement in the co-current mode along with the flow rate of 6.9 ml/min. The higher the flow rate of influent wastewater, the higher the performance of the MFCs.

https://doi.org/10.30501/jree.2022.290677.1218

1. INTRODUCTION

The know-how of electricity production processes from renewable resources has been known for many years; however, the critical need for the development of more practical and viable utilization of novel renewable technologies has been perceived on a global scale [1-4]. Microbial Fuel Cell (MFC) is known as a novel, useful and eco-friendly approach that not only generates clean energy but also solves the problems concerned with the contamination of water sources by treating the polluted waters and wastewaters [5-7]. Generally, Each MFC system consists of an anode chamber, a cathode chamber, and a membrane for exchanging the produced protons and separating the anode and cathode from each other [8, 9]. The source of electrical energy in MFCs is bacteria that reside in the biomass [10-12] and use the microbial-catalyzed redox reactions to produce bio-electricity directly [13]. The substrates are oxidized using the microorganisms presented in the wastewater medium and this results in electron and proton generation [11, 13]. Transfer of protons through the separator, followed by the combination of electrons with protons and oxygen results in the generation of water on the cathode surface. Electricity is simultaneously produced by the transportation of electrons through the external circuit [14]. By improving the performance of the MFC as well as reducing their component costs, it can be a promising source of energy generation in the future [15, 16].

Various parameters affecting the performance and overall cost of MFCs include their designs, operating conditions, and types of materials used for electrodes and separators. However, it seems that among many obstacles against the MFC scale-up, the challenge of finding an appropriate proton exchange medium that has low cost, efficient proton transferability, and long-term stability is of great importance. In this regard, many innovative separators have been used such as porous fabrics, nylon meshes, glass fiber, J-cloth, and ceramics, which are not ion-selective and the species are transferred based on their pore size [17-24]. Generally, these size-selective separators have a higher proton transfer capability and better applicability than the common Ion Exchange Membranes (IEM). However, higher oxygen and substrate permeation through these coarse-pore separators is their most important shortcoming [25, 26], especially for Separator-Electrode Assembly (SEA) design of MFCs whose electrodes were closely placed on both sides of the separator

*Corresponding Author's Email: davoodmk@eng.usb.ac.ir (D. Mohebbi-Kalhori)
URL: https://www.jree.ir/article_147027.html

Please cite this article as: Keshavarz, M., Mohebbi-Kalhori, D. and Yousefi, V., "Multi-response optimization of tubular microbial fuel cells using response surface methodology (RSM)", ***Journal of Renewable Energy and Environment (JREE)***, Vol. 9, No. 2, (2022), 49-58. (https://doi.org/10.30501/jree.2022.290677.1218).

[27, 28]. To address this problem and take advantage of different genera's benefits, an assemblage of various size-selective separators was utilized as a proton exchange medium in some studies. For instance, in our previous work, three layers of NC, JC, and Glass Fiber (GF) have been successfully assembled as a separator of the continuous tubular microbial fuel cell [20]. NC layer was placed next to the anode chamber and JC and GF layers were assembled afterward in three arrangements. Though implementation of GF layer after the JC layer increased the electrode thickness due to its relatively high thickness (4 mm), it could block the excess oxygen crossing between the chambers and hence, improve the power and current densities remarkably. Moreover, the effect of two other important parameters including Hydraulic Retention Time (HRT) and relative flow patterns of influent anode and cathode electrolytes were investigated and optimized separately [20].

However, this study with many other industrial and laboratory scale processes was conventionally investigated using One-Factor-At-a-Time (OFAT) optimization method, which was only functionalized for the examination of single varied factors and did not include the interaction of various factors. To solve this problem, statistical Response Surface Methodology (RSM) can be used to build an empirical model by analyzing the affecting parameters as well as their interactions. This useful technique has also become more popular in biochemical fields, where a distinct mechanistic model cannot be easily formulated [29-32].

Therefore, in this work, the effects of three important factors of separator layers arrangement, wastewater flow rate (or HRT), and the anolyte and catholyte flow patterns were statistically optimized by using RSM according to D-optimal design.

As the first categorical factor, three different combinations of cost-effective porous layers, i.e., including nylon cloth (NC), J-cloth (JC), and the absorbent layer of artificial rayon (AL), were selected to find the best design of Separator-Electrode Assembly (SEA) for continuous tubular MFCs. Two flow patterns of anolyte versus catholyte (co-current and counter-current) were also investigated simultaneously. The flow rate of influent wastewater to the anode chamber, the only numeric factor of this design, was controlled between as 2.9 and 6.9 ml/min at 5 levels. On the other hand, the Maximum Power Density (MPD) and Coulombic Efficiency (CE) of each experiment were adopted as two responses of this statistical optimization. There are many types of research on the optimization of microbial fuel cell's operational conditions as well as those types of researches that focused absolutely on finding appropriate low-cost separators. However, to the best of our knowledge, this study is the first one that statistically investigates and optimizes different separator-electrode assemblies as well as prominent operational parameters along with their interactive effects.

2. MATERIALS AND METHODS

2.1. MFC construction

The MFC designs are almost similar to our previous study except for minor design differences including use of brass valves instead of plastic cones for input and output sections of the anode and cathode chambers. Moreover, a new absorbent fabric layer is implemented instead of glass fiber in the proton exchange layers [20]. The schematic design along with visual preparation steps of the tubular MFCs is given in Figure 1. The two-chambered MFCs consist of the inner cylindrical anode chamber (diameter = 3 cm and long = 30 cm) and the outer coaxial cathode chamber (diameter = 6 cm and long =30 cm). The anode surface was perforated using a drill (100 homogenously pores, each diameter 3 mm) for crossing the protons (surface area of 0.0007 m^2).

The separators used in the MFCs as the proton exchange medium composed of Nylon Cloth (NC, 0.5 mm thick, 70 µm pore diameter, and polyamide material), J-cloth (JC, 1 mm thick, Canada), and artificial rayon cloth as the absorbent layer (AL, 3 mm thick) in three different arrangements.

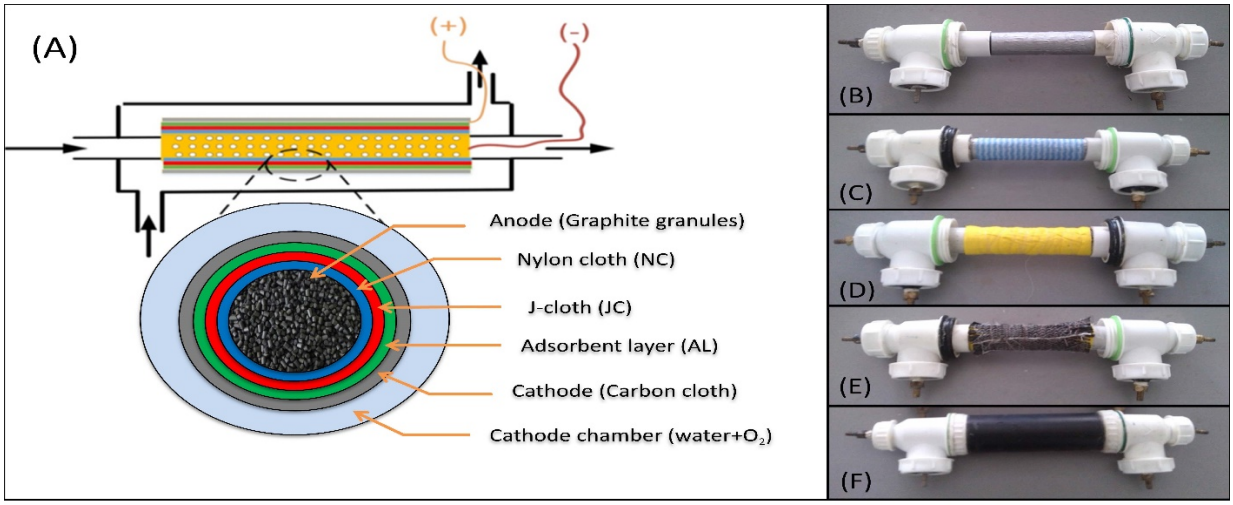

Figure 1. (A) schematic presentation of the tubular MFCs along with their cross-section details, (B) the assembled NC (thickness of 0.5 mm) over the perforated anode tube, (C) the J-cloth layer (1 mm thickness) wrapped around the nylon cloth, (D) the absorbent layer (3 mm thickness) over the previous layers, (E) the carbon cloth cathode, and (F) the completed MFC with an outer PVC tube as cathode chamber

The cathode electrode was made of carbon cloth (11 cm width and 13 cm length) wrapped on the applied multilayer separator (Figure 1E) and tightened using a thin pure copper wire as a collector for produced current. Granular graphite with an average diameter of 4 mm, the porosity of 9.39 %, and density of 1.77 g/cm^3 was used as an anode electrode accompanied by the spiral aluminum strip with a width of 0.9 cm and a length of 60 cm as the anode current collector, which was embedded into the anode compartment.

Fresh wastewater was continuously supplied from the septic tank of the sewage treatment plant of the University of Sistan and Baluchestan as anode electrolyte by a pump. Oxygen saturated tap water as catholyte was continuously fed into the cathode compartment. All experiments were triplicated by 3 similar MFCs in the same conditions, in which the temperature was controlled in the MFC containing chamber at 37 ºC, as depicted in Figure 2.

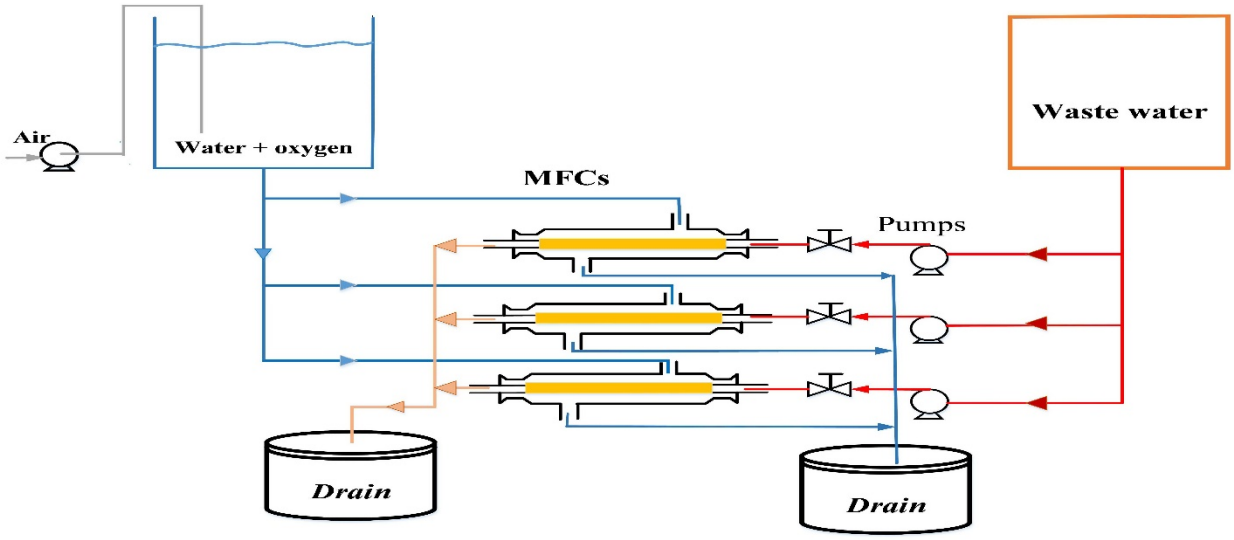

Figure 2. The process diagram of the experimental setup

2.2. Measurements and calculations

Open- and closed-circuit modes of three tubular MFCs operated and their voltages were recorded by a multimeter device (VC9805 Zhangzhou Weihua Electronic Co., Ltd., Fujian, China). The current (I) passing through the circuit was readily obtained using the well-known Eq. (1):

$$I = V/R_{ex} \quad (1)$$

where V is the voltage (V) and R_{ex} (1000 Ω) is the external resistance. Subsequently, the data for polarization were produced by varying the external resistances from 17 to 44000 Ω. The resulting voltages were recorded after stabilization. The Power Density (PD) and Current Density (CD) can be calculated through the following equations (Eq. 2 and Eq. 3):

$$PD = \frac{V^2}{R_{ext}A} \quad (2)$$

$$CD = \frac{V}{R_{ext}A} \quad (3)$$

where V, R_{ex}, and A represent the voltage (V), external resistance (Ω), and the effective surface area of proton transfer (m^2), respectively.

An instrument according to a standard method (photometer AL250 & CSB/COD-Reactor AL38, AQUALYTIC, Dortmund, Germany) was used to measure the Chemical Oxygen Demand (COD) for the fresh and treated wastewaters. Moreover, a Manometric BOD Measuring device (OxiTop®IS, USA) was used to obtain the Biological Oxygen Demand (BOD).

The Coulombic Efficiency (CE) was obtained using Eq. (4) [2].

$$CE(\%) = \frac{M\int_0^t I\,dt}{F\,b\,v_{An}\,\Delta COD} \quad (4)$$

where F represents Faraday's constant; b = 4 is the number of exchanged electrons per each mole of reacted oxygen; ΔCOD is the difference between inlet and outlet COD of anolyte; v_{An} is the volume of the anode compartment, and M represents the oxygen molecular weight.

2.3. Experimental design

The D-optimal method is one of the most useful techniques in the Response Surface Methodologies (RSM). D-optimal technique is well used for the curve fitting of complex problems, optimization, and experimental investigations. In addition, this method is applied to the chronological experimentation.

Several factors can influence the overall performance of microbial fuel cells. However, based on the experimental results of the previous work [20], three independent factors of anolyte flow rate, proton exchange layers arrangements, and flow pattern of anodic and cathodic influents were adopted as the most influencing parameters to be optimized using RSM. The independent parameters including flow rate of anolyte (2.9 to 6.9 (ml/min) at five levels), types and orders of the proton exchange layers (3 types, namely NC, JC, AL), and flow pattern in the cathode and anode compartments (2 patterns, i.e., co-current and counter-current) along with their experimental levels are shown in Table 1.

Table 1. Factors and levels of the experimental designs

Variables	Symbol	Variable levels				
Flow rate (ml/min)	A	2.9	3.9	4.9	5.9	6.9
Types and order of exchange layers	B	NC-JC	NC-JC-AL		NC-AL-JC	
Relative flow pattern of cathode and anode influents	C	Co-current		Counter-current		

The Maximum Power Density (MPD, mW/m^2) and the Coulombic Efficiency (CE, %) of the MFCs were defined as the responses of the statistical design. It is important to notice

that if RSM is not used in many experiments, higher expenses occur. Here, the nylon-cloth (NC), J-cloth (JC), and the absorbent layer (AL) of artificial rayon constitute the layers of the proton exchange medium in the MFCs with three distinct arrangements. The experimental designs and the RSM analysis were performed by means of Design-Expert software (version 8.0.0).

The experimental design of this study is represented in Table 2. The main responses in the statistical analysis are the MPD and CE of the microbial fuel cells. Table 2 shows the internal resistance of the microbial fuel cells for each experiment, which have been estimated from the concentration polarization plots. However, the internal resistance cannot be identified as the third independent response of RSM design, owing to its interconnection with the power density of microbial fuel cell.

Table 2. Design arrangement and experimental results for three responses of RSM design

Run	A: Anolyte flow rate (ml/min)	B: Types and orders of proton exchange layers	C: Flow patterns	Internal resistance (Ω)	R1: MPD (mW/m^2)	R2: CE (%)
1	2.9	NC-AL-JC	counter-current	546.3	197.659	1.8173
2	4.9	NC-AL-JC	co-current	383.1	222.700	3.7127
3	2.9	NC-JC	co-current	445.1	196.216	3.4912
4	6.9	NC-JC	counter-current	376.8	258.664	4.5321
5	3.9	NC-JC-Al	co-current	459.2	215.437	4.4341
6	2.9	NC-JC	co-current	445.2	225.601	3.1653
7	6.9	NC-JC-Al	co-current	343.8	276.915	4.0810
8	2.9	NC-JC-Al	counter-current	519.4	179.534	3.6810
9	4.9	NC-JC-Al	counter-current	584.2	188.260	3.3306
10	3.9	NC-JC	counter-current	476.9	203.812	3.8721
11	5.9	NC-JC	co-current	329.3	224.002	4.3174
12	6.9	NC-JC-Al	counter-current	344.2	274.692	4.4162
13	6.9	NC-AL-JC	co-current	323.9	285.895	4.9675
14	5.9	NC-JC	co-current	329.4	252.382	4.2385
15	6.9	NC-JC	counter-current	376.7	285.496	4.2995
16	5.9	NC-AL-JC	counter-current	410.1	212.175	1.6427
17	2.9	NC-AL-JC	co-current	433.4	201.272	3.2639

3. RESULTS AND DISCUSSION

3.1. Results for wastewater treatment

The COD and BOD of input wastewater were 1220 and 560 (mg/lit), respectively, with the BOD/COD ratio of 0.46. The BOD of the output stream was measured to be 95 (mg/lit), with 83 % percent of treatment, which seems to be an acceptable result [33].

3.2. Statistical optimization results

Microbial fuel cells are complex systems in which many factors can influence their performance. However, the performance of MFC systems can be optimized from different viewpoints such as maximizing the power generation, wastewater treatment, or current production. In the present study, two most important parameters of MPD and CE were adopted as the main responses of statistical optimization. Two distinct analyses of variance (ANOVA) were separately done for each response of RSM optimization, which is described in the following sections thoroughly.

3.2.1. The first response of RSM optimization: MPD

The results of ANOVA for MPD (Table 3) reveal that only A (flow rate), C (flow pattern), and A^2 can significantly affect (p-value < 0.05) the power generation of the MFCs. However, the order of separator layers (B) was not recognized as a significant parameter in the power production of the MFCs. Moreover, these results indicated that the influent flow rate of anolyte (A) was the most prominent parameter in the MPD of the MFCs.

The low p-value obtained for the model parameter indicates that the obtained model for the response is significant in terms of statistical analysis and there is a chance of 0.01 % in which the high amount of the model F-value (33.24) can occur due to existing noise. In addition, a value of 0.8847 was found for the coefficient of determination (R^2). Also, reasonable agreement between "Adjusted R^2" (0.8580) and "Predicted R^2" (0.8063) confirmed that the observed and predicted values had a good correlation. Comparison of the residual and pure errors in terms of replicated experimental design is obtained by the "lack of fit tests". In this regard, the p-values > 0.05 mean that there is an insignificant lack of fit. Furthermore, "Adequate

Precision" of 14.717, which presents the signal-to-noise ratio, implies an adequate signal. Overall, the obtained model can acceptably be employed to navigate the design space. Finally, an expression was produced mathematically from this statistical analysis. Equation 5 shows the mathematical expression in terms of the codded significant factors, and Equation 6 points to the correlation between the MPD and the actual factors of the analysis as follows:

$$MPD = 207.40 + 37.42 \times A - 8.30 \times C + 30.92 \times A^2 \quad (5)$$

$$MPD = k - 57.042 \times (F) + 7.729(F)^2 \quad (6)$$

where F represents the flow rate of anolyte and k is a constant value that is equal to 309.625 for co-current and 293.023 for counter-current flow patterns, respectively.

Table 3. The ANOVA analysis for the maximum power density (MPD) of the MFCs (the first response of RSM design)

Source	Sum of squares	df	Mean square	F-value	p-value	
Model	17999.26	3	5999.75	33.24	< 0.0001	significant
A-flow rate	15506.08	1	15506.08	85.90	< 0.0001	
C-flow pattern	1148.36	1	1148.36	6.36	0.0255	
A^2	2726.66	1	2726.66	15.11	0.0019	
Residual	2346.67	13	180.51			
Lack of fit	1152.22	10	115.22	0.29	0.9407	not significant
Pure error	1194.45	3	398.15			
Cor total	20345.93	16				
R^2= 0.8847 Adj. R^2= 0.8580						

3.2.2. The second response of RSM optimization: Coulombic Efficiency (CE)

The analysis of variance (ANOVA) for the CE has been done separately as the second response of the statistical optimization (Table 4). The results of this analysis reveal that all of three independent variables including anolyte flow rate (A), the orders of proton exchange layers (B), and relative flow patterns (C) of the anolyte and catholyte influents have statistically significant influence (p-value <0.05) on the CE of the MFCs. Interestingly, the orders of proton exchange layers (B), not recognized as a significant parameter in the analysis of variance of the first response, i.e., power density, has the highest F-value now. Therefore, although the orders of proton exchange layers may not have a significant impact on the power generation proficiency of microbial fuel cells, it can, however, control the rate of oxygen transportation between the cathode and anode compartment and hence, greatly affect the CE of the MFC systems. Comparison of the average values of coulombic efficiency for different arrangements shows that the addition of absorbent layer after the J-cloth improves the coulombic efficiency by about 15 %.

The prediction model for the CE has been modified using a reciprocal square root transformation to improve the normality of data. Results of ANOVA show that the resulting model is statistically significant. Acceptable proximity of R^2 (0.9436) value to 1.0 along with the agreement of the adjusted R^2 (0.9098) and the predicted R^2 (0.8868) values confirmed the model adequacy. Moreover, insignificant “lack of fit” along with the high value of "Adequate Precision" (17.622) indicates a sufficient signal-to-noise ratio and model adequacy.

Table 4. ANOVA for the coulombic efficiency (CE) of the MFCs as the second response of RSM

Source	Sum of squares	df	Mean square	F-value	p-value	
Model	0.12	6	0.021	27.90	< 0.0001	significant
A-flow rate	4.495E-003	1	4.495E-003	6.05	0.0337	
B-layers arrangement	0.046	2	0.023	30.89	< 0.0001	
C-flow pattern	0.020	1	0.020	26.76	0.0004	
BC	0.048	2	0.024	32.24	< 0.0001	
Residual	7.432E-003	10	7.432E-004			
Lack of fit	7.012E-003	7	1.002E-003	7.15	0.0671	not significant
Pure error	4.204E-004	3	1.401E-004			
Cor total	0.13	16				
R^2= 0.9436 Adj. R^2= 0.9098						

Finally, the following mathematical correlation was derived to predict the coulombic efficieny of microbial fuel cells based on the significant parameters of “proton exchange layers” (B), “flow rate” (A), and “flow patterns” (C) regarding the coded (Eq. 7) and the actual factors (Eq. 8).

$$\frac{1}{\sqrt{CE}} = 0.55 - 0.021 \times A - 0.044 \times B[1] + 0.091 \times B[2] + 0.040 \times C - 0.028 \times B[1]C + 0.078 \times B[2]C \quad (7)$$

$$\frac{1}{\sqrt{CE}} = C_1 - 0.0106 \times F \quad (8)$$

where F is the flow rate of anolyte influent and different values of C1 constant in Eq. 8 for each categorical factor are mentioned in Table 5.

Table 5. Constant values of correlated expressions for CE (Eq. 8)

Flow pattern (C)	Proton exchange layers arrangements (B)	C_1 (Eq.8)
Co-current	NC-JC-AL	0.5422
Counter-current	NC-JC-AL	0.5669
Co-current	NC-AL-JC	0.5708
Counter-current	NC-AL-JC	0.8077
Co-current	NC-JC	0.5627
Counter-current	NC-JC	0.5418

3.3. Investigation of the effects of the prominent parameters and their interactions

3.3.1. The effect of proton exchange layer arrangements

Microbial fuel cells are useful and eco-friendly technologies that can generate electricity from various waste materials. Generally, the organic matters are biologically degraded in the anode chamber using the exoelectrogens, and the produced electrons are transferred via the external circuit to react with the final electron-acceptor at the cathode (usually oxygen). The proton exchange membrane between the anode and cathode chambers transfers the generated protons in the anode to the cathode. It also provides a distance as close as possible between the electrodes and at the same time, prevents the short-circuiting, crosses the species between the chambers, and maintains anaerobic anodic environment by controlling the oxygen migration from the cathode to the anode compartment.

However, the objective of this paper is to substitute common highly expensive polymeric proton exchange membranes, with super-low-cost cloth layers. In this regard, the effect of different arrangements of three layers of nylon cloth (NC), J-cloth (JC), and glass fiber (GF) on the overall performance of MFCs was investigated statistically. The results of our previous research revealed that the placement of J-cloth fabric after the NC layer could sufficiently block the oxygen transportation between the MFC chambers due to the formation of good biofilm layer. However, the arrangement of NC-JC-GF was the best separator arrangement design since the addition of GF layer after the JC layer improved the power density by the 5.15 % compared to the NC-JC design [20]. In the present study, the application of another adsorbent layer, instead of the GF layer, after the j-cloth was examined thoroughly. Therefore, different arrangements of three layers of NC, JC, and absorbent rayon layer (AL) were investigated statistically. The power generation performance, cost, and coulombic efficiency of the present separator electrode assemblies were compared with the other low-cost porous fabric separators in Table 6.

Table 6. Comparison of the power output, coulombic efficiency, and cost of porous fabric separators

Separator	Thickness (mm)	Pore size (µm)	$K_o \times 10^{-4}$ (cm/s)	R_{ohm} (Ω)	R_{in} (Ω)	CE (%)	PD (mW/m^2)	Cost ($/$m^2$)	PO (mW/$)	Ref.
NWF1	0.13	2.01	Nd	60.1 ± 8.7	43 ± 2	Nd	40.8 ± 7.2	2	20.4	[34]
NWF2	0.18	1.78	Nd	59.2 ± 1.2	53 ± 6	Nd	79.2 ± 6.5	3	26.4	
NWF3	0.25	1.81	Nd	72.1 ± 9.5	37 ± 1	Nd	62.7 ± 6.9	4	15.6	
NWF4	0.13	1.21	7.0	46.9 ± 6.5	51 ± 7.5	20	97.0 ± 7.5	2	48.5	
Nafion 117	0.19	Nd	6.7	73.1 ±8.3	93 ± 2	22	57.5 ± 3.9	1400	0.04	
NWF-PP80	0.49	30	0.37 ± 0.2	9.29	Nd	22	Nd	0.57	Nd	[34]
NWF-PP100	0.54	42	0.73 ± 0.6	9.50	Nd	18	117	0.57	Nd	
PPS	0.52	40	0.75 ± 0.7	9.51	Nd	11	102	8.33	Nd	
S-PPS	0.54	44	0.72 ± 0.2	3.53	Nd	14	190	9.2	Nd	
CMI-7000	0.46	4-12	0.2	9.68	Nd	16	78	166	Nd	
Nafion 117	0.19	5×10^{-3}	0.75	3.13	Nd	19	24	2300	Nd	
J-Cloth	0.3	Nd	29.0	0.21± 0.08	38.1± 0.1	~40	786 ± 23	Nd	Nd	[34]
GF 1	1	Nd	0.50	2.26 ±0.1	38.1± 0.1	~80	791 ± 69	Nd	Nd	
GF 0.4	0.4	Nd	0.75	2.39 ± 0.3	40.1 ± 0.4	~78	623 ± 4	Nd	Nd	
CMI-7000	0.46	Nd	0.94	3.78 ± 0.4	131.7 ± 8.4	Nd	267 ± 22	Nd	Nd	
Nylon 0.2	0.170	0.2	Nd	Nd	84.6	70	443±27	Nd	Nd	[34]
Nylon 0.45	0.170	0.45	Nd	Nd	57.3	63	650 ± 7	Nd	Nd	
Nylon 10	0.045	10	Nd	Nd	41.4	55	769±65	Nd	Nd	
Nylon 60	0.050	60	Nd	Nd	39.5	45	816 ± 34	Nd	Nd	
Nylon 100	0.080	100	Nd	Nd	37.3	41	908 ± 24	Nd	Nd	
Nylon 160	0.100	160	Nd	Nd	35.7	31	941±47	Nd	Nd	
GF 0.7	0.380	0.7	Nd	Nd	40.4	56	732 ± 48	Nd	Nd	
GF 1	0.700	1.0	Nd	Nd	42.3	60	716 ±60	Nd	Nd	

GF 2	0.380	2.0	Nd	Nd	39.6	55	779 ±43	Nd	Nd	
NC-JC	0.15	Nd	Nd	Nd	576.09	6.03 ± 0.3	267.17 ± 30.6	7	38.2	[34]
NC-JC-GF	0.55	Nd	Nd	Nd	562.09	5.78 ± 0.3	281.30 ± 32.3	7.32	38.4	
NC-JC	1.5	Nd	Nd	Nd	397.1 ± 59	4.7	285.49	7	40. 8	This study*
NC-JC-AL	4.5	Nd	Nd	Nd	450.2 ± 106	4.08	276.91	~7.5	36.9	
NC-AL-JC	4.5	Nd	Nd	Nd	419.4 ± 82	4.26	285.89	~7.5	38.1	

Nd: not determined; NWF: non-woven fabric; NC: Nylon cloth, JC: J-cloth, GF: Glass fiber; AL: adsorbent layer.

* The highest values of power density obtained for each arrangement are provided in this table for comparison with the other separator types. The detailed results of experiments are listed in Table 2.

Figure 3 compares the results of two MFC experiments with different arrangements of NC-JC and NC-JC-AL. The other parameters of flow-patterns and flow-rate were similar in these experiments which were adjusted to counter-current and 6.9 ml/min, respectively. According to Figure 3, there is no marked difference in the open circuit voltages, currents, and polarization results of these MFCs. However, comparing the concentration polarization curves in Figure 3C revealed that although the overpotential and concentration losses were almost similar for these two arrangements, by taking into account the slope of the middle part of plots, the ohmic losses for the NC-JC-Al were slightly lower than the values for NC-JC. Altogether, unlike the glass fiber, the addition of rayon layer after the JC could not significantly improve the performance of MFC, as expected. However, as stated in the previous sections, ANOVA analysis confirmed that these different arrangements of proton exchange layers had only statistically significant impact on the CE of MFCs (p-value <0.05) and marginal differences in the maximum power densities of MFCs were not statistically significant.

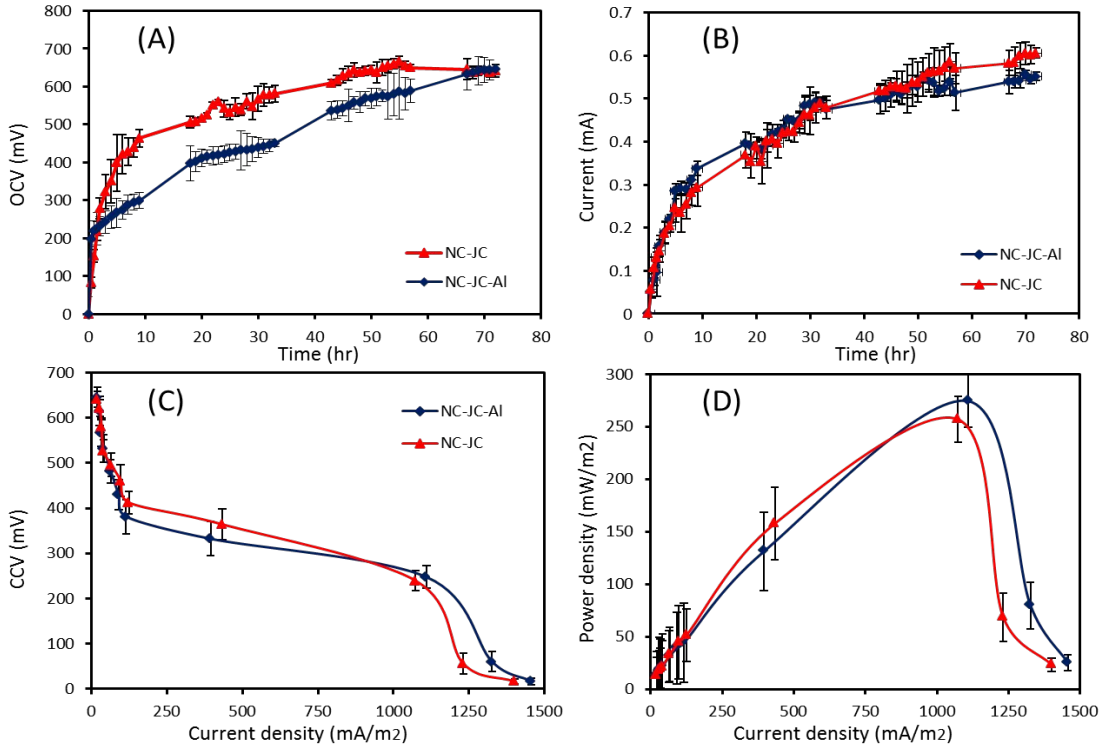

Figure 3. A comparison of the results of two experiments with different proton exchange layers of NC-JC and NC-JC-AL: (A) open circuit voltage, (B) current production, (C) closed circuit voltage, and (D) power density

Furthermore, the combined effects of independent variables on the two responses of RSM optimization were investigated as well as their individual effects. Figure 4 illustrates the combined effects of layer arrangements (B) and flow patterns of influents (C) on the two responses of MPD and CE.

Statistical analysis showed that although different arrangements of the above-mentioned cloths had no significant effect on the maximum generated power as well as open-circuit voltages of MFCs, it can seriously control the oxygen crossover between the chambers and affect the current production and CE of MFCs. Nevertheless, as can be seen in Figure 4B, the effect of layer arrangements on the CE was more pronounced in the counter-current mode of influents. It seems that higher pressure differences occurred in the counter-current mode result in the more oxygen passage across the separator layers, which hindered the performance of MFCs and decreased the CE. Moreover, the lowest CE was achieved when the absorbent rayon layer (AL) was placed next to the nylon cloth (NC) layer instead of J-Cloth (JC) since the high-porous rayon layer could not block the oxygen transfer

through the separator adequately. This fundamental role of J-cloth in the control of oxygen transportation rate is consistent with the results of our previous study [20].

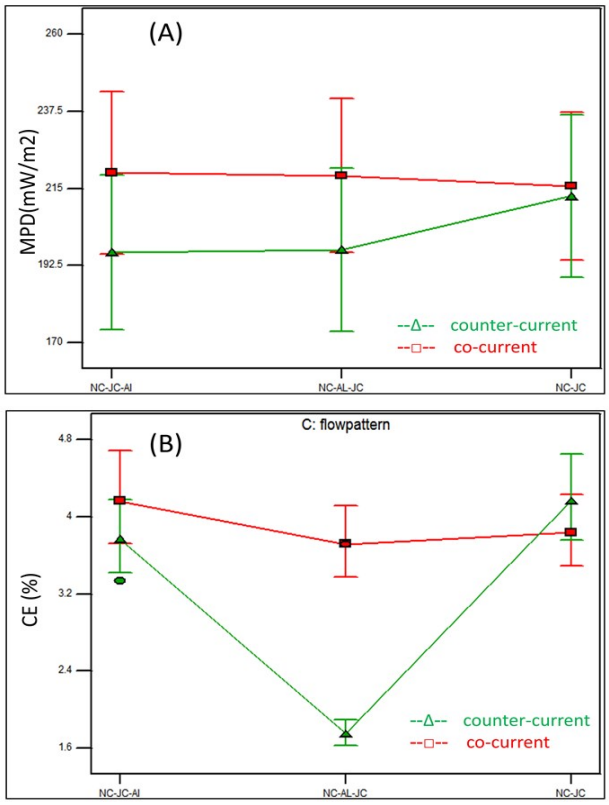

Figure 4. Combined effects of different separator layers (factor B) and flow patterns (factor C) on the two responses of RSM optimization: (A) MPD and (B) CE; the red squares and green triangles represent the co-current and counter-current modes, respectively

3.3.2. The effect of wastewater flow rate or Hydraulic Retention Time (HRT)

It is well known that the adoption of the appropriate HRT of anolyte in the anode compartment has a significant effect on the performance of MFCs with continuous flow mode, because it must be consistent with the generation rate of anodic bacteria and provide enough organic substrates for them. In this study, like many others, different anodic HRTs have been adjusted by changing the flow rates of influent wastewater.

The flow rate of wastewater effect on the two responses of MPD and CE is depicted in Figure 5. Consistent with our previous work, both the maximum power density and CE of MFCs were enhanced by increasing the flow rate or, in other words, by decreasing the wastewater HRT in the anode compartment. The rate of altering the responses by the change of wastewater flow rate was obviously different. The MPD of MFCs increased polynomial, whereas CE had a linear growth by increasing the flow rate of wastewater.

3.3.3. The effect of influent flow patterns on the performance of MFCs

Both responses of the statistical optimization are presented in Figure 6, which are affected by different modes of co-current and counter-current operations. Consistent with the results of our previous research, MFCs have better performance in the co-current configuration than the counter-current in terms of both the power production and CE. This priority of co-current over the counter-current mode is probably due to higher trans-membrane pressure and more oxygen crossover between the chambers in the counter-current design of MFCs, as described previously [20].

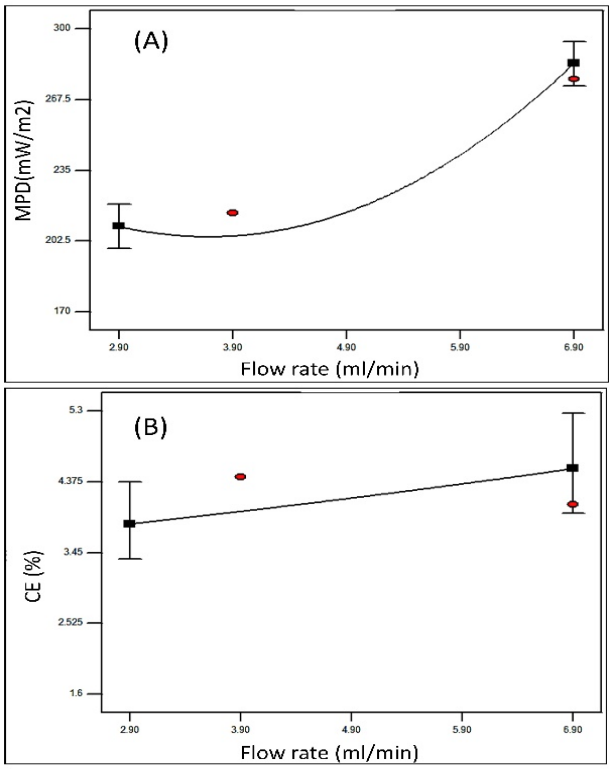

Figure 5. The effect of influent wastewater flow rate on (A) MPD and (B) CE of microbial fuel cells; red circles indicate the experimental design points

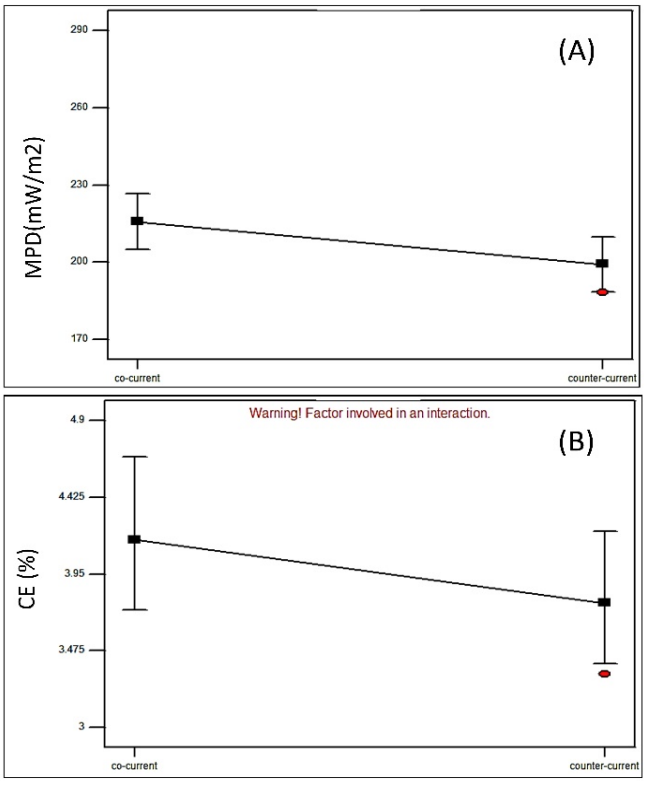

Figure 6. The effect of co-current and counter-current modes on the two responses of (A) MPD and (B) CE of MFCs; red circles indicate the experimental design points

4. CONCLUSIONS

In the present study, three more important operating parameters of influent flow patterns, different proton exchange layers, and the hydraulic retention time (HRT) of used wastewater in the anode compartment were statistically optimized by using the D-optimal-based response surface methodology (RSM). Two independent responses of maximum power density (MPD) and CE of MFCs were adopted for this optimization and two distinct ANOVA analyses were done for them. Statistical analyses confirmed that although different arrangements of nylon cloth, J-cloth, and absorbent rayon layer (AL) did not have a significant impact on the power production, it could critically influence the oxygen transfer rate between the anode and cathode chambers and thereby the CE of MFCs. Among the three configurations of NC-JC, NC-JC-AL, and NC-AL-JC, the first design of NC-JC-Al was the best arrangement. However, the addition of absorbent rayon layer after the J-cloth could not improve the MFC performance considerably. Since the application of rayon layer, with extremely high porosity, just increased the electrode distance without sufficient enhancement of the oxygen barrier property of separator. The MFC with NC-JC-AL assembly generated almost the same power density, but 8.2 % higher CE than the NC-JC design.

On the other hand, MFCs had superior performance in the co-current flow pattern compared to counter-current in terms of both the power production and CE. Moreover, investigation of the combined parameters effects revealed that the effect of separator layer arrangements was more pronounced in the counter-current flow patterns, owing to its higher-pressure difference and more oxygen penetration between the MFC chambers. Furthermore, the higher flow rates of wastewater improved the MFC performance due to the sufficiency of the organic substrate for the growth of anodic bacteria. Overall, the best conditions based on this optimization study were the co-current flow pattern, NC-JC-Al separator arrangement, and the anolyte flow rate of 6.9 (ml/min).

5. ACKNOWLEDGMENT

This research was supported by the University of Sistan and Baluchestan.

REFERENCES

1. Logan, B.E., Microbial fuel cells, John Wiley & Sons Inc., Hoboken, New Jersey, (2008). (https://doi.org/10.1002/9780470258590).
2. Logan, B.E., Hamelers, B., Rozendal, R., Schroder, U., Keller, J., Freguia, S., Aelterman P., Verstraete W. and Rabaey K., "Microbial fuel cells: Methodology and technology", ***Environmental Science and Technology***, Vol. 40, No. 17, (2006), 5181-5192. (https://doi.org/10.1021/es0605016).
3. Lovley, D.R., "The microbe electric: Conversion of organic matter to electricity", ***Current Opinion in Biotechnology***, Vol. 19, No. 6, (2008), 564-571. (https://doi.org/10.1016/j.copbio.2008.10.005).
4. El Haj Assad, M., Khosravi, A., Malekan, M., Rosen, M.A. and Nazari, M.A., "Chapter 14 - Energy storage", Design and performance optimization of renewable energy systems, Academic Press, (2021), 205-219. (https://doi.org/10.1016/B978-0-12-821602-6.00016-X).
5. Logan, B.E., "Exoelectrogenic bacteria that power microbial fuel cells", ***Nature Reviews Microbiology***, Vol. 7, No. 5, (2009), 375-381. (https://doi.org/10.1038/nrmicro2113).
6. Tan, W.H., Chong, S., Fang, H.-W., Pan, K.-L., Mohamad, M., Lim, J.W., Tiong, T.J., Chan, Y.J., Huang, C.-M. and Yang, T.C.-K., "Microbial fuel cell technology—A critical review on scale-up issues", ***Processes***, Vol. 9, No. 6, (2021), 985. (https://doi.org/10.3390/pr9060985).
7. Kataki, S., Chatterjee, S., Vairale, M.G., Sharma, S., Dwivedi, S.K. and Gupta, D.K., "Constructed wetland, an eco-technology for wastewater treatment: A review on various aspects of microbial fuel cell integration, low temperature strategies and life cycle impact of the technology", ***Renewable and Sustainable Energy Reviews***, Vol. 148, No. (2021), 111261. (https://doi.org/10.1016/j.rser.2021.111261).
8. You, S., Zhao, Q., Zhang, J., Jiang, J. and Zhao, S., "A microbial fuel cell using permanganate as the cathodic electron acceptor", ***Journal of Power Sources***, Vol. 162, No. 2, (2006), 1409-1415. (https://doi.org/10.1016/j.jpowsour.2006.07.063).
9. Fornero, J.J., Rosenbaum, M., Cotta, M.A. and Angenent, L.T., "Microbial fuel cell performance with a pressurized cathode chamber", ***Environmental Science & Technology***, Vol. 42, No. 22, (2008), 8578-8584. (https://doi.org/10.1021/es8015292).
10. Oh, S., Min, B. and Logan, B.E., "Cathode performance as a factor in electricity generation in microbial fuel cells", ***Environmental Science & Technology***, Vol. 38, No. 18, (2004), 4900-4944. (https://doi.org/10.1021/es049422p).
11. Rabaey, K. and Verstraete, W., "Microbial fuel cells: Novel biotechnology for energy generation", ***Trends in Biotechnology***, Vol. 23, No. 6, (2005), 291-298. (https://doi.org/10.1016/j.tibtech.2005.04.008).
12. Miroliaei, M.R., Samimi, A., Mohebbi-Kalhori, D., Khorram, M. and Qasemi, A., "Competition between *E. coli* and *Shewanella sp.* for electricity generation in air cathode MFC in presence of methylene blue as artificial mediator", ***Environmental Progress & Sustainable Energy***, Vol. 34, No. 4, (2015), 1097-1105. (https://doi.org/10.1002/ep.12111).
13. Zhuwei, D.U., Haoran, L.I. and Tingyue, G.U., "A state of the art review on microbial fuel cells: A promising technology for wastewater treatment and bioenergy", ***Biotechnology Advances***, Vol. 25, No. 5, (2007), 464-482. (https://doi.org/10.1016/j.biotechadv.2007.05.004).
14. Oh, S.T., Kim, J.R., Premier, G.C., Lee, T.H., Kim, C. and Sloan, W.T., "Sustainable wastewater treatment: How might microbial fuel cells contribute", ***Biotechnology Advances***, Vol. 28, No. 6, (2010), 871-881. (https://doi.org/10.1016/j.biotechadv.2010.07.008).
15. Ouitrakul, S., Sriyudthsak, M., Charojrochkul, S. and Kakizono, T., "Impedance analysis of bio-fuel cell electrodes", ***Biosensors and Bioelectronics***, , Vol. 23, No. 5, (2007), 721-772. (https://doi.org/10.1016/j.bios.2007.08.012).
16. Zhou , M.C., Luo , M.J., He, H. and Jin, T., "An overview of electrode materials in microbial fuel cells", ***Journal of Power Sources***, Vol. 196, No. 10, (2011), 4427-4443. (https://doi.org/10.1016/j.jpowsour.2011.01.012).
17. Khalili, H.-B., Mohebbi-Kalhori, D. and Afarani, M.S., "Microbial fuel cell (MFC) using commercially available unglazed ceramic wares: Low-cost ceramic separators suitable for scale-up", ***International Journal of Hydrogen Energy***, Vol. 42, No. 12, (2017), 8233-8241. (http://dx.doi.org/10.1016/j.ijhydene.2017.02.095).
18. Yousefi, V., Mohebbi-Kalhori, D. and Samimi, A., "Ceramic-based microbial fuel cells (MFCs): A review", ***International Journal of Hydrogen Energy***, Vol. 42, No. 3, (2017), 1672-1690. (https://doi.org/10.1016/j.ijhydene.2016.06.054).
19. Li, W.-W., Sheng, G.-P., Liu, X.-W. and Yu, H.-Q., "Recent advances in the separators for microbial fuel cells", ***Bioresource Technology***, Vol. 102, No. 1, (2011), 244-252. (https://doi.org/10.1016/j.biortech.2010.03.090).
20. Yousefi, V., Mohebbi-Kalhori, D., Samimi, A. and Salari, M., "Effect of separator electrode assembly (SEA) design and mode of operation on the performance of continuous tubular microbial fuel cells (MFCs)", ***International Journal of Hydrogen Energy***, Vol. 41, No. 1, (2016), 597-606. (https://doi.org/10.1016/j.ijhydene.2015.11.018).
21. Yousefi, V., Mohebbi-Kalhori, D. and Samimi, A., "Equivalent electrical circuit modeling of ceramic-based microbial fuel cells using the electrochemical impedance spectroscopy (EIS) analysis", ***Journal of Renewable Energy and Environment (JREE)***, Vol. 6, No. 1, (2019), 21-28. (https://doi.org/10.30501/JREE.2019.95555).
22. Cheraghipoor, M., Mohebbi-Kalhori, D., Noroozifar, M. and Maghsoodlou, M.T., "Comparative study of bioelectricity generation in a microbial fuel cell using ceramic membranes made of ceramic powder, Kalporgan's soil, and acid leached Kalporgan's soil", ***Energy***, Vol. 178, (2019), 368-377. (https://doi.org/10.1016/j.energy.2019.04.124).
23. Cheraghipoor, M., Mohebbi-Kalhori, D., Noroozifar, M. and Maghsoodlou, M.T., "Production of greener energy in microbial fuel cell with ceramic separator fabricated using native soils: Effect of lattice

and porous SiO_2", ***Fuel***, Vol. 284, (2021), 118938. (https://doi.org/10.1016/j.fuel.2020.118938).

24. Rodríguez, J., Mais, L., Campana, R., Piroddi, L., Mascia, M., Gurauskis, J., Vacca, A. and Palmas, S., "Comprehensive characterization of a cost-effective microbial fuel cell with Pt-free catalyst cathode and slip-casted ceramic membrane", ***International Journal of Hydrogen Energy***, Vol. 46, No. 51, (2021). (https://doi.org/10.1016/j.ijhydene.2021.01.066).
25. Yousefi, V., Mohebbi-Kalhori, D. and Samimi, A., "Application of layer-by-layer assembled chitosan/montmorillonite nanocomposite as oxygen barrier film over the ceramic separator of the microbial fuel cell", ***Electrochimica Acta***, Vol. 283, (2018), 234-247. (https://doi.org/10.1016/j.electacta.2018.06.173).
26. Yousefi, V., Mohebbi-Kalhori, D. and Samimi, A., "Start-up investigation of the self-assembled chitosan/montmorillonite nanocomposite over the ceramic support as a low-cost membrane for microbial fuel cell application", ***International Journal of Hydrogen Energy***, Vol. 45, No. 7, (2020), 4804-4820. (https://doi.org/10.1016/j.ijhydene.2019.11.216).
27. Zhang, F., Ahn, Y. and Logan, B.E., "Treating refinery wastewaters in microbial fuel cells using separator electrode assembly or spaced electrode configurations", ***Bioresource Technology***, Vol. 152, (2014), 46-52. (https://doi.org/10.1016/j.biortech.2013.10.103).
28. Ahn, Y. and Logan, B.E., "Domestic wastewater treatment using multi-electrode continuous flow MFCs with a separator electrode assembly design", ***Applied Microbiology and Biotechnology***, Vol. 97, No. 1, (2013), 409-416. (https://doi.org/10.1007/s00253-012-4455-8).
29. Steinberg, D.M. and Bursztyn, D., "Response surface methodology in biotechnology", ***Quality Engineering***, Vol. 22, No. 2, (2010), 78-87. (https://doi.org/10.1080/08982110903510388).
30. Yousefi, V. and Kariminia, H.-R., "Statistical analysis for enzymatic decolorization of acid orange 7 by *Coprinus cinereus* peroxidase", ***International Biodeterioration & Biodegradation***, Vol. 64, No. 3, (2010), 245-252. (https://doi.org/10.1016/j.ibiod.2010.02.003).
31. Kariminia, H.-R. and Yousefi, V., "Statistical optimization of reactive blue 221 decolorization by fungal peroxidise", Water production and wastewater treatment, NOVA publisher, (2011), Chap. 12, 215-224. (https://www.researchgate.net/publication/286857603_Statistical_optimization_of_reactive_blue_221_decolorization_by_fungal_peroxidise).
32. Raychaudhuri, A. and Behera, M., "Review of the process optimization in microbial fuel cell using design of experiment methodology", ***Journal of Hazardous, Toxic, and Radioactive Waste***, Vol. 24, No. 3, (2020), 04020013. (https://doi.org/10.1061/(ASCE)HZ.2153-5515.0000503).
33. Jang, J.K., Pham, T.H., Chang, I.S., Kang, K.H., Moon, H. and Chok, S., "Construction and operation of a novel mediator-and membraneless microbial fuel cell", ***Process Biochem***, Vol. 39, No. 8, (2004), 1007-1012. (https://doi.org/10.1016/S0032-9592(03)00203-6).
34. Choi, S., Kim, J.R., Cha, J., Kim, Y., Premier, G.C. and Kim, C., "Enhanced power production of a membrane electrode assembly microbial fuel cell (MFC) using a cost effective poly [2,5-benzimidazole] (ABPBI) impregnated non-woven fabric filter", ***Bioresource Technology***, Vol. 128, (2013), 14-21. (https://doi.org/10.1016/j.biortech.2012.10.013).

JREE: Vol. 9, No. 2, (Spring 2022) 59-74

Journal of Renewable Energy and Environment

Journal Homepage: www.jree.ir

Materials and Energy Research Center

MERC

Research Article

Reduction of Low Frequency Oscillations Using an Enhanced Power System Stabilizer via Linear Parameter Varying Approach

Vahid Nazari, Mohammad Hossein Mousavi, Hassan Moradi CheshmehBeigi *

Department of Electrical Engineering, Faculty of Engineering, Razi University, P. O. Box: 67144-14971, Kermanshah, Kermanshah, Iran.

PAPER INFO

Paper history:
Received: 27 September 2021
Revised in revised form: 23 December 2021
Scientific Accepted: 15 December 2021
Published: 12 April 2022

Keywords:
Power System Stabilizer,
Single Machine Infinite Bus Power System,
Linear Parameter Varying (LPV),
Linear Matrix Inequality (LMI)

ABSTRACT

Over the past decades, power engineers have begun to connect power grids to other networks such as microgrids associated with renewable units using long transmission lines to provide higher reliability and greater efficiency in production and distribution besides saving resources. However, many dynamic problems such as low frequency oscillations were observed as a result of these connections. Low frequency oscillation is a normal phenomenon in most power systems that causes perturbations and, thus, the grid stability and damping process are of paramount importance. In this paper, to attenuate these oscillations, a novel method for designing Power System Stabilizer (PSS) is presented via Linear Parameter-Varying (LPV) approach for a Single Machine Infinite Bus system (SMIB). Because the system under study is subject to frequent load and production changes, designing the stabilizer based on the nominal model may not yield the desired performance. To guarantee the flexibility of the stabilizer with respect to the aforementioned issues, the power system polytopic representation is used. In order to apply the new method, the nonlinear equations of the system at each operating point, located in a polytope, are parametrically linearized by scheduling variables. Scheduling variables can be measured online in any operating point. By using this model and following the H_∞ synthesis, feedback theories, and Linear Matrix Inequalities (LMIs), LPV controllers at all operating points are obtained. Finally, the simulation results verify the effectiveness of the proposed controller over classic and robust controllers with regard to uncertainties and changes in system conditions.

https://doi.org/10.30501/jree.2021.306909.1265

1. INTRODUCTION

Improving the stability of the power systems is one of the main goals, tasks, and aspirations of power engineers that has been of great significance in the last decades. The development of power grids, their diversity, and intertwining with renewable energies have brought about spontaneous low-frequency oscillations. Small and sudden disturbances in the grid cause natural fluctuations in the system. In the normal case, these oscillations die out rapidly and the amplitude of the oscillations does not exceed a certain amount. However, these fluctuations may continue for a long time and at worst, their amplitudes increase. Such fluctuations in the grid pose serious risks, making it difficult to exploit the system optimally. Various experiences of interconnected power systems indicate that these oscillations are caused by the excitation of electric modes of synchronous generators. Today, power system stabilizers are widely used to robustly improve the stability and overcome the perturbations [1-4].

*Corresponding Author's Email: ha.moradi@razi.ac.ir (H. Moradi CheshmehBeigi)
URL: https://www.jree.ir/article_148013.html

Several methods have been proposed in the literature to attenuate the low frequency oscillations of power systems. Planning a control strategy is essential to damping electromechanical oscillations while designing and creating a power system. Classic control systems, robust, adaptive, optimal, H_∞, fuzzy control-based methods, artificial neural networks, and a wide variety of optimization and artificial intelligence algorithms are some of the methods that have been developed in the field of stability and PSS design over the last years [5-10]. Utilizing fuzzy logic controller for designing a power system stabilizer was studied in an SMIB [11], showing the better performance of Fuzzy PSS (FPSS) over Classic PSS (CPSS) by considering the triangular and Gaussian functions to synthetize the controller. In [12], a predictive optimal adaptive PSS was presented for an SMIB. The simulation results of this optimization algorithm illustrated that the proposed POA-PSS method had preferable performance compared to CPSS. Another research was conducted to evaluate the output performance of CPSS and PID-PSS, which were optimized by Firefly and Bat algorithms. The results clarified that although CPSS with bat algorithm exhibited weak performance, the robust PID-PSS using firefly algorithm optimization could stabilize the proposed SMIB system for all operating conditions [13].

Please cite this article as: Nazari, V., Mousavi, M.H. and Moradi CheshmehBeigi, H., "Reduction of low frequency oscillations using an enhanced power system stabilizer via linear parameter varying approach", ***Journal of Renewable Energy and Environment (JREE)***, Vol. 9, No. 2, (2022), 59-74. (https://doi.org/10.30501/jree.2021.306909.1265).

Under [14] study, a stochastic metaheuristic population-based optimization algorithm named Sine Cosine Algorithm (SCA) was used for tuning PSS parameters. The research revealed that this technique was much more effective than other methods in exploration and exploitation to determine PSS parameters and improve the stability of a single machine connected to a large power system. An artificial intelligence method known as Ant Colony was employed to optimize a PID-PSS for an SMIB system. It was shown that the proposed control approach worked properly and the minimum overshoot for the frequency response and rotor angle were achieved [15].

In further studies, several methods have also been presented for multi-machine power systems. In [16], the design of PSS using the root locus method was investigated. The technique could be applied directly to the power systems and provided clear indication of damping degrees for various combination of PSS parameters. The result of this research indicated that the perturbations caused by noise input could be suppressed by the root locus-based PSS structure. In another study, the design of a fixed parameter PSS for synchronous performance in a multi-machine power system was executed. The stabilizer was designed to compensate for the transfer function. It was shown that the transfer function remained relatively constant over all working points. It was concluded that when facing disturbances, the PSS transfer function and dc gains were selected in a way that the phase and gain errors around the modal frequencies were kept to a minimum. [17]. In [18], a new evolutionary algorithm-based approach was proposed to perfectly design multi-machine power system stabilizers. The presented method used the Particle Swarm Optimization (PSO) algorithm to search for optimal settings of PSS parameters. Two objective functions based on eigenvalues were considered to increase the attenuation of the electromechanical modes of the system. Robustness of the proposed method also depended on the initial guess, which is considered as its drawback. Thus, the simulation results were analyzed to guarantee the desired performance of the proposed PSS in the presence of various perturbations and loading issues. It was demonstrated that the novel Modified PSO algorithm presented in the paper brought about some advantages compared to previous PSO approaches. Further research was conducted to design a PSS for the multi-machine power system using the output feedback sliding mode control technique. The nonlinear model of the multi-machine power system was linearized at different operating points. The slide signal was taken as output and the output feedback sliding mode control was applied at an appropriate sampling rate. This method did not require complete states feedback and was easy to implement [19]. The main result of this research is that the proposed controller can damp the oscillations much faster than the classical PSS, which increases the responsiveness of the control system. In [20], an adaptive fuzzy control method was employed to form a decentralized load frequency controller in a two-zone interconnected power system. The Adaptive Fuzzy Load Frequency Controller (AFLFC) was implemented to enhance the frequency dynamic performance and transmitted power through the transmission lines during sudden load changes. The results illustrated that this method provided good attenuation control and reduced the frequency deviation overshoot in both regions. Gray Wolf Optimization (GWO) algorithm was tested to create a Wide-Area Power System Stabilizer (WAPSS) and it was examined in some multi-machine power systems. It was observed that the proposed strategy came with a multitude number of advantages such as damping the inter-area oscillations and compensating the detrimental effects of communication delays [21]. In [22], an optimal Model Reference Adaptive System (MRAS) was addressed to devise an effective PSS utilizing in multi-machine power systems. Through the suggested strategy in this research, the speed profile of the generator was enhanced and much more damping torque was provided upon injecting the stabilizing signals to the excitation part of the control system. The robust approach has also been of interest to researchers in recent years due to its impacts on improving system performance. One novel research investigated a robust strategy for a single machine infinite linked to a static synchronous compensator (STATCOM). The purpose of employing STATCOM was to regulate voltage and lessen the fluctuations via NSGII algorithm. The proposed system acts like a PSS to deal with disturbances. There were three scenarios considering PID controllers for speed loop, voltage loop, and both. The results illustrated that the third scenario positively affected the damping degree for both speed and voltage control aims [23]. It was shown in [24] that a robust power system stabilizer for enhancement of stability in power system ensured better performance in comparison with the conventional fuzzy-PID controller. The methods mentioned in this section for designing and tuning power system stabilizers present many drawbacks. In addition to the random selection of the initial population, local entrapment and inopportune convergence are among the disadvantageous of heuristic algorithms. Then, meta-heuristic algorithms have been introduced to compensate earlier issues. Some other studies have focused on linear parameter varying to achieve good performance for power system stabilizers. A Least Mean Square (LMS) method was used as an LPV identification algorithm in [25]. This algorithm was composed of the LPV model based on the interpolation of m linear local models and active and reactive power were considered as scheduling parameters. The simulation and experimental test showed that the applied methodology had a desirable damping effect on electromechanical oscillating terms. Also, another LPV system identification methodology was presented in [26]. Principal Component Analysis-based (PCA-based) parameter set mapping was employed to decrease the number of models and create a simpler LPV model. In this way, the computational burden of the modeling strategy was reduced. The suggested LPV controller verified the suppressing features and damping properties against fluctuations, especially in multi-machine power systems facing different operating conditions. Despite the relatively good performances of different systems, a strong mathematical basis is not included and even much time may be spent for solving optimization problems. Also, getting an accurate response due to the complexity of the systems could be difficult to reach. Additionally, the proposed robust PSS and CPSS tested in the literature mainly offer one simple controller for all operating points which cannot work under some uncertainties and system disturbances. On the other hand, an enhanced LPV-PSS presents separate controllers for the whole working points and uncertain circumstances. Online parameter tuning in LPV control systems is a major privilege amongst other controllers to adjust the PSS parameters due to unpredictable performances of a system. It is to be mentioned that proven control theories and lemmas support the LPV systems.

Linear Parameter Varying (LPV) modeling refers to linear dynamical models and the description of their state space depends on an exogenous variable parameter. In these models, the exogenous parameter operates independently and the state space model is dependent on it, that is, the exogenous parameter changes are independent of the system and a unique linear state space model is defined for each parameter. Exogenous parameters are called scheduling parameters. LPV models have a profound relationship with gain-scheduling strategies which is, in fact, the extension of the classical gain-scheduling method. The only difference is that in gain-scheduling models, unlike LPV models, the free parameter is endogenous, meaning that it originates within the system. The basis of both theories is to parse a nonlinear controller and create a set of linear controllers for a nonlinear system [27-28].

The main purpose of this paper is to design a power system stabilizer using LPV control method which is used to enhance the oscillations' damping of a single-machine power system connected to an infinite bus in a wide range of operating conditions. In order to apply this new technique, the nonlinear equations of the system at any operating points in a polytopic space are parameterized linearly by setting online-measured parameters. Next, the search space is reduced from a non-convex space to a convex sub-space to solve the optimization problem. Considering H_∞ algorithm and optimization LMIs, the LPV controller is designed using output and state feedback theories. This way, contrary to the pre-mentioned controllers, there would be a controller for every single working point in the determined polytopic space. Hence, by taking online feedbacks, the PSS parameters can be tuned uniquely. In other words, by proceeding from one working point to another, the controller model also changes accordingly. This empowers the control system to perfectly perform during different conditions.This article is organized as follows. Introduction is presented in Section 1. In Section 2, preliminaries are introduced. In Section 3, the LPV modeling of Single Machine Infinite Bus Power System with polytopic representation is stated. Simulation and results are given in Section 4. Conclusion is discussed in Section 5.

2. PRELIMINARIES

2.1. LPV systems

The LPV model is a dynamic linear state space model. Although the matrices of this model are not specific, they depend on the system free parameter. The general form of such a model is as follows:

$$\begin{aligned}\dot{x} &= A(\theta)x + B(\theta)u\\ y &= C(\theta)x\end{aligned} \tag{1}$$

where θ is an exogenous parameter that can be time dependent; u and y are input and output. As can be seen, this is a typical representation of the state space. One thing to note is that within a given timeframe, the parameter can cross any arbitrary path whose quality is generally out of the system control. It is also worth mentioning that there are bounds on magnitude and rate of variation for exogenous parameters [27].

For all $t \geq 0$,

$$\begin{aligned}-\mu \leq \theta(t) \leq \mu\\ -\rho \leq \dot{\theta}(t) \leq \rho\end{aligned} \tag{2}$$

2.2. Output feedback LPV controller design

By expanding (1), the state space complete model of the LPV system is obtained as follows:

$$G(\theta):\begin{cases}\dot{x} = A(\theta)x + B_1(\theta)w + B_2u\\ z = C_1(\theta)x + D_{11}(\theta)w + D_{12}(\theta)u\\ y = C_2(\theta)x + D_{21}(\theta)w\end{cases} \tag{3}$$

where z is performance output, y sensed output, u control input, and w represents disturbance input. The state space model of the full-order output feedback controller is defined as follows:

$$K(\theta):\begin{cases}\dot{x}_k = A_K(\theta)x_K + B_K(\theta)y\\ u = C_K(\theta)x_K + D_K(\theta)y\end{cases} \tag{4}$$

The closed loop system consisting of plant (P) and output feedback controller (K) defined in (3) and (4) is expressed as follows:

$$H(\theta):\begin{cases}\dot{x}_{cl} = A_{cl}(\theta)x_{cl} + B_{cl}(\theta)w\\ z = C_{cl}(\theta)x_{cl} + D_{cl}(\theta)w\end{cases} \tag{5}$$

The generilized separate form is considered as follows:

$$\begin{pmatrix}A_{cl} & B_{cl}\\ C_{cl} & D_{cl}\end{pmatrix} = \begin{pmatrix}A + BD_KC & BC_K & B_w + BD_KD_w\\ B_KC & A_K & B_KD_w\\ C_z + D_zD_KC & D_zC_K & D_{zw} + D_zD_KD_w\end{pmatrix} \tag{6}$$

Figure 1 presents the block diagram of the closed loop system in the output feedback design.

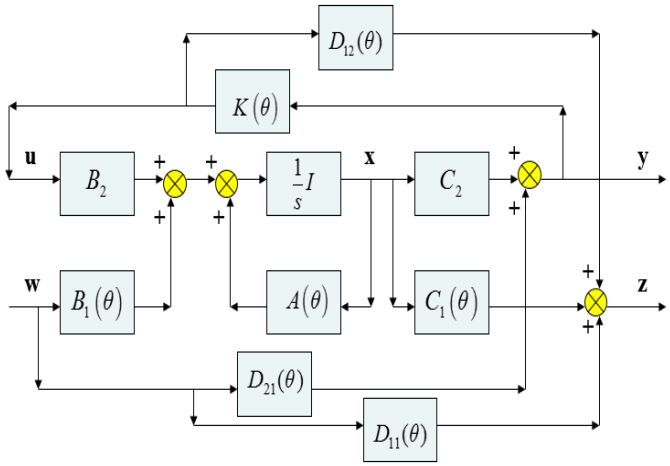

Figure 1. Block diagram of closed loop system in output feedback method

2.2.1. H_∞ based output feedback controller considering Single Quadratic Lyapunov Function (SQLF)

In this case, the variation rate of exogenous parameters is considered as desired. This method is stated through two approaches. The purpose to review these two perspectives is to figure out which one exhibits better performance and accuracy.

Theorem 1. If for a positive value of γ_∞, there will be a definite positive matrix of $X, Z \in S^n$ and the matrices of the dependent parameter $A_K(\theta) \in R^{n\times n}$, $B_K(\theta) \in R^{n\times n_y}$, $C_K(\theta) \in R^{n_u\times n}$, $D_K(\theta) \in R^{n_u\times n_y}$, respectively, so that the LMIs (7) and (8) are satisfied simultaneously, then the closed loop system $H(\theta)$ in (5) is exponentially stable and the constraint (norm) H_∞ of transfer function from disturbance input w to

performance output z in the closed loop system $H(\theta)$ becomes smaller than γ_∞ in (9) [29]. Therefore, the state space matrices of controller $K(\theta)$ can be obtained from Equation (10).

$$\Upsilon_\infty(\theta)=\begin{pmatrix}\mathrm{He}\left\{\begin{pmatrix}A(\theta)X+B_2C_K(\theta) & A(\theta)B_2D_K(\theta)C_2\\ A_K(\theta) & ZA(\theta)+B_K(\theta)C_2\end{pmatrix}\right\} & * & \begin{bmatrix}B_1(\theta)+B_2D_K(\theta)D_{21}\\ ZB_1(\theta)+B_K(\theta)D_{21}\end{bmatrix}\\ \begin{bmatrix}C_1(\theta)X+D_{12}C_K(\theta) & C_1(\theta)+D_{12}D_K(\theta)C_2\end{bmatrix} & -\gamma_\infty I_{nz} & D_{11}(\theta)+D_{12}D_K(\theta)D_{21}\\ * & * & -\gamma_\infty I_{nw}\end{pmatrix}<0 \tag{7}$$

The parameters used in the above LMI are state, input, and output matrices, which were introduced in Section 2.2. By solving this LMI, the controller matrices are obtained.

$$\begin{pmatrix}X & I_n\\ I_n & Z\end{pmatrix}>0 \tag{8}$$

$$\sup_{w\in L_2, w\neq 0}\frac{\|z\|_2}{\|w\|_2}<\gamma_\infty \tag{9}$$

$$\begin{cases}A_K(\theta)=Z^{-1}(ZA(\theta)X+ZB_2C_K(\theta)-A_K(\theta)\\ -\left(ZB_2D_K(\theta)-B_K(\theta)\right)C_2X)Y^{-1}\\ B_K(\theta)=Z^{-1}\left(ZB_2D_K(\theta)-B_K(\theta)\right)\\ C_K(\theta)=(C_K(\theta)-D_K(\theta)C_2X)Y^{-1}\\ D_K(\theta)=D_K(\theta)\end{cases} \tag{10}$$

where

$$Y=X-Z^{-1} \tag{11}$$

Theorem 2. For any given value of λ, the closed loop system consisting of the system (3) and the LPV controller is stable by displaying the given state space in (4) if and only if there are constant decision matrices $P_1\in R^{n\times n}$, $P_2\in R^{n\times n}$, $P_3\in R^{n\times n}$, and $Y\in R^{n\times n}$, as well as the dependent parameters $L_1(\theta)\in R^{n\times n}$, $L_2(\theta)\in R^{n\times r}$, $L_3(\theta)\in R^{p\times n}$ and $X(\theta)\in R^{n\times n}$, $S(\theta)\in R^{n\times n}$, so that Conditions (12) and (13) are satisfied simultaneously; then, the closed loop system $H(\theta)$ is exponentially stable in (5) and H_∞ norm of the transfer function from the disturbance input w to performance output z in the closed loop system $H(\theta)$ will be less than the value of γ_∞ in (16) [30]. Therefore, the state space matrices of the controller $K(\theta)$can be obtained from Equation (15):

$$\begin{pmatrix}P_1 & P_2\\ P_2' & P_3\end{pmatrix}>0 \tag{12}$$

$$\begin{pmatrix}\dot{P}_1-\mathrm{He}(A(\theta)X(\theta)+B_2(\theta)L_3(\theta)) & *\\ P_2'-L_1(\theta)-A'(\theta) & \dot{P}_3-\mathrm{He}(YA(\theta)+L_2(\theta)C_2(\theta))\\ -C_1(\theta)X(\theta)-D_2(\theta)L_3(\theta) & -C_1(\theta)\\ B_1' & B_1'(\theta)Y'+D_{21}'(\theta)L_2'(\theta)\\ X(\theta)-P_1-\lambda X'(\theta)A'(\theta)-\lambda L_3'(\theta)B_2'(\theta) & I-P_2-\lambda L_1'(\theta)\\ S(\theta)-P_2'-\lambda A'(\theta) & Y-P_3-\lambda A'(\theta)Y'-\lambda C_2'(\theta)L_2'(\theta)\end{pmatrix}$$
$$\begin{pmatrix}* & * & * & *\\ * & * & * & *\\ I & * & * & *\\ D_1'(\theta) & \gamma_\infty^2 I & * & *\\ -\lambda X'(\theta)C_1'(\theta)-\lambda L_3'(\theta)D_2'(\theta) & 0 & \lambda(\mathrm{He}(X(\theta))) & *\\ -\lambda C_1'(\theta) & 0 & \lambda S(\theta)+\lambda I & \lambda(\mathrm{He}(Y))\end{pmatrix}<0 \tag{13}$$

The output variables and the controller state space representation are achieved as follows:

$$\begin{cases}A_K(\theta)=V(L_1(\theta)-YA(\theta)X(\theta)-YB_2(\theta)L_3(\theta)-L_2(\theta)C_2(\theta)X(\theta))\\ B_K(\theta)=V\left(L_2(\theta)-YB_2(\theta)\right)\\ C_K(\theta)=L_3(\theta)\\ D_K(\theta)=0\\ \varepsilon_K(\theta)=V\left(S(\theta)-YX(\theta)\right)\end{cases} \tag{14}$$

where

$$\begin{cases}A_K(\theta)=A_K(\theta)\varepsilon_K^{-1}(\theta)\\ B_K(\theta)=B_K(\theta)\\ C_K(\theta)=C_K(\theta)\varepsilon_K^{-1}(\theta)\\ D_K(\theta)=D_K(\theta)\end{cases} \tag{15}$$

$$\|H_{zw}\|_\infty^2=\sup_{\|w(k)\|_2\neq 0}\frac{\|z(k)\|_2^2}{\|w(k)\|_2^2}<\gamma_\infty^2 \tag{16}$$

Matrix V is opted as desired, which can be an identity matrix with the appropriate dimension [30]. It should be noted that according to Theorem 2, various stabilizer controllers can be designed by selecting each different λ.

2.2.2. H∞ based output feedback controller considering Parameter Dependent Lyapunov Function (PDLF)

In this case, the variation rate of exogenous parameters is considered slow.

Theorem 3. For any given value of λ, the closed loop system consisting of the system (3) and the LPV controller is stable with the state space represntation in (4) if and only if there are symmetric dependent parameter $P_1\in R^{n\times n}$, $P_3\in R^{n\times n}$ and the dependent matrix parameters of $L_1(\theta)\in R^{n\times n}$, $L_2(\theta)\in R^{n\times r}$, $L_3(\theta)\in R^{p\times n}$ and $P_2\in R^{n\times n}$, $X(\theta)\in R^{n\times n}$, $S(\theta)\in R^{n\times n}$ and the constant decision matrix $Y\in R^{n\times n}$ so that the Conditions (17) and (18) are satisfied simultaneously. Then, the closed loop system $H(\theta)$ in (5) is exponentially stable and the H_∞ norm of the transfer function from disturbance input w to performance output z in the close loop system $H(\theta)$ will be smaller than the value of γ_∞ in (21). Therefore, the controller state space matrices $K(\theta)$ can be calculated from Equation (20) as follows [30]:

$$\begin{pmatrix}P_1(\theta) & P_2(\theta)\\ P_2'(\theta) & P_3(\theta)\end{pmatrix}>0 \tag{17}$$

$$\begin{pmatrix}\dot{P}_1(\theta)-\mathrm{He}(A(\theta)X(\theta)+B_2(\theta)L_3(\theta)) & *\\ P_2'(\theta)-L_1(\theta)-A'(\theta) & \dot{P}_3(\theta)-\mathrm{He}(YA(\theta)+L_2(\theta)C_2(\theta))\\ -C_1(\theta)X(\theta)-D_2(\theta)L_3(\theta) & -C_1(\theta)\\ B_1' & B_1'(\theta)Y'+D_{21}'(\theta)L_2'(\theta)\\ X(\theta)-P_1(\theta)-\lambda X'(\theta)A'(\theta)-\lambda L_3'(\theta)B_2'(\theta) & I-P_2(\theta)-\lambda L_1'(\theta)\\ S(\theta)-P_2'(\theta)-\lambda A'(\theta) & Y-P_3(\theta)-\lambda A'(\theta)Y'-\lambda C_2'(\theta)L_2'(\theta)\end{pmatrix}$$
$$\begin{pmatrix}* & * & * & *\\ * & * & * & *\\ I & * & * & *\\ D_1'(\theta) & \gamma_\infty^2 I & * & *\\ -\lambda X'(\theta)C_1'(\theta)-\lambda L_3'(\theta)D_2'(\theta) & 0 & \lambda(\mathrm{He}(X(\theta))) & *\\ -\lambda C_1'(\theta) & 0 & \lambda S(\theta)+\lambda I & \lambda(\mathrm{He}(Y))\end{pmatrix}<0 \tag{18}$$

The output variables and the controller state space reprentation are obtained as follows:

$$\begin{pmatrix}* & * & * & *\\ * & * & * & *\\ I & * & * & *\\ D_1'(\theta) & \gamma_\infty^2 I & * & *\\ -\lambda X'(\theta)C_1'(\theta)-\lambda L_3'(\theta)D_2'(\theta) & 0 & \lambda(\mathrm{He}(X(\theta))) & *\\ -\lambda C_1'(\theta) & 0 & \lambda S(\theta)+\lambda I & \lambda(\mathrm{He}(Y))\end{pmatrix}<0 \tag{19}$$

where

$$\begin{cases} A_K(\theta) = A_K(\theta)\varepsilon_K^{-1}(\theta) \\ B_K(\theta) = B_K(\theta) \\ C_K(\theta) = C_K(\theta)\varepsilon_K^{-1}(\theta) \\ D_K(\theta) = D_K(\theta) \end{cases} \quad (20)$$

$$\|H_{zw}\|_\infty^2 = \sup_{\|w(k)\|_2 \neq 0} \frac{\|z(k)\|_2^2}{\|w(k)\|_2^2} < \gamma_\infty^2 \quad (21)$$

Matrix V is opted as desired, which can be an identity matrix with the appropriate dimension [30]. It should be noted that according to Theorem 3, various stabilizer controllers can be designed by selecting each different λ.

2.3. State feedback LPV controller design

Theorem 4. If in the following optimization problem, for a positive ρ, there are positive and definite matrices $X(\theta)$ and $W(\theta)$ so that the LMI Condition in (22) for the system (3) can be satisfied, then the closed loop system $T(\theta)$ in (20) is stable and the norm of the closed loop (23) is met [31].

$$\begin{pmatrix} A(\theta)X(\theta) + B_2W(\theta) + (A(\theta)X(\theta) + B_2W(\theta))^T & & \\ B_1^T(\theta) & & \\ C_1(\theta)X(\theta) + D_{12}(\theta)W(\theta) & & \end{pmatrix}$$

$$\begin{matrix} B_1(\theta) & (C_1(\theta)X(\theta) + D_{12}W(\theta)^T \\ -I & D_{11}^T(\theta) \\ D_{11}(\theta) & -\rho I \end{matrix} \Bigg) < 0 \quad (22)$$

where $X(\theta), W(\theta) > 0$.

$$\|T_{wz}\|_\infty < \sqrt{\rho} \quad (23)$$

Then, the state feedback controller gain can be expressed through the following equation [30]:

$$K(\theta) = W(\theta) \times X^{-1}(\theta) \quad (24)$$

$$T(\theta): \begin{cases} \dot{x}_{cl} = A_{cl}(\theta)x_{cl} + B_{cl}(\theta)w \\ z = C_{cl}(\theta)x_{cl} \end{cases} \quad (25)$$

Figure 2 demonstrates the block diagram of the closed loop system in the state feedback design method.

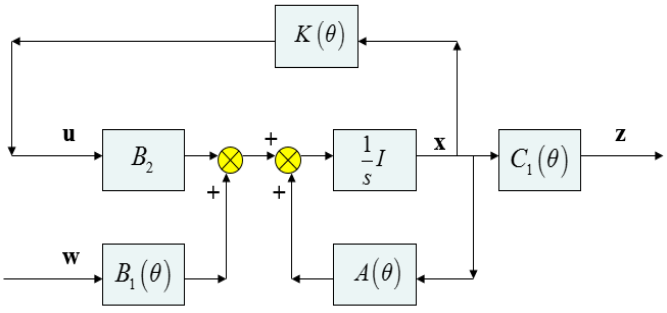

Figure 2. Block diagram of the closed loop system in state feedback method

In designing a controller using this technique, much progress has been made beyond stabilization (as minimum expectation of the controller), especially in the discussion of disturbances from LPV systems and minimization of inductive norms, improvements are significant [27]. It is to be noted that in most robust control topics, achieving a desirable function leads to minimization of inductive norm of a weighted function and progress in minimizing these norms provides progress in obtaining the desired system performance.

3. PROPOSED LPV MODELING of SINGLE MACHINE INFINTE BUS POWER SYSTEM

The system under study is a single machine infinite bus power system connecting via a transmission line. This system is represented by a fourth-order linear model [32]. The block diagram of this model is shown in Figure 3 below.

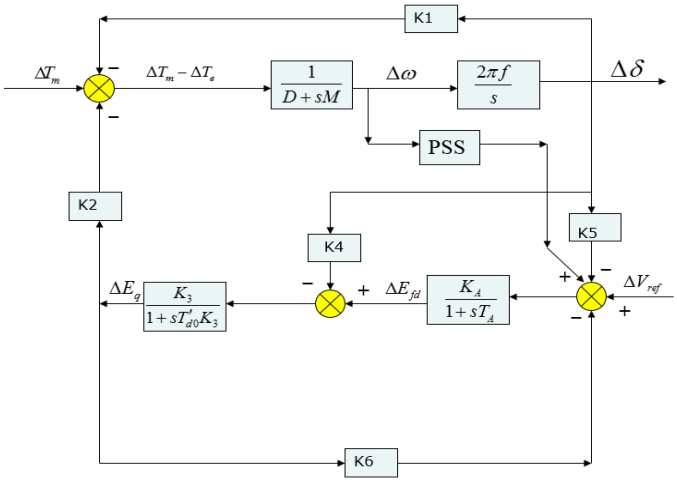

Figure 3. Mathematical model of the single machine infinite bus power system

In the proposed LPV modeling, to ensure the flexibility of the PSS, a polytopic representation of the power system is employed. As is clear from Fig. 3, $(k_1, k_2, k_3, k_4, k_5, k_6)$ are fourth-order model constants that remain dependent on the loading conditions of the active power (P), the reactive power (Q), and the external reactance of transmission line (x_e).

Mathematical equations concerned with how to convert $k_1 \dots k_6$ to P, Q, x_e were given in reference [33, 34]. In fact, Parameters $k_1 \dots k_6$ are obtained via linearized small perturbation relations of a single generator supplying an infinite bus through external impedance. In other words, the proposed model $k_1 \dots k_6$ emerges from the relationship between the concept of small perturbation analysis and synchronous generator elements. The proposed working points (P Q x_e) are per unit values which are arbitrarily determined from the specified intervals for each of the parameters. The LPV model of a single machine infinite bus power system can be written as follows:

$$G(\theta): \begin{cases} \dot{x} = A(k_p)x + B_w w + B_u u \\ z = C_z x + D_z u \\ y = C_y x \end{cases} \quad (26)$$

z, w and y are stabilizer output, the disturbance input, and the measured output, respectively. Here, the velocity change $\Delta\omega$ is considered as the measured output. Disturbance input can be selected as a change in the mechanical torque input or a change in the voltage reference. The state vector $x \in R^4$ is defined as $x = [\Delta\delta \quad \Delta\omega \quad \Delta E_q \quad \Delta E_{fd}]$, where $\Delta\delta$, ΔE_q, and ΔE_{fd} are load angle deviation, induced electromagnetic force deviation corresponding to the field current, and deviation in the generator field excitation voltage. The matrices for representing the state space are as follows [32].

$$(k_p)=\begin{pmatrix} 0 & \omega_0 & 0 & 0 \\ \frac{-k_1}{M} & \frac{-D}{M} & \frac{-k_2}{M} & 0 \\ \frac{-k_4}{T'_{d0}} & 0 & \frac{-1}{T'_{d0}k_3} & \frac{1}{T'_{d0}} \\ \frac{-K_E k_5}{T_E} & 0 & \frac{-K_E k_6}{T_E} & \frac{-1}{T_E} \end{pmatrix}, B_u=\begin{pmatrix} 0 \\ 0 \\ 0 \\ \frac{K_E}{T_E} \end{pmatrix}$$

$$B_w=\begin{pmatrix} 0 \\ \frac{1}{M} \\ 0 \\ 0 \end{pmatrix}, C_y=(0 \quad 1 \quad 1 \quad 1) \tag{27}$$

where T_E, K_E, T'_{d0} and M are exciter time constant, exciter gain, open circuit field time constant, and inertia coeficient, respectively.

Note: $C_1=C_z$ and $C_2=C_y$ may be selected as $C_z=C_y$ and also $D_z=0$. Doing this, the H_∞ norm of the closed loop system is reduced from the input w to z as well as the effect of external disturbance on the output performance. Based on the analysis performed in [33], k_4 can be written as $(x_d-x'_d)k_2$, in which x_d and x'_d are the d-axis synchronous reactance and the d-axis transient reactance, respectively. In addition, it can be written in the matrix (27):

$$k_{3i}=\frac{1}{k_3} \tag{28}$$

Therefore, system matrices can be expressed as follows:

$$(k_p)=\begin{pmatrix} 0 & \omega_0 & 0 & 0 \\ \frac{-k_1}{M} & 0 & \frac{-k_2}{M} & 0 \\ \frac{-(x_d-x'_d)k_2}{T'_{d0}} & 0 & \frac{-k_{3i}}{T'_{d0}} & \frac{1}{T'_{d0}} \\ \frac{-K_E k_5}{T_E} & 0 & \frac{-K_E k_6}{T_E} & \frac{1}{T_E} \end{pmatrix}, B_u=\begin{pmatrix} 0 \\ 0 \\ 0 \\ \frac{K_E}{T_E} \end{pmatrix}$$

$$B_w=\begin{pmatrix} 0 \\ \frac{1}{M} \\ 0 \\ 0 \end{pmatrix}, C_y=(0 \quad 1 \quad 0 \quad 0) \tag{29}$$

$$A(k_p)=A_0+k_1A_1+k_2A_2+k_{3i}A_3+k_5A_5+k_6A_6 \tag{30}$$

In Equation (30), the system matrix $A(k_p)$ is written as an expression and separated by parameters and constant matrices A_0, A_1, A_2, A_3, A_5 and $A_6$where each parameter changes within a certain range:

$$\begin{cases} k_1 \in [k_1^-, k_1^+] \\ k_2 \in [k_2^-, k_2^+] \\ k_{3i} \in [k_{3i}^-, k_{3i}^+] \\ k_5 \in [k_5^-, k_5^+] \\ k_6 \in [k_6^-, k_6^+] \end{cases}$$

under different loading conditions.

$k_i^-(k_i^+)$ represent the boundries of the k_i parameter corresponding to the $P \in [P^-, P^+]$, $Q \in [Q^-, Q^+]$and $x_e \in [x_e^-, x_e^+]$ values. The affine parameter-dependent model in (30) can be converted to a olytopic model as (32). The parametric vector $k=[k_1 \quad k_2 \quad k_{3i} \quad k_5 \quad k_6]$ creates a 32-corner polytope whose corners are as follows:

$$\begin{cases} k_{cor32}=[k_1^- \quad k_2^+ \quad k_{3i}^+ \quad k_5^+ \quad k_6^+] \\ k_{cor32}=[k_1^+ \quad k_2^- \quad k_{3i}^+ \quad k_5^+ \quad k_6^+] \\ \qquad\qquad . \\ \qquad\qquad . \\ \qquad\qquad . \\ k_{cor32}=[k_1^- \quad k_2^- \quad k_{3i}^- \quad k_5^- \quad k_6^-] \end{cases} \tag{31}$$

For all $P \in [P^-, P^+]$, $Q \in [Q^-, Q^+]$ and $x_e \in [x_e^-, x_e^+]$ values, the system matrix can be obtained as:

$$A(k_p)=A(k) \in S := Co\{A_1, A_2, \dots, A_{32}\}:$$

$$=\left\{\sum_{i=1}^{i=32} a_i A_i : a_i \geq 0, \sum_{i=1}^{i=32} a_i = 1\right\} \tag{32}$$

where $A_1=A(k_{cor1}), A_2=A(k_{cor2}), \dots, A_{32}=A(k_{cor32})$.

In this study, the design of PSS using the output feedback and the state feedback method via LPV approach for optimal placement of poles in accordance with the working conditions $P \in [P^-, P^+]$, $Q \in [Q^-, Q^+]$ and $x_e \in [x_e^-, x_e^+]$ is presented so that the H_∞norm of the closed loop system can be minimized. Furthermore, the PSS transfer function is strictly proper and its order is equal to the system order (full order controller). The state space representation of PSS controller and closed loop system are shown in accordance with (4) and (5) as follows:

$$K(k_p): \begin{cases} \dot{x}_K = A_K(k_p)x_K + B_K(k_p)y \\ u = C_K(k_p)x_K + D_K(k_p)y \end{cases} \tag{33}$$

The closed loop system consists of a plant (29) and a controller (33), as obtained below:

$$T(k_p): \begin{cases} \dot{x}_{cl} = A_{cl}(k_p)x_{cl} + B_{cl}(k_p)w \\ z = C_{cl}(k_p)x_{cl} + D_{cl}(k_p)w \end{cases} \tag{34}$$

where

$$\begin{pmatrix} A_{cl} & B_{cl} \\ C_{cl} & D_{cl} \end{pmatrix}=\begin{pmatrix} A+BD_KC & BC_K & B_w+BD_KD_w \\ B_KC & A_K & B_KD_w \\ C_z+D_zD_KC & D_zC_K & D_{zw}+D_zD_KD_w \end{pmatrix} \tag{35}$$

4. SIMULATION AND RESULTS

In this section, by employing the mentioned Theorems and Equations, simulations are done according to the defined scenarios. Optimization problems are solved using the YALMIP [35] and ROLMIP [36] toolboxes runnig in MATLAB software. SeDuMi and SPDT3 are used as LMI solvers.

4.1. Output feedback structure

Theorems 1 and 2 of Section 2.2.1. are used for system (29) with a 32-corner polytope corresponding to the following parameters:

$P \in [P^-, P^+]$, $Q \in [Q^-, Q^+]$and $x_e \in [x_e^-, x_e^+]$

$$\begin{cases} k_1 \in [k_1^-, k_1^+] \\ k_2 \in [k_2^-, k_2^+] \\ k_{3i} \in [k_{3i}^-, k_{3i}^+] \\ k_5 \in [k_5^-, k_5^+] \\ k_6 \in [k_6^-, k_6^+] \end{cases}$$

Finally, the control parameters of the output feedback design are obtained using Equation (10) and (15).

Considering the single machine infinite bus power system and the 32 corners obtained from its polytopic representation, the LPV stabilizer design is addressed. In the simulations performed, the range of changes in machine parameters is considered as follows [32]:

$$\begin{array}{l} P \in [0.2 \quad 1] \text{ p.u} \\ Q \in [-0.2 \quad 0.5] \text{ p.u} \\ x_e \in [0.4 \quad 0.8] \text{ p.u} \end{array} \tag{36}$$

The parameters k_1 to k_6 will also change as shown in Appendix B, in the specific period $[k_i^-, k_i^+]$ as follows:

$$\begin{cases} [k_1^- \quad k_1^+] = [0.67027 \quad 1.7130] \\ [k_2^- \quad k_2^+] = [0.0377 \quad 1.3255] \\ [k_{3i}^- \quad k_{3i}^+] = [2.14285 \quad 2.77778] \\ [k_5^- \quad k_5^+] = [-0.13991 \quad 0.16554] \\ [k_6^- \quad k_6^+] = [0.3810 \quad 0.82008] \end{cases} \quad (37)$$

To investigate the effectiveness of the proposed method, the simulation results of the stabilizer designed by Theorems 1 and 2 in Section 2.2.1 and a classical stabilizer [37] as well as a H_∞ robust stabilizer [32] are compared.

H_∞ Robust output feedback PSS

$$\frac{76.74\times(1+0.287s)(1+0.648s)(1+0.0126s)}{(1+0.0205s)(1+0.0324s)(1\times10^{-5}s^2+2.35\times10^{-3}s+1)} \quad (38)$$

$$C_{pss} = \frac{K_s T_w s}{1+T_w s} \times \frac{(1+T_1 s)(1+T_3 s)}{(1+T_2 s)(1+T_4 s)} = \frac{14\times10s}{1+10s} \times \frac{(0.08s^2+0.65s+1)}{(0.0052s^2+0.14s+1)} \quad (39)$$

K_s is the PSS gain, T_w is the Washout time constant, and $T_1 \ldots T_4$ are the time constants of the lead compensators.

Here are the simulation results of a sudden change in the input mechanical torque, which indicates a short circuit at a particular moment and its elimination after a certain period of time that occurs in three modes of operation.

Table 1. Summary of the considered operating conditions

Operating conditions	Values
1st: Lag power factor	$P = 1, Q = 0.2, x_e = 0.4$
2nd: Lead power factor	$P = 1, Q = -0.2, x_e = 0.8$
3rd: Lag power factor	$P = 0.2, Q = 0.5, x_e = 0.4$
4th: Lead power factor	$P = 0.3, Q = -0.1, x_e = 0.6$

In this case, first, using Theorems 1 and 2 in Section 2.2.1, the Liapanov function is fixed and as a result, the dynamics of the system are considered to be relatively fast. The simulation results are obtained as follows (Figure4 - Figure14).

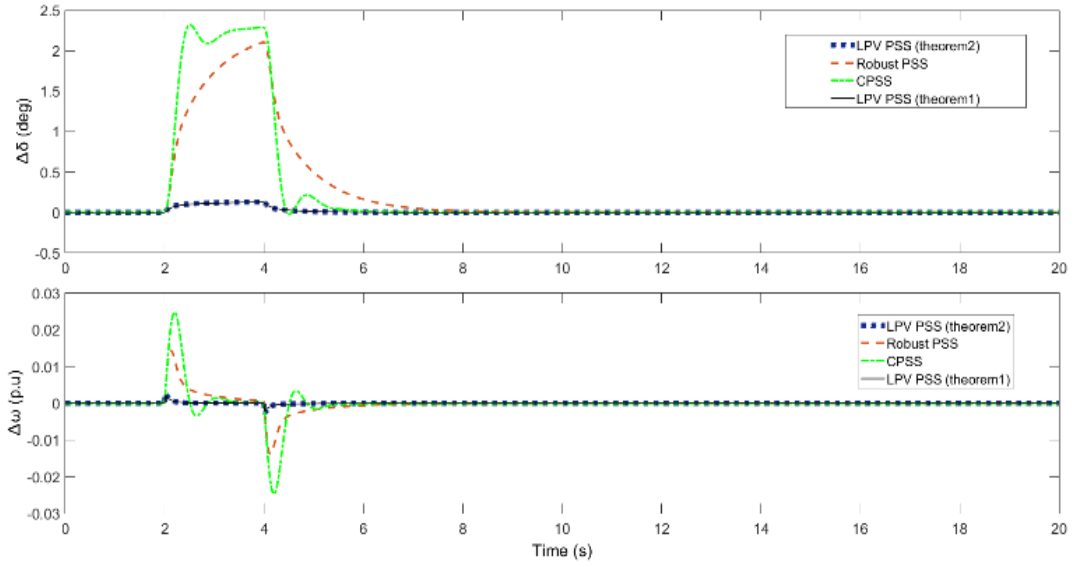

Figure 4. Comparison of LPV PSS, Robust PSS, and CPSS for the first working mode and a sudden change t = 2 s in the input mechanical torque

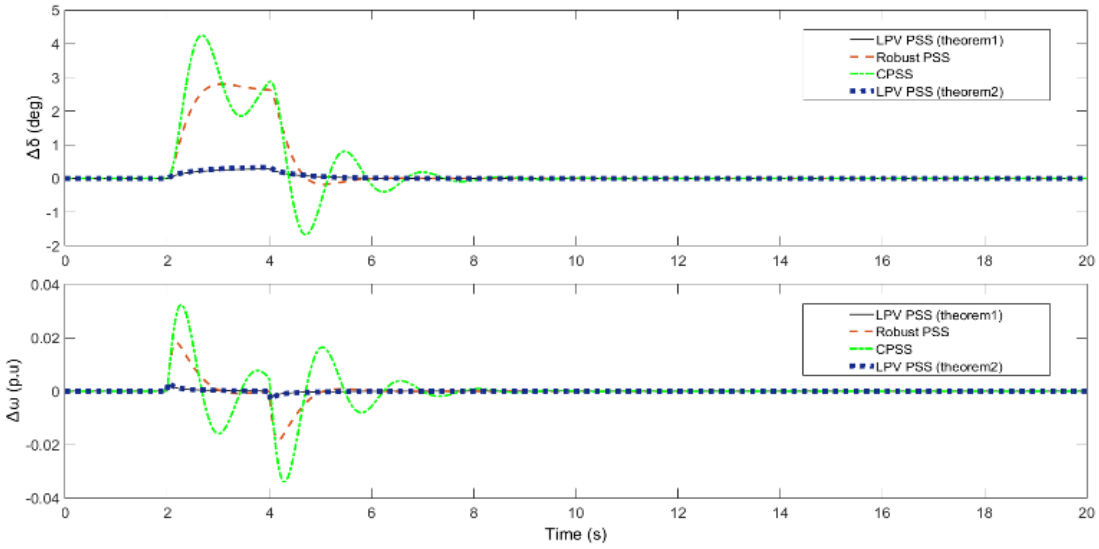

Figure 5. Comparison of LPV PSS, Robust PSS, and CPSS for the second working mode and a sudden change t = 2 s in the input mechanical torque

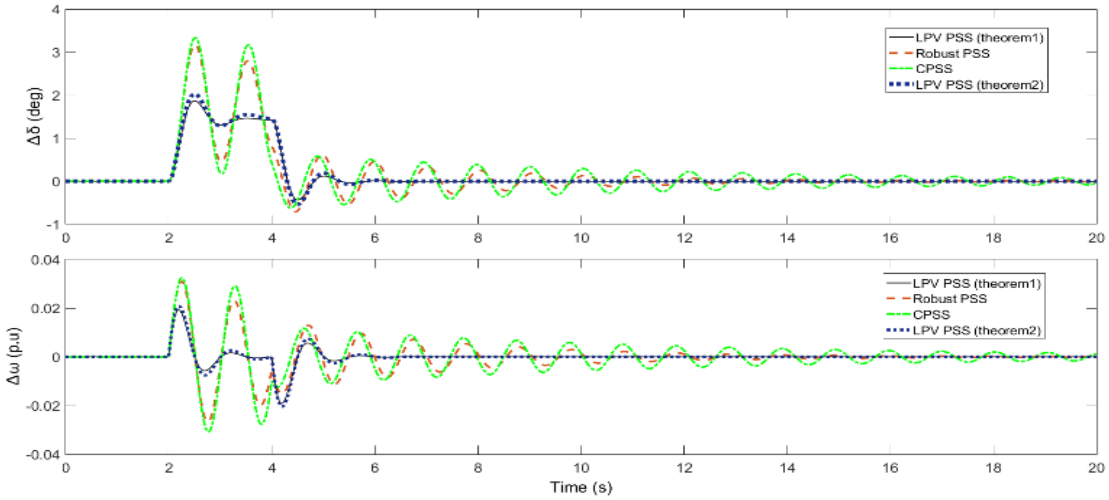

Figure 6. Comparison of LPV PSS, Robust PSS, and CPSS for the third working mode and a sudden change t = 2 s in the input mechanical torque

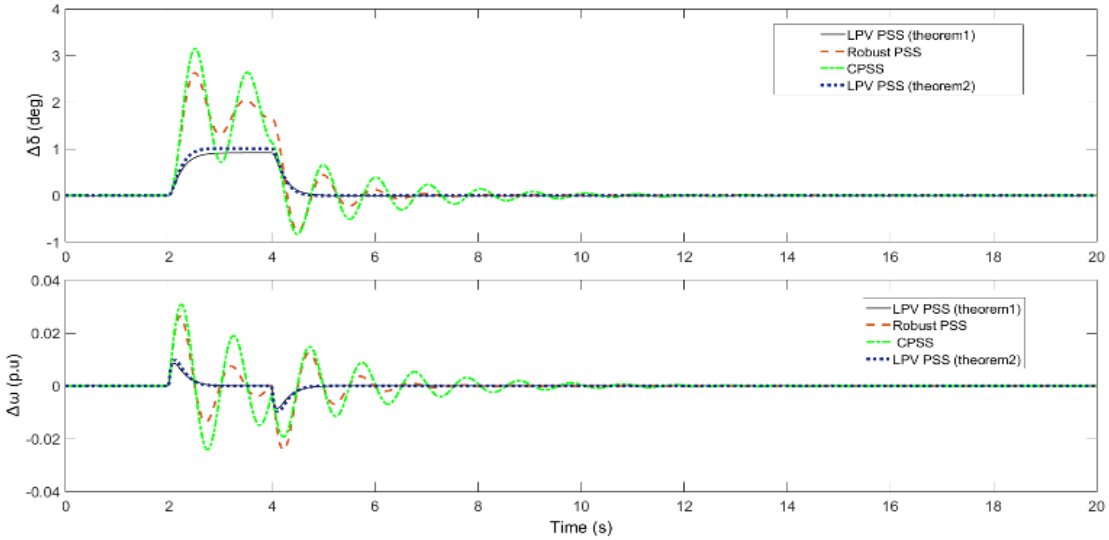

Figure 7. Comparison of LPV PSS, Robust PSS, and CPSS for the fourth working mode and a sudden change t = 2 s in the input mechanical torque

Figures 4-7 show comparisons between LPV controllers from Theories 1 and 2 as well as between the robust PSS and the classic PSS at the mentioned working points with changes in mechanical torque at t = 2 s. It can be observed that Theories 1 and 2 represent better performance in speed and load angle tracking after applying the disturbance and exhibit minmum deviation from the reference values. It should also be noted that the amplitude of overshoots and undershoots in the LPV controllers is much more limited than other control theorems, which is more desirable.

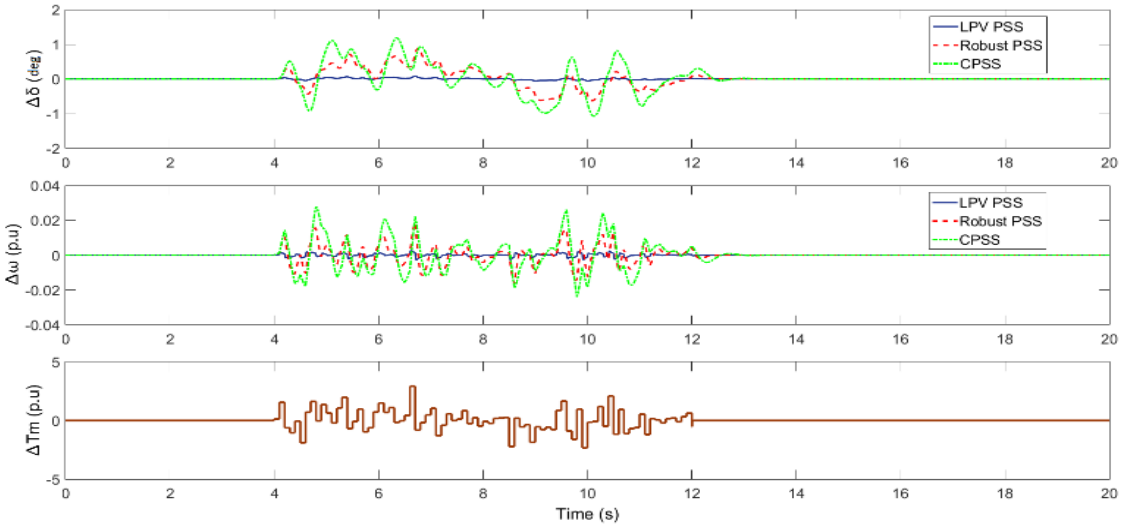

Figure 8. Comparison of LPV PSS, Robust PSS, and CPSS for the first working mode upon applying noise in the input mechanical torque

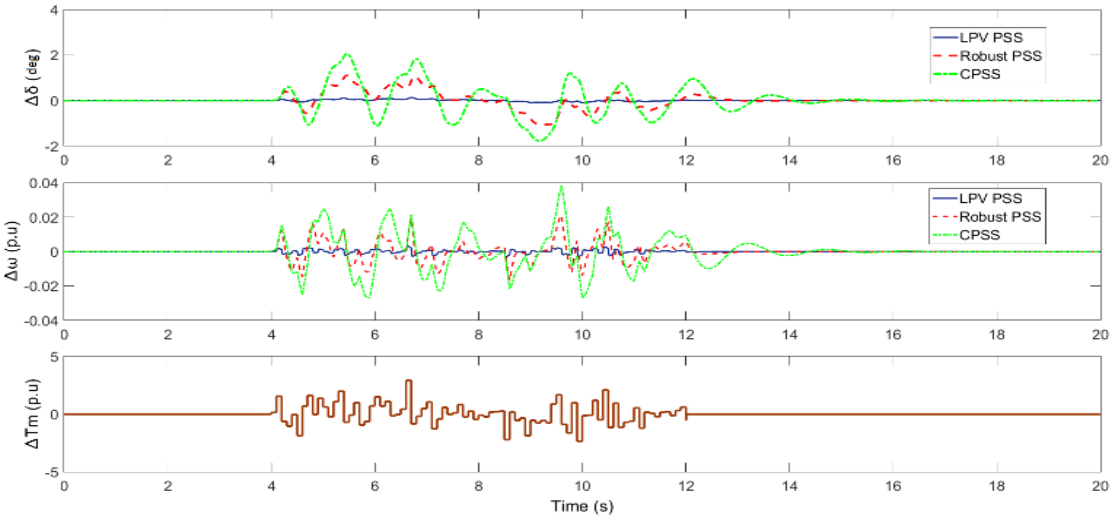

Figure 9. Comparison of LPV PSS, Robust PSS, and CPSS for the second working mode upon applying noise in the input mechanical torque

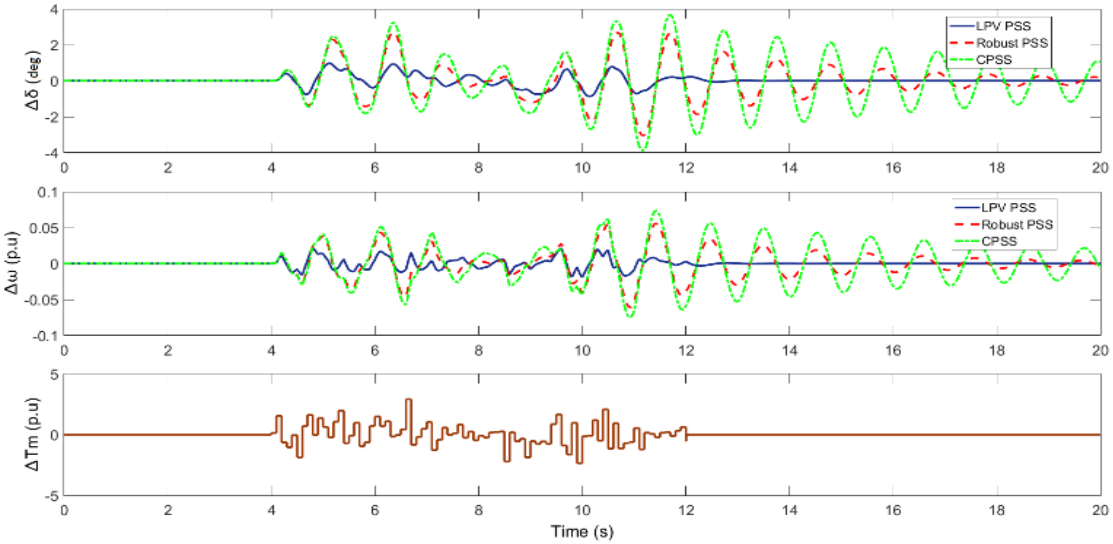

Figure 10. Comparison of LPV PSS, Robust PSS, and CPSS for the third working mode upon applying noise in the input mechanical torque

The variations in load angle, velocity, and mechanical torque in the presence of white noise are shown in Figures 8-10 for three operating points. As illustrated earlier, the proposed LPV controller senses much less perturbations than robust PSS and CPSS. In addition, it is crystal clear that the application of noise in robust and classic PSS creates instability for some operating points and makes $\Delta\delta$ and $\Delta\omega$ oscillate around the reference value. This verifes the incredible performance of the proposed LPV controller.

Now, using Theorem 3 in Section 2.2.2, the Liapanov function is considered as the dependent parameter and the system dynamics is relatively slow. The simulation results are shown in Figures 11-14.

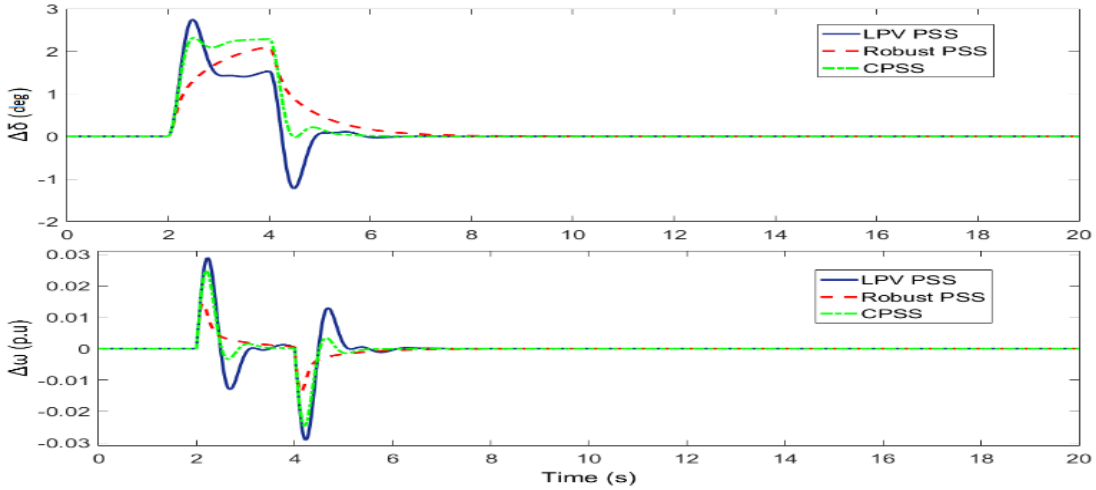

Figure 11. Comparison of LPV PSS, robust PSS, and CPSS for the first working mode and a sudden change t = 2 s in the input mechanical torque

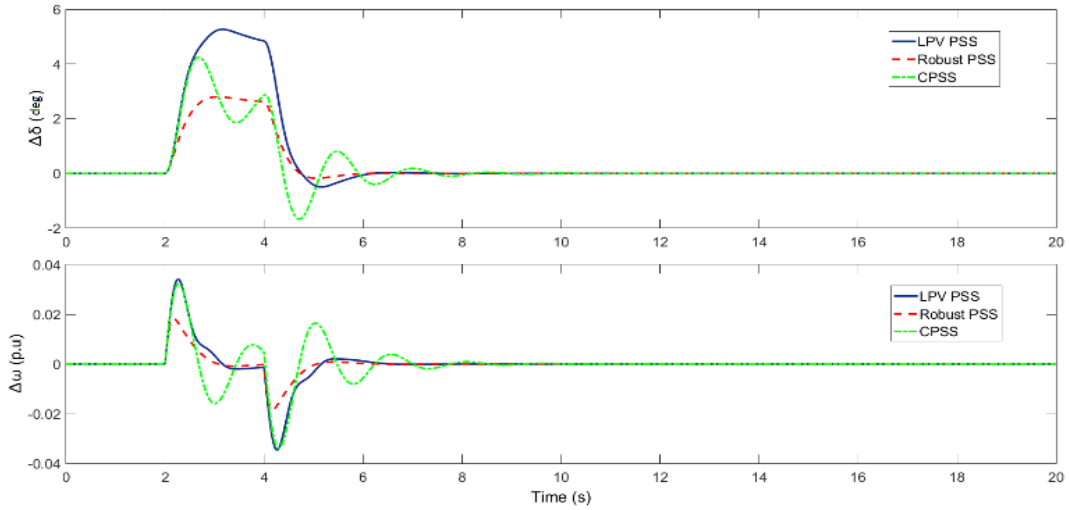

Figure 12. Comparison of LPV PSS, robust PSS, and CPSS for the second working mode and a sudden change t = 2 s in the input mechanical torque

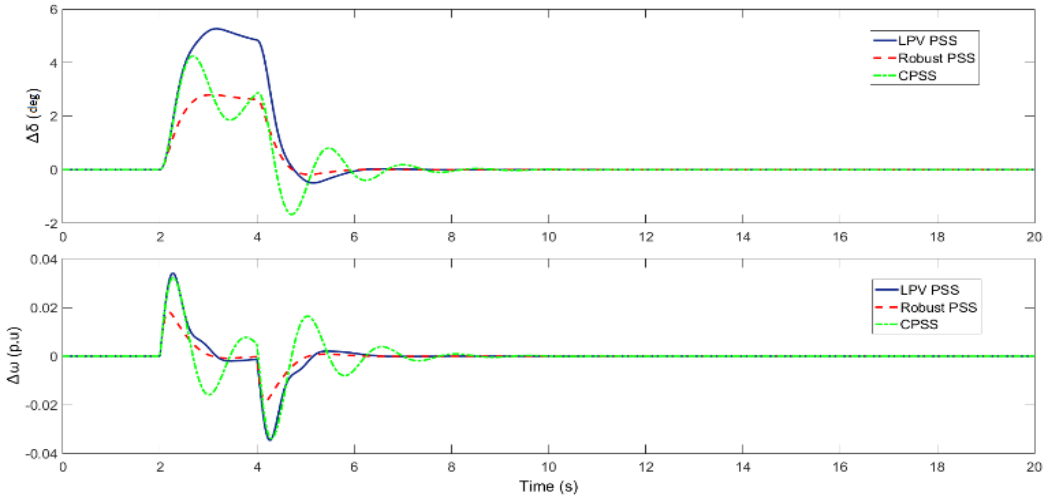

Figure 13. Comparison of LPV PSS, robust PSS, and CPSS for the third working mode and a sudden change t = 2 s in the input mechanical torque

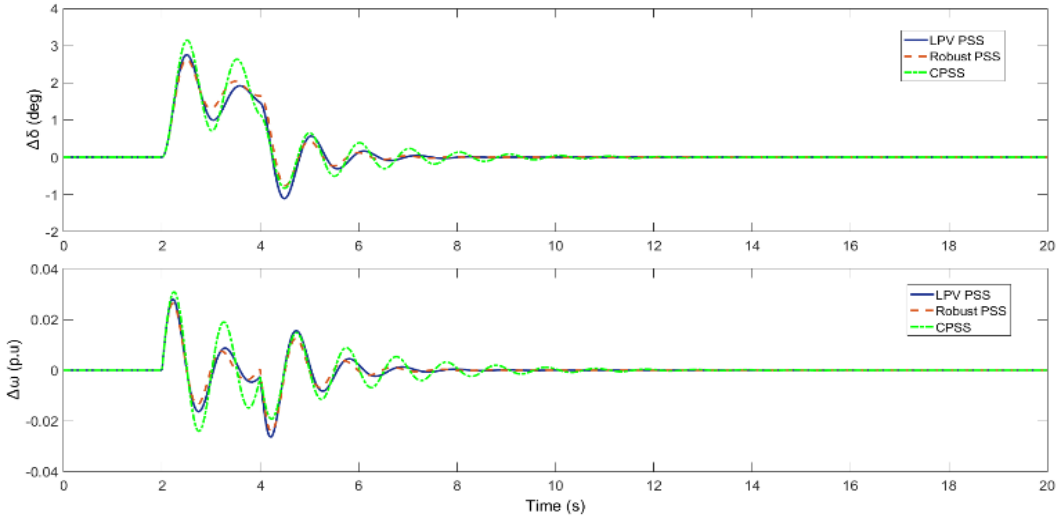

Figure 14. Comparison of LPV PSS, Robust PSS, and CPSS for the fourth working mode and a sudden change t = 2 s in the input mechanical torque

According to Figures 11 to 14, the performance of the LPV controller designed based on Theorem 3 with the proposed polytopic approach by assuming that the variation rate of exogenous parameters is slow (slow dynamic) is not as favorable as it should be and it is less valuable than robust and classic controllers. If Figures 4 to 10 are taken into account, it can be seen that the simulation results based on Theorems 1 and 2 are much more effective than robust and classic methods.

Table 2. Norm comparison in output feedback method related to Theorems 1, 2, and 3

PSS designing method	Largest closed-loop norm (γ_∞)	Iteration	l
Robust	0.023	25	-----
LPV (Theorem 1)	(0.236,0.234,0.228,0.205)	(1,2,3,4)	(0.01,0.001,0.00005,0.00001)
LPV (Theorem 2)	(4.18,2.38,1.115,0.797)	(1,2,3,4)	(0.01,0.005,0.0005,0.00005)
LPV (Theorem 3)	0.267	1	-----

By comparing the best design methods (based on Theorems 1 and 2-Liapanov's fixed function) in Section (2.2.1) and since these controllers are proper and strictly proper respectively, it can be concluded that the controller originated from Theorem 1 has a better performance than Theorem 2.

4.2. State feedback structure

Here, Theorem 4 in Section (2.3) for System (29) with 32-corner polytopes corresponding to the parameters:

$P \in [P^-, P^+]$, $Q \in [Q^-, Q^+]$and $x_e \in [x_e^-, x_e^+]$

$$\begin{cases} k_1 \in [k_1^-, k_1^+] \\ k_2 \in [k_2^-, k_2^+] \\ k_{3i} \in [k_{3i}^-, k_{3i}^+] \\ k_5 \in [k_5^-, k_5^+] \\ k_6 \in [k_6^-, k_6^+] \end{cases}$$

are employed and the state feedback controller gain is obtained.

The following are the simulation results of the stabilizer tuned by the state feedback technique according to Theorem 4 in Section (2.3.) and the output feedback technique in Theorem 1 in Section (2.2.1.). Figures 17-20 demonestrate the simulation results of the comparison of LPV PSS performance in output feedback and state feedback approaches.

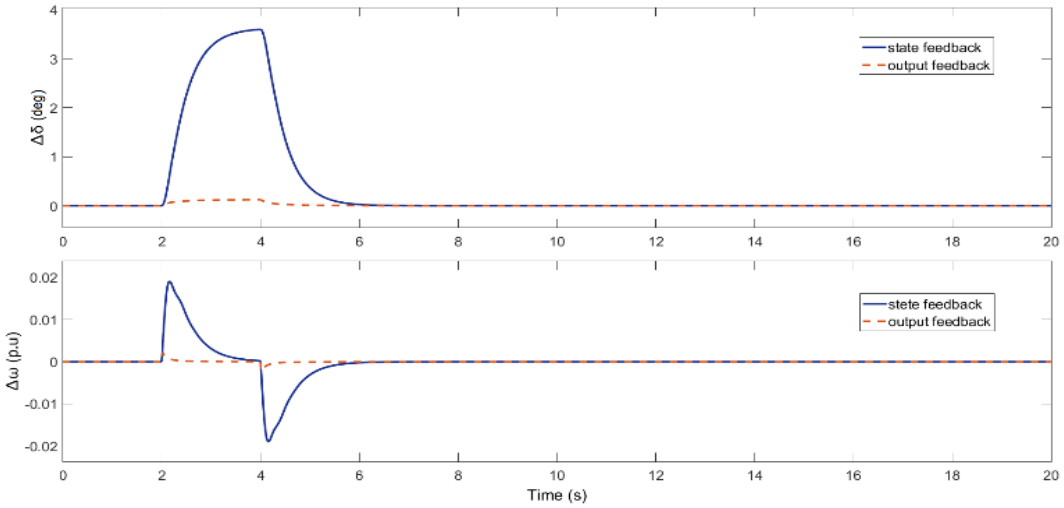

Figure 15. Comparison of LPV PSS performance in output feedback and state feedback methods for the first working mode and a sudden change t = 2 s in input mechanical torque

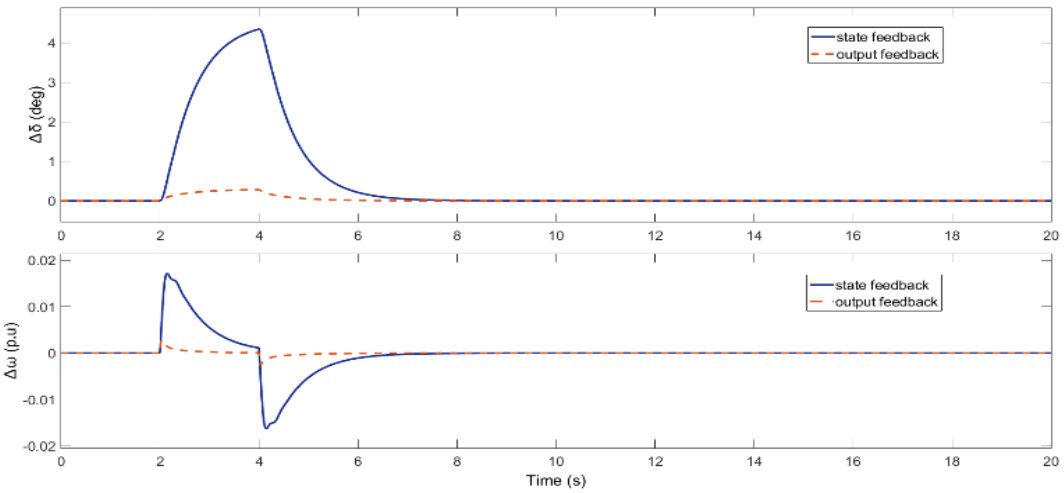

Figure 16. Comparison of LPV PSS performance in output feedback and state feedback methods for the second working mode and a sudden change t = 2 s in input mechanical torque

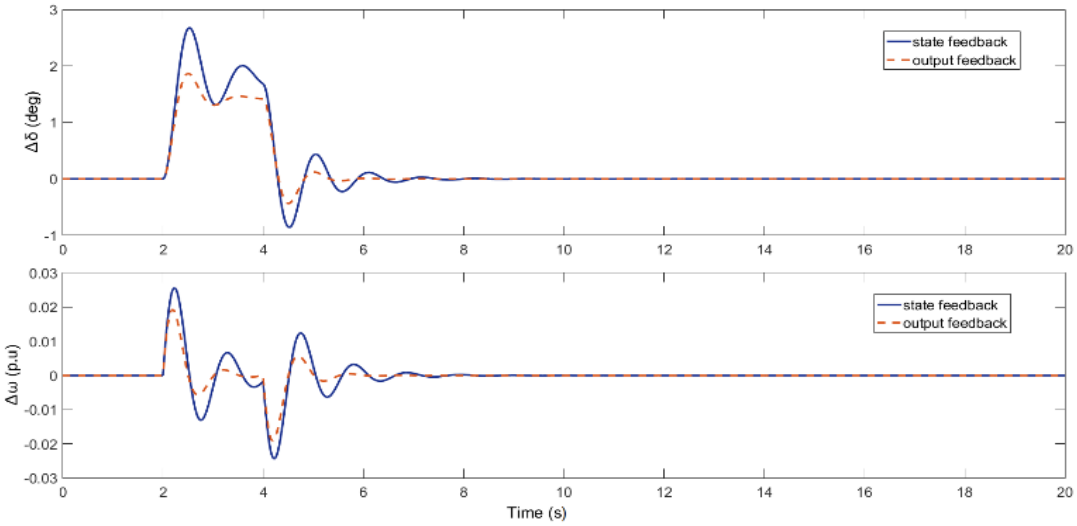

Figure 17. Comparison of LPV PSS performance in output feedback and state feedback methods for the third working mode and a sudden change t = 2 s in input mechanical torque

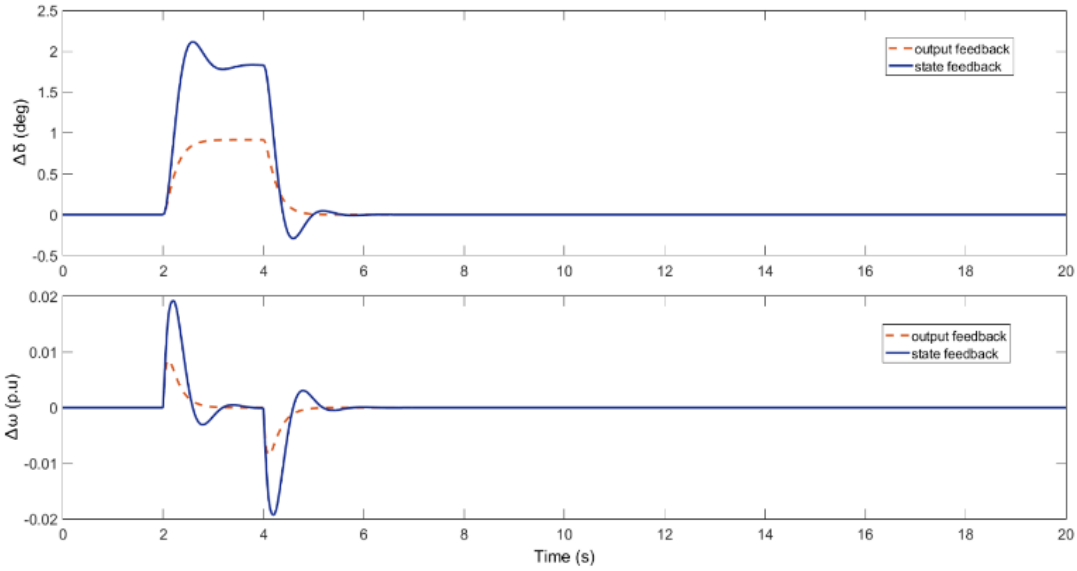

Figure 18. Comparison of LPV PSS performance in output feedback and state feedback methods for the fourth working mode and a sudden change t = 2 s in input mechanical torque

According to Figures 15-18, output feedback design works more presciely than state feedback design to damp the disturbances and minimize the errors. The range of overshoots and undershoots indicates that the proposed LPV PSS designed by output feedback theory is less affected by disturbances.

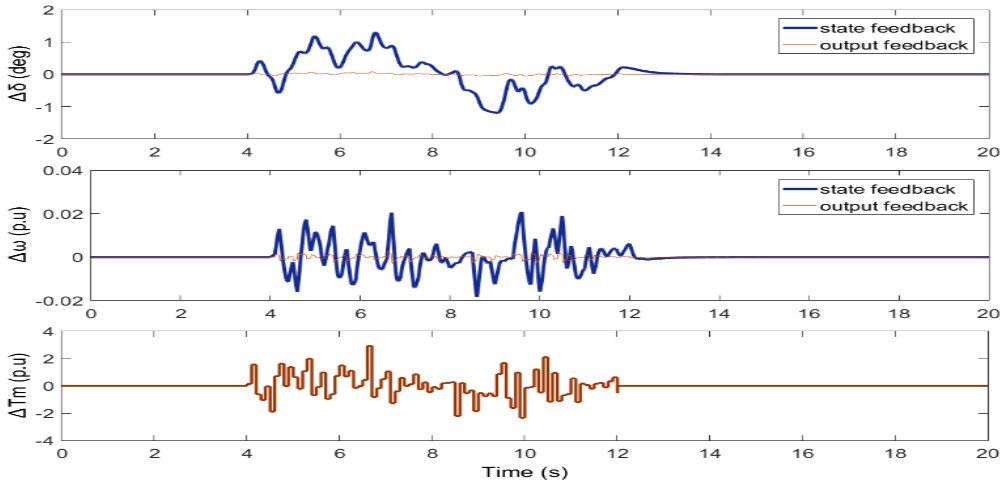

Figure 19. Comparison of LPV PSS performance in output feedback and state feedback methods for the first working mode upon applying noise in the input mechanical torque

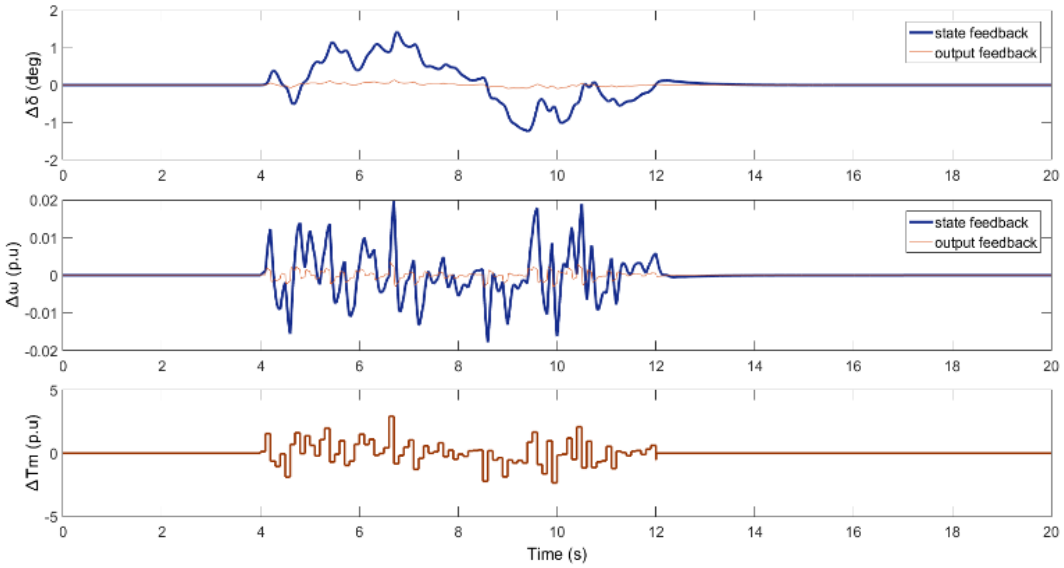

Figure 20. Comparison of LPV PSS performance in output feedback and state feedback methods for the second working mode upon applying noise in the input mechanical torque

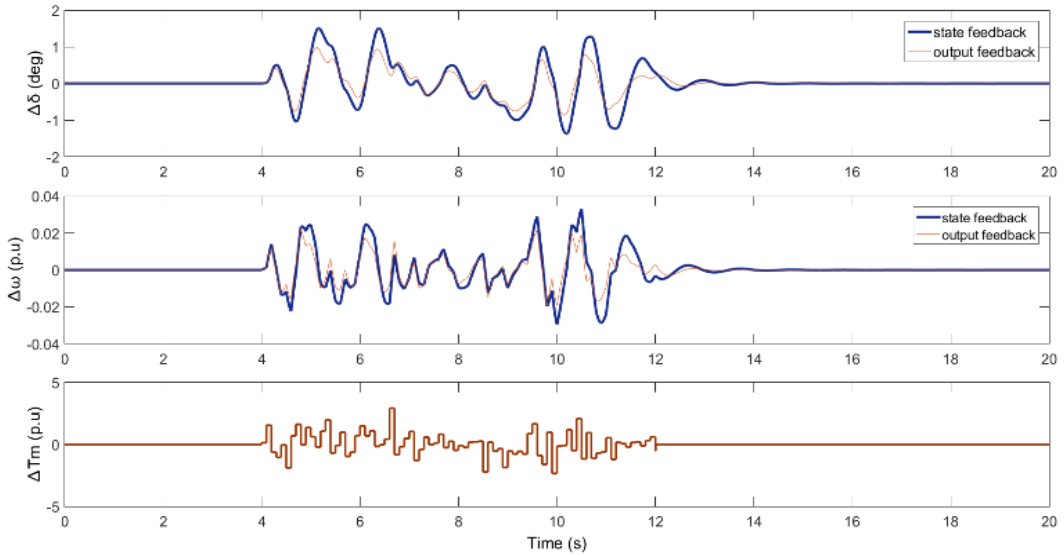

Figure 21. Comparison of LPV PSS performance in output feedback and state feedback methods for the third working mode upon applying noise in the input mechanical torque

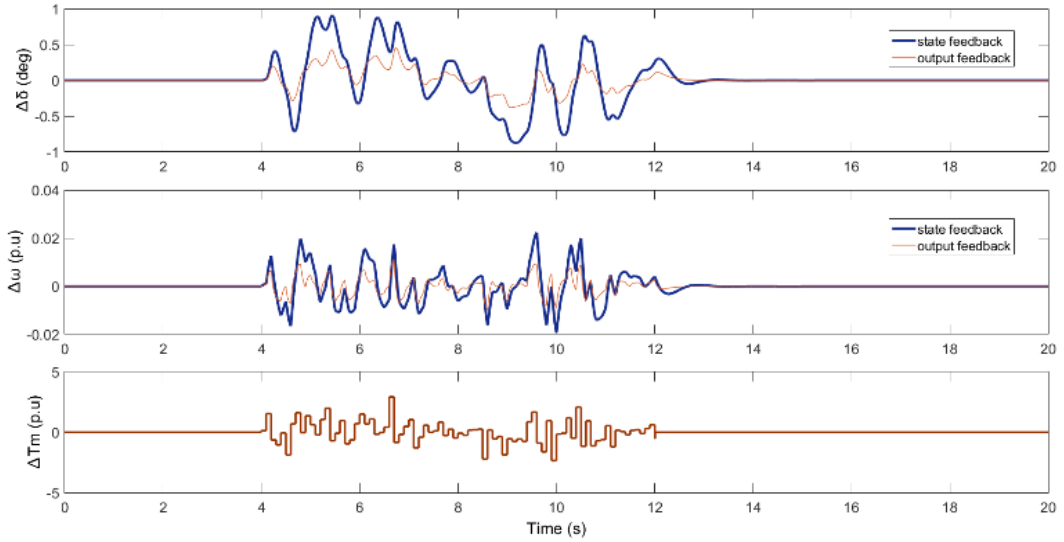

Figure 22. Comparison of LPV PSS performance in output feedback and state feedback methods for the fourth working mode upon applying noise in the input mechanical torque

According to the results derived from Figures 19-22, while noise is applied to the input mechanical torque, the state feedback control system performs weaker than the output feedback one. For a fair comparison, maximum error rates and for two scenarios and four operating points are denoted, as given in Figure 23-26.

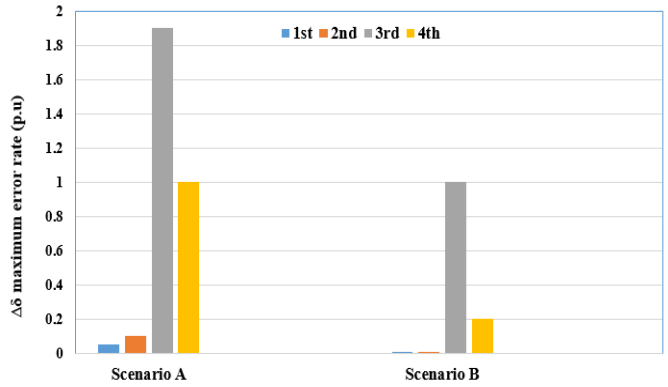

Figure 23. Maximum error rate-output feedback approach tested at four working points. Scenario A: Sudden change in input mechanical torque. Scenario B: Applying noise to input mechanical torque

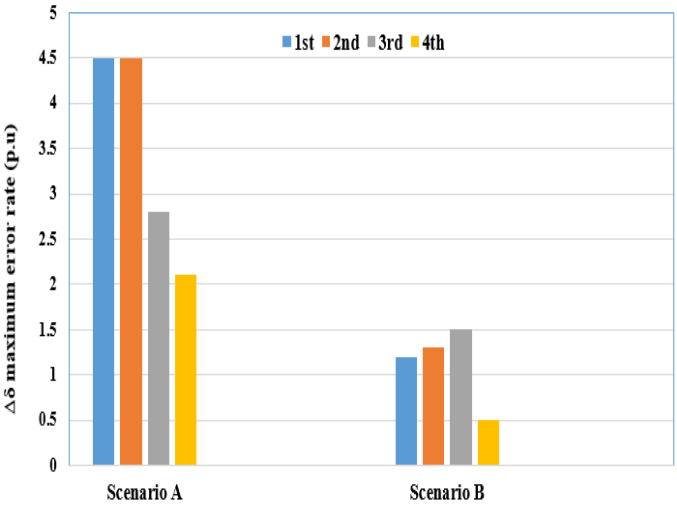

Figure 24. Maximum error rate-state feedback approach tested at 4 working points. Scenario A: Sudden change in input mechanical torque. Scenario B: Applying noise to input mechanical torque

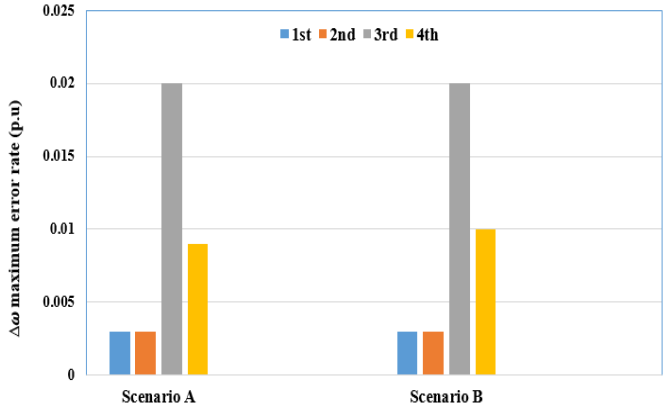

Figure 25. Maximum error rate-output feedback approach tested at 4 working points. Scenario A: Sudden change in input mechanical torque. Scenario B: Applying noise to input mechanical torque

…As can be concluded from the bar charts above, the output feedback theory while applying Scenario A for Δδ has an accurate performance to track reference value and the maximum error rate is 1.9. On the other hand, based on the state feedback theory, the maximum error rate is 4.5, which is much higher than the output feedback approach. Similarly, the rotor angle maximum error rate for the output and state feedback theories are 1 and 1.5, respectively.

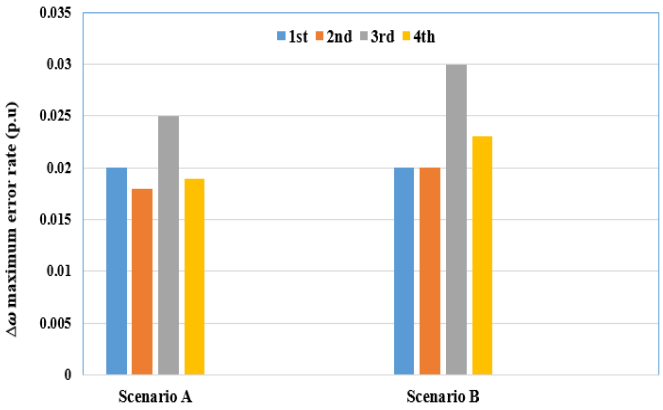

Figure 26. Maximum error rate- state feedback approach tested in 4 working points. Scenario A: Sudden change in input mechanical torque. Scenario B: Applying noise to input mechanical torque

Considering Δω graphs, it is evident that the maximum error rate for both state feedback and output feedback theories is almost the same between 0.02 and 0.03 p.u. Overall, it can be said that the PSS implemented via output feedback theory outweighs the state feedback approach.

Table 3. Norm comparison in output feedback and state feedback methods for Theorems 1 and 4

Largest closed-loop norm	Desired theorems
$\gamma_{\infty}=0.267$	Theorem 1 (Output feedback)
$\gamma_{\infty}=0.063$	Theorem 4 (State feedback)

In this paper, Matlab Software was used for the aim of simulation. The convergence time depends the order of generator model and on the polytope vertices. The higher the order of the system, the more complex the controller design and the longer the convergence time.

The proposed strategy flowchart is finally presented here for clarifying the overall methodolgy.

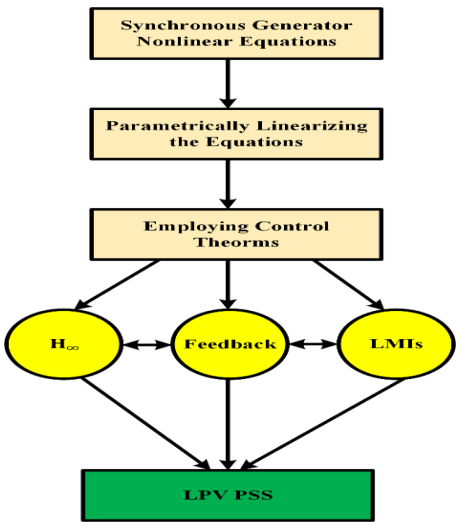

Figure 27. Overall proposed control strategy flowchart

5. CONCLUSIONS

Low frequency oscillations in interconnected power systems are considered as the main challenge. This paper suggests a control strategy based on LPV method to obtain an effective power system stabilizer rejecting noises and disturbances. This system was examined by applying different inputs as well as different operating conditions of the proposed stabilizing performance. Also, the effectiveness of the proposed controller design was compared to the robust and classic design considering the uncertainties of the model and changes in the working conditions. Polytopic representation and LMI optimization are employed to design output feedback and state feedback controllers in order to create a power system stabilizer. Upon comparing the proposed methods and controllers, it was found that PSS designed via LPV method and based on output feedback theory provided better results. In addition, good stability and damping over the whole range of system conditions are guaranteed. This designed PSS can be utilized in intertwined power systems including renewable units to suppress the oscillations.

6. ACKNOWLEDGEMENT

This research did not receive any specific grant from funding agencies in the public, commercial, or not-for-profit sectors.

NOMENCLATURE

P	Active power (w)
Q	Reactive power (var)
Xe	External reactance of transmission line (Ω)
$k_1 \dots k_6$	PSS fourth-order model constants
u	Stabilizer output
w	Disturbance input
y	Measured output
$\Delta\omega$	Velocity deviation (rad/s)
$\Delta\delta$	Load angle deviation
ΔE_q	Electromagnetic force deviation (kg. m/s^2)
ΔE_{fd}	Generator field excitation voltage deviation (v)
T_E	Exciter time constant (s)
K_E	Exciter gain
T'_{d0}	Open circuit field time constant (s)
M	Inertia constant (s)
D	Damping coefficient
x_d	d-axis transient reactance (Ω)
x_q	q-axis transient reactance (Ω)
x'_d	d-axis synchronous reactance (Ω)
K_s	PSS gain
T_w	Washout time constant (s)
$T_1 \dots T_4$	Time constant of lead compensator (s)

APPENDICES

Appendix A: System parameters

Parameter	Value
V	1 p.u
ω_0	314 rpm
M	10 s
x'_d	0.32 p.u
x_d	1.6 p.u
x_q	1.55 p.u
K_E	25
T_E	0.05 s
T'_{d0}	6 s
D	0.05 p.u

Appendix B: Calculation of k_1 to k_6

$$C_1 = \frac{V^2}{x_e + x_q}, \qquad C_3 = C_1\frac{x_q - x'_d}{x_e + x'_d}, \qquad C_4 = \frac{V}{x_e + x'_d}$$

$$C_5 = V\frac{x_d - x'_d}{x_e + x'_d}, \qquad C_6 = C_1\frac{x_q(x_q - x'_d)}{x_e + x'_d}, \qquad C_7 = \frac{x_e}{x_e + x'_d}$$

$$k_1 = C_3\frac{P}{P^2 + (Q + C_1)^2} + Q + C_1$$

$$k_2 = C_4\frac{P^2}{\sqrt{P^2 + (Q + C_1)^2}}, \qquad k_3 = \frac{x_e + x'_d}{x_d + x'_d}$$

$$k_4 = C_5\frac{P^2}{\sqrt{P^2 + (Q + C_1)^2}}$$

$$k_5 = C_4 x_e\frac{P}{V^2 + Qx_e}\left[C_6\frac{C_1 + Q}{P^2 + (C_1 + Q)^2} - x'_d\right]$$

$$k_6 = C_7\frac{\sqrt{P^2 + (Q + C_1)^2}}{V^2 + Qx_e}\left[x_e + \frac{C_1 x_q(C_1 + x_q)}{P^2 + (C_1 + Q)^2}\right]$$

REFERENCES

1. Kundur, P., Balu, N.J. and Lauby, M.G., Power system stability and control, Vol. 7, McGraw-Hill, New York, (1994). (http://dl.poweren.ir/downloads/PowerEn/Book/2019/Jun/Power%20System%20Stability%20and%20Control%20-%20Prabha%20Kundur%20%28PowerEn.ir%29.pdf).
2. Wang, S.K., "Coordinated parameter design of power system stabilizers and static synchronous compensator using gradual hybrid differential evaluation", ***International Journal of Electrical Power & Energy Systems***, Vol. 81, (2016), 165-174. (https://doi.org/10.1016/j.ijepes.2016.02.016).
3. Dey, P., Bhattacharya, A. and Das, P., "Tuning of power system stabilizer for small signal stability improvement of interconnected power system", ***Applied Computing and Informatics***, Vol. 16, (2017), 3-28. (https://doi.org/10.1016/j.aci.2017.12.004).
4. Jin, T., Liu, S., Flesch, R.C. and Su, W., "A method for the identification of low frequency oscillation modes in power systems subjected to noise", ***Applied Energy***, Vol. 206, (2017), 1379-1392. (https://doi.org/10.1016/j.apenergy.2017.09.123).
5. Eltag, K., Aslamx, M.S. and Ullah, R., "Dynamic stability enhancement using fuzzy PID control technology for power system", ***International Journal of Control, Automation and Systems***, Vol. 17, (2019), 234-242. (https://doi.org/10.1007/s12555-018-0109-7).
6. Suzuki, K., Kobayashi, J., Otani, T. and Iwamoto, S., "A multi-input lead-lag power system stabilizer with H_∞ control performance", ***Proceedings of 2015 IEEE Innovative Smart Grid Technologies-Asia (ISGT ASIA)***, Bangkok, Thailand, (2015), 1-6. (https://doi.org/10.1109/ISGT-Asia.2015.7387023).
7. Abido, M.A., "A novel approach to conventional power system stabilizer design using tabu search", ***International Journal of Electrical Power & Energy Systems***, Vol. 21, No. 6, (1999), 443-454. (https://doi.org/10.1016/S0142-0615 (99)00004-6).
8. Farahani, M. and Ganjefar, S., "Intelligent power system stabilizer design using adaptive fuzzy sliding mode controller", ***Neurocomputing***, Vol. 226, (2017), 135-144. (https://doi.org/10.1016/j.neucom.2016.11.043).
9. Bouchama, Z. and Harmas, M.N., "Optimal robust adaptive fuzzy synergetic power system stabilizer design", ***Electric Power Systems Research***, Vol. 83, No. 1, (2012), 170-175. (https://doi.org/10.1016/j.epsr.2011.11.003).
10. Guesmi, T. and Alshammari, B.M., "An improved artificial bee colony algorithm for robust design of power system stabilizers", ***Engineering Computations***, Vol. 34, No. 7, (2017), 2131-2153. (https://doi.org/10.1108/EC-12-2016-0459).

11. Sambariya, D.K. and Prasad, R., "Robust power system stabilizer design for single machine infinite bus system with different membership functions for fuzzy logic controller", ***Proceedings of 7th International Conference on Intelligent Systems and Control (ISCO)***, Coimbatore, India, (2013). (https://doi.org/10.1109/ISCO.2013.6481115).
12. Milla, F. and Duarte-Mermoud, M.A., "Predictive optimized adaptive PSS in a single machine infinite bus", ***ISA Transactions***, Vol. 63, (2016), 315-327. (https://doi.org/10.1016/j.isatra.2016.02.018).
13. Farhad, Z., Eke, H., Tezcan, S. and Safi, S., "A robust PID power system stabilizer design of single machine infinite bus system using firefly algorithm", ***Gazi University Journal of Science***, Vol. 31, No. 1, (2018), 155-172. (https://dergipark.org.tr/en/pub/gujs/issue/35772/346118).
14. Khawaja, A.W., Kamari, N.A.M. and Zainuri, M.A.A.M., "Design of a damping controller using the SCA optimization technique for the improvement of small signal stability of a single machine connected to an infinite bus system", ***Energies***, Vol. 14, No. 11, (2021), 2996. (https://doi.org/10.3390/en14112996).
15. Kadir, N. and Ruswandi Djalal, M., "Optimal design PSS-PID control on single machine infinite bus using ANT COLONY optimization", ***SINERGI***, Vol. 25, No. 2, (2021), 169-176. (http://doi.org/10.22441/sinergi.2021.2.008).
16. Bolinger, K., Laha, A., Hamilton, R. and Harras, T., "Power stabilizer design using root locus methods", ***IEEE Transactions on Power Apparatus and Systems***, Vol. 94, No. 5, (1975), 1484-1488. (https://doi.org/10.1109/T-PAS.1975.31990).
17. Gibbard, M.J., "Robust design of fixed-parameter power system stabilizers over a wide range of operating conditions", ***IEEE Transactions on Power Apparatus and Systems***, Vol. 6, No. 2, (1991), 794-800. (https://doi.org/10.1109/59.76727).
18. Abido, M.A., "Optimal design of power-system stabilizers using particle swarm optimization", ***IEEE Transactions on Energy Conversion***, Vol. 17, No. 3, (2002), 406-413. (https://doi.org/10.1109/TEC.2002.801992).
19. Bandal, V. and Bandyopadhyay, B., "Robust decentralised output feedback sliding mode control technique-based power system stabilizer (PSS) for multimachine power system", ***IET Control Theory Applications***, Vol. 1, (2007), 1512-1522. (https://doi.org10.1049/iet-cta:20060393).
20. El-Metwally, K.A., "An adaptive fuzzy logic controller for a two area load frequency control problem", ***Proceedings of 12th International Middle-East Power System Conference***, Aswan, Egypt, (2008), 300-306. (https://doi.org/10.1109/MEPCON.2008.4562327).
21. Shakarami, M.R. and Davoudkhani, I.F., "Wide-area power system stabilizer design based on grey wolf optimization algorithm considering the time delay", ***Electric Power Systems Research***, Vol. 133, (2016), 149-159. (https://doi.org/10.1016/j.epsr.2015.12.019).
22. Hemmati, R., "Power system stabilizer design based on optimal model reference adaptive system", ***Ain Shams Engineering Journal***, Vol. 9, No. 2, (2018), 311-318. (https://doi.org/10.1016/j.asej.2016.03.002).
23. Kashani, M., Alfi, A. and Arabkoohsar, A., "Optimal robust control scheme to enhance power system oscillations damping via STATCOM", ***Proceedings of 2020 International Conference on Smart Energy Systems and Technologies (SEST)***, Istanbul, Turkey, (2020), 1-6. (https://doi.org/10.1109/SEST48500.2020.9203361).
24. Guesmi, T., Farah, A., Abdallah, H.H. and Ouali, A., "Robust design of multi-machine power system stabilizers based on improved non-dominated sorting genetic algorithms", ***Electrical Engineering***, Vol. 100, (2018), 1351-1363. (https://doi.org/10.1007/s00202-017-0589-0).
25. Nogueira, F.G., Barra Jr, W., da Costa Jr, C.T., Barreiros, J.A. and de Lana, J.J., "Design and experimental tests of an LPV power system stabilizer on a 10kVA small-scale generating unit", ***IFAC-PapersOnLine***, Vol. 48, No. 26, (2015), 236-241. (https://doi.org/10.1016/j.ifacol.2015.11.143).
26. Jabali, M.B.A. and Kazemi, M.H., "A new LPV modeling approach using PCA-based parameter set mapping to design a PSS", ***Journal of Advanced Research***, Vol. 8, No. 1, (2017), 23-32. (https://doi.org/10.1016/j.jare.2016.10.006).
27. Shamma, J.S., "An overview of LPV system",Control of linear parameter varying systems with applications,Mohammadpour, J. and Scherer, C. eds., Springer, Boston, MA, (2012), 3-26. (https://doi.org/10.1007/978-1-4614-1833-7_1).
28. Bruzelius, F., "An approach to gain scheduling linear parameter varying system", ***Chalmers University of Technology***, (2004). (https://elibrary.ru/item.asp?id=8860385).
29. Sato, M. and Peaucelle, D., "Gain-scheduled output-feedback controllers using inexact scheduling parameters for continuoustime LPV systems", ***Automatica***, Vol. 49, No. 4, (2013), 1019-1025. (https://doi.org/10.1016/j.automatica.2013.01.034).
30. Sadeghzadeh, A., "Gain-scheduled filtering for linear parameter-varying systems using inexact scheduling parameters with bounded variation rates", ***International Journal of Robust and Nonlinear Control***, Vol. 26, No. 13, (2015), 2864-2879. (https://doi.org/10.1002/rnc.3482).
31. Xie, R., Wang, X. and Li, Y., "H Infinity State feedback control for the stabilization of the three Euler angles of helicopter based on LMI", ***Proceedings of International Conference on Intelligent Computation Technology and Automation***, Changsha, China, (2008). (https://doi.org/10.1109/ICICTA.2008.332).
32. Soliman, H.M., Emara, H., Elshafei, A.L., Bahgat, A. and Malik, O.P., "Robust output feedback power system stabilizer design: An LMI approach", ***2008 IEEE Power and Energy Society General Meeting–Conversion and Delivery of Electrical Energy in the 21st Century***, Pittsburgh, PA, USA, (2008), 1-8. (https://doi.org/10.1109/PES.2008.4596450).
33. Soliman, H.M., Elshafei, A.L., Shaltout. A.A. and Morsi, M.F., "Robust power system stabilizer", ***IET Proceedings - Generation Transmission and Distribution***, Vol. 147, No. 5, (2000), 285-291. (http://dx.doi.org/10.1049/ip-gtd:20000560).
34. Demello, F.P. and Concordia, C., "Concepts of synchronous machine stability as affected by excitation control", ***IEEE Transactions on Power Apparatus and Systems***, Vol. PAS-88, No. 4, (1969), 316-329. (https://doi.org/10.1109/TPAS.1969.292452).
35. Lofberg, J., "YALMIP: A toolbox for modeling and optimization in MATLAB", ***Proceedings of IEEE International Conference on Robotics and Automation***, Taipei, Taiwan, (2004). (https://doi.org/10.1109/CACSD.2004.1393890).
36. Agulhari, C.M., De Oliveira, R.C.L.F. and Peres, P.L.D., "Algorithm 998: The robust LMI parser—A toolbox to construct LMI conditions for uncertain systems", ***ACM Transactions on Mathematical Software***, Vol. 45, No. 3, (2019), 1-25. (https://doi.org/10.1145/3323925).
37. Yang, T.C., "Applying H_∞ optimization method to power system stabilizer design, Part 1: single-machine infinite-bus systems", ***International Journal of Electrical Power & Energy Systems***, Vol. 19, No. 1, (1997), 29-35. (https://doi.org/10.1016/S0142-0615 (96)00026-9).

JREE: Vol. 9, No. 2, (Spring 2022) 75-81

Journal of Renewable Energy and Environment

Journal Homepage: www.jree.ir

Materials and Energy Research Center

MERC

Research Article

CFD Analysis of the Most Favorable Gap Between the Main Runner and Booster Runner of Gravitational Water Vortex Turbine

Bharosh Kumar Yadav[a*], Amit Chandra Jyoti[a], Pintu Kr. Rajak[a], Ramesh Kr. Mahato[a], Deelip Kr. Chaudhary[a], Mehdi Jahangiri[b], Ram Dayal Yadav[a]

[a] *Department of Mechanical Engineering, Purwanchal Campus, Institute of Engineering, Tribhuvan University, Dharan-08, Nepal.*
[b] *Department of Mechanical Engineering, Shahrekord Branch, Islamic Azad University, Shahrekord, Iran.*

PAPER INFO

Paper history:
Received 20 September 2021
Revised in revised form: 06 November 2021
Scientific Accepted: 23 November 2021
Published: 19 April 2022

Keywords:
Low Head MHP,
Computational Fluid Dynamic (CFD),
Vortex Turbine,
Booster Runner,
Main Runner

ABSTRACT

The Gravitational Water Vortex Power Plant (GWVPP) is a power generation system designed for ultralow head and low flow water streams. Energy supply to rural areas using off-grid models is simple in design and structure and sustainable to promote electricity access through renewable energy sources in the villages of Nepal. The objective of this study is to determine the most favorable gap between the booster and main runners of a Gravitational Water Vortex Turbine (GWVT) to ensure maximum power output of the GWVPP. CFD analysis was used to evaluate the 30 mm gap between the main and booster runners, which was the most favorable gap for enhancing the plant's power. In this study, the optimum power and economic analysis of the entire plant was conducted in the case of mass flow rates of 4 kg/s, 6 kg/s, and 8 kg/s. The system was modeled in SolidWorks V2016 and its Computational Fluid Dynamic (CFD) analysis was performed utilizing ANSYS R2 2020 with varying multiple gaps between the main and booster runners to determine the most favorable gap of the plant's runner. This research concluded that optimum power could be achieved if the distance of the main runner's bottom position be fixed at 16.72 %, i.e., the distance between the top position of the conical basin and the top position of the booster runner. At a mass flow rate of 8 kg/s, the plant generated maximum electric energy (3,998,719.6 kWh) comparatively and economically contributed 268,870.10 USD on an annual basis.

https://doi.org/10.30501/jree.2022.298216.1237

1. INTRODUCTION

Water is a clean, inexpensive source of energy through which an environmentally benign generation of power can be ensured, and this is is of utmost importance for a sustainable future. Nevertheless, much of water energy remains underutilized [1]. The Gravitational Water Vortex Power Plant (GWVPP) uses a hydrokinetic technique to extract energy, in which case the kinetic energy of flowing water is immediately transformed into electricity by a turbine with low or no head [2]. The GWVT is a type of low-head turbine that can operate at 0.7-3.0 m head, which is conventional for the production of renewable energy and such hydro turbines have a positive impact on the environment. The GWVT turbine rotates in a co-axial manner and is a strike on its overall circumference. Water enters the cannel by a huge, straight intake and then, flows tangentially over the circular basin forming a vortex. Due to the dynamic force between the turbine and flowing water fluid, a vortex emerges that passes through the bottom of the basin, which is intentionally structured to maintain pressure differences. It not only provides electricity for households but also aerates the flow of water. Dhakal et al. performed a computational and experimental analysis for GWVPP with cylindrical and conical basins to determine the optimum position of the runner. They demonstrated that the power and efficiency were higher 65-75 % in the conical basin, compared to the cylindrical basin [3, 4]. The GWVT is beneficial for a variety of uses in human civilization and industry, e.g., it can be used in load-setting situations to light up home, community, run modest fans, etc. It can also be used for irrigation as a water delivery system with a motorized fountain spray. In industries, it is more useful to light up bulbs and preserve energy grids [5]. The concentration of dissolved oxygen may increase upon the formation of a vortex. It is more advantageous in geographical places such as mountain steep areas where transmission lines are not properly accessible.

Mulligan et al. adjusted the ratio of orifice diameter and tank diameter (d/D) in the range of 14-18 % for both in low-head and high-head locations and found the vortex power optimum [6]. Nepal is a landlocked country and 17 % of the total land is flat, known as Terai Madhesh Region (TMR). Tri Ratna Bajracharya et al. studied the free-flowing low-head water

*Corresponding Author's Email: bharosh@ioepc.edu.np (B. Kumar Yadav)
URL: https://www.jree.ir/article_148440.html

Please cite this article as: Kumar Yadav, B., Chandra Jyoti, A., Rajak, P.Kr., Mahato, R.Kr., Chaudhary, D.Kr., Jahangiri, M. and Dayal Yadav, R., "CFD analysis of the most favorable gap between the main runner and booster runner of gravitational water vortex turbine", ***Journal of Renewable Energy and Environment (JREE)***, Vol. 9, No. 2, (2022), 75-81. (https://doi.org/10.30501/jree.2022.298216.1237).

turbine of TMR, the condition of discharge, and length of the basin diameter, and they found that the vortex was minimum at the bottom level depending on the geometry of the basin's supply of discharge [7]. Wanchat et al. investigated the formation of a vortex in/of the water stream and found that the kinetic energy of the vortex of the water stream was the characteristic of the water height, diameter of the orifice, and basin of the structure. They also employed numerical and experimental analyses to evaluate the produced electric power of 60 W, which achieved 30 % efficiency for the plant [8, 9]. Rabin Dhakal et al. investigated the design method of the GWVPP runner and found the efficiency of the curved blade to be greater than a straight or twisted blade profile [10]. Manil Kayastha et al. suggested that the shifting of the runner downwards would increase the efficiency of the plant [11]. R. Ullah et al. conducted a performance analysis on multi-stage GWVT and found that the performance of the GWVPP could be increased using multistage, implying that the alignment manner of the two runners should be the same rotor to a basin with an identical diameter. He further analyzed experimentally the effect of the ratios of rotor diameter to basin diameter on multistage GWVPP with a conical basin of the plant for adequate power and efficiency [12, 13].

As a result of the literate review, some relevant research gaps have been identified. None of the scientific literature studies has focused on the measurement of the most favorable gap between the main and booster runners of the GWVPP plant. CFD analysis evaluated which gap between the main and booster runner would be the most favorable one to cover so as to enhance the plant's power. In this study, the optimum power and economic analysis of the entire plant was evaluated at mass flow rates of 4 kg/s, 6 kg/s, and 8 kg/s. Therefore, the present research work aims to bridge the research gap for ensuring reliable and sustainable energy in the installation of cum production in the GWVPP plant.

2. METHODOLOGY

In this work, a holistic approach was used for the analysis of two-stage GWVPP, as shown in Figure 1. In today's world where global warming is one of the greatest human challenges, sustainable energy generation is becoming increasingly relevant. The use of green and clean energy sources is the best way to minimize hazardous gases and other emissions of conventional energy usage.

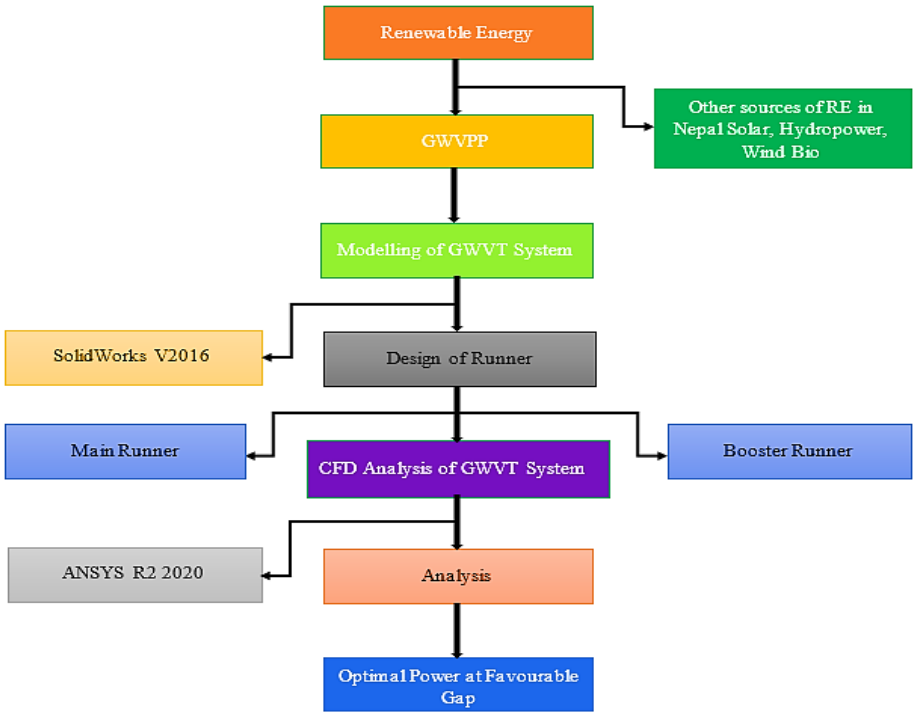

Figure 1. Flowchart describing the methodology of the study

The gravitational water vortex power plant is a form of micro-hydropower system that converts the energy of flowing fluid into rotational energy with a head between 0.7-3.0 meters. The GWVPP system is built with a circular/conical basin in which water creates a vortex above the drain used to drive a water turbine. By using the Navier-Stokes equation and the continuity equations, cylindrical coordinates can be described taking the assumption of steady, incompressible, and axis-symmetric flows as follows [14]:

$$\frac{\partial V_r}{\partial r} + \frac{\partial V_z}{\partial z} + \frac{V_r}{r} = 0 \quad (1)$$

$$V_r \frac{\partial V_\theta}{\partial r} + V_z \frac{\partial V_\theta}{\partial z} - \frac{V_r V_\theta}{r} = \nu\left(\frac{\partial^2 V_\theta}{\partial r^2} + \frac{\partial V_\theta}{r\,\partial r} - \frac{V_\theta}{r^2} + \frac{\partial^2 V_\theta}{\partial z^2}\right) \quad (2)$$

$$V_r \frac{\partial V_r}{\partial r} + V_z \frac{\partial V_r}{\partial z} - \frac{V_\theta^2}{r} + \frac{\partial \rho}{\rho \partial r} = \nu\left(\frac{\partial^2 V_r}{\partial r^2} + \frac{\partial V_r}{r\,\partial r} - \frac{V_r}{r^2} + \frac{\partial^2 V_r}{\partial z^2}\right) \quad (3)$$

$$V_r \frac{\partial V_z}{\partial r} + V_z \frac{\partial V_z}{\partial z} + \frac{\partial \rho}{\rho\,\partial z} = g + \nu\left(\frac{\partial^2 V_z}{\partial r^2} + \frac{\partial V_z}{r\,\partial r} + \frac{\partial^2 V_z}{\partial z^2}\right) \quad (4)$$

where V_θ = tangential velocity, V_r = radial velocity, V_z = axial velocity, ρ = density of fluid, g = gravitational acceleration, and ν = kinematic viscosity.

3. NUMERICAL SIMULATIONS

A numerical simulation as a computer-based calculation uses a program to implement a mathematical model of a physical system [15]. Most nonlinear systems require numerical

simulations to analyze their behavior because their mathematical models are too complex to provide analytical answers [16]. Computational fluid dynamics is a branch of fluid mechanics used for the analysis of and solution to the problem corresponding to the fluid flow involving data structures and the numerical analysis [17]. The calculations that are essential to the model with a free fluid stream and the interaction of the fluid with its surface area are defined by boundary conditions that can be solved using computers [18]. The SolidWorks V2016 was utilized for modeling the GWVPP system, and different gaps were provided such as 10mm, 20 mm, 30 mm, 40 mm, 50 mm, and 60 mm in between the main runner and booster runner of the GWVT. Finally, simulation results were analyzed using ANSYS R2 2020 and used to customize the favorable gap of the runners of the GWVPT for optimal power of the plants.

3.1. 3D modeling of runner

The 3D modeling of the GWVPP structure was performed using SolidWorks and various sections of GWVT such as canal, basin, and runners aligned together, as shown in Figure 2. In the design process, the booster runner was kept fixed at about 70 % of the total height of GWVT from the top position of the conical basin and, simultaneously, the main runner varied at different gaps such as 10 mm, 20 mm, 30 mm, 40 mm, 50 mm, and 60 mm to achieve optimum and sustainable power of the plant.

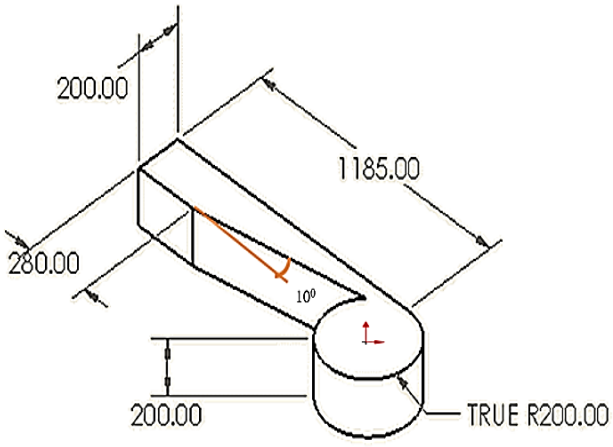

a) Canal

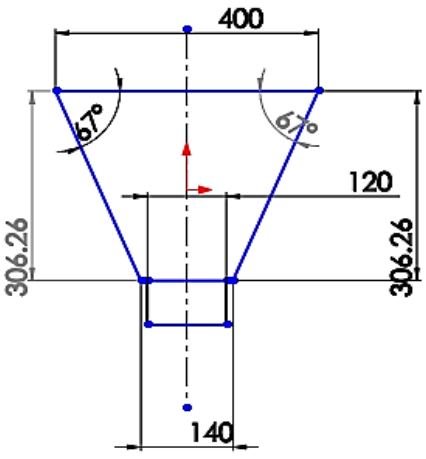

b) Conical basin

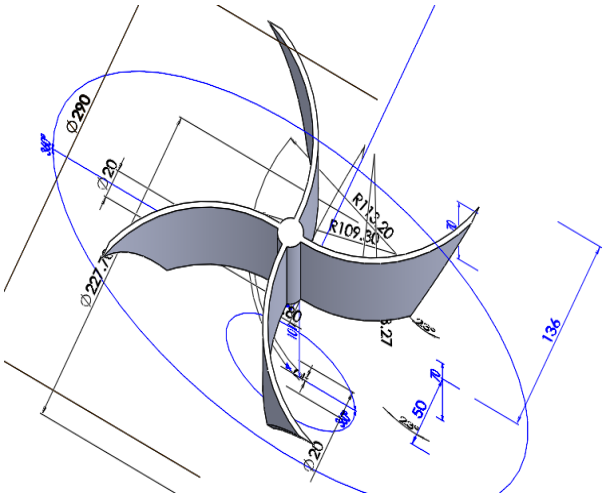

c) Main runner

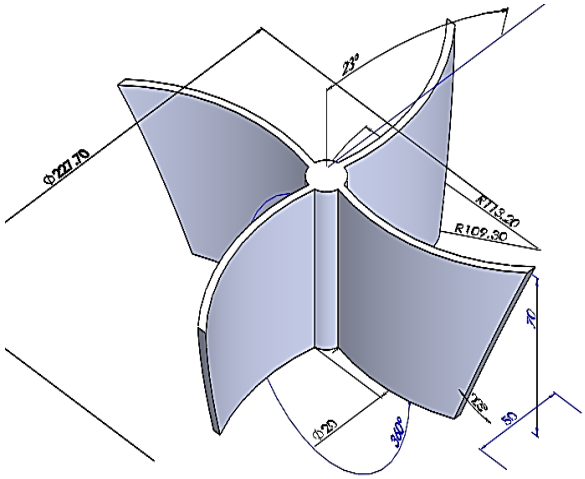

d) Booster runner

Figure 2. 3D modeling of GWVPP system

3.2. Meshing and boundary condition

Meshing is one of the processes of engineering simulation that is used for breaking complex geometries into simple parts which can facilitate discretizing local approximations into wider domains. The mesh has an impact on the speed, accuracy, and convergence of simulation because this meshing takes a large percentage of total simulation time to give the most possible results [19]. There are two types of domains: rotatory and stationary. The domain of the booster runner and the main runner is used as a rotatory domain and the domain of canal, basin, and a draft tube is used as the stationary domain of the GWVPP structure, which is shown in Figure 3.

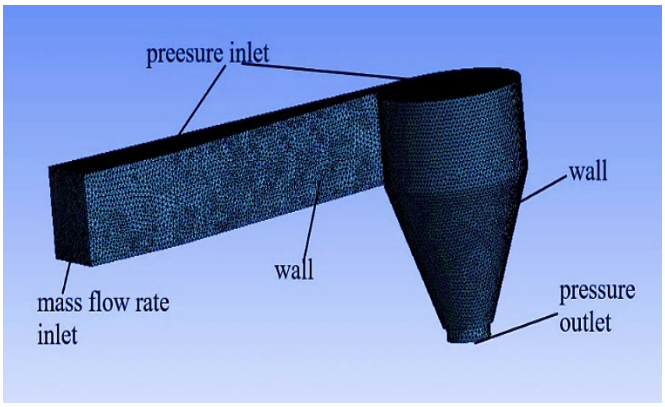

a) Stationary domain

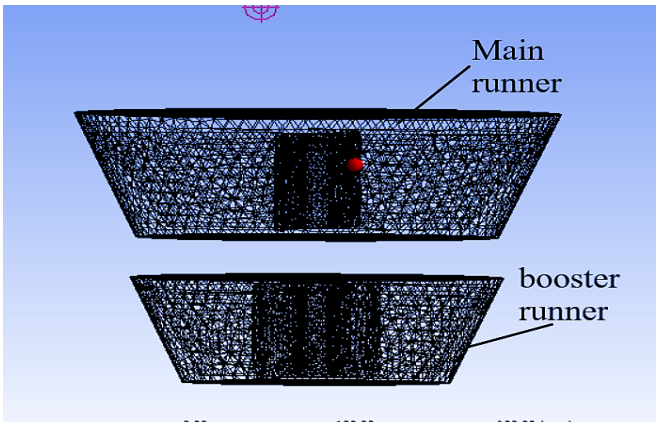

(b) Wireframe view of a rotatory domain

Figure 3. Mesh generation (a) Stationary and (b) Rotatory domain of GWVT system

In this work, the very popular Finite Element (FE) computational simulating software ANSYS R2 2020 was used for numerical analysis. During the process of meshing the structure of the GWVT with a different individual component, the elements in orthogonal shape were provided as 9 mm to 18 mm, and the rest of the parameters were set to be the default of the plant. Table 1 summarizes the mesh analysis results of the plant setup.

Table 1. Results obtained from mesh analysis

Name	Obtained results
Number of elements	475188
Orthogonal quality minimum size	0.013535
Orthogonal quality maximum size	0.99366
Aspect ratio	1.15
Number of nodes	95941

After meshing the whole structure of the GWVPP, the boundary conditions of mass flow rates of 4 kg/s, 6 kg/s, and 8 kg/s were set fixed at the inlet and outlet of the plant following the conservation of mass with variable angular velocities in the range of 1-4 rad/s. The method of formulation, solving, and summary of boundary conditions are depicted in Table 2. A difficut task is to set the condition to get maximum angular velocities (in the range of 1-4 rad/s) so as to choose the favorable gap (out of 10 mm, 20 mm, 30 mm, 40 mm, 50 mm, and 60 mm) after performing various simulations to achieve the maximum output power of the GWVPP.

Table 2. Summary of boundary conditions and features

1.	**Boundary type**	**Operating conditions**
i.	Mass flow rate inlet	4 kg/s, 6 kg/s, 8 kg/s
ii.	Pressure inlet	Atmospheric pressure
iii.	Wall	Steel wall
iv	Pressure outlet	Atmospheric pressure
2.	**Feature**	**Technique**
i.	Method of coupling velocity and pressure terms	Simple
ii.	Gradient discretization	Least square cell based
iii.	Pressure discretization	Second order
iv.	Momentum discretization	Second-order upwind
v.	Turbulent kinetic energy discretization	Second-order upwind
vi.	Specific dissipation rate	Second-order upwind
vii.	Maximum number of iterations	350
viii.	Mesh movement algorithm	Smoothing and re-meshing
ix.	Mesh movement algorithm over the fluid-solid interface	System coupling and deformation

4. RESULTS AND DISCUSSION

The simulation results are presented in this section. Three mass flow rates (i.e., 4 kg/s, 6 kg/s, and 8 kg/s) were set fixed at the inlet and outlet of the plant and angular velocities changed in the range of 1-4 rad/s in three conditions of the vortex flow of water. In the meantime, the gaps/spacing was increasing correspondingly from the top position of the conical basin and the top position of the booster runner's distances to predict the main runner position set to be fixed in between them. The seven input parameters of angular velocities set fixed in the ANSYS at an equal interval of 0.5 rad/s (in between 1-4 rad/s range) and the power produced through the main runner and booster runners obtained from the numerical simulations at the gaps of 10 mm, 20 mm, 30 mm, 40 mm, 50 mm, and 60 mm with three different mass flow rates are shown in Figure 4.

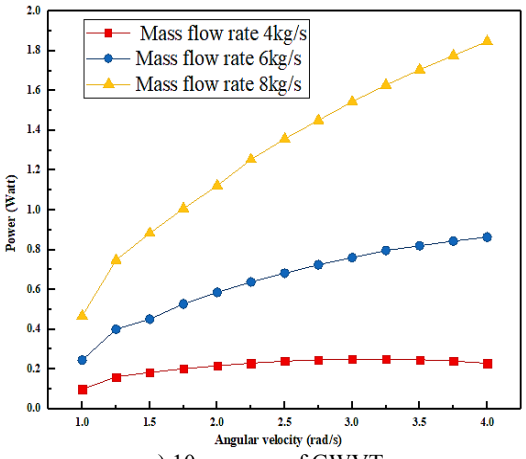

a) 10 mm gap of GWVT

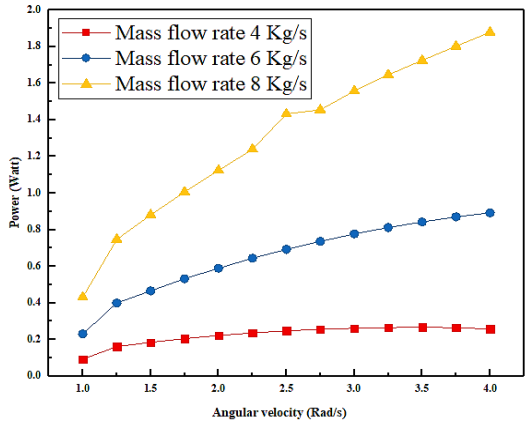

b) 20 mm gap of GWVT

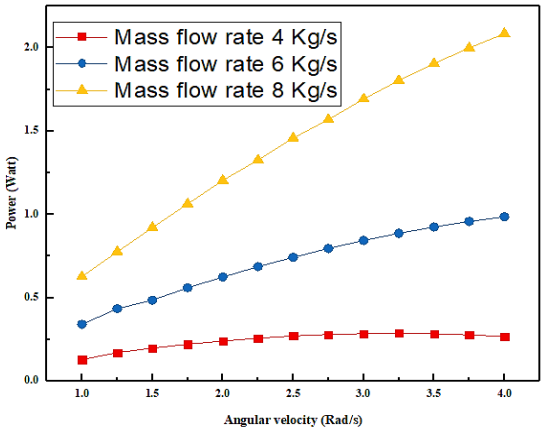

c) 30 mm gap of GWVT

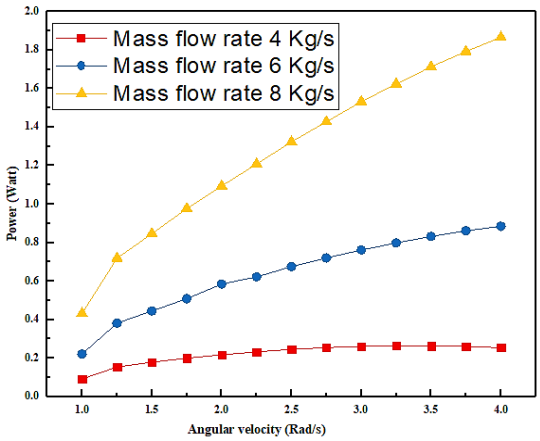

d) 40 mm gap of GWVT

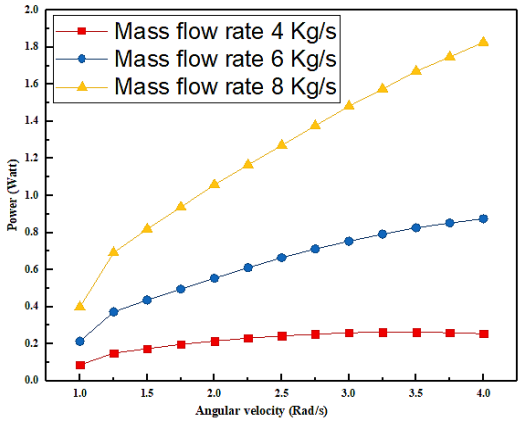

e) 50 mm gap of GWVT

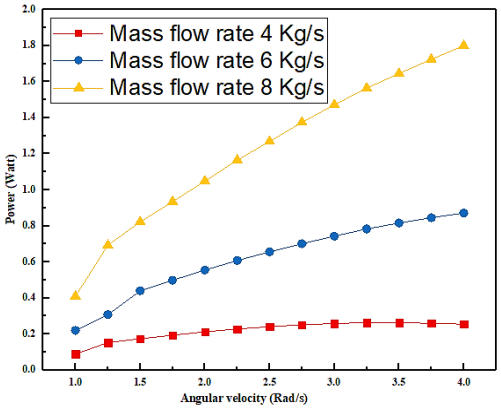

f) 60 mm gap of GWVT

Figure 4. Power output vs. Angular velocity of the main runner and booster runner at various gaps of the GWVT system

The optimum power generation at the gap of 30 mm in between the main runner and booster runner for 4 kg/s, 6 kg/s, and 8 kg/s mass flow rates was found as 0.2862522 Watt, 0.9852612 Watt, and 2.084236 Watt, respectively, as shown in Figure 5. According to the appendix, if the GWVPP plant is installed considering 10 hours of electric use every day, then the plant with a mass flow rate of 4 kg/s will produce an electric energy of 549157.671 kWh in a year, which will be about 43,93,261.37 Rupees (36924.84 $). Likewise, the annual economic analysis for mass flow rates of 6 kg/s and 4 kg/s GWVPP plant can produce 1890164.5 kWh and 3998719.6 kWh electric energies, which will be around 15121316 Rupees (127092.86 $) and 31989756.8 (268870.1 $), respectively. The optimum and cost-effective production of electric energy by the GWVPP plant can be ensured when 30 mm gap be considered in between the main and booster runner at a mass flow rate of 8 kg/s.

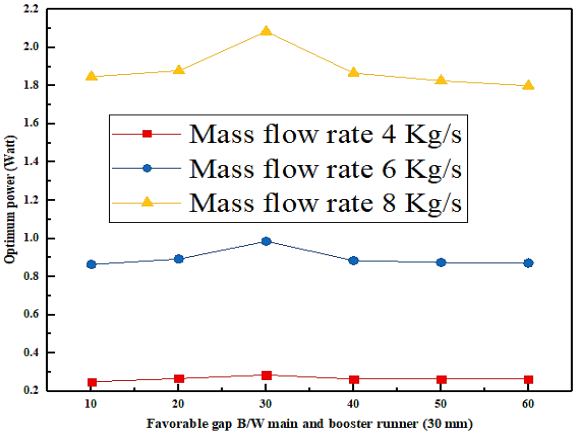

Figure 5. Optimum power of GWVT system and the corresponding favorable gap

5. CONCLUSIONS

This study concluded that the optimum power of the GWVPP plant could be enhanced upon fixing the main runner bottom position at 16.72 % of the distances in between the top position of the conical basin and the top position of the booster runner. CFD analysis of this study illustrated that the 30 mm gap was the most favorable gap between the main runner and booster runner. Also, the optimum power was found to be maximum at the same gap of the main runner and booster runner of the GWVT and the values obtained were

0.2862522 Watt, 0.9852612 Watt, and 2.084236 Watt, respectively. The distance between the top position of the conical basin and the top position of the booster runner taken was 179.39 mm; therefore, the favorable position of the main runner would be 16.72 % of 179 mm, i.e., 29.9940 mm ~ 30 mm gap. This finding was validated according to the computational simulation result. Thus, the present research work aimed to bridge the research gap concerning the optimal power and favorable gap of the main and booster runners of the GWVT system. The optimum power and economic analysis of the entire plant were evaluated at mass flow rates of 4 kg/s, 6 kg/s, and 8 kg/s, respectively. The GWVPP plant being installed considering 10 hours of daily electric use, compared to one year, with a mass flow rate of 4 kg/s will produce 549157.671 kWh electric energy, which will be about 43,93,261.37 Rupees (36924.84 $). Likewise, the yearly economic analysis for the mass flow rates of 6 kg/s and 8 kg/s can produce 1890164.5 kWh and 3998719.6 kWh electric energy, which will be around 15121316 Rupees (127092.86 $) and 31989756.8 (268870.1 $), respectively. At a mass flow rate of 8 kg/s, the plant produces optimum electric energy economically when a 30 mm gap is maintained between the main and booster runners. In addition, the installation of GWVPP by the general public or government authorities and stakeholders will lead to greater convenience, implementation confidence, proper utilization of green energy, thus enhancing a plant's power, cost-effectiveness, and efficiency output. Future related work may focus on the validation of computational numerical simulation results in experimental terms.

6. ACKNOWLEDGEMENT

This research was supported by the "Students Final Year Research Fund" of Tribhuvan University, Institute of Engineering, Purwanchal Campus, Dharan-08, Nepal.

APPENDIX

The economic analysis was carried out based on the mass flow rates of 4 kg/s, 6 kg/s, and 8 kg/s shown below:

For 4 kg/s, we can have 0.2862522 Watt power. Then, the total power in one year = 0.2862522*60*24*365 = 150454.156 Watt.

As is already known, 1 kWh = 1 unit considering that 10 hours of electricity is being used by the consumers every day. Then, the yearly electricity consumed by the consumer = 10 * 365 = 3650 hours/Year.

Also, kWh = 1540454.156 * 3650/1000 = 549157.671 kWh

or Units

549157.671 kWh = 549157.671 units

According to Nepal Electrical Authority, each unit costs 8 Rupees Nepali currency (0.067 $). Therefore,

549157.671 units = Rs. 549157.671* 8 = Rs. 4393261.37 (36924.84 $)

From the above calculation, it can be seen that when the mass flow rate is 4 kg/s, the GWVPP plant can produce 549157.671 kWh electricity power which will be around Rs. 4393261.37 (36924.84 $), yearly.

Likewise, a calculation was done for mass flow rates 6 kg/s and 8 kg/s and it was found that When the mass flow rate was 6 kg/s, GWVPP would generate 1890164.5 kWh, which would be around 15121316 Nepalese Rupees (127092.86 $) yearly; and when the mass flow rate was 8 kg/s, the plant would generate maximum electric energy of 3998719.6 kWh, which is around 31989756.8 Nepalese Rupees (268870.1 $) yearly.

It can be concluded that 8 kg/s mass flow rate will be more economical and optimum electric energy can be harnessed when the gap in between the main and booster runners is maintained at 30 mm.

REFERENCES

1. Dhakal, R., Bajracharya, T.R., Shakya, S.R., Kumal, B., Kathmandu, N., Khanal, K. and Ghale, D.P., "Computational and experimental investigation of runner for gravitational water vortex power plant", ***Proceedings of IEEE 6th International Conference on Renewable Energy Research and Applications (ICRERA 2017)***, San Diego, California, USA, (5-8 November 2017), 365-373. (https://doi.org/10.1109/ICRERA.2017.8191087).
2. Kaygusuz, K., "Energy for sustainable development: A case of developing countries", ***Renewable and Sustainable Energy Reviews***, Vol. 16, No. 2, (2012), 1116-1126. (https://doi.org/10.1016/j.rser.2011.11.013).
3. Dhakal, S., Timilsina, A.B., Dhakal, R., Fuyal, D., Bajracharya, T.R., Pandit, H.P. and Nakarmi, A.M., "Comparison of cylindrical and conical basins with optimum position of runner: Gravitational water vortex power plant", R***enewable and Sustainable Energy Reviews***, Vol. 48, (2015), 662-669. (https://doi.org/10.1016/j.rser.2015.04.030).
4. Dhakal, R., Dhakal, S., Timilsina, A.B. and Fuyal, D., "Design optimization of basin and testing of runner for gravitational water vortex power plant", ***Proceedings of The 2015 International Capstone Design Contest on Renewable Energy Technology***, Mokpo National University, Mokpo, Korea, (07 January 2015). (https://www.researchgate.net/publication/297967445_Design_Optimization_of_Basin_and_Testing_of_Runner_for_Gravitational_Water_Vortex_Power_Plant).
5. Dhakal, S., Timilsina, A.B., Dhakal, R., Fuyal, D., Bajracharya, T.R., Pandit, H.P. and Amatya, N., "Mathematical modeling, design optimization and experimental verification of conical basin: Gravitational water vortex power plant", ***Proceedings of Dalam World Largest Hydro Conference***, (2015), 1-23. (https://www.academia.edu/43393673/Mathematical_modeling_design_optimization_and_experimental_verification_of_conical_basin_Gravitational_water_vortex_power_plant?from=cover_page).
6. Mulligan, S. and Casserly, J., "The hydraulic design and optimisation of a free water vortex for the purpose of power extraction", ***BE Project Report***, Institute of Technology, Sligo, (2010). (https://scholar.google.com/scholar?cluster=17970346606563119939&hl=en&as_sdt=2005).
7. Bajracharya, T.R. and Chaulagai, R.K., "Developing innovative low head water turbine for free-flowing streams suitable for micro-hydropower in flat (Terai) regions in Nepal", ***Center for Applied Research and Development (CARD), Institute of Engineering***, Tribhuvan University, Kathmandu, Nepal, (2012). (https://scholar.google.com/scholar?cluster=9996932610268160475&hl=en&oi=scholarr).
8. Wanchat, S. and Suntivarakorn, R., "Preliminary design of a vortex pool for electrical generation", ***Advanced Science Letters***, Vol. 13, No. 1, (2012), 173-177. (https://doi.org/10.1166/asl.2012.3855).
9. Wanchat, S., Suntivarakorn, R., Wanchat, S., Tonmit, K. and Kayanyiem, P., "A parametric study of a gravitation vortex power plant", ***Advanced Materials Research***, Vol. 805, (2013), 811-817. (https://doi.org/10.4028/www.scientific.net/AMR.805-806.811).
10. Dhakal, R., Bajracharya, T.R., Shakya, S.R., Kumal, B., Khanal, K., Williamson, S.J. and Ghale, D.P., "Notice of violation of IEEE publication principles: Computational and experimental investigation of runner for gravitational water vortex power plant", ***Proceedings of IEEE 6th International Conference on Renewable Energy Research and Applications (ICRERA)***, San Diego, CA, USA, (2017), 365-373. (https://doi.org/10.1109/ICRERA.2017.8191087).
11. Kayastha, M., Raut, P., Subedi, N.K. and Ghising, S.T., "CFD evaluation of performance of gravitational water vortex turbine at different runner position", ***Proceedings of KEC Conference***, Kantipur

Engineering College, Dhapakhel Lalitpur, (2019), 17-25. (https://doi.org/10.31224/osf.io/d9qn3).

12. Ullah, R., Cheema, T.A., Saleem, A.S., Ahmad, S.M., Chattha, J.A. and Park, C.W., "Performance analysis of multi-stage gravitational water vortex turbine", ***Energy Conversion and Management***, Vol. 198, (2019), 111788. (https://doi.org/10.1016/j.enconman.2019.111788).
13. Ullah, R., Cheema, T.A., Saleem, A.S., Ahmad, S.M., Chattha, J.A. and Park, C.W., "Preliminary experimental study on multi-stage gravitational water vortex turbine in a conical basin", ***Renewable Energy***, Vol. 145, (2020), 2516-2529. (https://doi.org/10.1016/j.renene.2019.07.128).
14. Wang, Y.K., Jiang, C.B. and Liang, D.F., "Investigation of air-core vortex at hydraulic intakes", ***Journal of Hydrodynamics***, Vol. 22, No. 1, (2010), 673-678. (https://doi.org/10.1016/S1001-6058(10)60017-0).
15. Jahangiri, M., Saghafian, M. and Sadeghi, M.R., "Numerical simulation of hemodynamic parameters of turbulent and pulsatile blood flow in flexible artery with single and double stenoses", ***Journal of Mechanical Science and Technology***, Vol. 29, No. 8, (2015), 3549-3560. (https://doi.org/10.1007/s12206-015-0752-3).
16. Jahangiri, M., Saghafian, M. and Sadeghi, M.R., "Effects of non-Newtonian behavior of blood on wall shear stress in an elastic vessel with simple and consecutive stenosis", ***Biomedical and Pharmacology Journal***, Vol. 8, No. 1, (2015), 123-131. (https://dx.doi.org/10.13005/bpj/590).
17. Jahangiri, M., Haghani, A., Ghaderi, R. and Hosseini Harat, S.M., "Effect of non-Newtonian models on blood flow in artery with different consecutive stenosis", ***ADMT Journal***, Vol. 11, No. 1, (2018), 79-86. (http://admt.iaumajlesi.ac.ir/article_538372.html).
18. Jahangiri, M., Saghafian, M. and Sadeghi, M.R., "Effect of six non-Newtonian viscosity models on hemodynamic parameters of pulsatile blood flow in stenosed artery", ***Journal of Computational & Applied Research in Mechanical Engineering***, Vol. 7, No. 2, (2018), 199-207. (https://dx.doi.org/10.22061/jcarme.2017.1433.1114).
19. Sharifzadeh, B., Kalbasi, R., Jahangiri, M., Toghraie, D. and Karimipour, A., "Computer modeling of pulsatile blood flow in elastic artery using a software program for application in biomedical engineering", ***Computer Methods and Programs in Biomedicine***, Vol. 192, (2020), 105442. (https://doi.org/10.1016/j.cmpb.2020.105442).

Journal of Renewable Energy and Environment

Journal Homepage: www.jree.ir

Materials and Energy Research Center

MERC

Research Article

Sustainability and Environmental Impact of Hydroxy Addition on a Light-Duty Generator Powered with an Ethanol–Gasoline Blend

Padmanabhan Sambandam [a*], Parthasarathy Murugesan [a], Mohamed Iqbal Shajahan [a], Balaguru Sethuraman [b], Hussein Mohamed Abdelmoneam Hussein [c]

[a] School of Mechanical and Construction, Vel Tech Rangarajan Dr. Sagunthala R&D Institute of Science and Technology, Avadi, Chennai, Tamil Nadu, India.
[b] School of Mechanical Engineering, VIT Bhopal University, Madhya Pradesh, India.
[c] Department of Mechanical Engineering, Faculty of Engineering, Helwan University, Cairo, Egypt.

PAPER INFO

Paper history:
Received: 11 August 2021
Revised in revised form: 18 October 2021
Scientific Accepted: 26 November 2021
Published: 08 May 2022

Keywords:
Gasoline Engine,
Light Duty Generator,
Ethanol,
Hydroxy Gas,
Emission Characteristics

ABSTRACT

Environmental sustainability encompasses various problems including climate change, clean air, renewable energy, non-toxic environments, and capacity to live in a healthy community. Many researchers focus their attention on alternative energy sources, such as ethanol and hydroxy gas, to enhance environmental health and quality of life. The introduction of hydroxy gas as a clean source of energy is gaining significant traction. Also, ethanol has a greater octane number than gasoline. Therefore, the ethanol–gasoline blend has a higher octane number than conventional gasoline. A new combination of hydroxy gas, ethanol, and gasoline is environmentally benign while significantly improving the performance of gasoline engines. This paper tested hydroxy gas in a 197-cc gasoline engine power generator powered with ethanol–gasoline blend. The results demonstrated that thermal efficiency increased up to 23.6 % and fuel consumption decreased up to 36 % on a volume basis, which was a significant improvement over the base engine. Furthermore, the hazardous carbon monoxide reduction reached 11.45 % and the unburned hydrocarbon emissions reached 17.6 %.

https://doi.org/10.30501/jree.2021.299136.1241

1. INTRODUCTION

An enormous research opportunity has opened up due to the rapid depletion of fossil resources and the global rise in the pace of crude oil production. To meet the increasing demand for fuel, researchers in the automobile industry, in particular, should seek firm and ecologically friendly alternatives. Urban environmental authorities have raised awareness about the effects of using up to 20 % ethanol blends in current vehicles without changing the engine design. Global warming and climate change are still major issues according to climate scientists. Many studies have shown that the main cause of this man-made disaster is excessive atmospheric gas emissions from industry and automobiles. Incomplete combustion releases toxic hydrocarbons into the air.

The researcher has studied ethanol combustion in an internal combustion engine. The use of high compression hydrous ethanol reforming and supercharging lean-burn conditions was explored to enhance thermal efficiency and performance [1]. The amount of ethanol utilized with gasoline blend increased the emission of Nitrogen Oxide (NOx). Total carbon monoxide (CO) and hydrocarbon emissions were reduced. It was determined that various ethanol–gasoline mix ratios produced different levels of energy efficiency and pollution under varied loading circumstances. The results showed that the emission concentration increased with engine load, but decreased with ethanol content [2]. The effect of ethanol-gasoline blend on power, torque, fuel consumption, and emissions was studied analytically to evaluate steady-state engines [3]. There has been a recent interest in the performance of spark-ignition engines operating on ethanol-gasoline blends with a constant fuel-air ratio [4, 5]. Low ethanol blends under 20 % pointed to a significant effect on engine efficiency or torque.

Hydroxy gas (HHO) is one of the potential energy sources that may be used as a viable alternative fuel to fossil fuels. In some instances, the electrolysis of water may be used to create it. HHO increases the power and thermal efficiency of the engine while simultaneously reducing the formation of hazardous carbon deposits, nitrogen oxides, and hydrocarbons. Hydroxy gas is a blend of hydrogen (H_2) and oxygen (O_2) gases. Theoretically, a ratio of 2:1 hydrogen:oxygen is adequate to attain maximum efficiency while burning [6]. In terms of fuel chemistry, HHO is superior to gasoline with an efficient fuel structure. HHO has two atoms of hydrogen and oxygen per combustion unit, while gasoline has thousands of huge molecules of hydrocarbons. HHO gas improves combustion by improving engine thermal

*Corresponding Author's Email: padmanabhan.ks@gmail.com (P. Sambandam)
URL: https://www.jree.ir/article_149434.html

Please cite this article as: Sambandam, P., Murugesan, P., Iqbal Shajahan, M., Sethuraman, B. and Mohamed Abdelmoneam Hussein, H., "Sustainability and environmental impact of hydroxy addition on a light-duty generator powered with an ethanol–gasoline blend", ***Journal of Renewable Energy and Environment (JREE)***, Vol. 9, No. 2, (2022), 82-92. (https://doi.org/10.30501/jree.2021.299136.1241).

efficiency and decreasing specific fuel consumption. Because hydrogen and oxygen atoms immediately interact, there are no ignition propagation delays owing to surface transit time. A greater velocity flame front shoots through the cylinder wall upon ignition. By boosting reaction rate and flame speed, HHO's heat energy is able to improve combustion efficiency [7]. It is used as a fuel made of hydrogen and oxygen gases. When heated to the auto-ignition temperature at 570 °C at atmospheric pressure with a ratio of 2:1 hydrogen:oxygen, hydroxy gas burns. When ignited, the gas combination turns to water vapor, releasing energy that drives the reaction at 242 kJ per mole of hydrogen. The quantity of heat produced is independent of combustion mode, although flame temperature changes [6]. Many researchers have been developing HHO as a potential engine enhancer for gasoline and diesel engines and other power source applications [8, 9].

Plexiglas-based water-cooled variable compression gasoline-powered four-stroke engine using a potassium hydroxide electrolyte has been investigated for the experiment. The engine test findings indicate that the overall energy consumption decreases while the brake thermal efficiency improves as the flame velocity increases [10]. A simple novel HHO generator was employed to study the impact of adding HHO as an engine performance enhancement additive. The findings found that the thermal efficiency of the engine was improved by 10 %; fuel consumption was decreased by 35 %; and exhaust emissions were reduced nearly 15 % [10]. A single-cylinder engine confirmed that the novel device generated 25 % fuel savings, decreased exhaust temperature, and cut pollutants. A blend of HHO, air, and gasoline effectively decreased pollutant emissions and increased engine efficiency [11]. The unique blend was tested using a series of engine speeds. The emission of nitrogen oxides was cut by almost half. Additionally, the emission of CO was found to be decreased by 20 % and fuel usage was reduced by 25 % [12]. A HHO system that resulted in the overall improvement of 19 % for engine torque, a 14 % reduction in fuel consumption, and a nominal reduction in exhaust emissions [13]. Upon investigating various hydrogen concentrations, researchers have discovered that the CO emission rate did not change regardless of the concentration of hydrogen and that the hydrogen concentration might regulate the particle emission size [14].

Apart from this, HHO gas is added to the gasoline engine and the quantity of gas fluctuates depending on the current supply. Brake thermal efficiency and specific fuel usage were enhanced under HHO [15]. A comprehensive review of hydrogen blended with enhanced natural gas was provided and an experimental study of hydrogen-natural gas was completed [16]. The process of making HHO using variations in current, voltage, temperature, chemical concentration, and reaction time was performed [17]. The study found a 35 % rise in HHO with little electrical energy and also, production rose upon increasing voltage, temperature, and alkaline electrolyte concentration. Because of its better combustion characteristics, hydrogen has been preferred [18].

Furthermore, it was found that biodiesel generated combustion, reduced efficiency, raised carbon dioxide (CO_2) emissions, and caused low combustion. In case of hydrogen-biodiesel, we can see a significant reduction in CO and HC emissions. In a study, 5-25 % HHO in air intake on a single-cylinder SI gasoline engine was evaluated. The findings revealed that when hydroxy levels increased, thermal efficiency and HC emissions also increased. Additionally, the findings revealed that NOx emissions increased as the percentage of HHO increased. The authors calculated the performance of a four-cylinder gasoline engine using an electronically controlled hydrogen injection system. The addition of hydrogen reduced cyclic engine fluctuation, according to the testing findings [19]. Accordingly, the engine performance was evaluated by mixing oxygen-hydrogen (H_2/O_2) with gasoline and liquefied petroleum gas. These experiments were conducted by varying the engine load and emission and performance parameters were evaluated [20]. By using H_2/O_2 mixture in compression, ignition engines reduced fuel consumption and pollutants. The performance test was applied to a constant/test mix using diesel engine. Thermal efficiency was enhanced by 3 %, while CO_2 and H_2O emissions were reduced [21]. The addition of hydrogen to a gasoline methanol engine increased the braking mean effective pressure. The addition of 3 % hydrogen to the fuel source improved both the thermal and volumetric efficiency [22].

The findings indicated that the addition of HHO gas improved brake thermal efficiency by 13 % and reduced brake-specific fuel consumption by 11 %. The HHO gas enrichment reduced CO by 9 % and HC by 21 % while increasing NOx by 6.5 %. The findings demonstrated that the addition of HHO gas raised the lean operating limit of Liquefied Petroleum Gas (LPG) from 1.35 to 1.56 [8]. It was found that the SI engines had lower NOx concentrations, whereas the diesel engines had higher NOx concentrations. While HC concentrations fell by 24 %, CO concentrations rose by 34 %, and NOx remained stable [23]. *Moringa oleifera* biodiesel exhibited a minor increase in brake thermal efficiency owing to the HHO gas. However, adding HHO gas to the mixes reduced the brake specific fuel usage. In terms of emissions, adding biodiesel blends decreased CO, HC, and CO_2 concentrations. No decrease in NOx was seen. However, adding HHO to biodiesel decreased the average NOx by 6 %, which is a significant impact. Overall, HHO enhancing biodiesel blends may replace current fossil fuels due to their better fuel characteristics [24]. The Compressed Natural Gas (CNG) with HHO blend demonstrated superior performance, with a 15 % improvement in average brake power when compared with CNG and yet, with a 15 % reduction when compared with gasoline. CNG-HHO beat gasoline and CNG in terms of emission of HC, CO_2, CO, and brake specific fuel consumption were all reduced by 31 % when compared to gasoline. In comparison to CNG, CNG–HHO generated an average of 13 % more NOx [25].

When the current experimental research on hydrogen supplementation in SI engines is compared with the earlier literatures, many researchers have tried experimental studies for hydrogen supplementation in spark-ignition engines (as shown in Table 1). In general, researchers concentrate on gasoline with hydrogen supplemental experiments in Spark Ignition (SI) and Compression Ignition (CI) engines using LPG, biofuel and alcohol addition for performance improvement.

In India, light-duty power generator engines are still widely used that have high emission. Since renewable energy is not accessible in all locations and seasons in India, certain modifications are required to enhance the combustion rate and thermal efficiency. It is produced from agricultural resources such as sugarcane and maize, making it a viable alternative to gasoline to reduce dependence on fossil fuels and net carbon emissions. It may enhance the performance of a light-duty

gasoline generator engine. Completing the burning of HHO with gasoline minimizes harmful pollutants [33, 34].

The key motivation for concentrating on the SI engine study was to improve the thermal efficiency and minimize the global emission. Accordingly, the present work was carried out on a light-duty power generator engine. Hydroxy gas was regulated at two flow variations of 0.15 kg/hr and 0.25 kg/hr on 10 % ethanol-blended gasoline (E10) fuel. Installation of an electrolyser that continuously supplies hydroxy gas to the engine is simple, effective, and ecologically beneficial.

Table 1. Studies on the effect of HHO addition on SI and CI engines

Authors	Engine	Fuel used	BTE	SFC	CO	HC	NOx
Cakmak et al., 2021 [8]	SI engine	HHO + LPG	12.9 %⇧	11.2 %⇩	8.7 %⇩	21 %⇩	6.42 %⇧
Gatot Setyono et al., 2020 [26]	SI engine	Ethanol + HHO	5 %⇧	6 %⇩	–	–	–
Bahman Najafi et al., 2021 [27]	Diesel engine dual fuel	B20 + HHO	3.2 %⇧	13.5 %⇩	21.2 %⇩	–	13.7 %⇧
Usman et al., 2020 [28]	SI engine @219 cc	HHO + LPG	7 %⇧	15 %⇩	21 %⇩	21.8 %⇩	16.1 %⇧
Shajahan et al., 2020 [29]	SI engine	HHO	22.8 %⇧	36.4 %⇩	10.5 %⇩	24 %⇩	–
Hariharan et al., 2019 [18]	SI engine @ 553 cc	HHO	4.5 %⇧	12 %⇩	48.5 %⇩	47.5 %⇩	20.5 %⇧
Baltacioglu et al., 2019 [30]	Diesel engine @ 219 cc	B10 + E5 + HHO	2.82 %⇧	8.39 %⇩	–	–	8.57 %⇧
Karagoz et al., 2018 [31]	SI engine @1124 cc	H_2/O_2	10.4 %⇧	3.3 %⇩	12.5 %⇩	25 %⇩	23 %⇧
Brayek et al., 2016 [32]	SI engine @ 98 cc	H_2/O_2	–	10.4 %⇩	42 %⇩	20.5 %⇩	20 %⇧
Kassaby et al., 2016 [7]	SI engine @ 1289 cc	HHO	10 %⇧	34 %⇩	18 %⇩	14 %⇩	15 %⇩

The necessary test runs with and without hydroxy gas were conducted under four different load conditions from zero to full load to ensure the optimum performance and lowest pollutant emissions. The objective of the present work is to: (1) study the impact of hydroxy gas on the improvement of performance parameters in small generator SI engine powered with ethanol gasoline blend; (2) investigate the engine performance and emission characteristics adoption with hydroxy gas and choose an optimized injection rate of hydroxy gas to enhance the thermal efficiency and minimize the HC and CO emission.

2. EXPERIMENTAL DETAILS

2.1. Hydroxy gas production

Hydrogen is the most reliable alternative due to the current worldwide lack of energy. The practicality of electrolysis lies in the production of hydrogen. HHO is still widely recognized in vehicles that use water as fuel. Despite the tremendous amount of energy required to decompose water molecules, several controversial ideas persist about HHO fuel or fuel additives. In this research, HHO was generated by electrolysis of water utilizing titanium electrodes as both cathode and anode. Sodium sulfate was employed as an electrolyte in an electrolytic cell, and it decomposed water with the liberation of heat. Heat control techniques were sufficient. The electrolysis process also liberated energy. The pulse width modulation technique for HHO production was invented and produced by Baltacıoglu (2019) [30]. In this procedure, the hydroxy output is regulated under the operating requirements of internal combustion engines. A 12-volt, 14-amp battery was employed to provide current to the anode, which was subsequently transferred to the cathode through the electrolyte. The electrolytic glass chamber contained everything required to handle the ingredients and HHO delivery and production. The properties of base fuel gasoline, ethanol, and HHO are tabulated in Table 2.

Table 2. Properties of gasoline, ethanol, and hydroxy gas

Properties	Ethanol	Gasoline	Hydroxy gas
Chemical formula	C_2H_5OH	C_8H_{18}	HHO
Density at 20 °C (kg/m^3)	789	765	600
Molecular weight (g/mole)	46.07	114.18	17.01
Stoichiometric air-to-fuel ratio	8.94	14.49	34
Autoignition temperature (°C)	363	257	585
Net heating value (MJ/kg)	26.8	44	55
Octane number (research)	111	92	130
Oxygen content wt. %	35	0	33

A hydroxy generator generated HHO when installed in the engine without any modifications to the engine assembly. Electrolysis of different molar concentrations of aqueous catalyst was employed to generate much of the gas generated. Sodium hydroxide (NaOH) aqueous solutions were utilized as electrolytes in this research. Further separating the anode and cathode electrodes is done by a semipermeable membrane which is immersed in the electrolyte. The primary chemical component is a catalyst composed of sodium hydroxide, often referred to as caustic soda. It is a salt composed of sodium and hydroxide ions. In the creation of hydrogen, the use of sodium hydroxide leads to high hydrogen generation rates and

reduced operating temperatures. The positively charged anodes were successful in decomposing the water molecules contained in the electrolyte, allowing for the release of oxygen and hydrogen gases over the top surface of the reactor's upper surface. Although the simple mixing of HHO and hydrogen had little effect on lowering fuel consumption, the mixture had a significant impact on improving the competency of the fuel. Although the HHO composition of 1/3 volume percent and 2/3 volume percent hydrogen with an octane rating of 130 has reduced in recent years, it still provides adequate performance in engines that run on gaseous fuels or gasoline. Greater fuel combustion translates into less waste being released into the environment. It is then necessary to supply the combustion chamber with the hydroxy gas produced [35].

2.2. Engine setup

The engine utilized in the test was built according to the specifications (Table 3). It was decided to conduct this investigation using a spark-ignition engine at a compression ratio of 4.5:1 and a peak output of 3 kW at an engine speed of 3600 rpm, as a single-cylinder, four-stroke air-cooled engine. After injecting the controlled volume of hydroxy gas into the air intake manifold and mixing it with gasoline and air, the engine was ready to go. It is the primary job of hydrogen to enrich the reaction and that of oxygen to support the process of oxygen to enrich the reaction.

Table 3. Experimental engine specification

Parameter	Description
Engine type	Four-stroke, single-cylinder
Power	3 kW @ 3600 rpm
Fuel	Gasoline and kerosene
Displacement	197 cc
Bore and stroke	67 × 56 mm
Compression ratio	4.5:1
Cooling system	Air-cooled engine
Load type	Mechanical type

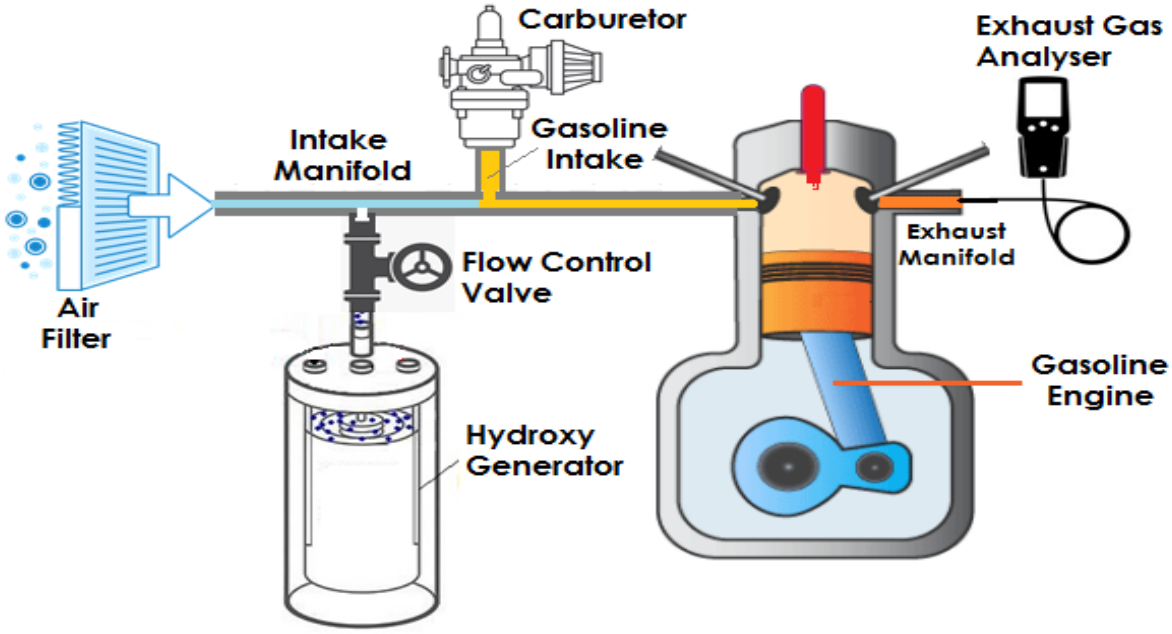

(a) Schematic diagram of the experimental setup

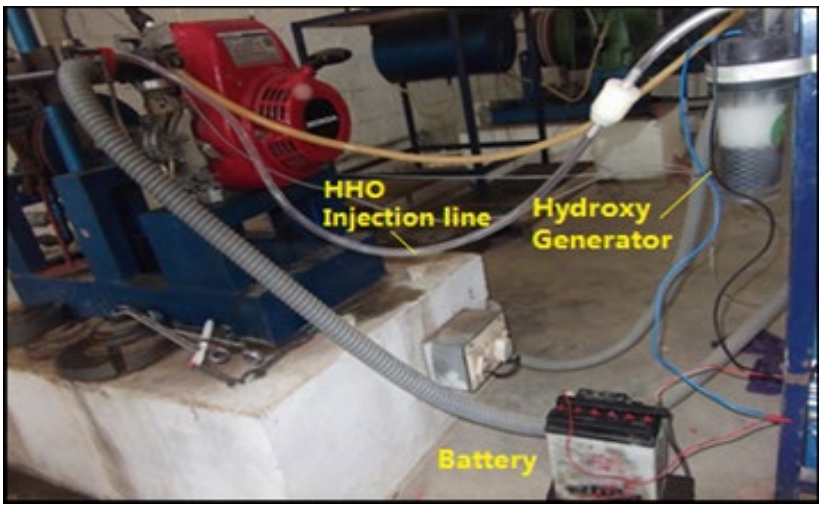

(b) Experimental engine setup with Hydroxy gas

(c) Experimental engine setup with loading setup

Figure 1. Experimental setup

A single-cylinder four-stroke air-cooled, spark-ignition engine with an incremental load was used in this study to examine the ethanol blend and HHO performance and emission characteristics. The incremental load was changed by mechanical loading. A schematic diagram of the use of hydroxy gas in a light-duty power generator engine is shown in Figure 1 (a) and gasoline engine experimental setup is shown in Figure 1 (b) and (c). The engine was first started using gasoline and was, then, subjected to a series of tests until steady-state operating conditions were achieved. Thermal efficiency, specific fuel consumption, HC, CO, and oxygen emissions were measured. The test runs were carried out according to the weight of the load. Similar procedures were used when using ethanol-blended gasoline with HHO enrichment. The HHO was tested for two different contributions of 0.15 kg/hr and 0.25 kg/hr. At the time of the experiment, the atmospheric pressure was 1.013 bar and the temperature was approximately 30 °C. To achieve greater precision, all possible measurable parameters were gathered in each trial and the mean values were calculated.

2.3. Experimental analysis

The experiment was performed in the single cylinder gasoline engine specified in Table 3. The thermal efficiency and specific fuel consumption were analyzed using the following equations:

Thermal efficiency = (Indicated power / Head supplied) × 100

Indicated power = Friction power + Brake power

Brake power = (2π NT) / 60

Torque = Weight × Radius

Head supplied = Fuel consumption × Calorific value

Fuel consumption = (Q*10-6 / t) × Density

Specific fuel consumption = Total fuel consumption / Brake power

where N is the speed of the engine in rpm, T is torque (Nm), Weight is used for loading on the engine (kg), Radius is radius of drum used for loading (m), Q is sample fuel consumption measured as 10 ml, and t is the time taken for fuel consumption (sec).

On the analysis of emission measurement, Crypton 680 series Analyser was used for this research. It is a fully microprocessor-controlled exhaust gas analyzer employing Non-Dispersive Infra-Red (NDIR) Techniques. The unit measures carbon monoxide, carbon dioxide, and hydrocarbons. A further channel is provided employing electrochemical measurement of oxygen and chemical sensor used for nitrogen oxides. It has a response time of 11 seconds to 95 % of final reading under the Operating Pressure of 750-1100 bar. It operates at a minimum flow rate of 5 litres/min. The technical details of Crypton 680 emission analyzer are tabulated in Table 4.

Table 4. Details of emission analyser

Measurement	Range	Accuracy	Resolution	Instrument
CO	0 to 10 %	± 0.03 %	0.01 % vol.	Crypton 680 series analyzer, NDIR technique
HC	0 to 10000 ppm	± 10 ppm	1 ppm vol.	Crypton 680 series analyzer, NDIR technique
Oxygen	0 to 25 %	± 0.10 %	0.01 % vol.	Crypton 680 series analyzer, Electrochemical measurement
NOx	0 to 5000 ppm	± 25 ppm	1 ppm	Crypton 680 series analyzer, chemical sensor

On the experimentation, the Crypton 680 series Analyzer was connected at the exhaust system and the emission values were observed for different fuel blends in different loading conditions. The percentage of variation for each parameter can be observed in comparison with base gasoline readings.

3. RESULTS AND DISCUSSION

3.1. Impact on thermal efficiency

The maximum thermal efficiency of gasoline engines is about 30 %. This implies that the remaining 70 % of the heat energy

was lost, but it was used to maintain engine temperature and extend the engine span life. Accordingly, half of heat energy was injected into the exhaust gases. The other half of the heat energy was carried out with the cooling unit of the engine through the radiator. Figure 2 depicts the change in thermal efficiency as a function of load, while the blending of HHO results in increased combustion, as previously stated. The thermal efficiency achieved using HHO at full load was raised from 13 % to 23.6 % at two flow variations along with ethanol blend because the flame speed of hydrogen was three times greater than the gasoline and the extensive flammability of hydrogen that scattered throughout the chamber achieved complete combustion. Moreover, hydrogen enables combustion to finish in a shorter amount of time [19].

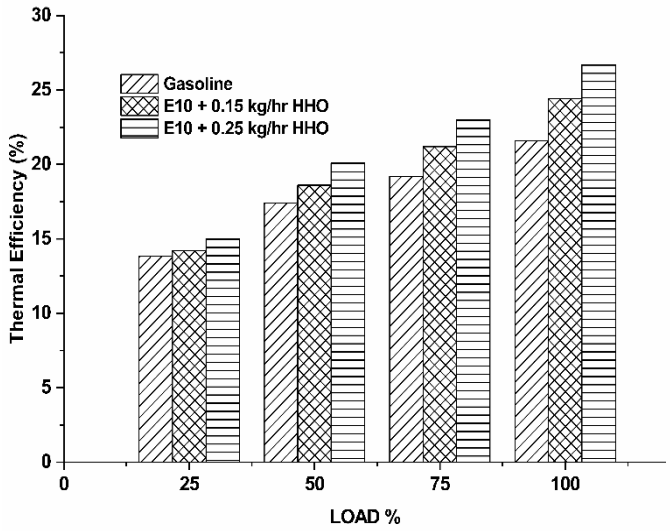

Figure 2. Impact of HHO of thermal efficiency on ethanol-gasoline engine

The cycle exhibits characteristics that are closer to perfect constant volume combustion and an improvement in efficiency. The improved thermal efficiency was recorded by 15 %, 20 %, 23.6 %, and 26.7 % for 0.25 kg/hr HHO injection with ethanol blend in load conditions of 25 %, 50 %, 75 %, and 100 %, respectively. This is due to stratified charges surrounding the spark plug. The remainder of the region is occupied by the lean mixture, resulting in a higher combustion rate than when running an engine test with gasoline alone [21]. Consequently, the characteristics of hydroxy gas lead to complete combustion and high thermal efficiency in large quantities. The enrichment of 0.25 kg/hr HHO was noted to be 19.1 % and 8.6 % higher than conventional fuel and lower than hydroxy gas induction rate. Upon the adoption of HHO, this improvement was noticed by enhanced flame velocity and greater air utilization, which resulted in better power output of the engine. In contrast, the combustion efficiency of the engine operating without HHO under various load conditions declined [30]. Moreover, the thermal efficiency of ethanol blend gasoline was lower than that of gasoline and HHO enrichment because ethanol had a lower stoichiometric ratio than gasoline, which enabled greater fuel mass to be burned with the same quantity of air [26].

3.2. Impact on brake specific fuel consumption

Figure 3 shows the impacts of the induction of HHO into ethanol mixed gasoline on brake specific fuel consumption under four different loads conditions. From the result, it was found that specific fuel consumption in the initial load condition was higher for all test fuel. This result was responsible for high friction power and inferior combustion in the initial load condition. Similar to a previous related work, the higher fuel consumption than other load results from the HHO generator's partial power absorption being more significant than that of the other loads [31]. The result was noted that specific fuel consumption (BSFC) of ethanol blend was observed to be higher than other fuel. It could be attributed to lower heating value of ethanol which required a greater amount of fuel to produce the same power output of the engine. The effect of HHO injection on an ethanol blend demonstrated that BSFC increased from 27 % to 36 % as compared to gasoline operated engine.

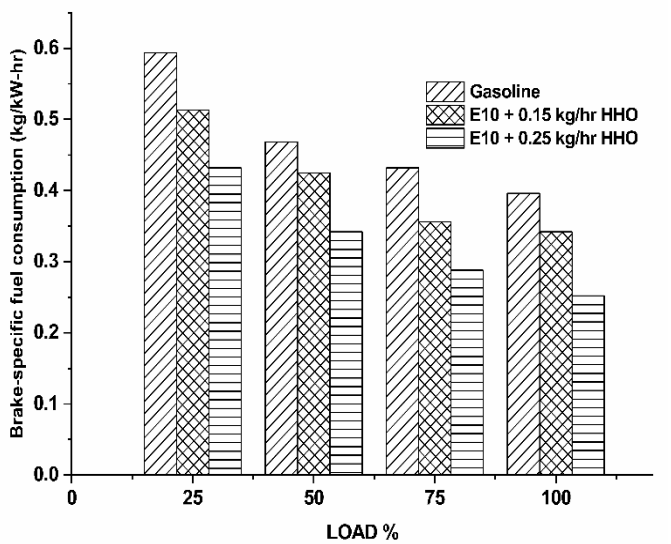

Figure 3. Impact of HHO of brake specific fuel consumption on the ethanol-gasoline engine

The result of BSFC was 0.396, 0.342, and 0.252 kg/kW.hr for gasoline, 0.15 kg/hr and 0.25 kg/hr of HHO injection with ethanol blend, respectively. It was clearly identified that the association of HHO with gasoline minimized the fuel consumption owing to enhanced flame propagation and less flame-quenching zones, which exhibited a better combustion rate [33]. From the results, 0.15 kg/hr HHO addition resulted in decreased fuel consumption between 9.2 % and 17.5 % relative to gasoline in initial and peak load conditions. The least BSFC was noticed for 0.25 kg/hr of HHO addition at peak load owing to better flame speed and enriched energy value of A/F mixture which led to consumption of less fuel quantity to produce the same brake power [22].

3.3. Impact of carbon monoxide emissions

With regard to CO concentrations in the air, they are deficient and restricted, but are primarily used in the formation of a low-level ozone. Figure 4 presents the CO emission rate as a function of different load conditions for gasoline and its ethanol blend with HHO induction. The Air-Fuel (A/F) ratio and combustion efficiency are the prime reason for the formation of CO emission in internal combustion engines. In the engine, a mid-range load condition led to a drop in CO emission. It was mainly due to chemically correct A/F mixture condition that enhanced the combustion rate [2]. CO emissions might have been reduced by adding oxygenated

compounds, which promoted CO combustion in the cylinder or post-combustion processes. It was evident that the inherent O_2 content in the ethanol would lead to a reduction in CO emissions. However, dilution of the fuel may not be the only way to decrease CO emissions. When rising the hydrogen concentration with the ethanol blend, a drastic reduction in CO emission was observed for all load ranges, mainly because the lower C/H ratio in the hydrogen fuel restricts the CO formation [12].

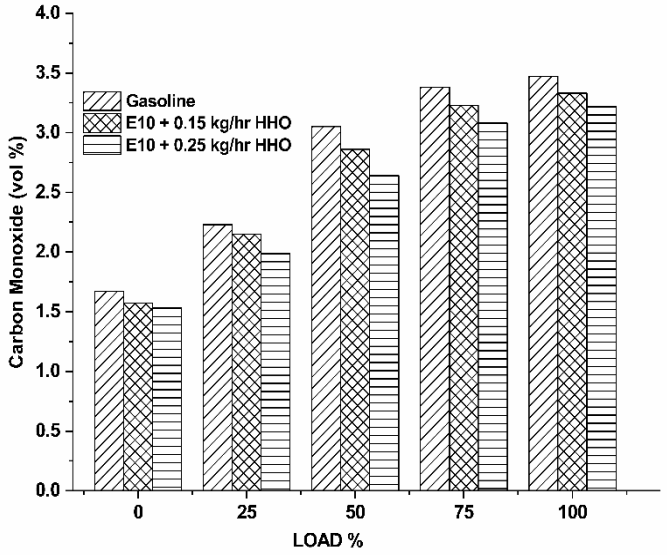

Figure 4. Impact of HHO of carbon monoxide on ethanol-gasoline engine

Improved combustion and lean engine operation caused by the blending of HHO resulted in CO volume percentage reduction rates of 7.2 % to 11.5 % and 3.85 % to 9.2 % for 0.25 kg/hr and 0.15 kg/hr, respectively, as related to gasoline fuel. Moreover, the absence of carbon in HHO substantially reduced CO generation. HHO allows the engine to operate even at a low level of load condition. This result might result from the superior properties of HHO such as wide range of flammability and high flame velocity [15]. High diffusivity of HHO could be easily prepared by the homogenous ethanol blend that leads to a shorter combustion period and promotes the conversion rate of CO_2, thereby reducing CO emission drastically [26].

3.4. Impact on oxygen

Figure 5 exhibits the presence of oxygen content in exhaust gas as a function of engine load for gasoline and its blends with HHO. The leaning action of ethanol also has the additional effect of raising the A/F fuel ratio to a higher value, resulting in the combustion process being closer to stoichiometric conditions and decreasing the oxygen concentration in the exhaust [21]. The test results showed that increase in the engine load causes a reduction in oxygen emissions for all test fuels because of their enhanced combustion rate. The combustion process is expedited under greater engine load circumstances, as seen in the graph. It is possible to infer that the addition of HHO to gasoline resulted in a reduction in the quantity of oxygen produced during the post combustion process [23].

This is mainly due to the high stoichiometric A/F ratio of HHO that utilizes much air during combustion and leads to the insignificant presence of O_2 in exhaust gas. The addition of HHO resulted in complete combustion and lean engine performance and led to a reduction in oxygen concentration from 13.1 vol. % to 7.4 vol. % for 0.15 kg/hr HHO enrichment. Moreover, the rate of adding 0.25 kg/hr HHO enhanced the combustion rate, which led to a substantial increase in heat conversion. It is evident that the amount of oxygen availability in the exhaust for 0.25 kg/hr of HHO addition was 7 %, 22 %, 28 %, and 44 % lower when compared with gasoline in the four load conditions, respectively.

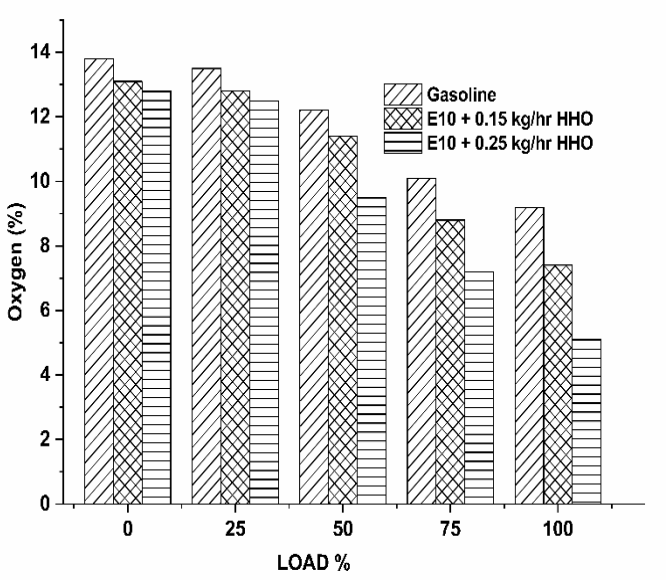

Figure 5. Impact of HHO of oxygen on ethanol-gasoline engine

3.5. Impact on unburned hydrocarbon emissions

The results demonstrated the quantity of unburned hydrocarbons (UBHCs) released into the atmosphere. Figure 6 displays the difference in HC emission with various engine load conditions for gasoline and its blend with enriched hydrogen. It was found that HC emission gradually dropped up to a mid-range load condition and then, it drastically increased due to fuel rich zone which was higher in peak load conditions [31]. Incomplete combustion of fuel is a significant reason for the presence of UBHC in exhaust. UBHC emissions in the exhaust were reduced by 17.6 % at a maximum load and 22 % at a minimum load in the presence of 0.25 kg/hr of HHO when compared with gasoline. HHO with ethanol blend was adopted and it was found that the significant reduction of HC emission was observed for all load conditions. A greater degree of complete combustion and improved engine performance with the addition of HHO influenced lower HC emission formation [34]. Consequently, percentage reduction in UBHC volume ranged between 5 % and 10 % when measured at a volumetric flow rate of 0.15 kg/hr as related to gasoline. It might be due to the enhanced chemical reaction and lack of carbon in the reaction mixture, which led to promotion of the complete oxidation of HC. The result of HC emission from gasoline and 0.15 kg/hr and 0.25 kg/hr of HHO with ethanol bend was 272, 245, and 224 ppm, respectively. The high rate of HHO results in scattered throughput from the cylinder, thereby promoting uniform combustion. Hydrogen reacts within a shorter quenching time than gasoline and results in a reduction in HC emissions. The strong flammability limits of ethanol and the relatively high in-cylinder pressure as well as the temperature generated by

the fast flame velocity and the ethanol blends resulted in a decrease in the volume of HC emissions. Increase in oxygen by blending with ethanol led to complete combustion and, as a consequence, reduced levels of UBHC emissions [36].

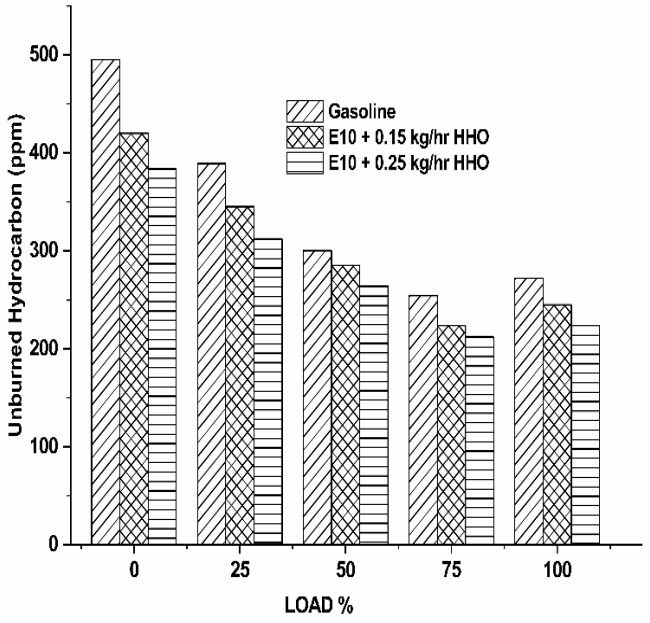

Figure 6. Impact of HHO of UBHC on ethanol-gasoline engine

3.6. Impact on nitrogen oxides emissions

The influence of hydrogen enrichment with ethanol blend on the formation of NOx emission in SI engine is presented in Figure 7. Production of high cylinder temperature during combustion results in NOx formation in the engine; similarly, with a gradual increase in the concentration of HHO, the NOx gradually increased in SI engine. It could be attributed to the higher heat value of hydrogen that dissipates a greater amount of heat during combustion and also aids in the promotion of nitrogen oxidation. In addition, the presence of HHO in the combustion chamber enhanced both the intensity of combustion and the temperature of the combustion chamber and this resulted in increase in the NOx emission [31]. NOx emissions in the exhaust were recorded to be 25 % higher than base gasoline as compared with the presence of 0.25 kg/hr of HHO in the mid-range load condition. However, the rate of increase was 33 % in the maximum load condition at a HHO injection of 0.15 kg/hr on the ethanol-gasoline blend. The primary cause for this was a greater concentration of HHO in the combustion chamber, which increased the temperature of the combustion chamber and resulted in the production of NOx in the process [24]. In the cylinder, the probe's temperature and the excess quantity of oxygen concentration have the most significant effect on the production of NOx emissions. When exposed to high temperatures, the nitrogen chains were eventually decomposed and dissolved. Next, these nitrogen bonds combined with the oxygen molecules in the monotonic form was contained inside the cylinder. The formation of NOx emissions was also influenced by the rate at which nitrogen molecules reacted throughout combustion when the temperature increased beyond a threshold [16].

3.7. Comparison of present investigation with literatures

The current experimental study of ethanol and HHO fuel in the SI engine is compared to the literature, which indicates that many researchers have experimentally investigated HHO supplementary fuel in the engine. Table 5 compares the present study's performance and emissions to those of Hariharan et al., 2019 [18], Usman et al., 2020 [28], and Çakmak et al., 2021 [8].

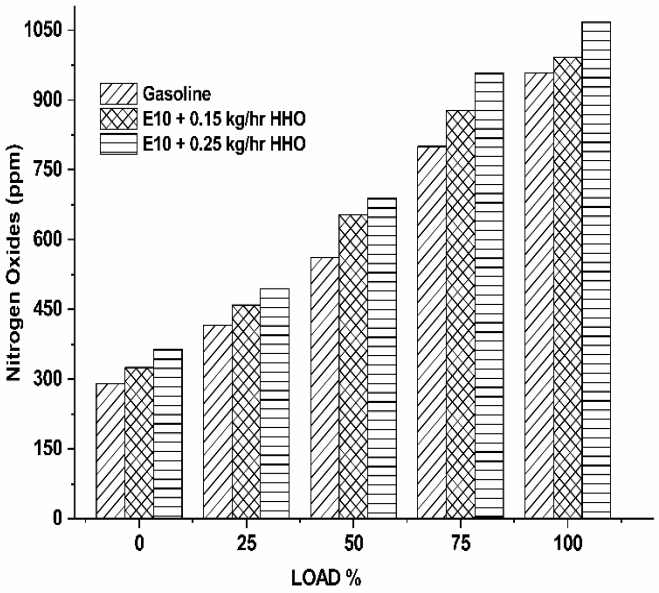

Figure 7. Impact of HHO of nitrogen oxides on the ethanol-gasoline engine

Table 5. Comparison of experimental results of SI engine

Parameters	Hariharan et al., 2019 [18]	Usman et al., 2020 [28]	Çakmak et al., 2021 [8]	Present study
Engine Specification	CI engine, 3.7 kW @ 6000 rpm	SI engine, 219 cc Single cylinder	SI engine Single cylinder	SI engine, 3 kW @ 3600 rpm
Supplementary fuel	HHO	HHO + LPG	HHO + LPG	HHO + E10
Thermal efficiency (%)	4.5 %⇧	7 %⇧	12.9 %⇧	23.6 %⇧
Specific fuel consumption (kg/kW-hr)	12 %⇩	15 %⇩	11.2 %⇩	36 %⇩
CO (%)	48.5 %⇩	21 %⇩	8.7 %⇩	11.5 %⇩
HC (ppm)	47.6 %⇩	-	21 %⇩	22 %⇩
NOx (ppm)	20.5 %⇧	16.1 %⇧	6.42 %⇧	25 %⇧

These experimental studies demonstrated that Brake specific fuel consumption figures might be improved. The current research looked into a greater decrease in specific fuel consumption than previous studies; this is because the engine

capacity is smaller and the combustion conduit is smaller, which enables a wider variety of flames and a quicker combustion rate. The greater thermal efficiency obtained compared to previous studies is due to the hydrogen sharing affecting the pace of combustion. Emissions in all previous investigations, including this experimental study, revealed that harmful compounds such as unburned hydrocarbons and carbon monoxide were significantly reduced. This is because of the increased flame velocity and calorific value induced by hydrogen enrichment. On the other hand, the higher temperature generated by HHO supplemented combustion led to the generation of more nitrogen oxides.

3.8. Environmental impact of HHO on gasoline engine

This study mainly focuses on reducing harmful emissions of CO and HC from a small gasoline power generator. CO harms human health by decreasing the ability of blood to transport oxygen to and from tissues. Furthermore, CO enters the circulation rapidly, converting hemoglobin to carboxyhemoglobin (COHb). Similarly, when CO is found in the lungs, hemoglobin does not reach 100 % oxygen saturation. The American Heart Association reports that COHb values of 10 % cause headaches, 25 % cause nausea and weakness, and 35 % cause coma or death in otherwise healthy people. CO affects human health by impairing the capacity of the blood to carry oxygen to and from the body's tissues. CO is breathed and quickly crosses the lung alveolar epithelium into the bloodstream, where it converts hemoglobin to COHb.

Changes in cognitive functioning, psychological issues, and respiratory system damage are all related to HC exposure. Apart from this, cancer and other general health problems are also linked to HC exposure. There has also been an effort to measure toxicity. One example is benzene, which causes leukemia in humans and is present in gasoline and crude oil. This HC is also known to decrease white blood cell synthesis, suppress the immune system, and increase white blood cell susceptibility to infection. There is evidence that reactive and hydrophobic aromatic compounds such as benzenes, naphthalene, styrene, or xylene isomers that harm seed germination in many plants. Additionally, the phototoxicity of contaminants changes with plant growth stage [33].

The present investigation revealed that HHO on an ethanol mix improved fuel economy and efficiency. The smaller engine capacity and combustion conduit enable a broader spectrum of flames and a faster combustion rate. Because hydrogen sharing influenced the fastness of fuel burning, this research generated higher thermal efficiency. Other studies, such as the current research, showed that pollution emissions such as UBHCs and CO were greatly decreased. This is because hydrogen enrichment increases the flame velocity and calorific value. The greater temperature in hydrogen-added combustion produces more nitrogen. To run this engine with a hydrogen electrolyzer, the values of increased thermal efficiency and reduced pollution emissions have been highlighted.

4. CONCLUSIONS

The fossil fuel industry now supplies a significant portion of the world's energy requirements, particularly in transportation. As a result of the scarcity of fossil fuels and the increasing release of hazardous pollutants into the environment, experts have turned their attention to alternative energy sources such as ethanol and HHO. An experimental investigation was conducted on a light-duty power generator powered by an ethanol-gasoline blend with HHO to improve the engine's performance and reduce harmful emissions. HHO was generated by an electrolysis process and added to the intake manifold at two different flow rates and in 10 % ethanol-blended gasoline. The further advantages include the following:

- With the addition of HHO, the thermal efficiency at the maximum load increased to 13 % and 23.6 % at 0.15 kg/hr and 0.25 kg/hr, respectively, owing to the boost produced by increased hydrogen flame velocity and a more comprehensive range of flames when using HHO.
- The combustion rate of ethanol-gasoline with a mixture of HHO was significantly enhanced. Fuel consumption was remarkably enhanced from 9 % to 36 % on a volume basis in different loading conditions.
- Enhanced and lean engine operation caused by the injection of HHO resulted in the CO volume reduction of 7.2 % to 11.5 % and 3.85 % to 9.2 % at volumes of 0.25 kg/hr and 0.15 kg/hr, respectively. In addition, the oxygen present in the exhaust was considerably reduced by 44 % due to the greater volume of complete combustion.
- The concentration of UBHCs was reduced by 17.6 % at maximum load and by 22 % at minimum load in the presence of 0.25 kg/hr of HHO, owing to the increased chain reaction caused by hydrogen and the absence of carbon in the system.
- NOx emissions were recorded to be 25 % more than base gasoline at minimum load in the presence of 0.25 kg/hr HHO and 33 % high at the maximum load with 0.15 kg/hr of HHO due to an increase in combustion chamber temperature.

In the future, the present study can be protracted in the case of high-speed SI engine to enhance the performance and combustion characteristics using doping of nanoparticle with gasoline. The numerical study may target SI engine fuelled with another alternative energy to increase performance parameters. Furthermore, this research may be enhanced by including exhaust gas recirculation assistance to decrease NO_X emissions and be modified to run in the dual fuel mode.

5. ACKNOWLEDGEMENT

We would like to show our gratitude to our institute Vel Tech Rangarajan Dr. Sagunthala R&D Institute of Science and Technology, Chennai, India for providing space to carry out this research in successful manner.

NOMENCLATURE

BSFC	Brake Specific Fuel Consumption
BTE	Brake Thermal Efficiency
CO_2	Carbon dioxide
CO	Carbon monoxide
COHb	Carboxyhemoglobin
CNG	Compressed Natural Gas
CI	Compression Ignition
E10	10 % Ethanol-blended gasoline
HC	Hydrocarbon

H_2	Hydrogen
HHO	Hydroxy gas
LPG	Liquefied Petroleum Gas
NOx	Nitrogen Oxide
NDIR	Non-Dispersive Infra-Red
O_2	Oxygen
NaOH	Sodium hydroxide
SI	Spark Ignition
UBHC	Unburned Hydrocarbons

REFERENCES

1. Shimada, A., Shirakawa, Y. and Ishikawa, T., "Improved thermal efficiency using hydrous ethanol reforming in advanced spark-ignition engines", ***Proceedings of SAE 2016 International Powertrains, Fuels & Lubricants Meeting***, (2016). (https://doi.org/10.4271/2016-01-2262).
2. Köten, H., Karagöz, Y. and Balcı, Ö., "Effect of different levels of ethanol addition on performance, emission, and combustion characteristics of a gasoline engine", ***Advances in Mechanical Engineering***, Vol. 12, No. 7, (2020), 1-13. (https://doi.org/10.1177/1687814020943356).
3. Tibaquirá, J.E., Huertas, J.I., Ospina, S., Quirama, L.F. and Niño, J.E., "The effect of using ethanol-gasoline blends on the mechanical, energy and environmental performance of in-use vehicles", ***Energies***, Vol. 11, No. 1, (2018), 221. (https://doi.org/10.3390/en11010221).
4. Doğan, B., Derviş, E., Hayri, Y. and Evren, K., "The effect of ethanol-gasoline blends on performance and exhaust emissions of a spark ignition engine through exergy analysis", ***Applied Thermal Engineering***, Vol. 120, (2017), 433-443. (https://doi.org/10.1016/J.APPLTHERMALENG.2017.04.012).
5. Najafi, G., Ghobadian, B., Yusaf, T., Safieddin Ardebili, S.M. and Mamat, R., "Optimization of performance and exhaust emission parameters of a SI (Spark Ignition) engine with gasoline–ethanol blended fuels using response surface methodology", ***Energy***, Vol. 90, Part 2, (2015), 1815-1829. (https://doi.org/10.1016/J.ENERGY.2015.07.004).
6. Najafi, B., Haghighatshoar, F., Ardabili, S., Band, Sh.S., Chau, K.W., and Mosavi, A., "Effects of low-level hydroxy as a gaseous additive on performance and emission characteristics of a dual fuel diesel engine fueled by diesel/biodiesel blends", ***Engineering Applications of Computational Fluid Mechanics***, Vol. 15, No. 1, (2021), 236-250. (https://doi.org/10.1080/19942060.2021.1871960).
7. El-Kassaby, M.M., Eldrainy, Y.A., Khidr, M.E. and Khidr, K.I., "Effect of hydroxy (HHO) gas addition on gasoline engine performance and emissions", ***Alexandria Engineering Journal***, Vol. 55, No. 1, (2016), 243-251. (https://doi.org/10.1016/J.AEJ.2015.10.016).
8. Çakmak, A., Girisen, A.R. and Ozcan, H., "Effects of hydroxy gas addition on the performance and emission characteristics of liquefied petroleum gas-powered lean-operated spark-ignition engine", ***SAE International Journal of Fuels and Lubricants***, Vol. 14, No. 1, (2021), 41-54. (https://doi.org/10.4271/04-14-01-0004).
9. Arjun, T.B., Atul, K.P., Muraleedharan, A.P., Walton, P.A., Bijinraj, P.B. and Raj, A.A., "A review on analysis of HHO gas in IC engines", ***Materials Today: Proceedings***, Vol. 11, Part 3, (2019), 1117-1129. (https://doi.org/10.1016/J.MATPR.2018.12.046).
10. Murali, K.V., Haritha, R.A., Sandeep, K.M. and Raghu, A., "Effect of hydroxy gas addition on performance and exhaust emissions in variable compression spark ignition engine", ***Materials Today: Proceedings***, Vol. 24, Part 2, (2020), 930-936. (https://doi.org/10.1016/J.MATPR.2020.04.404).
11. Badr, M.H., Hassan, M.I. and EL-Hamalawy, A.A., "An on-demand hydrogen cell for automobile fuel consumption efficiency", ***International Journal of Green Energy***, Vol. 12, No. 11, (2015), 1086-1090. (https://doi.org/10.1080/15435075.2014.890105).
12. Musmar, S.A. and Al-Rousan., A.A, "Effect of HHO gas on combustion emissions in gasoline engines", ***Fuel***, Vol. 90, No. 10, (2011), 3066-3070. (https://doi.org/10.1016/J.FUEL.2011.05.013).
13. Yilmaz, A.C., Uludamar, E. and Aydin, K., "Effect of hydroxy (HHO) gas addition on performance and exhaust emissions in compression ignition engines", ***International Journal of Hydrogen Energy***, Vol. 35, No. 20, (2010), 11366-11372. (https://doi.org/10.1016/J.IJHYDENE.2010.07.040).
14. Wang, S., Ji, C., Zhang, B. and Liu, X., "Performance of a hydroxygen-blended gasoline engine at different hydrogen volume fractions in the hydroxygen", ***International Journal of Hydrogen Energy***, Vol. 37, No. 17, (2012), 13209-13218. (https://doi.org/10.1016/J.IJHYDENE.2012.03.072).
15. Patil, N.N., Chavan, C.B., More, A.S. and Baskar, P., "Generation of oxy-hydrogen gas and its effect on performance of spark ignition engine", ***IOP Conference Series: Materials Science and Engineering***, Vol. 263, No. 6, (2017). (https://doi.org/10.1088/1757-899X/263/6/062036).
16. Nanthagopal, K., Subbarao, R., Elango, T., Baskar, P. and Annamalai, K., "Hydrogen enriched compressed natural gas - A futuristic fuel for internal combustion engines", ***Thermal Science***, Vol. 15, No. 4, (2011), 1145-1154. (https://doi.org/10.2298/TSCI100730044N).
17. Alam, N. and Pandey, K.M., "Experimental study of hydroxy gas (HHO) production with variation in current, voltage and electrolyte concentration", ***IOP Conference Series: Materials Science and Engineering***, Vol. 225, No. 1, (2017). (https://iopscience.iop.org/article/10.1088/1757-899X/225/1/012197/meta).
18. Hariharan, N., Senthil, V., Karthic, S.V. and Krishnamoorthi, M., "Influence of hydrogen enrichment on the combustion, efficiency and emissions of dual fuel engine", ***Energy Sources, Part A: Recovery, Utilization, and Environmental Effects***, (2019), 1-18. (https://doi.org/10.1080/15567036.2019.1675816).
19. Shivaprasad, K.V., Raviteja, S., Chitragar, P. and Kumar, G.N., "Experimental investigation of the effect of hydrogen addition on combustion performance and emissions characteristics of a spark ignition high speed gasoline engine", ***Procedia Technology***, Vol. 14, (2014), 141-148. (https://doi.org/10.1016/J.PROTCY.2014.08.019).
20. Rajasekaran, T., Duraiswamy, K., Bharathiraja, M. and Poovaragavan., S., "Characteristics of engine at various speed conditions by mixing of HHO with gasoline and LPG", ***ARPN Journal of Engineering and Applied Sciences***, Vol. 10, No. 1, (2015), 46-51. (https://citeseerx.ist.psu.edu/viewdoc/download?doi=10.1.1.1086.1341&rep=rep1&type=pdf).
21. Bari, S. and Mohammad, E.M., "Effect of H_2/O_2 addition in increasing the thermal efficiency of a diesel engine", ***Fuel***, Vol. 89, No. 2, (2010), 378-383. (https://doi.org/10.1016/J.FUEL.2009.08.030).
22. Ji, C., Zhang, B. and Wang, S., "Enhancing the performance of a spark-ignition methanol engine with hydrogen addition", ***International Journal of Hydrogen Energy***, Vol. 38, No. 18, (2013), 7490-7498. (https://doi.org/10.1016/J.IJHYDENE.2013.04.001).
23. Jakliński, P. and Czarnigowski, J., "An experimental investigation of the impact of added HHO gas on automotive emissions under idle conditions", ***International Journal of Hydrogen Energy***, Vol. 45, No. 23, (2020), 13119-13128. (https://doi.org/10.1016/J.IJHYDENE.2020.02.225).
24. Kanimozhi, B., Kumar, G., Alsehli, M., Elfasakhany, A., Veeman, D., Balaji, S., Thiran, T., Praveen K.T.R. and Sekar, M., "Effects of oxyhydrogen on the CI engine fueled with the biodiesel blends: A performance, combustion and emission characteristics study", ***International Journal of Hydrogen Energy***, (2021). (https://doi.org/10.1016/J.IJHYDENE.2021.08.054).
25. Usman, M., Hayat, N. and Bhutta, M.M.A., "SI engine fueled with gasoline, CNG and CNG-HHO blend: comparative evaluation of performance, emission and lubrication oil deterioration", ***Journal of Thermal Science***, Vol. 30, No. 4, (2021), 1199-1211. (https://doi.org/10.1007/s11630-020-1268-4).
26. Setyono, G., Anas, A.A. and Lillahulhaq, Z., "Hydroxy gas (HHO) supplement of ethanol fuel mixture in a single-cylinder spark-ignition matic-engine", ***Journal of Mechanical Engineering and Mechatronics***, Vol. 5, No. 2, (2020), 114-121. (https://doi.org/10.33021/jmem.v5i2.1136).
27. Thangavel, V., Momula, S.Y., Gosala, D.B. and Asvathanarayanan, R., "Experimental studies on simultaneous injection of ethanol–gasoline and n-butanol–gasoline in the intake port of a four stroke SI Engine", ***Renewable Energy***, Vol. 91, (2016), 347-360. (https://doi.org/10.1016/J.RENENE.2016.01.074).
28. Usman, M., Farooq, M., Naqvi, M., Saleem, M.W., Hussain, J., Naqvi, S.R., Jahangir, S., Jazim, U.H.M., Idrees, S. and Anukam, A., "Use of gasoline, LPG and LPG-HHO blend in SI engine: A comparative performance for emission control and sustainable environment", ***Processes***, Vol. 8, No. 1, (2020). (https://doi.org/10.3390/pr8010074).

29. Shajahan, M.I., Sambandam, P., Michael, J.J. and Abdelmoneam, H.H.M., "Environmental impact of oxyhydrogen addition on high-speed gasoline engine characteristics", ***Energy Sources, Part A: Recovery, Utilization, and Environmental Effects***, (2020), 1-14. (https://doi.org/10.1080/15567036.2020.1812768).

30. Baltacioglu, M.K., Kenanoglu, R. and Aydın, K., "HHO enrichment of bio-diesohol fuel blends in a single cylinder diesel engine", ***International Journal of Hydrogen Energy***, Vol. 44, No. 34, (2019), 18993-18994. (https://doi.org/10.1016/J.IJHYDENE.2019.02.060).

31. Karagöz, Y., Balcı, Ö., Orak, E. and Habib, M.S., "Effect of hydrogen addition using on-board alkaline electrolyser on SI engine emissions and combustion", ***International Journal of Hydrogen Energy***, Vol. 43, No. 24, (2018), 11275-11285. (https://doi.org/10.1016/J.IJHYDENE.2018.04.235).

32. Brayek, M., Jemni, M.A., Kantchev, G. and Abid, M.S., "Effect of hydrogen–oxygen mixture addition on exhaust emissions and performance of a spark ignition engine", ***Arabian Journal for Science and Engineering***, Vol. 41, No. 11, (2016), 4635-4642. (https://doi.org/10.1007/s13369-016-2228-x).

33. Kazim, A.H., Khan, M.B., Nazir, R., Shabbir, A., Abbasi, M.S., Abdul Rab, H., Shahid, Q.N., "Effects of oxyhydrogen gas induction on the performance of a small-capacity diesel engine", ***Science Progress***, Vol. 103, No. 2, (2020). (https://doi.org/10.1177/0036850420921685).

34. Lin, W.Y., Chang, Y.Y. and Hsieh, Y.R., "Effect of ethanol-gasoline blends on small engine generator energy efficiency and exhaust emission", ***Journal of the Air & Waste Management Association***, Vol. 60, No. 2, (2010), 142-148. (https://doi.org/10.3155/1047-3289.60.2.142).

35. Baltacıoğlu, M.K., "A novel application of pulse width modulation technique on hydroxy gas production", ***International Journal of Hydrogen Energy***, Vol. 44, No. 20, (2019), 9726-9734. (https://doi.org/10.1016/J.IJHYDENE.2018.10.228).

36. Guillin-Estrada, W., Maestre-Cambronel, D., Bula-Silvera, A., Gonzalez-Quiroga, A. and Duarte-Forero, J., "Combustion and performance evaluation of a spark ignition engine operating with acetone–butanol–ethanol and hydroxy", ***Applied Sciences***, Vol. 11, No. 11, (2021). (https://doi.org/10.3390/app11115282).

JREE: Vol. 9, No. 2, (Spring 2022) 93-106

Journal of Renewable Energy and Environment

Journal Homepage: www.jree.ir

Materials and Energy Research Center

MERC

Technical Note

Policy Model of Renewable Energy Development in Iran's Agriculture Sector

Somayeh Dehhaghi [a], Shahla Choobchian [a*], Barat Ghobadian [b], Homayon Farhadian [a]

[a] *Department of Agricultural Extension and Education, University of Tarbiat Modares (TMU), P. O. Box: 14115-336, Tehran, Tehran, Iran.*
[b] *Department of Mechanics of Biosystems Engineering, University of Tarbiat Modares, P. O. Box: 14115-336, Tehran, Tehran, Iran.*

PAPER INFO

Paper history:
Received: 18 October 2021
Revised in revised form: 11 January 2022
Scientific Accepted: 25 December 2021
Published: 10 May 2022

Keywords:
Renewable Energy,
Policymaking,
Policymaking Mode,
Energy Policy,
Agriculture

ABSTRACT

The purpose of this study is to present a renewable energy policy model in the agricultural sector of Iran. To achieve this goal, a questionnaire consisting of 57 items was designed. The reliability of the questionnaire was confirmed by Cronbach's alpha (0.916). Also, to analyze the validity and reliability of the research tool, the Average Variance Extracted (AVE) and Composite Reliability (CR) were calculated. The validity of the questionnaire was determined using face validity, Content Validity Ratio (CVR), and Content Validity Index (CVI). The statistical population of the study consists of energy policymaking experts who were estimated at about 80 people. The sampling method was random and 70 samples answered the questionnaire using the Krejcie and Morgan table. Using structural equation modeling and the maximum likelihood method and using LISREL software, the model fit was estimated at a favorable level. Based on the findings, it was found that the priorities of the agricultural sector and the needs of this sector had not been considered in renewable energy policymaking. Policymaking is done top-down and stakeholders are not considered. Renewable equipment market policies are not adequate and the market is not properly managed. Interaction between policymaking institutions is not in good shape. The results of this study can help address the various shortcomings of the renewable energy policy as well as reduce the common inconsistencies in this area. Finally, suggestions were made for the development and promotion of policies in the field of renewable energy in the agricultural sector of Iran.

https://doi.org/10.30501/jree.2022.311064.1273

1. INTRODUCTION

In today's world, non-renewable energy sources are running low. Moreover, the price of this type of resource in global markets fluctuates quite a lot. The limited resources of fossil fuels and the problems caused by the emission of greenhouse gases have made it necessary to pay much more attention to renewable energy.

Ensuring a secure and sustainable supply of energy at all times has encouraged countries to adopt the best and most appropriate policies. Energy policy is a very important issue that can restore the true identity of energy. In energy policymaking, governments seek to solve problems and the national energy policy underlies the formulation and implementation of a set of measures to oversee energy sector activities. Developing the right policy ensures the confidence of investors and encourages them to participate [1].

The path of renewable development is difficult without government support. Governments are implementing supportive policy packages for the development of renewable energy. The favorable policy package takes into account the current state of the global market and adaptation to changing barriers. As mentioned, these policies need to take into account changes in technology and its market position on a global scale. In other words, a country that uses renewable energy needs to constantly adapt its policymaking tools. Putting the right action package at the right time is the key to the successful use of renewables [2]. Therefore, policymaking must move to support investment in renewable energy on a larger and more integrated scale [3]. In the meantime, special attention should be paid to the agricultural sector, because agriculture plays a key role both in the discussion of food security and of economic development. One of the challenges facing sustainable agriculture is that most farms still rely on fossil fuels. Energy consumption in the domain of agriculture is a global concern [4] because CO_2 emissions from fossil fuels, which are used as the main source of energy, have increased rapidly [4, 5]. Agriculture plays an important role in global warming through greenhouse gases due to activities such as tillage operations, methane emissions from livestock, etc. [6]. On the other hand, the cost of agricultural production depends on the price of fuel [7]. Therefore, reducing the share of fossil fuels and increasing the share of biofuels are two of the most important future goals in this sector. Renewable resources in agriculture are a good alternative to conventional fuels which can ensure energy security and at the same time, they have the least destructive effect on the environment [5,

*Corresponding Author's Email: shchoobchian@modares.ac.ir (S. Choobchian)
URL: https://www.jree.ir/article_149614.html

Please cite this article as: Dehhaghi, S., Choobchian, Sh., Ghobadian, B. and Farhadian, H., "Policy model of renewable energy development in Iran's agriculture sector", ***Journal of Renewable Energy and Environment (JREE)***, Vol. 9, No. 2, (2022), 93-106. (https://doi.org/10.30501/jree.2022.311064.1273).

8]. For this reason, investment in this type of energy is increasing worldwide [9].

Currently, the share of renewable energy in Iran's energy portfolio is very small [8, 9]. One of the reasons for the failure to use renewable energy is inefficient policies. A review of renewable energy policies in Iran reveals that there have been repeated challenges in adopting and implementing the necessary policies.

A look into global experience shows that the agricultural sector is still supported by governments; however, in most countries, the structure of support has shifted to environmentally friendly support and the support that increases the efficiency and productivity of the agricultural sector. There are many successful experiences and innovations in this field. However, it requires a reform of protectionist policies. In order to adopt the right policy, it is necessary to know all aspects of the main issue. It is also necessary to identify the needs of the agricultural community correctly and with the least deviation in this field.

Due to the unscientific nature of energy policies in Iran, there are problems such as organizational interference and overlap, managerial interference, lack of cooperation between responsible institutions and organizations, inattentiveness to differences in the needs and potentials of different regions, and lack of evaluation of renewable energy policymaking. One of the reasons for the failure in the development of renewable energy is the lack of a coherent and complete policymaking framework and model in the field of renewable energy [10], which also affects the agricultural sector. Unfortunately, in Iran, there is no regular policymaking cycle and the policymaking model is not used to better manage the renewable energy policymaking process. Systematic scientific knowledge of the disadvantages of planning and policy-making structure in the country's renewable energy sector, compliance of existing policies with the needs of renewable energy development in the agricultural sector, correction of the existing incomplete cycle, designing of a policymaking model appropriate to Iran's agricultural conditions are necessary. Providing a model that is compatible with Iran's conditions can facilitate the process of policymaking and achieving energy goals in Iran, especially in the agricultural sector. Studies show that unfortunately, enough research has not been done in this area and the field of renewable energy is suffering severe information weakness in the field of policy conditions. The novelty of this study shows its significance. Analysis of renewable energy policies is a necessity that is felt in this area because to improve or eliminate problems, it is necessary to fully identify the shortcomings and weaknesses. Despite the great significance of renewable energy in the agricultural sector, it has not yet received much attention and energy policies in this sector have not been analyzed as necessary. This study seeks to answer these questions: 1-What are the weaknesses in Iran's renewable energy policies in the agricultural sector? 2-What is the current state of renewable energy policies in Iran's agricultural sector? 3-What policies should be revised and reformed? In this regard, this study is a pioneer and tries to examine the status of renewable energy policies by using the structural equation modeling method and to identify and examine weaknesses. The purpose of this research is to design an appropriate policy model for the development of renewable energy in the agricultural sector. This research helps to identify weaknesses and shortcomings in the development of renewable energy and because of its uniqueness in this field can help managers and policymakers to identify shortcomings and in order to take steps to fix these problems. The results of this study can be used in countries with similar conditions to Iran. In order to achieve the mentioned goals, the following studies and literature are studied and policymaking models are reviewed to design the default model. Then, the research methodology is explained and in the next section, the research model is presented. Finally, suggestions are provided to solve the existing problems.

2. THEORETICAL FRAMEWORK

2.1. Agriculture and renewable energy

For decades, developed and developing countries have been using fossil fuels extensively to promote their goals in all economic sectors such as manufacturing, tourism, transportation, and agriculture. This led to the emission of carbon dioxide in almost all parts of the world.

In fact, the use of fossil fuel farm equipment, water pumping for irrigation, animal husbandry, and use of nitrogen-rich fertilizers have all contributed significantly to greenhouse gas emissions from agriculture. Also, a strong relationship between energy consumption and agricultural productivity has been proven; for this reason, politicians support the use of energy in agriculture [11].

As GDP increases, so does diesel and electricity consumption in the long run. In this regard, researchers recommend that governments should improve infrastructure and provide subsidies for rural and agricultural electricity to increase agricultural production [12]. However, Sabri and Obaid believe that if proper management in the field of energy is not done, energy can also act as a limiting factor for agriculture and shock it [12]. However, the Food and Agriculture Organization of the United Nations believes that the agricultural sector has significant potential to reduce greenhouse gas emissions. In fact, many agricultural activities, such as irrigation, can be sourced from renewable energy sources [19]. Therefore, renewable energy can be a good solution [17, 18] and plays an important role in improving agricultural production [13, 14]. They also can help to reduce emissions [15]. Therefore, reducing the share of fossil fuels and increasing the share of biofuels is one of the most important future goals in this sector. The development of renewables, especially biofuels, in addition to reducing global warming, is effective in creating employment and encouraging the agricultural sector [16, 17]. Subsidy policies and tax concessions facilitate the rapid expansion of renewable energy in agriculture. Items such as setting guaranteed rates minimize the investment risk and make the investor more confident [23]. Appropriate policies are the main driver of investment in the renewable sector. In this regard, many policies such as feed in tariffs, insurance tariffs, financial incentives, etc. are implemented in the world and are very diverse, but the most important and most widely adopted policy is feed in tariffs [24-26].

The development of renewables, especially biofuels, in addition to reducing global warming, is effective in creating employment and encouraging the agricultural sector [16, 17]. Biomass energy has great potential to meet the challenges of rural development and environmental damage. Biomass, like agricultural residues, has a high potential for energy production. After oil, natural gas, and coal, biomass is one of the most important energy sources worldwide [18-20].

Agricultural residues are a potential source of energy that can be used in the energy production process [21].

Iran has many agricultural products and wastes that can be used to produce biofuels. Biomass resources from agricultural waste, including fruits, can be used to generate energy and renewable resources [9]. According to the production capacity of agricultural products in 2018, from the residues of oilseeds and products, approximately 4.8 billion liters of bioethanol and about 526 thousand tons of biodiesel could be obtained [22]. Nonetheless, the share of biofuels in Iran is very small [23]. So far in Iran, biofuels remain at the level of research and development. There is no suitable market for this type of fuel. The lack of appropriate supportive policies in this area is one of the reasons [21].

2.2. Renewable energy policy

Global warming is a serious problem for the global environment [24]. Rising temperatures affect agricultural productivity [25], human health [26, 27], infrastructure, and many other aspects of society. In this regard, policy-making and modeling for the energy system play a key role in the development of a sustainable energy system. Different energy models are useful tools for identifying changes in the implementation of different policies. Policymakers always need to be equipped with up-to-date information, meaningful figures, and analysis of the impact of the adopted policy. Renewable energy policies will be crucial to achieving the goals of energy policy and other benefits of renewable energy such as reducing climate change and air pollution, improving energy security, and increasing access to energy. Because a development that relies on the use of non-renewable resources affects the well-being of future generations in terms of resource depletion, environmental impacts, and unsustainable development [28]. A proper understanding of the complex interactions between the factors affecting the development of renewable energy is essential to designing appropriate economic, environmental, and energy policies and achieving goals in this field [29]. Today, renewable energy policies are prescribed as a pillar of energy security and sustainable development in all countries. Countries rich in fossil fuels and oil exporters are usually less inclined to use renewable energy [30]. Designing and evaluating renewable energy policies is difficult because policymakers and decision-makers must consider several aspects [31]. They need to evaluate the impact of their strategies and policies [32].

Many studies have been conducted in the field of renewable energy policies, and most of them have concluded that existing policies need to be reformed and revised. Radmehrder et al. (2021) concluded that policymakers should increase their support for universities and research centers so as to reduce the cost of producing energy from renewable sources. Radmehr's findings also show that policies that increase the cost of using fossil fuels must be adopted [29]. The study by Ghorashi (2021) and Maranlou demonstrated that the power purchase agreement and feed-in-tariff had positive effects on the renewable energy market in Iran [33]. The study of Norouzi et al. (2021) demonstrated that the level of achievement of the goals stated in the renewable energy policies in Iran remains generally low. The multiplicity of documents and institutions involved in RE, lack of operational plans, and lack of optimal use of private sector capacity are the main weaknesses. They further conclude that Iran can take an effective step in the development of renewables if the conditions for private sector participation be more favorable and appropriate operational and practical plans be considered. Finally, they suggest that the adoption of a comprehensive and integrated RE policy, as well as the centralization of RE management in a small number of institutions, represent an important factor in facilitating the success of renewable energy in Iran [34].

The results obtained by Arizen et al. identified weaknesses in renewable energy policies. This study illustrated that the carbon tax was not high enough to act as an incentive to invest in renewable technologies. To make renewable energy competitive in the electricity market, public support is essential through public subsidies through carbon taxes. Technology-driven policies are more appropriate than demand-driven policies [35].

A study conducted in ASEAN countries also pointed to policymaking weakness. This study concluded that policy of ASEAN countries is to increase the share of biofuels in the energy basket to reduce dependence on oil imports and climate change is not their priority. Malaysia and the Philippines, although having national biofuels policies and biofuels law, respectively, have weak policies on biofuels development [36].

Banse and colleagues also conducted research on renewable energy policies in the agricultural sector. The results of this study make it clear that without a combination of laws or subsidies to stimulate the use of biofuels, the goals of the EU Biofuels Directive will not be achieved. By combining the rules, the increased demand for biofuel products has a severe impact on agriculture globally and in Europe. Excess demand from the energy sector may slow or reverse the long-term trend of declining agricultural prices. Providing subsidies is essential to stimulating the production of biofuel products [37].

The Rajagopal study in India concluded that the focus of renewal policies is on Jatropha, and this is wrong because there are better options. Biofuel policies should focus on short-term, versatile, and drought-resistant crops such as sweet sorghum. Reform policies should focus on broader options, which can provide benefits that are more direct to the rural poor [38]. The study of Jeli and Yusuf (2015) also proved the importance of policies in the agricultural sector. They note that subsidizing renewable energy consumption in the agricultural sector helps the sector be more competitive in global markets while leaving less pollution [39]. Experimental results from a study by Hong et al. (2020) in China showed that investing in renewable energy, including bioenergy, solar, and hydropower, actually enhanced China's rural household economy [40]. Esmailzadeh et al. (2020) used interpretive structural modeling techniques in their study and concluded that government policies, oil crisis, economic growth, and recession were the most important factors affecting the photovoltaic technological innovation system in Iran [41].

Oryani et al. (2021) reached a conclusion that based on the effects of increased energy consumption and environmental degradation, switching from conventional energy to renewable energy sources should be considered in national energy policies. Accordingly, they believe that market-based intervention policies and non-market-based interventions are necessary [42]. A study by Muhammed and Tekbiyik (2020) demonstrated that renewable policies would increase the development of RE installation capacity in three countries, China, the United States, and Brazil [43].

In a research paper, Hafeznia et al. (2017) studied renewable energy policies in Iran. The results indicated that policies to support photovoltaic technologies were equal in all regions and that the government needed to differentiate between different regions with different potentials in designing new policies [44]. The results of the Onifade study revealed that the current policies were outdated and ineffective and that policies such as incentive tariffs and quota commitments needed to be used. It is also necessary to develop a market for renewables [45]. A study in Pakistan discussed RE policies in Pakistan. They argue that existing policies and activities have not been sufficient to increase significant change in the country's renewable sector. Renewable technology equipment must be imported, which increases the cost of RE projects. Government subsidies reduce the energy costs of crude oil. The complete lack of a marketing and advertising strategy is another weakness of RE policies in Pakistan. Mutual communication and partnerships between different government agencies are also weak. Smyth et al. (2010) concluded that at the national level, biofuel policies were poorly implemented and it would be necessary to establish an effective and efficient framework for the development of biofuels [46]. In a study on renewable policies in Canada, the results showed that under the combination of market incentives and the policy guidelines scenario, biomass-based ethanol and electricity generation could increase significantly and potentially lead to fundamental changes in land use practices. In general, agriculture enjoys significant potential for biomass production for energy and significant potential for reducing greenhouse gas emissions. However, the appropriate combination of market policies and incentives will have significant impact on the type of bioenergy produced [47].

2.3. Policymaking models

Iran lacks a proper policymaking framework for renewable energy and this is a major challenge for developing renewable energy technologies in the country. Although it seems that laws are enacted and directives are issued, it lacks executive instructions. An appropriate and precise policy can reduce the conflict between renewable and non-renewable energies. Success in the development of renewable energy depends on good political decision-making [48]. In this regard, many policymaking models have been presented over the years. The most basic policymaking model belongs to Laswell, which consists of seven main stages. These stages are knowledge, promotion, prescription, invocation, implementation, termination, and evaluation [49, 50]. The Purdon model consists of six steps: identifying the problem, setting criteria, identifying options, evaluating and selecting, evaluating the process, and evaluating the consequences [51]. The models of Lin [52], Ghavifekr et al. [53], Dye [54], Denhardt et al. [55], Ahrens [56], Janssen and Helbig [57], and Onifade [45] were also studied. Many policymaking models were presented that led to the diversity of these models. However, most researchers consider similar steps for the policymaking including the process of problem identification, policy formulation or development, decision-making, policy implementation, and policy evaluation [57-60] (Figure 1).

The model presented in Figure 1 was used as the default model in this research.

3. METHODOLOGY

The method of this research is quantitative and is applied in terms of purpose and survey in terms of strategy. Structural Equation Modeling (SEM) was used for the statistical analysis of research data. SEM is a data analytical approach that shows causal relations between measured and/or latent variables. For model analysis, SEM is not considered as a purely statistical technique, but as an analytical process involving model conceptualization, parameter identification and estimation, and data model fit assessment [61]. Researchers have become highly aware of the need to use multiple observed variables to understand their field of research better. Basic statistical methods consider only a limited number of variables simultaneously that are incapable of dealing with more advanced and complex theories. Using a small number of variables to understand complex phenomena is limited by itself. However, structural equation modeling allows researchers to statistically model and test complex phenomena. Structural equation modeling techniques are methods for confirming or rejecting theoretical models in a quantitative way. Another important point is the attention to the high importance of the validity and reliability of observation scores obtained by measuring instruments, e.g., in particular, measurement error, which is a fundamental issue in all disciplines. For analyzing data statistically, structural equation modeling techniques also took into account measurement errors. However, in classical statistical methods, measurement error and statistical analysis of data are done separately. Structural equation modeling programs can be used as easily as possible and be run with a Windows system. Therefore, structural equation modeling software is now easier to use and has features similar to other software packages under Windows [62-66].

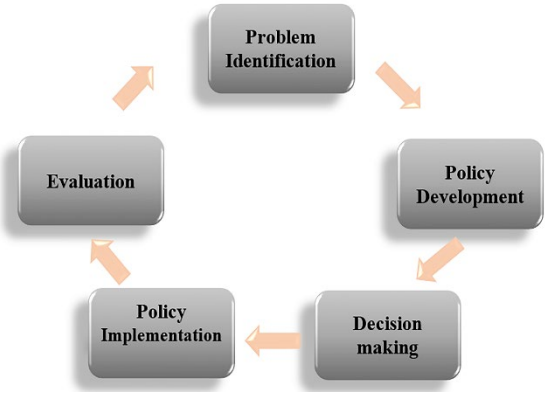

Figure 1. Default policy model.

The statistical population of this study consisted of all experts who had experience, expertise, and activities in the field of renewable energy policymaking. Although there is no exact information in this field for various reasons such as irregular retirements and returning to work after retirement in different areas of operation, according to the collected statistics, about 80 people are active in official and administrative affairs in this field and using the Krejcie and Morgan table, 70 samples must be considered. Therefore, the questionnaire was given to 70 energy policymaking experts who constituted the statistical sample to collect their opinions. Random sampling was used for this study. The main tool for data collection was a questionnaire designed based on the Likert spectrum, which was presented in two parts: demographic characteristics and main variables of the

research. The research variables consist of five main variables, each of which is composed of a number of items. These variables are problem identification (10 items), policy formulation (16 items), decision-making (8 items), policy implementation (17 items), and policy evaluation (6 items).

The validity of the research tool was determined using face validity, Content Validity Ratio (CVR), and Content Validity Index (CVI). Face validity determines whether the appearance of the questionnaire is appropriately designed to assess the researcher's intended purpose [67]. In this section, experts were asked about the appropriateness, attractiveness, and logical sequence of items, as well as the brevity and comprehensiveness of the questionnaire.

CVR is used to determine if the most important and correct content has been selected [68]. To determine the CVR, experts are asked to examine each item in the following three terms: "necessary", "useful but not necessary", and "not necessary". Finally, the CVR is calculated according to the following formula:

$$CVR = \frac{n_E - \frac{N}{2}}{\frac{N}{2}}$$

In this case, n_E is the number of specialists who answered the "necessary" option and N is the total number of specialists. Table 1 specifies the minimum amount of validity to be accepted. In determining this amount, the number of respondents is also considered. If the value obtained is greater than the value of the table (Table 1), the validity of the content of that item is accepted [69].

Table 1. Deciding on a CVR

Number of specialists	Minimum amount of validity
5	0.99
6	0.99
7	0.99
8	0.85
9	0.78
10	0.62
15	0.49
20	0.42
25	0.37
30	0.33
40	0.29
Reference: [69].	

The reliability of the questionnaire was calculated using Cronbach's alpha, the values of which are shown in Table 3. SPSS 25 and LISREL 80.8 software products were used to analyze the research data.

The CVI also determines whether the questionnaire items are best designed to measure content [68, 70]. The CVI is calculated by dividing the approximate scores for each item that scored "relevant but in need of review" and "fully relevant" by the total number of professionals. If the value is less than 0.7, the item is rejected. If it is between 0.7 and 0.79, a review should be performed and if it is greater than 0.79, it is acceptable [71]. In the pilot test, 30 experts were consulted to achieve CVI and CVR values and an initial questionnaire was provided to them, the results of which are given in Table 2.

Table 2. Calculated CVI and CVR questionnaire

Abbreviation	Items		
	Item	**CVI**	**CVR**
	Problem identification (pi)		
P1	In the renewable energy policy-making process, the priorities of the agricultural sector are considered.	0.80	0.66
P2	Renewable policies are adopted according to the needs of the country and the agricultural sector.	0.83	0.53
P3	There is a lack of management in setting priorities.	0.90	0.86
P4	Targeting in the adoption of renewable energy policies is well done.	0.86	0.60
P5	Strategic study to identify priority technologies has not been done according to the needs of each region.	0.83	0.46
P6	Accurate identification of stakeholders in the agricultural sector is not done.	0.80	0.93
P7	Support for renewable energy research in the agricultural sector is not well done.	0.93	0.93
P8	Policy-making is based on personal desires, aspirations, and interests.	0.86	0.60
P9	The development of policies for the use of agricultural waste for biogas production will play an important role in the development of renewable energy.	0.83	0.66
P10	Policy-making is done without considering the existing facts and objective problems and regional and local issues.	0.83	0.86
	Average	0.85	0.71
	Policy formulation (pf)		
Pf1	Policies to motivate the private sector to encourage the production of renewable energy are at a desirable level.	0.86	80.0
Pf2	It seems necessary to highlight the role of the Ministry of Agriculture in renewable energy policymaking.	0.90	73.0
Pf3	In the process of renewable energy policymaking, there is a lack of policy coherence.	0.80	1
Pf4	Lack of focus on renewable energy matters does not contribute much to development in this area.	0.80	0.80
Pf5	The focus of policy-making in a single organization helps develop renewable energy policies.	0.93	0.86
Pf6	Renewable equipment market development policies are in good condition.	0.86	0.53
Pf7	Simplification of laws and regulations related to renewables seems to be necessary, especially in the agricultural sector.	0.93	0.80

Pf8	Subsidies for the "consumption" of renewable energy should be increased, especially in the agricultural sector.	0.90	0.73
Pf9	Subsidies for the "production" of renewable energy, especially in the agricultural sector, should be increased.	0.96	0.86
Pf10	Renewable energy education and promotion policies have good conditions, especially in the agricultural sector.	0.80	0.60
Pf11	Organizational interference in policy-making is clearly observed as a problem in the policy-making path.	0.83	0.86
Pf12	At present, the parallelism of organizations and institutions in the implementation of adopted policies and programs acts as an obstacle.	0.80	0.93
Pf13	Real policymakers are not employed in the renewable energy policymaking cycle.	0.83	0.60
Pf14	There is a top-down approach to renewable energy policymaking in the agricultural sector.	0.83	0.46
Pf15	Policies should be adopted to reduce the role of fossil fuels in the agricultural sector.	0.90	1
Pf16	Relevant authorities have a high level of awareness in the field of renewable policymaking.	0.80	0.53
Average		0.81	0.76
Decision making (dm)			
Dm1	Participation of all stakeholders in renewable energy policymaking is low.	0.90	0.53
Dm2	There is a bottom-up approach to renewable energy policymaking in the agricultural sector.	0.83	0.66
Dm3	The setting of criteria and indicators and standards related to renewable energy production is well managed.	0.80	0.33
Dm4	The participation of agricultural stakeholders in renewable energy policymaking is adequate.	0.80	0.86
Dm5	It is necessary to eliminate subsidies for fossil fuels to encourage the production of renewable energy.	0.80	0.46
Dm6	Consumption pattern modification is one of the programs that can help the development of renewables.	0.83	0.53
Dm7	Policies to use incentives for farmers to produce and use renewables need to be considered.	0.93	0.60
Dm8	The adopted solutions are presented and selected according to the problem diagnosis stage.	0.83	0.60
Average		0.84	0.57
Policy implementation (pim)			
Pim1	The management of culture making and public awareness about renewable energy is in a convincing position.	0.83	0.66
Pim2	It does not seem necessary to highlight the role of the Ministry of Agriculture in the use of renewable energy.	0.80	0.73
Pim3	Planning to implement priorities suffers from severe managerial weakness.	0.90	0.86
Pim4	Government direct investment in the renewable energy sector is sufficient and appropriate.	0.80	0.66
Pim5	Groups involved in policy-making also monitor implementation.	0.83	0.60
Pim6	The necessary human resources are considered in the implementation of renewable energy policies.	0.86	0.73
Pim7	Coordination between the various departments enforcing renewables laws needs to be strengthened.	0.90	0.93
Pim8	Necessary executive resources are considered in the implementation of renewable energy policies.	0.93	0.80
Pim9	Adoption of policies without executive guarantees is widespread.	0.93	0.93
Pim10	Policy implementation is well managed.	0.86	0.86
Pim11	Sufficient work force is employed in the renewal policy cycle.	0.86	0.73
Pim12	Expert manpower has a high level of awareness.	0.80	0.66
Pim13	There are no enforcement guarantees for the policies adopted.	0.90	0.80
Pim14	All adopted policies are properly transformed to program.	0.86	0.40
Pim15	Cooperation between institutions and organizations in the implementation of renewable energy policies is adequate.	0.83	0.53
Pim16	The necessary financial resources are considered in the implementation of renewable energy policies.	0.86	0.25
Pim17	The relationship between academia and industry and policy-making institutions should be reviewed and strengthened.	0.80	0.46
Average		0.85	0.69
Policy evaluation (pe)			
Pe1	Evaluation of executive policies is done appropriately.	0.96	0.86
Pe2	Evaluations are used to address issues.	0.80	0.86
Pe3	The multiplicity of regulatory organizations is a major barrier to policy evaluation.	0.93	0.66
Pe4	There is no evaluation of implemented policies.	0.86	0.86
Pe5	Renewable development projects in the agricultural sector without subsidies are not economically justified.	0.80	0.33
Pe6	Evaluation takes place during the implementation of renewable development policies.	0.90	0.80
Average		0.87	0.72

Table 3. Cronbach's alpha values of different parts of the questionnaire

Latent variable name	Cronbach's alpha
Problem identification	0.919
Policy formulation	0.925
Decision making	0.951
Policy implementation	0.933
Policy evaluation	0.853
Total	0.916

A summary of the research methodology framework is shown in Figure 2.

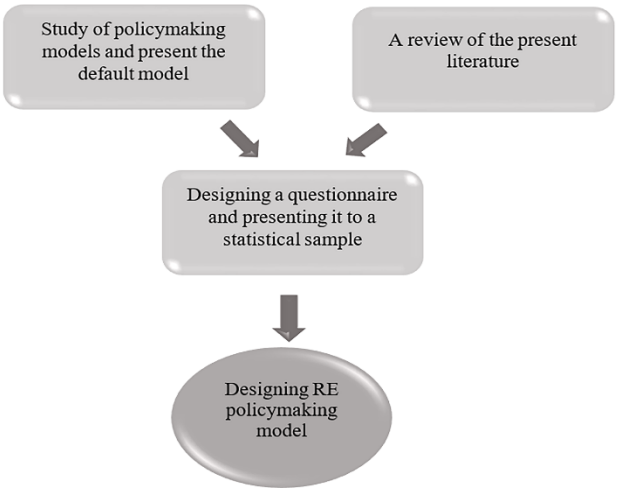

Figure 2. A summary of the research methodology framework

4. FINDINGS

In this section, descriptive statistics related to individual characteristics including age, education, field of study, and work experience in the field of renewables were examined.

Respondents in this study included 70 people. In terms of gender distribution, all respondents were male and their mean age was 54.12 years. People ranged in age from 40 to 69 years. In terms of records and experience, the subjects who aged 15.38 years on average have had experience in this field (Table 4).

Table 4. Age, gender, and work experience of the respondents

Variable	Gender	Age	Work experience
Mean	-	54.12	15.38
Max	-	69	35
Min	-	40	7
-	Male	-	-
Number	70	70	70

Out of 70 respondents, 64 (91.4 %) had a doctoral degree and six respondents (8.6 %) had a Master's degree (Table 5).

Table 5. Level of education of the respondents

Educational degree	Frequency	Percentage
Ph.D.	64	91.4
Masters	6	8.6
Total	70	100

The variety of fields of study was so great that about 23 fields of study were registered. Among them, 12 people (17.1 %) stated that their field of study was chemistry. The lowest number was related to the fields such as management and water resources (1.4 %).

4.1. Structural equation modeling

The results of the validity and reliability analysis and the structural model obtained from the analysis of the five Latent Variables of "problem identification", "policy formulation", "decision making", "policy implementation", and "policy evaluation" are as follows (Table 6):

Table 6. Validity and reliability results of research factors

latent factors	Cronbach's alpha	AVE	CR
Problem identification	0.919	0.700	0.930
Policy formulation	0.925	0.746	0.947
Decision making	0.951	0.701	0.949
Policy implementation	0.933	0.736	0.951
Policy evaluation	0.853	0.817	0.914
Total	0.916	0.704	0.938

4.2. Validity and reliability analysis of research variables

For each factor, two indices of Average Variance Extracted (AVE) and Composite Reliability (CR) were calculated. These two indicators are used to measure the validity and reliability of factors. The AVE index shows what percentage of the variance of the studied factors has been affected by the variables of those factors. Researchers have set a value of 0.5 or higher for the appropriateness of this index [72, 73]. Regarding the value of CR, it is stated that if it is greater than 0.7 for each of the factor, they exhibit acceptable reliability and the closer this value is to one for each factor, the reliability of that factor is higher. Based on the results, the values of the AVE and the CR calculated for all five factors named in the present study are listed in Table 6. In general, according to the obtained results, it can be said that the research tool had good validity and reliability.

To continue the analysis, a structural equation modeling technique was used and Confirmatory Factor Analysis (CFA) was selected. In this step, upon adding five factors "problem identification", "policy formulation", "decision making", "policy implementation", and "policy evaluation" and their items into LISREL software, the structural model of the research was presented. The question is whether the existing relationships between latent variables based on the previous studies, extracted and plotted, are confirmed. The presented final model states that the markers considered in the research could have properly confirmed their relationship. As shown in Figure 3, all relationships are significant ($t \geq 1.96$). Figure 4 shows the structural model of the research. For example, the factor load of the first observed variable "problem identification" variable is 0.63. The larger the factor load and the closer it is to the number one, the better the observed variable can explain the independent variable. If the factor load is less than 0.3, a weak relationship is considered and it is ignored. The factor load between 0.3 to 0.6 is acceptable; and if it is greater than 0.6, it is desirable [74].

In the problem identification factor, the factor load p1, which is related to considering the priorities of the agricultural sector, is 0.63. This factor load indicates the amount of variance that the item has explained. The factor load of item p2, which indicated how much attention was paid to the needs of the agricultural sector, was 0.66. In addition, the factor load of considering technology and its priority in each region is estimated to be 0.64. Lack of support for renewable energy research in agriculture (p7) also exhibited a factor load of 0.66. All of these items indicated a factor load greater than 0.6, implying that these observations could explain the problem identification variable well. In addition, the lowest factor loading is related to managing priorities (p3) and identifying stakeholders (p6) in the agricultural sector. In the policy formulation, item pf6, which measures the status of

policies of renewable equipment market development, had a factor load of 0.73. Item pf11, with a factor load of 0.76, examines organizational interference in policymaking. The parallel work of organizations and institutions in the implementation of adopted policies and programs (pf12) demonstrated a factor load of 0.78, which indicated that observations could explain the variable well (Table 7) in this factor. Accordingly, the items that examined the role of the Ministry of Agriculture in the renewables policymaking (pf2) and the condition of renewable energy education (pf10) were lower than the other items.

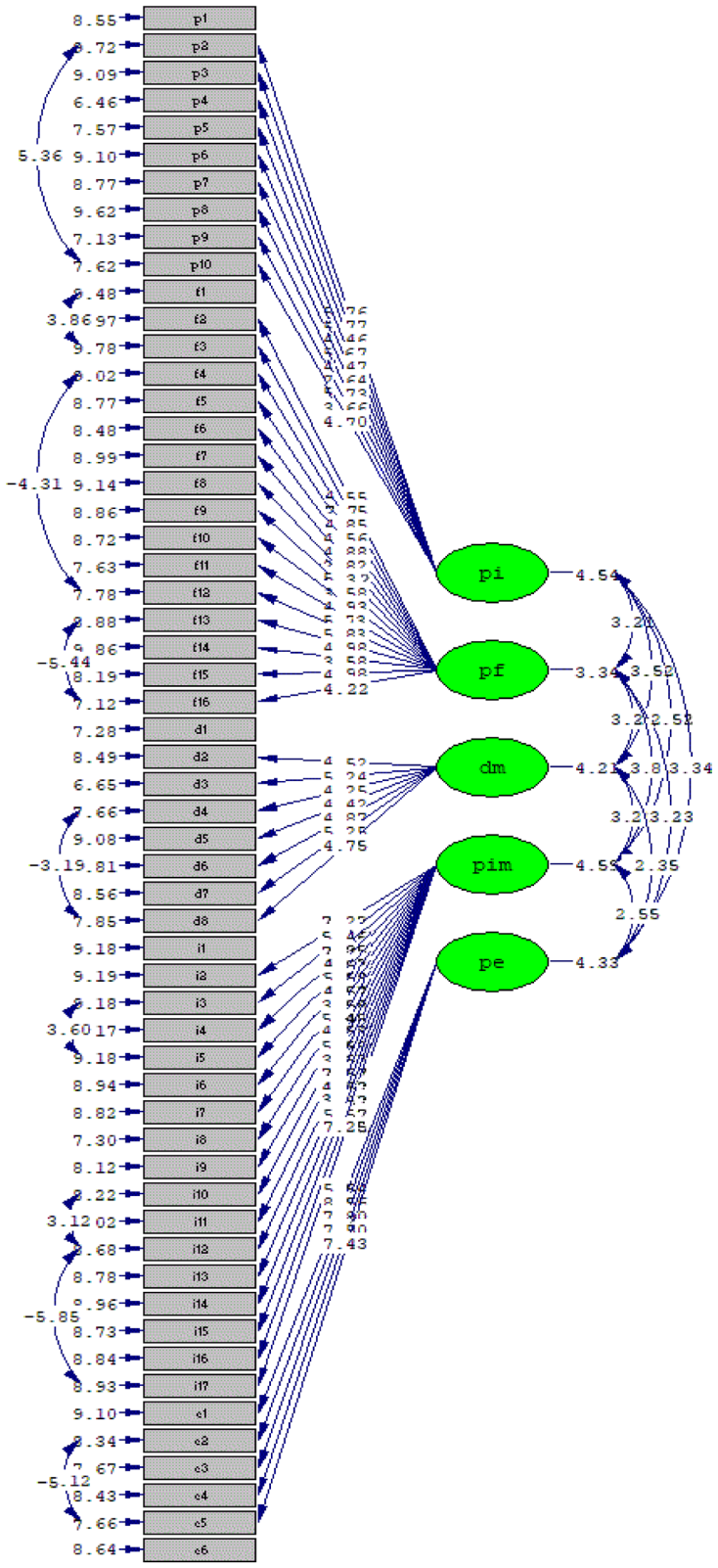

Figure 3. T-values in the structural model of renewable energy policymaking in the agricultural sector

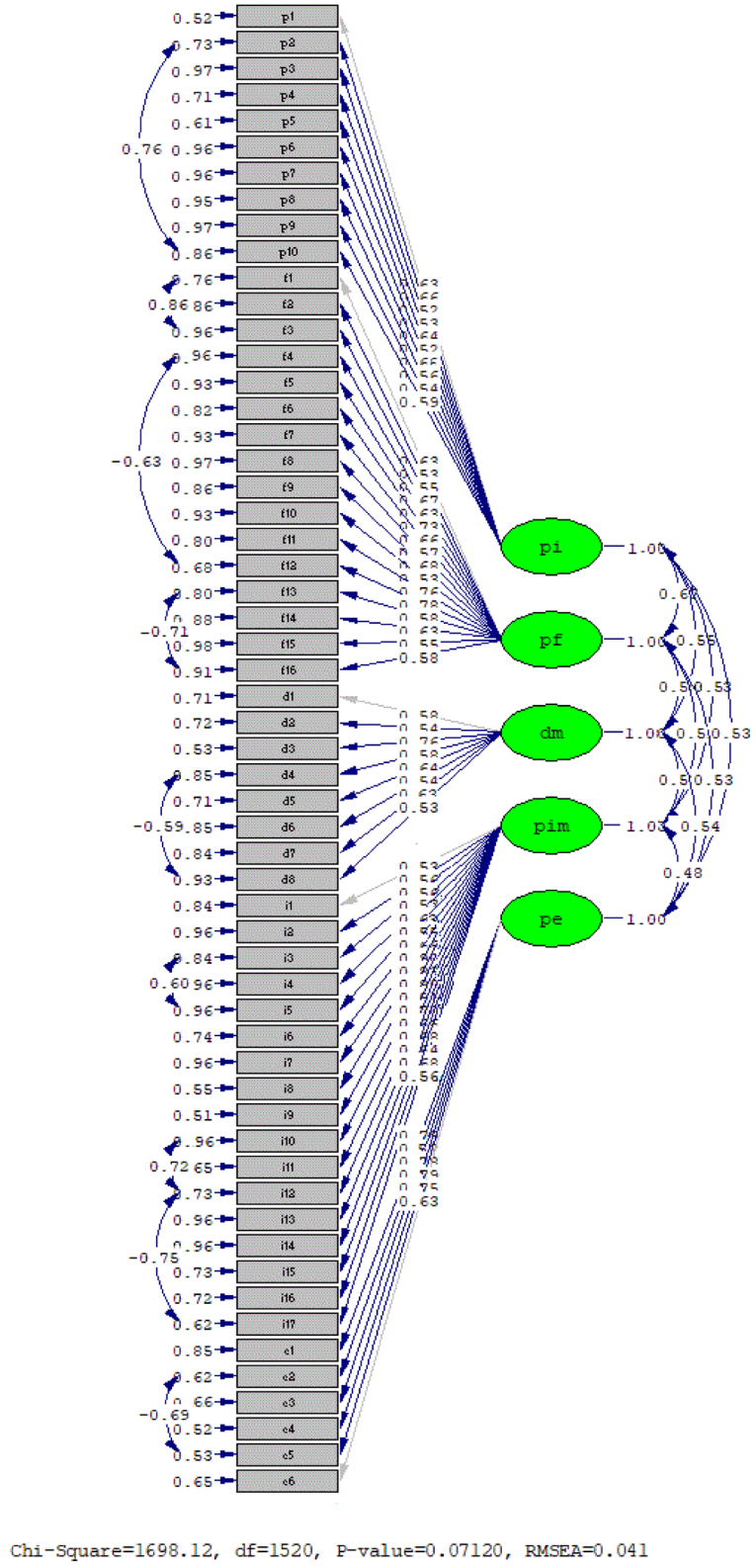

Figure 4. Structural model of renewable energy policymaking in agriculture

Table 7. Factor loads in the final model

Item		Factor loading
Problem identification (pi)		
P7	Support for renewable energy research in the agricultural sector is not well done.	0.66
P2	Renewable policies are adopted according to the needs of the country and the agricultural sector.	0.66
P5	Strategic study to identify priority technologies has not been done according to the needs of each region.	0.64

P1	In the renewable energy policy-making process, the priorities of the agricultural sector are considered.	0.63
P10	Policy-making is done without considering the existing facts and objective problems and regional and local issues.	0.59
P8	Policy-making is based on personal desires, aspirations, and interests.	0.56
P9	The development of policies for the use of agricultural waste for biogas production plays an important role in the development of renewable energy.	0.54
P4	Targeting in the adoption of renewable energy policies is well done.	0.53
P3	There is a lack of management in setting priorities.	0.52
P6	Accurate identification of stakeholders in the agricultural sector is not done.	0.52
Policy formulation (pf)		
Pf12	At present, the parallelism of organizations and institutions in the implementation of adopted policies and programs acts as an obstacle.	0.78
Pf11	Organizational interference in policy-making is clearly observed as a problem in the policy-making path.	0.75
Pf6	Renewable equipment market development policies are in good condition.	0.73
Pf9	Subsidies for the "production" of renewable energy, especially in the agricultural sector, should be increased.	0.68
Pf4	Lack of focus on renewable energy matters does not contribute much to development in this area.	0.67
Pf7	Simplification of laws and regulations related to renewables seems to be necessary, especially in the agricultural sector.	0.66
Pf1	Policies to motivate the private sector to encourage the production of renewable energy are at a desirable level.	0.63
Pf14	There is a top-down approach to renewable energy policymaking in the agricultural sector.	0.63
Pf5	The focus of policy-making in a single organization helps to develop renewable energy policies.	0.63
Pf16	Relevant authorities have a high level of awareness in the field of renewable policymaking.	0.58
Pf13	Real policymakers are not employed in the renewable energy policymaking cycle.	0.58
Pf8	Subsidies for the "consumption" of renewable energy should be increased, especially in the agricultural sector.	0.57
Pf3	In the process of renewable energy policymaking, there is a lack of policy coherence.	0.55
Pf15	Policies should be adopted to reduce the role of fossil fuels in the agricultural sector.	0.55
Pf2	It seems necessary to highlight the role of the Ministry of Agriculture in renewable energy policymaking.	0.53
Pf10	Renewable energy education and promotion policies have good conditions, especially in the agricultural sector.	0.53
Decision making (dm)		
Dm3	The setting of criteria and indicators and standards related to renewable energy production is well managed.	0.76
Dm5	It is necessary to eliminate subsidies for fossil fuels to encourage the production of renewable energy.	0.64
Dm7	Policies to use incentives for farmers to produce and use renewables need to be considered.	0.63
Dm4	The participation of agricultural stakeholders in renewable energy policymaking is adequate.	0.58
Dm1	Participation of all stakeholders in renewable energy policymaking is low.	0.58
Dm2	There is a bottom-up approach to renewable energy policymaking in the agricultural sector.	0.54
Dm6	Consumption pattern modification is one of the programs that can help the development of renewables.	0.54
Dm8	The adopted solutions are presented and selected according to the problem diagnosis stage.	0.53
Policy implementation (pim)		
Pim12	Expert manpower has a high level of awareness.	0.70
Pim14	All adopted policies are properly transformed to program.	0.68
Pim16	The necessary financial resources are considered in the implementation of renewable energy policies.	0.68
Pim8	Necessary executive resources are considered in the implementation of renewable energy policies	0.67
Pim7	Coordination between the various departments enforcing renewables laws needs to be strengthened.	0.66
Pim13	There are no enforcement guarantees for the policies adopted.	0.66
Pim15	Cooperation between institutions and organizations in the implementation of renewable energy policies is adequate.	0.64
Pim5	Groups involved in policy-making also monitor implementation.	0.63
Pim9	Adoption of policies without executive guarantees is widespread.	0.56
Pim10	Policy implementation is well managed.	0.56
Pim17	The relationship between academia and industry and policy-making institutions should be reviewed and strengthened.	0.56
Pim6	The necessary human resources are considered in the implementation of renewable energy policies.	0.55
Pim4	Government direct investment in the renewable energy sector is sufficient and appropriate.	0.53
Pim1	The management of culture making and public awareness about renewable energy is in a convincing position.	0.53
Pim11	Sufficient workforce is employed in the renewal policy cycle.	0.53
Pim2	It does not seem necessary to highlight the role of the Ministry of Agriculture in the use of renewable energy.	0.50

Pim3	Planning to implement priorities suffers from severe managerial weakness.	0.50
Policy evaluation (pe)		
Pe1	Evaluation of executive policies is done appropriately.	0.79
Pe4	No evaluation of implemented policies is done.	0.79
Pe3	The multiplicity of regulatory organizations is a major barrier to policy evaluation.	0.78
Pe5	Renewable development projects in the agricultural sector without subsidies are not economically justified.	0.75
Pe6	Evaluation takes place during the implementation of renewable development policies.	0.63
Pe2	Evaluations are used to address issues.	0.58

In the decision-making variable, item dm3, which is related to the management of regulatory criteria, indicators, and standards in the production of renewable energy, could explain the main variable more strongly than other cases. Factor loads of other items such as the elimination of fossil fuel subsidies (dm5) and consideration of incentive policies for farmers (dm7) were also recorded above 0.6. In the policy implementation variable, the factor load of nine items above 0.6 and three items exhibited a factor load above 0.7, indicating a good explanation of the variable by these items. In the last variable, policy evaluation, four items could elaborate the main variable with a factor load greater than 0.7. These items examined and measured the extent of policy evaluation (pe1), the multiplicity of regulatory organizations in policy evaluation (pe3), and the existence of policy implementation evaluation (pe4). It should be noted that the factor loads in this factor exhibited higher values than other factors.

It was mentioned above that the research model was in good condition in terms of AVE and CR. Table 8 shows that the model has good fitness. Root Mean Square Residual (RMR), Standardized Root Mean Square Residual (SRMR), Goodness of fit index (GFI), Normed Fit Index (NFI), Normalized Fit Index (NNFI), Incremental Fit Index (IFI), Comparative Fit Index (CFI), and Root Mean Square Error of Approximation (RMSEA) were employed to evaluate the fitness of the model. The information in Table 4-27 shows the value of each of these indicators in the research model. As can be seen, the overall research model has a goodness of fit.

Table 8. Results of the values of compliance of the research model with fitness indicators

	$(\frac{x^2}{df})$ **Relative chi-square**	**RMSEA**	**RMR**	**SRMR**	**CFI**	**GFI**	**NFI**	**NNFI**
Reception area*	3>	0.08>	Close to zero	0.08>	0.90≤	0.90≤	0.90≤	0.90≤
Research finding	1.11	0.041	0.21	0.053	0.99	0.99	0.99	0.99

5. DISCUSSION

The designed model shows that in the problem identification stage of the policymaking cycle, the priorities of the agricultural sector and the needs of the country in this sector are not considered. Selection of technologies is not based on the priority of this section and no strategic study is done in this area. Another important issue is the lack of accurate and correct identification of stakeholders in the agricultural sector. This will lead to wrong policy in the next step because it will suggest adopting policies that are unrelated to the target group. Ferris's findings also confirm that stakeholder participation increases the chances of achieving goals [59].

Analysis of the opinions of responsive experts indicated that at the policy-making stage, policies related to the market for renewable equipment are not in good condition. Problems related to organizational interference as well as parallelism in policymaking were acknowledged. These cases were identified as one of the most important problems of this step because they had the highest factor load (above 0.7) and could explain the highest variance. After these cases, another important issue is the simplification of laws and regulations related to this area. Cumbersome laws and troublesome bureaucracy prevent the facilitation of administrative and executive affairs. Another issue is the production subsidy for renewable energy. These subsidies and protections need to moderate the difference between the cost of conventional and renewable fuels. Mezher et al. (2012) came to the same conclusion. They argued that fossil fuel subsidies and a lack of economic support for renewable resources hindered active private sector participation [75]. Radmehr also believed that policies that increase the cost of using fossil fuels must be adopted [29]. It is necessary to correct the top-down approach in decision-making to bridge the gap between what is needed and what is offered. Lieu's findings also suggest that the interaction between all institutions at the policymaking stages, policymakers, and stakeholders can be beneficial, because ignoring stakeholder responses can lead to a set of policies that may seem very strong in theory and policy design but are inconsistent in practice [76]. At the decision-making stage, it is necessary to better define the criteria, indicators, and standards related to renewable energy production. There should also be incentives for farmers to encourage them to use and produce renewables.

Expert opinions on policy implementation showed that expert manpower needed more training because they did not have the necessary level of knowledge in this area. Mechanisms must also be put in place to ensure that policies are implemented and that all of these policies are well planned and effective. Policy evaluation also indicates that the need for effort and review in this step is necessary because the weakness in policy evaluation is clearly observed and policy evaluation is not done. This problem is similar to what Chapman et al. (2016) stated in their findings [77]. The multiplicity of monitoring organizations acts as a barrier. Nowruzi also confirmed the claim that the centralization of RE management in a small number of institutions would facilitate the success of renewable energy in Iran [34]. As demonstrated by the results, it is necessary to provide subsidies for renewable development projects in the agricultural sector in order to justify their economic value. In general, it should be noted that the factor loadings in the

policy evaluation factor showed higher values than other factors. It can be implied that the proposed model indicates the greatest weaknesses and shortcomings in policy evaluation. It is clear that evaluating the implementation of policies and programs as well as examining the effects and extent of achieving predetermined goals are essential. This helps better identify existing errors or shortcomings and fix these problems more easily. However, now, lack of proper evaluation is one of the major problems in renewable energy policy.

6. CONCLUSIONS

In conclusion, it can be said that with the depletion of fossil fuel resources in the world, all countries are looking to replace these fuels with renewable energy sources, especially in agriculture, to avoid any disruption in the economy, because energy is very important for comprehensive development. In this regard, appropriate policies are necessary for the utilization of renewable resources and success in this field, which will not be possible unless we have an effective and efficient policymaking cycle. The role and ability of organizations and institutions should be carefully considered and each of them, according to their capacity and importance, plays a role in different stages of the renewable policymaking cycle. Greater attention should be paid to the evaluation stage and the role of individuals and groups involved in this stage of policymaking should be taken seriously. While economic growth is dependent on energy, governments should consider renewables as a substitute for non-renewables and adopt appropriate policies. Energy policy is an important issue, especially for a country like Iran, because Iran's economy is based on oil and fossil fuels. Iran performed poorly in the development and use of renewable energy in the past. Considering the institutions and organizations involved in policymaking in Iran, it is necessary to use an appropriate model for policymaking and the development of renewables. Iran performed poorly in the development and use of renewable energy in the past. It is necessary to make up for the loss by revising policies and measures in this area.

For future studies, issues such as how policies are implemented, the extent to which defined goals have been achieved, and the needs assessment for each agricultural region for the development of renewable energy can be considered by researchers. Also by conducting research and model design in other communities, comparative validation is also possible.

7. ACKNOWLEDGEMENT

The authors acknowledge the financial support of Tarbiat Modares University during the project.

NOMENCLATURE

RE	Renewable energy
CFA	Confirmatory factor analysis
AVE	Average variance extracted
CR	Composite reliability
CVR	Content validity ratio
CVI	Content validity index
Pi	Policy identification
Pf	Policy formulation
Dm	Decision making
Pim	Policy implementation
Pe	Policy evaluation

REFERENCES

1. Nicolini, M. and Tavoni, M., "Are renewable energy subsidies effective? Evidence from Europe", ***Renewable and Sustainable Energy Reviews***, Vol. 74, (2017), 412-423. (https://doi.org/10.1016/j.rser.2016.12.032).
2. Müller, S., Brown, A. and Ölz, S., "Renewable energy: Policy considerations for deploying renewables", International Energy Agency, (IEA), Paris, France, (2011). (https://citeseerx.ist.psu.edu/viewdoc/download?doi=10.1.1.378.1540&rep=rep1&type=pdf).
3. Griffiths, S., "A review and assessment of energy policy in the Middle East and North Africa region", ***Energy Policy***, Vol. 102, (2017), 249-269. (https://doi.org/10.1016/j.enpol.2016.12.023).
4. Ikram, M., Zhang, Q., Sroufe, R. and Shah, S.Z.A., "Towards a sustainable environment: The nexus between ISO 14001, renewable energy consumption, access to electricity, agriculture and CO_2 emissions in SAARC countries", ***Sustainable Production and Consumption***, Vol. 22, (2020), 218-230. (https://doi.org/10.1016/j.spc.2020.03.011).
5. Testa, R. and Tudisca, S., "An opportunity for the agricultural sector: The renewable energy sources", ***American Journal of Agricultural and Biological Science***, Vol. 11, No. 3, (2016), 100-102. (https://doi.org/10.3844/ajabssp.2016.100.102).
6. Fami, H.S., Ghasemi, J., Malekipoor, R., Rashidi, P., Nazari, S. and Mirzaee, A., "Renewable energy use in smallholder farming systems: A case study in tafresh township of Iran", ***Sustainability***, Vol. 2, No. 3, (2010), 702-716. (https://doi.org/10.3390/su2030702).
7. Panwar, N., Kaushik, S. and Kothari, S., "Role of renewable energy sources in environmental protection: A review", ***Renewable and Sustainable Energy Reviews***, Vol. 15, No. 3, (2011), 1513-1524. (https://doi.org/10.1016/j.rser.2010.11.037).
8. Aghahosseini, A., Bogdanov, D., Ghorbani, N. and Breyer, C., "Analysis of 100 % renewable energy for Iran in 2030: Integrating solar PV, wind energy and storage", ***International Journal of Environmental Science and Technology***, Vol. 15, (2018), 17-36. (https://doi.org/10.1007/s13762-017-1373-4).
9. Solaymani, S., "A review on energy and renewable energy policies in Iran", ***Sustainability***, Vol. 13, No. 13, (202), 73-28. (https://doi.org/10.3390/su13137328).
10. Vatankhah, S., Mousavi, M. and Shabanikia, A., Energy policy making in Iran, Interviwer: Dehhaghi, S., (2018).
11. Türkekul, B. and Unakıtan, G., "A co-integration analysis of the price and income elasticities of energy demand in Turkish agricultur", ***Energy Policy***, Vol. 39, No. 5, (2011), 2416-2423. (https://doi.org/10.1016/j.enpol.2011.01.064).
12. Mushtaq, K., Abbas, F. and Ghafoor, A., "Energy use for economic growth: Cointegration and causality analysis from the agriculture sector of Pakistan", ***The Pakistan Development Review***, (2007), 1065-1073. (https://www.jstor.org/stable/41261213).
13. Chel, A. and Kaushik, G., "Renewable energy for sustainable agriculture", ***Agronomy for Sustainable Development***, Vol. 31, (2011), 91-118. (https://doi.org/10.1051/agro/2010029).
14. Sutherland, L.A., Peter, S. and Zagata, L., "Conceptualising multi-regime interactions: The role of the agriculture sector in renewable energy transitions", ***Research Policy***, Vol. 44, No. 8, (2015), 1543-1554. (https://doi.org/10.1016/j.respol.2015.05.013).
15. Jebli, M.B. and Youssef, S.B., "The role of renewable energy and agriculture in reducing CO_2 emissions: Evidence for North Africa countries", ***Ecological Indicators***, Vol. 74, (2017), 295-301. (https://doi.org/10.1016/j.ecolind.2016.11.032).
16. Crutzen, P.J., Mosier, A.R., Smith, K.A. and Winiwarter, W., "N_2O release from agro-biofuel production negates global warming reduction by replacing fossil fuels", Paul J. Crutzen: A pioneer on atmospheric chemistry and climate change in the anthropocene, Springer, (2016), 227-238. (https://doi.org/10.1007/978-3-319-27460-7_12).
17. Dehhaghi, S. and Choobchian, S.H., "The Role of photovoltaic water pumps in development of agricultural sector", ***Journal of Solar Energy Research***, Vol. 2, No. 4, (2017), 281-285. (https://jser.ut.ac.ir/article_64915.html).
18. Naqvi, S.R., Jamshaid, S., Naqvi, M., Farooq, W., Niazi, M.B.K. and Aman, Z., "Potential of biomass for bioenergy in Pakistan based on present case and future perspectives", ***Renewable and Sustainable Energy Reviews***, Vol. 81, Part. 1, (2018), 1247-1258. (https://doi.org/10.1016/j.rser.2017.08.012).

19. Proskurina, S., Heinimö, J., Schipfer, F. and Vakkilainen, E., "Biomass for industrial applications: The role of torrefaction", ***Renewable Energy***, Vol. 111, (2017), 265-274. (https://doi.org/10.1016/j.renene.2017.04.015).
20. Toklu, E., "Biomass energy potential and utilization in Turkey", ***Renewable Energy***, Vol. 107, (2017), 235-244. (https://doi.org/10.1016/j.renene.2017.02.008).
21. Samadi, S.H., Ghobadian, B. and Nosrati, M., "Prediction and estimation of biomass energy from agricultural residues using air gasification technology in Iran", ***Renewable Energy***, Vol. 149, (2020), 1077-1091. (https://doi.org/10.1016/j.renene.2019.10.109).
22. ME | Ministry of Energy, (2017). (https://irandataportal.syr.edu/energy-environment), (Accessed: 11 Desember 2019).
23. Kheybari, S. and Rezaie, F.M., "Selection of biogas, solar, and wind power plants' locations: An MCDA approach", ***Journal of Supply Chain Management Science***, Vol. 1, No. 1-2, (2020), 45-71. (https://doi.org/10.18757/jscms.2020.4805).
24. Haque, U., Da Silva, P.F., Devoli, G., Pilz, J., Zhao, B. and Khaloua, A., "The human cost of global warming: Deadly landslides and their triggers (1995–2014)", ***Science of the Total Environment***, Vol. 682, (2019), 673-684. (https://doi.org/10.1016/j.scitotenv.2019.03.415).
25. Agovino, M., Casaccia, M., Ciommi, M., Ferrara, M. and Marchesano, K., "Agriculture, climate change and sustainability: The case of EU-28", ***Ecological Indicators***, Vol. 105, (2019), 525-543. (https://doi.org/10.1016/j.ecolind.2018.04.064).
26. Ahima, R.S., "Global warming threatens human thermoregulation and survival", ***The Journal of Clinical Investigation***, Vol. 130, No. 2, (2020), 59-61. (https://doi.org/10.1172/JCI135006).
27. Marshall, D.J., Pettersen, A.K., Bode, M. and White C.R., "Developmental cost theory predicts thermal environment and vulnerability to global warming", ***Nature Ecology & Evolution***, Vol. 4, (2020), 406-411. (https://doi.org/10.1038/s41559-020-1114-9).
28. Tiba, S. and Belaid, F., "Modeling the nexus between sustainable development and renewable energy: The African perspectives", ***Journal of Economic Surveys***, Vol. 35, No. 1, (2021), 307-329. (https://doi.org/10.1111/joes.12401).
29. Radmehr, R., Henneberry, S.R. and Shayanmehr, S., "Renewable energy consumption, CO_2 emissions, and economic growth nexus: A simultaneity spatial modeling analysis of EU countries", ***Structural Change and Economic Dynamics***, Vol. 57, (2021), 13-27. (https://doi.org/10.1016/j.strueco.2021.01.006).
30. Gatto, A. and Drago, C., "When renewable energy, empowerment, and entrepreneurship connect: Measuring energy policy effectiveness in 230 countries", ***Energy Research & Social Science***, Vol. 78, (2021), 19-77. (https://doi.org/10.1016/j.erss.2021.101977).
31. Horschig, T. and Thrän, D., "Are decisions well supported for the energy transition? A review on modeling approaches for renewable energy policy evaluation", ***Energy, Sustainability and Society***, Vol. 7, (2017), 1-14. (https://doi.org/10.1186/s13705-017-0107-2).
32. Boulanger, P.M. and Bréchet, T., "Models for policy-making in sustainable development: The state of the art and perspectives for research", ***Ecological Economics***, Vol. 55, No. 3, (2005), 337-350. (https://doi.org/10.1016/j.ecolecon.2005.07.033).
33. Ghorashi, A.H. and Maranlou, H., "Essential infrastructures and relevant policies for renewable energy developments in oil-rich developing countries: Case of Iran", ***Renewable and Sustainable Energy Reviews***, Vol. 141, (2021), 110839. (https://doi.org/10.1016/j.rser.2021.110839).
34. Norouzi, M., Yeganeh, M. and Yusaf, T., "Landscape framework for the exploitation of renewable energy resources and potentials in urban scale (case study: Iran)", ***Renewable Energy***, Vol. 163, (2021), 300-319. (https://doi.org/10.1016/j.renene.2020.08.051).
35. Argentiero, A., Bollino, C.A., Micheli, S. and Zopounidis, C., "Renewable energy sources policies in a Bayesian DSGE model", ***Renewable Energy***, Vol. 120, (2018), 60-68. (https://doi.org/10.1016/j.renene.2017.12.057).
36. Kumar, S., Shrestha, P. and Salam, P.A., "A review of biofuel policies in the major biofuel producing countries of ASEAN: Production, targets, policy drivers and impacts", ***Renewable and Sustainable Energy Reviews***, Vol. 26, (2013), 822-836. (https://doi.org/10.1016/j.rser.2013.06.007).
37. Banse, M., van Meijl, H., Tabeau, A. and Woltjer, G., "Will EU biofuel policies affect global agricultural markets?", ***European Review of Agricultural Economics***, Vol. 35, No. 2, (2008), 117-141. (https://doi.org/10.1093/erae/jbn023).
38. Rajagopal, D., "Implications of India's biofuel policies for food, water and the poor", ***Water Policy***, Vol. 10, (2008), 95-106. (https://doi.org/10.2166/wp.2008.055).
39. Jebli, M.B. and Youssef, S.B., "The environmental Kuznets curve, economic growth, renewable and non-renewable energy, and trade in Tunisia", ***Renewable and Sustainable Energy Reviews***, Vol. 47, (2015), 173-185. (https://doi.org/10.1016/j.rser.2015.02.049).
40. Huang, J., Li, W., Guo, L., Hu, X. and Hall, J.W., "Renewable energy and household economy in rural China", ***Renewable Energy***, Vol. 155, (2020), 669-676. (https://doi.org/10.1016/j.renene.2020.03.151).
41. Esmailzadeh, M., Noori, S., Nouralizadeh, H. and Bogers, M.L., "Investigating macro factors affecting the technological innovation system (TIS): A case study of Iran's photovoltaic TIS", ***Energy Strategy Reviews***, Vol. 32, (2020), 100577. (https://doi.org/10.1016/j.esr.2020.100577).
42. Oryani, B., Koo, Y., Rezania, S. and Shafiee, A., "Investigating the asymmetric impact of energy consumption on reshaping future energy policy and economic growth in Iran using extended Cobb-Douglas production function", ***Energy***, Vol. 216, (2021), 119187. (https://doi.org/10.1016/j.energy.2020.119187).
43. Muhammed, G. and Tekbiyik-Ersoy, N., "Development of renewable energy in China, USA, and Brazil: A comparative study on renewable energy policies", ***Sustainability***, Vol. 12, No. 21, (2020), 91-36. (https://doi.org/10.3390/su12219136).
44. Hafeznia, H., Aslani, A., Anwar, S. and Yousefjamali, M., "Analysis of the effectiveness of national renewable energy policies: A case of photovoltaic policies", ***Renewable and Sustainable Energy Reviews***, Vol. 79, (2017), 669-680. (https://doi.org/10.1016/j.rser.2017.05.033).
45. Onifade, T.T., "Hybrid renewable energy support policy in the power sector: The contracts for difference and capacity market case study", ***Energy Policy***, Vol. 95, (2016), 390-401. (https://doi.org/10.1016/j.enpol.2016.05.020).
46. Smyth, B., Gallachóir, B.Ó., Korres, N. and Murphy, J., "Can we meet targets for biofuels and renewable energy in transport given the constraints imposed by policy in agriculture and energy?", ***Journal of Cleaner Production***, Vol. 18, No. 16-17, (2010), 1671-1685. (https://doi.org/10.1016/j.jclepro.2010.06.027).
47. Liu, T., McConkey, B., Huffman, T., Smith, S., MacGregor, B. and Yemshanov, D., "Potential and impacts of renewable energy production from agricultural biomass in Canada", ***Applied Energy***, Vol. 130, (2014), 222-229. (https://doi.org/10.1016/j.apenergy.2014.05.044).
48. Ghobadian, B., Najafi, G., Rahimi, H. and Yusaf, T., "Future of renewable energies in Iran", ***Renewable and Sustainable Energy Reviews***, Vol. 13, No. 3, (2009), 689-695. (https://doi.org/10.1016/j.rser.2007.11.010).
49. Ferretti, V., Pluchinotta, I. and Tsoukiàs, A., "Studying the generation of alternatives in public policy making processes", ***European Journal of Operational Research***, Vol. 273, No. 1, (2019), 353-363. (https://doi.org/10.1016/j.ejor.2018.07.054).
50. Wegrich, K. and Jann, W., Theories of the policy cycle, Handbook of public policy analysis, CRC Press, New York, United States of America, (2007). (https://scholar.google.com/scholar?hl=en&as_sdt=0%2C5&q=Theories+of+the+Policy+Cycle.+Handbook+of+Public+Policy+Analysis%2C+New+York%2C+United+States+of+America%3A+CRC+Press%3B&btnG=).
51. Purdon, S., Lessof, C., Woodfield, K. and Bryson, C., Research methods for policy evaluation, Social Research Branch, London, (2001), 1-37. (http://www.thesummerinstitute.ca/wp-content/uploads/Research-Methods-for-Policy-Evaluation.pdf).
52. Lin, C.H., Wen, L. and Tsai, Y.M., "Applying decision-making tools to national e-waste recycling policy: An example of analytic hierarchy process", ***Waste Management***, Vol. 30, No. 5, (2010), 863-869. (https://doi.org/10.1016/j.wasman.2009.11.012).
53. Ghavifekr, S., Hussin, S. and Ghani, M.F.A., "The process of Malaysian smart school policy cycle: A qualitative analysis", ***Journal of Research & Reflections In Education (JRRE)***, Vol. 5, (2011). (https://web.p.ebscohost.com/abstract?direct=true&profile=ehost&scope=site&authtype=crawler&jrnl=19955243&AN=70299848&h=QgOVisLkY%2fs0vCsIXp3BDXjyRnnsGTRh7TvwjUbohIzpMSzBzLnlWdmhUqBTM1ahQIQvnWpRKv5IPBZ4k%2bqxIg%3d%3d&crl=c&resultNs=AdminWebAuth&resultLocal=ErrCrlNotAuth&crlhashurl=login.aspx%

3fdirect%3dtrue%26profile%3dehost%26scope%3dsite%26authtype%3dcrawler%26jrnl%3d19955243%26AN%3d70299848).

54. Dye, T.R., Understanding public policy, Pearson, (2013). (https://repository.vnu.edu.vn/handle/VNU_123/89996).
55. Denhardt, R.B., Denhardt, J.V. and Blanc, T.A., Public administration: An action orientation, Cengage Learning, (2013). (https://books.google.com/books?hl=en&lr=&id=DaYWAAAAQBAJ&oi=fnd&pg=PR4&dq=TA.,+Public+administration:+An+action+orientation:+Cengage+Learning,+(2013&ots=5PAiwpcS4t&sig=CQ-Coy2WYyTOfFBJVV6YexluOSk#v=onepage&q&f=false).
56. Ahrens, N., China's industrial policymaking process, Center for Strategic & International Studies, (2013). (http://csis-website-prod.s3.amazonaws.com/s3fs-public/legacy_files/files/publication/130124_Ahrens_ChinaPolicymaking_Web.pdf).
57. Janssen, M. and Helbig, N., "Innovating and changing the policy-cycle: Policy-makers be prepared!", ***Government Information Quarterly***, Vol. 35, No. 4, Supplement, (2018), S99-S105. (https://doi.org/10.1016/j.giq.2015.11.009).
58. Chapman, A., McLellan, B. and Tezuka, T., "Strengthening the energy policy making process and sustainability outcomes in the OECD through policy design", ***Administrative Sciences***, Vol. 6, No. 3, (2016), 9. (https://doi.org/10.3390/admsci6030009).
59. Ferris, T., "Reflections on the public policy process in Ireland", ***Journal of Administration***, Vol. 62, No. 4, (2015), 87-106. (http://regulatoryreform.com/wp-content/uploads/2015/03/Ireland-Reflections_onthe_PublicPolicy_Process-Tom-Ferris-2015.pdf).
60. Gerston, L.N., Public policy making: Process and principles, Routledge, (2014). (https://books.google.com/books?hl=en&lr=&id=WD3fBQAAQBAJ&oi=fnd&pg=PP1&dq=Gerston,+LN.,+Public+policy+making:+Process+and+principles:+Routledge,+(2014&ots=YEla5Bp_Mh&sig=p9APB2NPcfSkDC-cPhYo_SGjxwY#v=onepage&q=Gerston%2C%20LN.%2C%20Public%20policy%20making%3A%20Process%20and%20principles%3A%20Routledge%2C%20(2014&f=false).
61. Mueller, R.O. and Hancock, G.R., Structural equation modeling, Routledge, (2019), 176. (https://doi.org/10.4324/9781315755649-33).
62. Jais, S.D., Structural equation modeling, The successful use of information in multinational companies: An exploratory study of individual outcomes and the influence of national culture, (2007). (https://books.google.com/books?hl=en&lr=&id=NS5SI_1ywEgC&oi=fnd&pg=PR5&dq=Structural+equation+modeling.+The+Successful+Use+of+Information+in+Multinational+Companies:+An+exploratory+study+of+individual+outcomes+and+the+influence+of+national+culture&ots=nlJQyzrtaA&sig=VyLTkE4iS2xnWogGVtQUX_muQ44#v=onepage&q=Structural%20equation%20modeling.%20The%20Successful%20Use%20of%20Information%20in%20Multinational%20Companies%3A%20An%20exploratory%20study%20of%20individual%20outcomes%20and%20the%20influence%20of%20national%20culture&f=false).
63. Nachtigall, C., Kroehne, U., Funke, F. and Steyer, R., "Pros and cons of structural equation modeling", ***Methods Psychological Research Online***, Vol. 8, (2003), 1-22. (https://citeseerx.ist.psu.edu/viewdoc/download?doi=10.1.1.329.7618&rep=rep1&type=pdf).
64. Burnette, J.L. and Williams, L.J., Structural equation modeling (SEM): An introduction to basic techniques and advanced issues, Research in organizations: Foundations and methods of inquiry, (2005), 143-160. (https://books.google.com/books?hl=en&lr=&id=AyMZt9AodEEC&oi=fnd&pg=PA143&dq=Structural+equation+modeling+(SEM):+An+introduction+to+basic+techniques+and+advanced+issues.+&ots=N6qoLv3Lb9&sig=8i7sxmGwdy1G4Dd8H8ujM6jnLe4#v=onepage&q=Structural%20equation%20modeling%20(SEM)%3A%20An%20introduction%20to%20basic%20techniques%20and%20advanced%20issues.&f=false).
65. Kock, N., "Factor-based structural equation modeling with WarpPLS", ***Australasian Marketing Journal***, Vol. 27, (2019), 57-63. (https://doi.org/10.1016/j.ausmj.2019.02.002).
66. Keith, T.Z., Multiple regression and beyond: An introduction to multiple regression and structural equation modeling (3rd ed.), Routledge, (2019), 654. (https://doi.org/10.4324/9781315162348).
67. Holden, R.R., "Face validity", The corsini encyclopedia of psychology, (2010), 1-2. (https://doi.org/10.1002/9780470479216.corpsy0341).
68. Taherdoost, H., "Validity and reliability of the research instrument; how to test the validation of a questionnaire/survey in a research", ***International Journal of Academic Research in Management***, Vol. 5, No. 3, (2016), 28-36. (https://papers.ssrn.com/sol3/papers.cfm?abstract_id=3205040).
69. Baghestani, A.R., Ahmadi, F., Tanha, A. and Meshkat, M., "Bayesian critical values for Lawshe's content validity ratio", ***Measurement and Evaluation in Counseling and Development***, Vol. 52, No. 1, (2019), 69-73. (https://doi.org/10.1080/07481756.2017.1308227).
70. Polit, D.F., Beck, C.T. and Owen, S.V., "Is the CVI an acceptable indicator of content validity? Appraisal and recommendations", ***Research in Nursing & Health***, Vol. 30, (2007), 459-467. (https://doi.org/10.1002/nur.20199).
71. Hajizadeh, A. and Asghari, M., Statistical methods and analysis with a view to research methods in biological and health sciences, University Jihad, (2011), 536. (In Farsi). (https://www.gisoom.com/book/1744928/%DA%A9%D8%AA%D8%A7%D8%A8-%D8%B1%D9%88%D8%B4-%D9%87%D8%A7-%D9%88-%D8%AA%D8%AD%D9%84%DB%8C%D9%84-%D9%87%D8%A7%DB%8C-%D8%A2%D9%85%D8%A7%D8%B1%DB%8C-%D8%A8%D8%A7-%D9%86%DA%AF%D8%A7%D9%87-%D8%A8%D9%87-%D8%B1%D9%88%D8%B4-%D8%AA%D8%AD%D9%82%DB%8C%D9%82-%D8%AF%D8%B1-%D8%B9%D9%84%D9%88%D9%85-%D8%B2%DB%8C%D8%B3%D8%AA%DB%8C-%D9%88-%D8%A8%D9%87%D8%AF%D8%A7%D8%B4%D8%AA%DB%8C-%D8%A8%D9%87-%D9%87%D9%85%D8%B1%D8%A7%D9%87-%D8%B1%D8%A7%D9%87%D9%86%D9%85%D8%A7%DB%8C-SPSS/).
72. Ahmad, S., Zulkurnain, N.N.A. and Khairushalimi, F.I., "Assessing the validity and reliability of a measurement model in Structural Equation Modeling (SEM)", ***Journal of Advances in Mathematics and Computer Science***, (2016), 1-8. (https://doi.org/10.9734/BJMCS/2016/25183).
73. dos Santos, P.M. and Cirillo, M.Â., "Construction of the average variance extracted index for construct validation in structural equation models with adaptive regressions", ***Communications in Statistics-Simulation and Computation***, (2021), 1-13. (https://doi.org/10.1080/03610918.2021.1888122).
74. Mahmoudi, M.T., Azar, M. and Bahrami, R., "The impact of organizational happiness on the working life quality: A case study among Isfahan University's staff", ***International Journal of Advanced Studies in Humanities and Social Science***, Vol. 8, No. 3, (2019), 255-265. (https://dx.doi.org/10.33945/SAMI/IJASHSS.2019.3.3).
75. Mezher, T., Dawelbait, G. and Abbas, Z., "Renewable energy policy options for Abu Dhabi: Drivers and barriers", ***Energy Policy***, Vol. 42, (2012), 315-328. (https://doi.org/10.1016/j.enpol.2011.11.089).
76. Lieu, J., Spyridaki, N.A., Alvarez-Tinoco, R., Van der Gaast, W., Tuerk, A. and Van Vliet, O., "Evaluating consistency in environmental policy mixes through policy, stakeholder, and contextual interactions", ***Sustainability***, Vol. 10, No. 6, (2018), 18-96. (https://doi.org/10.3390/su10061896).
77. Chapman, A.J., McLellan, B. and Tezuka, T., "Proposing an evaluation framework for energy policy making incorporating equity: Applications in Australia", ***Energy Research & Social Science***, Vol. 21, (2016), 54-69. (https://doi.org/10.1016/j.erss.2016.06.021).

ABSTRACTS

Control of Pitch Angle in Wind Turbine Based on Doubly Fed Induction Generator Using Fuzzy Logic Method

Ehsan Hosseini [a,b], Neda Behzadfar [a,b*], Mahnaz Hashemi [a,b], Majid Moazzami [a,b], Majid Dehghani [a,b]

[a] *Department of Electrical Engineering, Najafabad Branch, Islamic Azad University, Najafabad, Isfahan, Iran.*
[b] *Smart Microgrid Research Center, Najafabad Branch, Islamic Azad University, Najafabad, Isfahan, Iran.*

PAPER INFO

Paper history:
Received: 07 July 2021
Revised in revised form: 17 November 2021
Scientific Accepted: 11 January 2022
Published: 11 January 2022

Keywords:
Doubly Fed Induction Generator (DFIG),
Fuzzy Logic Controller,
PI Controller,
Pitch Angle,
Wind Turbine

ABSTRACT

Wind turbines can be controlled by controlling the generator speed and adjusting the blade angle and the total rotation of a turbine. Wind energy is one of the main types of renewable energy and is geographically extensive, scattered and decentralized and is almost always available. Pitch angle control in wind turbines with Doubly Fed Induction Generator (DFIG) has a direct impact on the dynamic performance and oscillations of the power system. Due to continuous changes in wind speed, wind turbines have a multivariate nonlinear system. The purpose of this study is to design a pitch angle controller based on fuzzy logic. According to the proposed method, nonlinear system parameters are automatically adjusted and power and speed fluctuations are reduced. The wind density is observed by the fuzzy controller and the blade angle is adjusted to obtain appropriate power for the system. Therefore, the pressure on the shaft and the dynamics of the turbine are reduced and the output is improved, especially in windy areas. Finally, the studied system is simulated using Simulink in MATLAB and the output improvement with the fuzzy controller is shown in the simulation results compared to the PI controller. Fuzzy control with the lowest cost is used to control the blade angle in a wind turbine. Also, in this method, the angle is adjusted automatically and it adapts to the system in such a way that the input power to the turbine is limited. Compared to the PI controller, by calculating different parameters, the power quality for fuzzy controller is enhanced from 2.941 % to 4.762 % for wind with an average speed of 12 meters per second.

https://doi.org/10.30501/jree.2021.293546.1226

چکیده

انرژی باد یکی از انواع اصلی انرژی‌های تجدیدپذیر است و از نظر جغرافیایی، گسترده و پراکنده و غیر متمرکز است و تقریباً همیشه در دسترس است. کنترل زاویه گام در توربین های بادی با ژنراتور القایی دوسو تغذیه (DFIG) تأثیر مستقیمی بر عملکرد پویایی و نوسانات سیستم قدرت دارد. با توجه به تغییرات پیوسته در سرعت باد، توربین‌های بادی دارای سیستم چند ورودی غیر خطی هستند. هدف از این مطالعه طراحی کنترل‌کننده زاویه گام با استفاده از منطق فازی است. با توجه به روش پیشنهادی، پارامترهای سیستم غیر خطی به‌طور خودکار تنظیم شده و نوسانات قدرت و سرعت کاهش می یابد. چگالی باد توسط کنترل‌کننده فازی مشاهده می‌شود و زاویه تیغه برای به دست آوردن قدرت مناسب برای سیستم تنظیم می‌شود. بنابراین، فشار روی شفت و دینامیک توربین کاهش می‌یابد و خروجی به خصوص در مناطق بادخیز بهبود می‌یابد. در نهایت، سیستم مورد مطالعه با استفاده از سیمولینک در متلب شبیه‌سازی شده و بهبود خروجی با کنترلر فازی در نتایج شبیه‌سازی در مقایسه با کنترلر PI نشان داده شده است. برای کنترل زاویه پره در توربین بادی از کنترل فازی با کمترین هزینه استفاده می‌شود. همچنین در این روش، زاویه به طور خودکار تنظیم می‌شود و به گونه‌ای با سیستم سازگار می‌شود که قدرت ورودی به توربین محدود شود. با محاسبه پارامترهای مختلف، در مقایسه با کنترل کننده PI، بهبود کیفیت توان از ۲/۹۴۱ ٪ تا ۴/۷۶۲ ٪ برای باد با سرعت متوسط ۱۲ متر در ثانیه بدست می‌آید.

Environmental and Economic Sustainability Assessment of Rainfed Agro-Systems in Northern Iran

Alireza Taheri-Rad, Abbas Rohani *, Mehdi Khojastehpour

Department of Biosystems Engineering, Ferdowsi University of Mashhad, P. O. Box: 91779-48974, Mashhad, Khorasan Razavi, Iran.

PAPER INFO

Paper history:
Received: 26 May 2021
Revised in revised form: 25 November 2021
Scientific Accepted: 11 October 2021
Published: 29 January 2022

Keywords:
Barley,
Canola,
Eco-Efficiency,
Triticale,
Wheat

ABSTRACT

Environmental and economic aspects are two remarkable pillars toward a sustainable agro-system. Accordingly, this study aimed to assess the sustainability of autumn rainfed agro-systems in northern Iran by the Eco-Efficiency (EF) indicator. The data of the production processes of wheat, barley, canola, and triticale were collected in the three crop years of 2016-2019. Results indicated that the canola production system with 720 $kgCO_{2eq}$ ha^{-1} had the highest greenhouse gas (GHG) emissions; however, wheat with 604 $kgCO_{2eq}$ ha^{-1} was attributed to the lowest GHG emissions. The results of the economic analysis also highlighted that the barley production system had the lowest while the canola production system had the highest production costs. The canola production system had the highest profitability, while the barley production system had the lowest in terms of net income and average benefit to cost ratio indicators. The EF indicator for wheat, barley, canola, and triticale was determined to be 1.4, 0.6, 1.8, and 1.1, respectively, indicating the highest EF value for the canola production system.

https://doi.org/10.30501/jree.2021.287947.1212

چکیده

جنبه‌های زیست‌محیطی و اقتصادی دو رکن مهم در حرکت به‌سوی سیستم‌های کشاورزی پایدار هستند. بنابراین، این مطالعه با هدف ارزیابی پایداری سیستم‌های کشت دیم پاییزه در شمال ایران به کمک شاخص اقتصادی-زیست‌محیطی بوده است. داده‌های فرایند تولید گندم، جو، کلزا و تریتیکاله در طول سه سال زراعی ۲۰۱۶ تا ۲۰۱۹ جمع‌آوری شد. نتایج نشان داد که سیستم تولید کلزا با ۷۲۰ کیلوگرم کربن‌دی‌اکسید معادل در هکتار، بیش‌ترین میزان انتشار گازهای گلخانه‌ای را داشت؛ در حالی‌که گندم با ۶۰۴ کیلوگرم کربن‌دی‌اکسید معادل در هکتار دارای کم‌ترین میزان انتشار بود. نتایج تحلیل اقتصادی هم‌چنین نشان داد که جو و کلزا به ترتیب کم‌ترین و بیش‌ترین هزینه تولید را داشتند. سیستم تولید کلزا دارای بیش‌ترین بهره‌وری و سیستم تولید جو دارای کم‌ترین مقدار شاخص‌های درآمد خالص و متوسط نسبت سود به هزینه بود. شاخص کارایی اقتصادی-زیست‌محیطی برای گندم، جو، کلزا، و تریتیکاله به‌ترتیب برابر ۱/۴، ۰/۶، ۱/۸، و ۱/۱ به‌دست آمد، که نشان‌دهنده آن بود که سیستم تولید کلزا بیش‌ترین مقدار شاخص کارایی اقتصادی-زیست‌محیطی را داشت.

Performance of Microtabs and Trailing Edge Flaps in Wind Turbine Power Regulation: A Numerical Analysis Using WTSim

Alireza Maheri [a*], I. Kade Wiratama [b], Terence Macquart [c]

[a] *School of Engineering, Centre for Energy Transition, University of Aberdeen, Aberdeen, Scotland, United Kingdom.*
[b] *Faculty of Engineering, University of Mataram, Mataram, West Nusa Tenggara, Indonesia.*
[c] *Department of Aerospace Engineering, University of Bristol, Bristol, England, United Kingdom.*

PAPER INFO

Paper history:
Received: 27 June 2021
Revised in revised form: 15 November 2021
Scientific Accepted: 10 September 2021
Published: 20 February 2022

Keywords:
Microtab,
Trailing Edge Flap,
Smart Blade,
Power Control,
Load Alleviation,
WTSim

ABSTRACT

The effectiveness of trailing-edge flaps and microtabs in damping 1P-3P loads has been proven through a series of research work during the past decade. This paper presents the results of an investigation into the effectiveness of these devices in power enhancement and power control for responding to the issue of where these devices can be used with dual function of load and power control on a medium size turbine. The 300 kW-AWT27 wind turbine is used as the base wind turbine and the effects of adding trailing-edge flaps and string of microtabs of different lengths positioned at different span locations on the aerodynamic performance of the rotor are studied. In each case, the wind turbine simulator WTSim is used to obtain the aerodynamic performance measures. In the next step, the original blade twist is redesigned to ensure that the blade is optimized upon the addition of these active flow controllers. It is found that blades equipped with flaps can increase the annual average power and reduce the blade loading at the same time for constant speed and variable speed generators. Power enhancement is more visible on constant speed rotors, while load reduction is more significant on variable speed rotors. To achieve constant speed rotors, an average power enhancement of around 12 % is achieved for a flap of size 25 % of the blade span located at about 72 % of the blade span. Microtabs are less effective in power control and can improve the produced power only by a few percentage points.

https://doi.org/10.30501/jree.2021.291397.1220

چکیده

اثربخشی لبه انتهایی برآافزاها و میکرو زبانه‌ها در تعدیل بارهای الکتریکی 1P-3P از طریق یک سری کار تحقیقاتی در طول دهه گذشته ثابت شده است. این مقاله، نتایج یک بررسی در مورد اثربخشی این دستگاه‌ها در افزایش و کنترل توان را برای پاسخ مناسب به این موضوع که در کجا می‌توان از این دستگاه‌ها با عملکرد دوگانه در کنترل بار و توان روی یک توربین با اندازه متوسط استفاده کرد، ارائه می‌نماید. از یک توربین بادی ۳۰۰ کیلووات-AWT27 به عنوان توربین بادی پایه استفاده شده است و اثرات افزودن لبه انتهایی برآافزاها و رشته هایی از میکرو زبانه‌ها با طول‌های مختلف که در مکان‌های دهانه مختلف قرار گرفته‌اند، بر عملکرد آیرودینامیکی گردان مورد مطالعه قرار گرفته اند. در هر مورد، توربین بادی شبیه سازی شده WTSim برای به دست آوردن معیارهای عملکرد آیرودینامیکی استفاده می‌شود. در مرحله بعد، پره چرخان اصلی دوباره طراحی شده تا اطمینان حاصل شود که پره با اضافه شدن این کنترل کننده‌های جریان فعال بهینه شده است. در بررسی مشخص شد که پره های مجهز به برآافزاها می توانند میانگین سالانه توان را افزایش داده و بارگذاری تیغه را در همان زمان برای ژنراتورهای سرعت ثابت و سرعت متغیر کاهش دهند. افزایش توان در چرخانه‌های سرعت ثابت بیشتر قابل مشاهده است، در حالی که کاهش بار در چرخانه‌های سرعت متغیر قابل توجه تر است. برای دستیابی به چرخانه‌های سرعت ثابت، افزایش توان متوسط حدود ۱۲ درصد برای برآافزاهای به اندازه ۲۵ درصد دهانه تیغه واقع در حدود ۷۲ درصد دهانه تیغه به دست می آید. میکروتب ها در کنترل توان کارایی کمتری دارند و فقط چند درصد توان تولیدی را بهبود می‌بخشند.

Dynamic Simulation of Solar-Powered Heating and Cooling System for an Office Building Using TRNSYS: A Case Study in Kerman

Hadi Farzan *

Department of Mechanical Engineering, Faculty of Engineering, Higher Education Complex of Bam, P. O. Box: 76615-314, Bam, Kerman, Iran.

P A P E R I N F O

Paper history:
Received: 18 October 2021
Revised in revised form: 18 December 2021
Scientific Accepted: 07 December 2021
Published: 05 March 2022

Keywords:
Solar-Powered Heating System,
Solar-Powered Cooling System,
Evacuated-Tube Collectors,
Energy Saving,
TRNSYS,
Transient Dynamics Simulation

A B S T R A C T

Recently, novel techniques have been developed in building industries to use solar heating and cooling systems. The current study develops a Solar-powered Heating and Cooling (SHC) system for an office building in Kerman and assesses the transient dynamics of this system and office indoor temperature. To this end, TRNSYS simulation software is utilized to simulate system dynamics. The developed system comprises Evacuated-Tube solar Collectors (ETCs), heat storage tank, heat exchanger, circulating pumps, axillary furnace, cooling tower, single-effect absorption chiller, and air handling unit. The office indoor temperature is assessed in two scenarios, including commonly-insulated and well-insulated envelopes, while window awnings are used to prevent the sun from shining directly through the windows. The results illustrate that the SHC system can meet the thermal loads and provide thermal comfort in line with ASHRAE standards. The indoor temperature reaches 21 °C and 24 °C on cold winter and hot summer days by using the SHC system; however, without the SHC system, the indoor temperature experiences 15 °C and 34 °C on cold and hot days, respectively. The SHC system provides 45 °C and 15 °C supply air on cold and hot days to keep the indoor temperature in the desired range. A thermostat monitors the indoor temperature and saves energy by turning off the system when no heating or cooling is required. Furthermore, the ETCs can run the SHC system for a long time during daytime hours, but the axillary heater is still essential to work at the beginning of the morning.

https://doi.org/10.30501/jree.2021.310980.1272

چکیده

اخیراً روش‌های جدیدی برای استفاده از سیستم‌های گرمایشی و سرمایشی خورشیدی توسعه داده شده است که سبب افزایش بهره‌وری انرژی ساختمان و افزایش استفاده از انرژیهای نو می‌گردد. مطالعه حاضر یک سیستم گرمایشی و سرمایشی خورشیدی برای یک ساختمان اداری در شهر کرمان توسعه داده و به ارزیابی رفتار دینامیکی سیستم و دمای داخلی ساختمان اداری می‌پردازد. برای این منظور از نرم افزار شبیه ساز ترنسیس (TRNSYS) برای شبیه سازی دینامیک سیستم و ساختمان استفاده شده است. سیستم توسعه داده شده شامل: گردآورنده‌های لوله خلأ، تانک ذخیره، مبدل حرارتی، پمپ‌های سیرکلاسیون، اجاق کمکی، برج خنک کن، چیلر جذبی تک اثره و دستگاه هواساز است. دمای داخلی ساختمان در دو حالت شامل ساختمان با عایق بندی معمولی و عایق بندی بالا بررسی شده است و از سایبان بر روی دیواره‌های خارجی استفاده شده است تا از ورود مستقیم نور خورشید جلوگیری شود. نتایج مطالعه نشان می‌دهد سیستم خورشیدی توسعه داده شده به خوبی توانایی تأمین بارهای گرمایشی و سرمایشی و تأمین آسایش حرارتی را بر اساس استاندارد اشری (ASHRAE) دارد. دمای داخلی ساختمان در صورت استفاده از سیستم گرمایشی و سرمایشی خورشیدی به مقادیر ۲۱ °C و ۲۴ °C به ترتیب در روزهای سرد و گرم سال می‌رسد. در حالیکه در صورت عدم استفاده از سیستم گرمایشی و سرمایشی خورشیدی، دمای داخل ساختمان به ترتیب مقادیر ۱۵ °C و ۳۴ °C را در روزهای سرد و گرم سال تجربه می‌کند. سیستم گرمایشی و سرمایشی خورشیدی هوای با درجه حرارت ۴۵ °C و ۱۵ °C را برای ایجاد آسایش حرارتی در ساختمان تأمین می‌کند. یک ترموستات وظیفه کنترل دمای داخلی ساختمان و افزایش راندمان انرژی با خاموش کردن سیستم در لحظاتی که سرمایش و گرمایش مورد نیاز نیست، را به عهده دارد. این نکته حائز اهمیت است که گردآورنده‌های لوله خلأ توانایی راه اندازی سیستم خورشیدی را برای مدت ط ولانی در طول روز دارا می‌باشند، اما استفاده از اجاق کمکی برای ابتدای صبح امری ضروری است.

Analytical Approach to Exploring the Missing Data Behavior in Smart Home Energy Consumption Dataset

Kasaraneni Purna Prakash [a], Yellapragada Venkata Pavan Kumar [b*]

[a] *School of Computer Science and Engineering, VIT-AP University, Amaravati-522237, Andhra Pradesh, India.*
[b] *School of Electronics Engineering, VIT-AP University, Amaravati-522237, Andhra Pradesh, India.*

PAPER INFO

Paper history:
Received: 04 November 2021
Revised in revised form: 04 December 2021
Scientific Accepted: 12 December 2021
Published: 07 March 2022

Keywords:
Behavior Analysis,
Data Analysis,
Energy Consumption Data,
Missing Data Anomalies,
Smart Homes,
Smart Meter Data

ABSTRACT

Smart homes are considered to be the subset of smart grids that have gained widespread popularity and significance in the present energy sector. These homes are usually equipped with different kinds of sensors that communicate between appliances and the metering infrastructure to monitor and trace the energy consumption details. The smart meters trace the energy consumption data continuously or in a period of intervals as required. Sometimes, these traces will be missed due to errors in communication channels, an unexpected breakdown of networks, malfunctioning of smart meters, etc. This missingness greatly impacts smart home operations such as load estimation and management, energy pricing, optimizing assets, planning, decision making, etc. Moreover, to implement a suitable precautionary measure to eliminate missing of data traces, it is required to understand the past behavior of the data anomalies. Hence, it is essential to comprehend the behavior of missing data in the smart home energy consumption dataset. In this regard, this paper proposes an analytical approach to detect and quantify the missing data instants in all days for all appliances. Using this quantification, the behavior of missing data anomalies is analyzed during the day. For the analysis, a practical smart home energy consumption dataset 'Tracebase' is considered. Initially, the existence and the count of missing instants are computed. From this, the appliance 'MicrowaveOven' is considered for further analysis as it comprises the highest count of missing instants (84740) in a day when compared to all other appliances. Finally, the proposed analysis reveals that the large number of missing instants is occurring during the daylight period of a day.

https://doi.org/10.30501/jree.2021.313536.1277

چکیده

خانه‌های هوشمند زیرمجموعه‌ای از شبکه‌های هوشمند در نظر گرفته می‌شوند که محبوبیت و اهمیت گسترده‌ای در بخش صنعت انرژی کنونی پیدا کرده‌اند. این خانه‌ها معمولاً به انواع مختلفی از سنسورها مجهز هستند که بین دستگاه‌ها و زیرساخت‌های اندازه‌گیری ارتباط برقرار می‌کنند تا جزئیات مصرف انرژی را نظارت و ردیابی کنند. کنتورهای هوشمند، داده‌های مصرف انرژی را به طور مداوم در بازه‌های زمانی مورد نیاز ردیابی می‌کنند. گاهی اوقات، این ردیابی‌ها به دلیل خطا در کانال‌های ارتباطی، خرابی غیرمنتظره شبکه‌ها، عملکرد نادرست کنتورهای هوشمند و غیره از بین می‌روند. نبود چنین ردیابی‌هایی بر عملیات خانه‌های هوشمند مانند برآورد و مدیریت عملکرد، قیمت‌گذاری انرژی، بهینه‌سازی دارایی‌ها، برنامه ریزی، تصمیم گیری و غیره تأثیر زیادی دارد. علاوه بر این، برای اجرای یک اقدام پیشگیرانه مناسب برای از بین بردن ردیابی داده‌ها، نیاز به درک رفتار گذشته ناهنجاری داده‌ها است. از این رو، فهم رفتار داده‌های از دست رفته در مجموعه مصرف داده‌های انرژی خانه هوشمند ضروری است. در این راستا، این مقاله یک رویکرد تحلیلی برای شناسایی و تعیین کمّیت لحظه‌ای برای داده‌های از دست رفته در تمام روزها و برای همه دستگاه‌ها پیشنهاد می‌کند. با استفاده از این کمّیت، ناهنجاری رفتارهای داده‌های از دست رفته در طول روز تجزیه و تحلیل می‌شود برای تجزیه و تحلیل، یک مجموعه داده کاربردی مصرف انرژی خانه هوشمند "Tacebase" در نظر گرفته شده است. در ابتدا، وجود و تعداد لحظه‌های از دست رفته محاسبه می‌شود. از این رو، دستگاه «مایکروویو» برای تجزیه و تحلیل بیشتر در نظر گرفته می‌شود، زیرا در مقایسه با همه دستگاه‌های دیگر، بیشترین تعداد لحظه‌های از دست رفته (۸۴۷۴۰) در روز را دارد. در نهایت، تحلیل پیشنهادی نشان می‌دهد که تعداد زیادی از لحظه‌های از دست رفته در طول روز رخ می‌دهد.

Multi-Response Optimization of Tubular Microbial Fuel Cells Using Response Surface Methodology (RSM)

Maryam Keshavarz [a], Davod Mohebbi-Kalhori [a,b*], Vajihe Yousefi [a]

[a] *Department of Chemical Engineering, Faculty of Engineering, University of Sistan and Baluchestan, Zahedan, Sistan and Baluchestan, Iran.*
[b] *University of Sistan and Baluchestan Central Laboratory, Zahedan, Sistan and Baluchestan, Iran.*

PAPER INFO

Paper history:
Received: 14 June 2021
Revised in revised form: 03 January 2022
Scientific Accepted: 11 October 2021
Published: 19 March 2022

Keywords:
Microbial Fuel Cell,
Response Surface Methodology (RSM),
Separator-Electrode Assembly,
J-Cloth,
Nylon-Cloth,
Domestic Wastewater Treatment

ABSTRACT

Response surface methodology is employed to statistically identify the significance of three parameters of separator assembly arrangement, wastewater flow rate, and relative flow patterns of anode and cathode influencing the generation of power and coulombic efficiency of Microbial Fuel Cells (MFCs). Three different assemblies of Nylon-Cloth (NC), artificial rayon cloth as Absorbent Layer (AL), and J-Cloth (JC) were investigated as proton exchange mediums instead of common expensive polymeric membranes. Statistical analyses (ANOVA) revealed that although the addition of the AL after the JC layer had no significant impact on the enhancement of maximum power density, it could improve the coulombic efficiency of the MFCs by 15 %, owing to the crucial impact of oxygen permeability control between the MFC chambers. In the counter-current flow pattern, higher trans-membrane pressure and more oxygen concentration differences diminished the MFC performance and marked the importance of efficient separator layer arrangement, compared to co-current influents. The maximum power density of 285.89 mW/m^2, the coulombic efficiency of 4.97 %, and the internal resistance of 323.9 Ω were achieved for the NC-JC-Al arrangement in the co-current mode along with the flow rate of 6.9 ml/min. The higher the flow rate of influent wastewater, the higher the performance of the MFCs.

https://doi.org/10.30501/jree.2022.290677.1218

چکیده

در این تحقیق، روش پاسخ سطحی جهت بررسی آماری میزان اهمیت فاکتورهای ترتیب چینش لایه‌های غشای جداکننده، شدت جریان فاضلاب و آرایش جریان ورودی به محفظه آندی و کاتدی بر توان و بازده کولومبیک پیل‌های سوختی میکروبی، به کارگرفته شده است. به جای استفاده از غشاهای تبادل پروتون پلیمری گران‌قیمت متداول، از سه لایه متفاوت شامل پارچه نایلونی (NC)، پارچه ریون مصنوعی به عنوان لایه جاذب (AL) و لایه جی-کلات (JC) به عنوان محیط تبادل پروتون استفاده گردید. تحلیل آماری (ANOVA) نشان داد که با وجود اینکه افزودن لایه جاذب بعد از جی کلات تأثیر قابل اهمیتی در حداکثر توان تولیدی ندارد، اما به دلیل نقش تعیین‌کننده چینش لایه‌ها در کنترل اکسیژن عبوری بین محفظه‌های آندی و کاتدی، سبب بهبود بازده کولومبیک پیل‌های سوختی میکروبی می‌گردد. در آرایش جریان ناهمسو، اختلاف فشار بیشتر و اختلاف غلظت بیشتر اکسیژن در مقایسه با جریان همسو، سبب کاهش بازده پیل سوختی میکروبی و برجسته شدن اهمیت انتخاب بهینه چینش لایه‌های تبادل پروتون می‌گردد. در پیل سوختی با ترتیب لایه های NC-JC-AL با جریان همسو و شدت جریان برابر با ۶/۹ ml/min، حداکثر توان تولیدی برابر با ۲۸۵/۸۹ mW/m^2، بازده کولومبیک برابر با ۴/۹۷ ٪ و مقاومت داخلی برابر با ۳۲۳/۹ Ω به دست آمد. افزایش شدت جریان فاضلاب ورودی سبب افزایش کارایی پیل سوختی میکروبی شد.

Reduction of Low Frequency Oscillations Using an Enhanced Power System Stabilizer via Linear Parameter Varying Approach

Vahid Nazari, Mohammad Hossein Mousavi, Hassan Moradi CheshmehBeigi *

Department of Electrical Engineering, Faculty of Engineering, Razi University, P. O. Box: 67144-14971, Kermanshah, Kermanshah, Iran.

PAPER INFO

Paper history:
Received: 27 September 2021
Revised in revised form: 23 December 2021
Scientific Accepted: 15 December 2021
Published: 12 April 2022

Keywords:
Power System Stabilizer,
Single Machine Infinite Bus Power System,
Linear Parameter Varying (LPV),
Linear Matrix Inequality (LMI)

ABSTRACT

Over the past decades, power engineers have begun to connect power grids to other networks such as microgrids associated with renewable units using long transmission lines to provide higher reliability and greater efficiency in production and distribution besides saving resources. However, many dynamic problems such as low frequency oscillations were observed as a result of these connections. Low frequency oscillation is a normal phenomenon in most power systems that causes perturbations and, thus, the grid stability and damping process are of paramount importance. In this paper, to attenuate these oscillations, a novel method for designing Power System Stabilizer (PSS) is presented via Linear Parameter-Varying (LPV) approach for a Single Machine Infinite Bus system (SMIB). Because the system under study is subject to frequent load and production changes, designing the stabilizer based on the nominal model may not yield the desired performance. To guarantee the flexibility of the stabilizer with respect to the aforementioned issues, the power system polytopic representation is used. In order to apply the new method, the nonlinear equations of the system at each operating point, located in a polytope, are parametrically linearized by scheduling variables. Scheduling variables can be measured online in any operating point. By using this model and following the H_∞ synthesis, feedback theories, and Linear Matrix Inequalities (LMIs), LPV controllers at all operating points are obtained. Finally, the simulation results verify the effectiveness of the proposed controller over classic and robust controllers with regard to uncertainties and changes in system conditions.

https://doi.org/10.30501/jree.2021.306909.1265

چکیده

طی دهه‌های گذشته، مهندسان برق با استفاده از خطوط انتقال طولانی، شبکه‌های برق را به شبکه‌های دیگر مانند ریزشبکه‌های شامل واحدهای تجدیدپذیر متصل کرده‌اند تا علاوه بر صرفه‌جویی در منابع، قابلیت اطمینان بالاتر و کارایی بیشتری را در تولید و توزیع ارائه دهند. با این حال، بسیاری از مشکلات دینامیکی مانند نوسانات فرکانس پایین در نتیجه این اتصالات مشاهده شدند. نوسان فرکانس پایین یک پدیده طبیعی در اکثر سیستم‌های قدرت است که اختلالاتی را ایجاد می‌کند و لذا ثبات و میرایی شبکه در این زمینه بسیار حائز اهمیت می‌باشد. در این مقاله به منظور کاهش این نوسانات، یک روش کارامد برای طراحی پایدارساز سیستم قدرت (PSS) از طریق روش پارامترهای خطی متغیر (LPV) برای یک سیستم تک ماشینه متصل به شین بی‌نهایت (SMIB) ارائه شده است. از آنجا که سیستم مورد مطالعه تحت بار و تغییرات مکرر تولید قرار دارد، طراحی پایدارساز بر اساس مدل نامی ممکن است عملکرد مطلوبی را ارائه ندهد. برای تضمین انعطاف‌پذیری پایدارساز با توجه به موارد فوق، از نمایش چند سقفی (چند بر) سیستم قدرت استفاده می‌شود. برای اعمال روش کارآمد جدید، معادلات غیرخطی سیستم در هر نقطه کاری که در یک فضای چند سقفی قرار دارد، با استفاده از متغیرهای برنامه‌ریزی به صورت پارامتری خطی‌سازی می‌شوند. متغیرهای برنامه‌ریزی را می‌توان بصورت آنلاین در هر نقطه کار اندازه‌گیری کرد. با استفاده از این مدل و پیروی از سنتز H_∞، نظریه‌های بازخورد و نامساوی‌های ماتریس خطی (LMI)، کنترل‌کننده‌های LPV در تمام نقاط عملیاتی بدست می‌آید. در نهایت، نتایج شبیه‌سازی اثربخشی کنترل‌کننده پیشنهادی و برتری آن را بر کنترل‌کننده‌های کلاسیک و مقاوم با در نظر گرفتن عدم قطعیت‌ها و تغییرات در شرایط سیستم تأیید می‌کند.

CFD Analysis of the Most Favorable Gap Between the Main Runner and Booster Runner of Gravitational Water Vortex Turbine

Bharosh Kumar Yadav [a*], Amit Chandra Jyoti [a], Pintu Kr. Rajak [a], Ramesh Kr. Mahato [a], Deelip Kr. Chaudhary[a], Mehdi Jahangiri[b], Ram Dayal Yadav[a]

[a] *Department of Mechanical Engineering, Purwanchal Campus, Institute of Engineering, Tribhuvan University, Dharan-08, Nepal.*
[b] *Department of Mechanical Engineering, Shahrekord Branch, Islamic Azad University, Shahrekord, Iran.*

PAPER INFO

Paper history:
Received 20 September 2021
Revised in revised form: 06 November 2021
Scientific Accepted: 23 November 2021
Published: 19 April 2022

Keywords:
Low Head MHP,
Computational Fluid Dynamic (CFD),
Vortex Turbine,
Booster Runner,
Main Runner

ABSTRACT

The Gravitational Water Vortex Power Plant (GWVPP) is a power generation system designed for ultralow head and low flow water streams. Energy supply to rural areas using off-grid models is simple in design and structure and sustainable to promote electricity access through renewable energy sources in the villages of Nepal. The objective of this study is to determine the most favorable gap between the booster and main runners of a Gravitational Water Vortex Turbine (GWVT) to ensure maximum power output of the GWVPP. CFD analysis was used to evaluate the 30 mm gap between the main and booster runners, which was the most favorable gap for enhancing the plant's power. In this study, the optimum power and economic analysis of the entire plant was conducted in the case of mass flow rates of 4 kg/s, 6 kg/s, and 8 kg/s. The system was modeled in SolidWorks V2016 and its Computational Fluid Dynamic (CFD) analysis was performed utilizing ANSYS R2 2020 with varying multiple gaps between the main and booster runners to determine the most favorable gap of the plant's runner. This research concluded that optimum power could be achieved if the distance of the main runner's bottom position be fixed at 16.72 %, i.e., the distance between the top position of the conical basin and the top position of the booster runner. At a mass flow rate of 8 kg/s, the plant generated maximum electric energy (3,998,719.6 kWh) comparatively and economically contributed 268,870.10 USD on an annual basis.

https://doi.org/10.30501/jree.2022.298216.1237

چکیده

نیروگاه گرانشی چرخشی آب، یک سیستم تولید برق است که برای جریان‌های آب کم و بسیار کم طراحی شده است. تأمین انرژی مناطق روستایی با استفاده از مدل‌های خارج از شبکه از نظر طراحی و ساختار ساده بوده و روشی پایدار برای ارتقای دسترسی به برق از طریق منابع انرژی تجدیدپذیر در روستاهای نپال است. هدف از این مطالعه، تعیین مطلوب‌ترین فاصله بین گرداننده و تقویت کننده اصلی یک توربین گرانشی-چرخشی آب (GWVT) برای اطمینان از حداکثر توان خروجی GWVPP است. از آنالیز دینامیک سیالات محاسباتی (CFD) برای ارزیابی فاصله‌های مختلف بین گرداننده اصلی و تقویت کننده استفاده شد که مطلوب‌ترین فاصله برای افزایش قدرت نیروگاه ۳۰ میلی‌متر بود. در این مطالعه، توان بهینه و تحلیل اقتصادی کل نیروگاه در نرخ جریان‌های جرمی ۴ کیلوگرم بر ثانیه، ۶ کیلوگرم بر ثانیه و ۸ کیلوگرم بر ثانیه انجام شد. این سیستم در SolidWorks V2016 مدل‌سازی شد و تجزیه و تحلیل دینامیک سیالات محاسباتی آن با استفاده از ANSYS R2 2020 با فاصله‌های متعدد بین گرداننده اصلی و تقویت‌کننده منبع اصلی برای تعیین مطلوب‌ترین شکاف گرداننده کارخانه انجام شد. این تحقیق به این نتیجه رسید که اگر فاصله موقعیت پایین گرداننده اصلی در ۱۶/۷۲ ٪ ثابت شود، یعنی فاصله بین موقعیت بالای حوضه مخروطی و موقعیت بالایی گرداننده تقویت-کننده، می‌توان به قدرت بهینه دست یافت. با نرخ جریان جرمی ۸ کیلوگرم بر ثانیه، این نیروگاه حداکثر انرژی الکتریکی (۳،۹۹۸،۷۱۹/۶ کیلووات ساعت) را تولید کرد و از نظر اقتصادی ۲۶۸،۸۷۰/۱۰ دلار آمریکا به صورت سالانه کمک کرد.

Sustainability and Environmental Impact of Hydroxy Addition on a Light-Duty Generator Powered with an Ethanol–Gasoline Blend

Padmanabhan Sambandam [a*], Parthasarathy Murugesan [a], Mohamed Iqbal Shajahan [a], Balaguru Sethuraman [b], Hussein Mohamed Abdelmoneam Hussein [c]

[a] *School of Mechanical and Construction, Vel Tech Rangarajan Dr. Sagunthala R&D Institute of Science and Technology, Avadi, Chennai, Tamil Nadu, India.*
[b] *School of Mechanical Engineering, VIT Bhopal University, Madhya Pradesh, India.*
[c] *Department of Mechanical Engineering, Faculty of Engineering, Helwan University, Cairo, Egypt.*

PAPER INFO

Paper history:
Received: 11 August 2021
Revised in revised form: 18 October 2021
Scientific Accepted: 26 November 2021
Published: 08 May 2022

Keywords:
Gasoline Engine,
Light Duty Generator,
Ethanol,
Hydroxy Gas,
Emission Characteristics

ABSTRACT

Environmental sustainability encompasses various problems including climate change, clean air, renewable energy, non-toxic environments, and capacity to live in a healthy community. Many researchers focus their attention on alternative energy sources, such as ethanol and hydroxy gas, to enhance environmental health and quality of life. The introduction of hydroxy gas as a clean source of energy is gaining significant traction. Also, ethanol has a greater octane number than gasoline. Therefore, the ethanol–gasoline blend has a higher octane number than conventional gasoline. A new combination of hydroxy gas, ethanol, and gasoline is environmentally benign while significantly improving the performance of gasoline engines. This paper tested hydroxy gas in a 197-cc gasoline engine power generator powered with ethanol–gasoline blend. The results demonstrated that thermal efficiency increased up to 23.6 % and fuel consumption decreased up to 36 % on a volume basis, which was a significant improvement over the base engine. Furthermore, the hazardous carbon monoxide reduction reached 11.45 % and the unburned hydrocarbon emissions reached 17.6 %.

https://doi.org/10.30501/jree.2021.299136.1241

چکیده

پایداری محیطی شامل مشکلات مختلفی از جمله تغییرات آب و هوایی، هوای پاک، انرژی های تجدیدپذیر، محیطهای غیر سمّی و ظرفیت زندگی در یک جامعه سالم است. بسیاری از محققان توجه خود را بر منابع انرژی جایگزین، مانند اتانول و گاز هیدروکسی، برای افزایش سلامت محیط و کیفیت زندگی متمرکز می‌کنند. معرفی گاز هیدروکسی به عنوان یک منبع پاک انرژی در حال افزایش است. همچنین اتانول دارای عدد اکتان بیشتری نسبت به بنزین است. بنابراین، ترکیب اتانول–بنزین دارای عدد اکتان بالاتری نسبت به بنزین معمولی است. ترکیب جدیدی از گاز هیدروکسی، اتانول و بنزین از نظر زیست‌محیطی بی خطر است و در عین حال عملکرد موتورهای بنزینی را به طور قابل توجهی بهبود می‌بخشد. این مقاله گاز هیدروکسی را در یک ژنراتور برق ۱۹۷ سی سی موتور بنزینی که با ترکیب اتانول-بنزین تغذیه می‌شود، آزمایش کرد. نتایج نشان داد که راندمان حرارتی تا ۲۳/۶ درصد افزایش یافته و مصرف سوخت تا ۳۶ درصد بر اساس حجم کاهش یافته است که نسبت به موتور پایه، بهبود قابل توجهی داشته است. علاوه بر این، کاهش خطرناک مونوکسید کربن به ۱۱/۴۵ درصد و انتشار هیدروکربن نسوخته به ۱۷/۶ درصد رسید.

Policy Model of Renewable Energy Development in Iran's Agriculture Sector

Somayeh Dehhaghi [a], Shahla Choobchian [a*], Barat Ghobadian [b], Homayon Farhadian [a]

[a] *Department of Agricultural Extension and Education, University of Tarbiat Modares (TMU), P. O. Box: 14115-336, Tehran, Tehran, Iran.*
[b] *Department of Mechanics of Biosystems Engineering, University of Tarbiat Modares, P. O. Box: 14115-336, Tehran, Tehran, Iran.*

PAPER INFO

Paper history:
Received: 18 October 2021
Revised in revised form: 11 January 2022
Scientific Accepted: 25 December 2021
Published: 10 May 2022

Keywords:
Renewable Energy,
Policymaking,
Policymaking Mode,
Energy Policy,
Agriculture

ABSTRACT

The purpose of this study is to present a renewable energy policy model in the agricultural sector of Iran. To achieve this goal, a questionnaire consisting of 57 items was designed. The reliability of the questionnaire was confirmed by Cronbach's alpha (0.916). Also, to analyze the validity and reliability of the research tool, the Average Variance Extracted (AVE) and Composite Reliability (CR) were calculated. The validity of the questionnaire was determined using face validity, Content Validity Ratio (CVR), and Content Validity Index (CVI). The statistical population of the study consists of energy policymaking experts who were estimated at about 80 people. The sampling method was random and 70 samples answered the questionnaire using the Krejcie and Morgan table. Using structural equation modeling and the maximum likelihood method and using LISREL software, the model fit was estimated at a favorable level. Based on the findings, it was found that the priorities of the agricultural sector and the needs of this sector had not been considered in renewable energy policymaking. Policymaking is done top-down and stakeholders are not considered. Renewable equipment market policies are not adequate and the market is not properly managed. Interaction between policymaking institutions is not in good shape. The results of this study can help address the various shortcomings of the renewable energy policy as well as reduce the common inconsistencies in this area. Finally, suggestions were made for the development and promotion of policies in the field of renewable energy in the agricultural sector of Iran.

https://doi.org/10.30501/jree.2022.311064.1273

چکیده

این مطالعه با هدف طراحی مدل سیاست‌گذاری انرژی‌های تجدیدپذیر در بخش کشاورزی ایران انجام شده است. برای دستیابی به این هدف، پرسشنامه‌ای شامل ۵۷ گویه طراحی شد. جامعه آماری پژوهش، متخصصان سیاست‌گذاری انرژی با تعداد ۸۰ نفر بودند. روش نمونه‌گیری تصادفی بوده و بر اساس جدول مورگان ۷۰ نفر به پرسشنامه پاسخ دادند. در تست پایلوت، پرسشنامه بین ۳۰ نفر از متخصصان توزیع شد. روایی پرسشنامه حاضر با استفاده از روایی صوری، نسبت اعتبار محتوا (CVR)، شاخص روایی محتوا (CVI) تعیین شد. پایایی آن با استفاده از آلفای کرونباخ (۰/۹۱۶) به دست آمد. همچنین ، برای تجزیه و تحلیل اعتبار و پایایی متغیرهای تحقیق، میانگین شاخص های واریانس استخراج شده (AVE) و پایایی مرکب (CR) محاسبه گردید. با استفاده از مدل‌سازی معادلات ساختاری و روش حداکثر درست‌نمایی و با استفاده از نرم افزارLISREL، برازش مدل در سطح خوبی برآورد شد. بر اساس یافته ها مشخص شد که اولویت‌های بخش کشاورزی و نیازهای این بخش در سیاست‌گذاری انرژی‌های تجدید پذیر در نظر گرفته نشده است. سیاست گذاری از بالا به پایین انجام می شود و ذینفعان در نظر گرفته نمی‌شوند. سیاست‌های بازار تجهیزات تجدیدپذیر در وضعیت خوبی نیست. تعامل بین نهادهای سیاست‌گذار در شرایط مناسبی نیست. نتایج این مطالعه می‌تواند به رفع نواقص مختلف چرخه سیاست‌گذاری انرژی‌های تجدیدپذیر و همچنین کاهش تناقضات رایج در این چرخه کمک نماید. در نهایت، پیشنهاداتی برای توسعه و ارتقای سیاست‌گذاری در زمینه انرژی‌های تجدیدپذیر در بخش کشاورزی ایران ارائه شده است.

CONTENTS

Journal Homepage: www.jree.ir